

GAS PERMEATION AND SORPTION PROPERTIES OF ZIF-8 FILLED
POLYMERIC MEMBRANES PREPARED BY INFRARED AND
INCANDESCENT LIGHT INDUCED LIQUID AND VAPOR PHASE
INVERSION

A THESIS SUBMITTED TO
THE GRADUATE SCHOOL OF NATURAL AND APPLIED SCIENCES
OF
MIDDLE EAST TECHNICAL UNIVERSITY

BY

BURCU TÜZÜN ANTEPLİ

IN PARTIAL FULFILLMENT OF THE REQUIREMENTS
FOR
THE DEGREE OF DOCTOR OF PHILOSOPHY
IN
CHEMICAL ENGINEERING

DECEMBER 2017

Approval of the thesis:

**GAS PERMEATION AND SORPTION PROPERTIES OF ZIF-8 FILLED
POLYMERIC MEMBRANES PREPARED BY INFRARED AND
INCANDESCENT LIGHT INDUCED LIQUID AND VAPOR PHASE
INVERSION**

submitted by **BURCU TÜZÜN ANTEPLİ** in partial fulfillment of the requirements for the degree of **Doctor of Philosophy in Chemical Engineering Department, Middle East Technical University** by,

Prof. Dr. Gülbin Dural Ünver
Dean, Graduate School of **Natural and Applied Sciences**

Prof. Dr. Halil Kalıpçılar
Head of Department, **Chemical Engineering**

Prof. Dr. Halil Kalıpçılar
Supervisor, **Chemical Engineering Dept., METU**

Prof. Dr. Levent Yılmaz
Co-Supervisor, **Chemical Engineering Dept., METU**

Examining Committee Members:

Prof. Dr. Nihal Aydoğan
Chemical Engineering Dept., Hacettepe University

Prof. Dr. Halil Kalıpçılar
Chemical Engineering Dept., METU

Assoc. Prof. Dr. Zeynep Çulfaz Emecen
Chemical Engineering Dept., METU

Assoc. Prof. Dr. Çerağ Dilek Hacıhabiboğlu
Chemical Engineering Dept., METU

Asst. Prof. Dr. Berna Topuz
Chemical Engineering Dept., Ankara University

Date: 11.12.2017

I hereby declare that all information in this document has been obtained and presented in accordance with academic rules and ethical conduct. I also declare that, as required by these rules and conduct, I have fully cited and referenced all material and results that are not original to this work.

Name, Last name: Burcu Tüzün Antepli

Signature:

ABSTRACT

GAS PERMEATION AND SORPTION PROPERTIES OF ZIF-8 FILLED POLYMERIC MEMBRANES PREPARED BY INFRARED AND INCANDESCENT LIGHT INDUCED LIQUID AND VAPOR PHASE INVERSION

Antepli Tüzün, Burcu

Ph.D., Department of Chemical Engineering

Supervisor: Prof. Dr. Halil Kalıpcılar

Co-Supervisor: Prof. Dr. Levent Yılmaz

December 2017, 307 pages

In this study, the effects of production method parameters, zeolitic imidazole framework (ZIF-8) as filler and para-nitro aniline (pNA) as low molecular weight additive on membrane morphology and gas separation properties were investigated. Membranes were characterized by single gas permeability measurements and sorption measurements of CO₂ and CH₄ as well as scanning electron microscopy (SEM).

In the first part of this study, asymmetric PES membranes were produced by wet phase inversion method. The polymeric membranes prepared in isopropanol (IPA) coagulation bath with 25% v.l. dimethylformamide (DMF) have CO₂ permeance 44% higher than that of prepared with pure IPA. The polymeric membranes prepared in IPA coagulation bath with 10% v.l. water have CO₂ permeance 175% higher as compared to the one prepared with pure IPA. Observations show that 10% loading of ZIF-8 with 60 nm crystal size results in 86% increase in CO₂ permeance and 13% increase in CO₂/CH₄ selectivity of PES membrane.

In the second part, PI membranes prepared via light induced dry-wet phase inversion method. This is a new method and is not used in literature before. Infrared (IR) and incandescent lamp (IL) light were used as energy source during dry inversion step in order to control the rate and extent of evaporation of volatile solvent. When the IR exposure was less than 60 s at dry inversion, the membrane permeance sharply increased with IR exposure and then decreased slightly. Further increase in IR exposure period created denser and low permeate PI membranes. The maximum permeance was observed when the IR exposure took less than 10 s. The permeance was about 8.51 GPU, 2.44 GPU and 0.13 GPU for H₂, CO₂ and CH₄, respectively. Solvent ratio THF/DMF was the other parameter whose effect was studied. CO₂ permeance of PI membranes was measured 0.81 GPU, 2.55 GPU and 6.65 GPU corresponding to the 0.80, 0.42, 0.17 THF/DMF ratio of casting solution, respectively. For PI membranes, ZIF-8 loading resulted in thicker skin layer and lower permeance.

In the third part, asymmetric PI membranes were produced via light induced dry-vapor phase inversion method. This study is different from literature in terms of both being developed a new method and producing the first gas separation and the first mixed matrix membrane by this new method. This method led to slow phase inversion, closed pores and thicker skin layer, thereby lower permeance was observed. The two important opportunities of this method were fixing the ZIF-8 crystals in the skin layer and incorporating of pNA into the membrane. Previously, pNA diffused into coagulation bath during wet phase inversion and could not be incorporated into the membrane. For mixed matrix-pNA membranes produced by this method, the maximum selectivity was about 3.24, 132.68, and 40.9 for H₂/CO₂, H₂/CH₄ and CO₂/CH₄, respectively.

In the last part, effect of ZIF-8 loading on sorption capacity of dense PI mixed matrix membrane (MMM) was investigated. CO₂ sorption capacity increased by 22% and 40% at 10 bar corresponding to ZIF-8 loading by 10% and 20 %. The

enhancement in CH₄ sorption capacity was 20% and 60% at 10 bar corresponding to 10% and 20% ZIF-8 addition. Dual mode sorption parameters of neat PI and PI/ZIF-8 MMM were calculated. k_D and b increased and C_H decreased due to incorporation of ZIF-8. Based on the variation in the dual-mode parameters, the free volume of MMM decreased, nevertheless sorption capacity increased because the affinity between membrane and penetrant enhanced. Mixture gas sorption experiment was carried out for three different compositions namely 30:70, 50:50, 70:30 CO₂:CH₄. In the multicomponent sorption in glassy polymers the solubility of all gases depressed with different extents due to a competitive effect. The competition has a much stronger impact on methane than on carbondioxide solubility. For example, for mixture containing %49 CH₄- %51 CO₂, solubility of CH₄ decreased about 75% with respect to pure CH₄, while the solubility of CO₂ decreased by 35% with respect to pure CO₂.

Keywords: Gas separation, Asymmetric PI and PES mixed matrix membranes, Gas sorption, Light induced phase inversion, Zeolitic Imidazole Framework (ZIF-8)

ÖZ

KIZILÖTESİ VE AMPUL IŞIĞI YARDIMIYLA SIVI VE BUHARDA FAZ DEĞİŞİM YÖNTEMLERİYLE ÜRETİLEN ZIF-8 DOLGULU POLİMERİK MEMBRANLARIN GAZ GEÇİRİM VE SOĞURMA ÖZELLİKLERİ

Antepli Tüzün, Burcu

Doktora, Kimya Mühendisliği Bölümü

Tez Yöneticisi: Prof. Dr. Halil Kalıpçılar

Ortak Tez Yöneticisi: Prof. Dr. Levent Yılmaz

Aralık 2017, 307 sayfa

Bu çalışmada, üretim yöntemlerinin değişkenlerinin, dolgu maddesi olarak ZIF-8 ve düşük molekül ağırlıklı uyumlaştırıcı olarak pNA kullanımının membranın morfolojik ve gaz geçirim özelliklerine etkisi incelenmiştir. Membranlar, H₂, CO₂ ve CH₄ tek gaz geçirgenlik ölçümleri, taramalı electron mikroskopu (SEM) ve gaz soğurma ölçümleriyle test edilmiştir.

Bu çalışmanın ilk bölümünde, asimetric PES membranlar ıslak faz değişim yöntemiyle üretilmiştir. İzo-propanol (IPA) çökeltme banyosunda 25% hacimce dimetilformamide (DMF) eklenmesi PES membranın CO₂ akısının 44% arttırmıştır. IPA çökeltme banyosunda hacimce 10% su eklenmesiyle CO₂ geçirimliliği saf IPA banyosunda hazırlanan membranlara kıyasla 175% oranında artmıştır. Kütlece polimerin 10%'u oranında, 65 nm kristal boyutunda ZIF-8 eklenmesiyle CO₂ geçirgenliği 86% CO₂/CH₄ ideal seçiciliği 13% oranında artmıştır.

İkinci bölümde, PI membranlar daha önce literatürde hiç denenmemiş bir yöntem olan ışık yardımıyla kuru-ıslak faz değişim yöntemiyle üretilmiştir. Bu yöntemde

kızılötesi yada aydınlatma ampülünün enerjisi kuru faz değişimi süresince uçucu çözücünün buharlaşmasını kontrol etmek amacıyla kullanılmıştır. Kuru faz değişimi süresince IR maruziyetinin 60 saniyeden az olduğu durumlarda, membran gaz geçirgenlik değerleri önce birden artmış, daha sonra azalan bir eğilim göstermiştir. IR maruziyetinin 60 saniyeyi aştığı durumlarda, elde edilen membran daha kalın, daha yoğun bir gözeneksiz seçici tabaka kalınlığına ve görece daha düşük geçirgenliğe sahiptir. En yüksek geçirgenlik değeri, IR maruziyetinin 10 saniyeden daha az olduğu üretim koşullarında elde edilmiştir ve yaklaşık olarak H₂ için 8.51 GPU, CO₂ için 2.44 GPU ve CH₄ için 0.13 GPU olarak ölçülmüştür. Uçucu ve uçucu olmayan çözücünün birbirlerine oranı incelenen bir diğer değişkendir. 0.80, 0.42 ve 0.17 THF/DMF oranıyla hazırlanmış membranlara karşılık gelen CO₂ geçirgenliği sırasıyla 0.81 GPU, 2.55 GPU ve 6.65 GPU olarak ölçülmüştür. PI/ZIF-8 karışık matrisli membranlarda, ZIF-8 eklenmesi daha kalın bir seçici kabuk tabaka oluşumunu ve daha düşük geçirgenlik değerlerinin elde edilmesini sağlamıştır.

Çalışmanın üçüncü bölümünde, asimetrik PI membranlar ışık yardımıyla kuru-buharda faz değişim yöntemiyle üretilmiştir. Çalışmamız, literatürde daha önce denenmemiş bir yöntemin geliştirilmesi ve yine bu yöntemle üretilmiş ilk karışık matrisli gaz ayırım membranlarının çalışılması yönünden farklıdır. Bu yöntem kuru-ıslak faz değişim yöntemine kıyasla çok daha yavaş bir faz değişimi, kapalı gözenekler, nispeten daha kalın bir seçici kabuk tabaka ve dolayısıyla düşük geçirimli bir membran oluşumuna neden olur. Bu yöntemin en önemli avantajı, ZIF-8 kristallerini çökmeden ince kabuk tabakanın içinde sabitlemesi ve pNA'nın polimere tutunmasını sağlamasıdır (pNA ıslak faz değişimi süresince polimer çözeltilisinden ayrılarak çökeltme banyosunun içine geçmektedir). Bu yöntemle üretilmiş PI/ZIF-8/pNA karışık matrisli membranlar için tespit edilmiş en yüksek ideal seçicilik değerleri sırasıyla H₂/CO₂ için 3.24, H₂/CH₄ için 132.68 ve CO₂/CH₄ için 40.9.

Son bölümde ise karışık matrisli simetrik gözeneksiz PI/ZIF-8 membranların ZIF-8 eklenmesine bağlı olarak değişen CO₂ ve CH₄ soğurma kapasiteleri incelenmiştir. PI'ın kütlece %10'u ve %20'si oranında ZIF-8 eklenmesiyle, membranın 10 bar'da CO₂ soğurma kapasitesi sırasıyla 22% ve 40% artmıştır. Aynı şartlarda CH₄ soğurma kapasitesi ise sırasıyla 20% ve 60% yükselmiştir. Eldeki soğurma kapasitesi verilerine bağlı olarak simetrik gözeneksiz saf PI ve PI/ZIF-8 karışık matrisli membranların ikili-kipli soğurma kapasite sabitleri hesaplanmıştır. Membrana ZIF-8 eklenmesiyle Henry tipi soğurma sabiti k_D ve benzetimlik sabiti b artarken, Langmuir tipi soğurma sabiti C_H 'ın azaldığı tespit edilmiştir. Bu durum membranın dengede olmayan boşluk hacminin ZIF-8 eklenmesiyle azaldığı ancak membranın gazlarla olan etkileşiminin artmasından kaynaklı olarak soğurma kapasitesinin arttığı tespit edilmiştir. Karışım gaz soğurma deneyleri 30:70, 50:50, 70:30 CO₂:CH₄ olmak üzere üç farklı derişimde gerçekleştirilmiştir. Camsı polimerlerde nüfuz eden gazların rekabetinden kaynaklı olarak her iki gazında soğurulma kapasitelerinde azalma görülmüştür. Rekabetçi çözünenin metan üzerine etkisi karbondoksitten çok daha baskındır. Örneğin, 49:51 CH₄:CO₂ karışımında saf hallerine kıyasla, metan çözünlüğü 75% azalırken, karbondioksitin çözünlüğü 35% oranında azalmıştır.

Anahtar Kelimeler: Gaz ayırımı, asimetrik PI ve PES karışık matrisli membranlar, Gaz soğurulumu, ışık yardımıyla faz değişim yöntemi, Zeolitik İmidazolat Kafes-8 (ZIF-8)

To my family

ACKNOWLEDGEMENTS

First of all, I would like to present my sincere thanks to my supervisor Prof. Dr. Halil Kalıpçılar for his significant contributions and guidance during this study and to my co-supervisor Prof. Dr. Levent Yılmaz for his precious suggestions and support.

I'm deeply grateful to my thesis committee members Prof. Dr. Nihal Aydoğan, Assoc. Prof. Dr. Zeynep Çulfaz Emecen, Assoc. Prof. Dr. Çerağ Dilek Hacıhabiboğlu, and Asst. Prof. Dr. Berna Topuz for reading my thesis and sharing their invaluable consideration.

I would like to thank the financial supports from The Scientific and Technological Research Council of Turkey (TUBITAK) through the grant number 213M546.

My very special and deeply appreciations go to my family for their moral and material support, encouragement and unlimited patience.

TABLE OF CONTENTS

ABSTRACT	v
ÖZ.....	viii
ACKNOWLEDGEMENTS	xii
LIST OF TABLES	xvii
LIST OF FIGURES.....	xxi
LIST OF SYMBOLS AND ABBREVIATIONS.....	xxvi
CHAPTERS	
1 INTRODUCTION	1
1.1 Objective and Thesis Outline.....	13
REFERENCES.....	17
2 ASYMMETRIC NEAT PES MEMBRANES AND ASYMMETRIC PES/ZIF-8 MIXED MATRIX MEMBRANES PRODUCED BY WET PHASE INVERSION	21
2.1 Theoretical Background about Polymeric Membrane Formation via Phase Inversion	22
2.1.1 Formation of Membrane Surface based on Ternary System Thermodynamics	27
2.1.2 Formation of Pores based on Ternary System Thermodynamics....	29
2.2 Selection of Solvent and Non-Solvent Pair	30
2.3 Materials and Experimental Method	37
2.3.1 Materials.....	37
2.3.2 Preparation of ZIF-8.....	38
2.3.3 Characterization of ZIF-8 Crystals.....	39
2.3.4 Membrane Preparation	40
2.3.5 Membrane Characterization	42
2.4 Characterization of ZIF-8 Crystals	44
2.5 Morphology of pure PES Asymmetric Membranes (SEM Results).....	49
2.6 Morphology of Mixed Matrix PES-ZIF-8 Membranes	66
2.7 Gas Separation Test Results of neat PES Membranes.....	75
2.8 Gas Separation Test Results of PES/ZIF-8 Mixed Matrix Membranes .	83

2.9 Conclusion.....	87
REFERENCES.....	89
3 LIGHT INDUCED DRY-WET PHASE INVERSION METHOD FOR ASYMMETRIC NEAT PI AND PI/ZIF-8 MIXED MATRIX MEMBRANES ..	97
3.1 Evolution and Development of Dry-Wet Phase Inversion Method for Gas Separation Asymmetric Membranes.....	98
3.2 Experimental Method and Materials	108
3.2.1 Materials.....	108
3.2.2 Light Induced Dry-Wet Phase Inversion Method	109
3.2.3 Light Induced Dry-Wet Phase Inversion (LIDWPI) for neat PI, PI/ZIF-8 Membranes	111
3.3 Experimental Results of PI Membranes Produced via LWDPI Method	117
3.3.1 Effect of THF/DMF Ratio on Membrane Morphology	119
3.3.2 Effect of THF/DMF Ratio on Membrane Gas Separation Properties	122
3.3.3 Importance of Light Source.....	125
3.3.4 Effect of Light Source on Membrane Morphology.....	127
3.3.5 Effect of Light Source on Membrane Gas Separation Properties .	128
3.3.6 Effect of IR Exposure Period on Membrane Morphology.....	130
3.3.7 Effect of IR Exposure Period on Membrane Gas Separation Properties.....	135
3.3.8 Effect of IR Exposure Period with Humidity Control Membrane Gas Separation Properties.....	139
3.3.9 Effect of ZIF-8 loading on Membrane Morphology	141
3.3.10Effect of ZIF-8 loading on Membrane Gas Separation Performance	144
3.4 Conclusion.....	146
REFERENCES.....	149
4 ASYMMETRIC NEAT PI MEMBRANES AND ASYMMETRIC PI/ZIF-8/PNA MIXED MATRIX MEMBRANES BY LIGHT INDUCED DRY-VAPOR-PHASE INVERSION.....	155
4.1 Theoretical Background about Vapor Phase Inversion	155
4.2 Materials and Experimental Method of PI Membrane Production via Light Induced Dry-VIPS.....	163

4.2.1	Materials	163
4.2.2	Preparation of neat PI, PI/ZIF-8 and pNA/PI/ZIF-8 Membranes via VIPS	164
4.2.3	Gas Separation Test of neat PI, PI/ZIF-8 and pNA/PI/ZIF-8 Membranes	165
4.3	Morphological Investigation of VIPS Membranes.....	168
4.3.1	IR Exposure Effect on Membrane Morphology.....	168
4.3.2	Incandescent Lamp Light Exposure Effect on Membrane Morphology	174
4.3.3	Effect of Light Exposure on Membrane Surface.....	175
4.3.4	Morphological Properties of PI/ZIF-8 Mixed Matrix Membrane prepared via IR Exposure during VIPS	179
4.3.5	Morphological Properties of PI/ZIF-8/pNA Mixed Matrix Membrane including Compatibilizer prepared via IR Exposure during VIPS	187
4.4	Gas Separation Performance of VIPS Membranes.....	191
4.4.1	Effect of IR Exposure on Neat PI Membranes prepared via VIPS	192
4.4.2	Effect of IL Exposure on Neat PI Membranes prepared via VIPS	193
4.4.3	Effect of Containing ZIF-8 and Containing ZIF-8 with pNA on Gas Separation Performance.....	194
4.5	Comparison of The Membranes	204
4.6	Conclusions.....	205
	REFERENCES	207
5	SORPTION CAPACITY OF DENSE-SYMMETRIC NEAT PI AND PI/ZIF-8 MIXED MATRIX MEMBRANES PRODUCED BY SOLVENT EVAPORATION.....	211
5.1	Theoretical Background about Sorption Mechanism of Polymers.....	211
5.1.1	Dual Mode Sorption Model.....	212
5.1.2	Parameters Effect on Sorption Capacity	217
5.1.3	Mixed Gas Sorption in Glassy Polymer	218
5.1.4	A Brief Literature Survey About CO ₂ and CH ₄ Sorption Capacity of PI Membranes and ZIF-8 Crystals.....	220
5.1.5	CH ₄ and CO ₂ Sorption Behavior of ZIF-8	232
5.2	Materials and Experimental Methods of PI Membrane Production and Sorption Test.....	234

5.2.1	Materials.....	234
5.2.2	Preparation of Dense Symmetric neat PI and PI/ZIF-8 Membranes via Solvent Evaporation	234
5.2.3	Experimental Test Set-up and Sorption Test.....	235
5.3	Sorption Capacity Test Results of the Neat Dense Symmetric PI Membranes.....	246
5.3.1	CO ₂ - CH ₄ Mixture Sorption Capacity of Neat Symmetric Dense Polyimide Membrane	253
5.4	Sorption Capacity of the Mixed Matrix Dense Symmetric PI/ZIF-8 Membranes.....	257
5.4.1	Mixed Gas Sorption Behavior of the Mixed Matrix Dense Symmetric PI/ZIF-8 Membranes.....	262
5.5	Conclusions	269
	REFERENCES.....	271
	APPENDICES.....	277
	A. EXPERIMENTAL RESULTS OF PES MEMBRANES PRODUCED VIA LIDWPI METHOD	277
	Production Method	277
	B. CALIBRATION OF GC	302
	CURRICULUM VITAE	305

LIST OF TABLES

TABLES

Table 1.1 Commerically polymeric gas separation membranes (Basu et al., 2010).	3
Table 1.2 Permeability of polymeric membranes at 30 °C (^a Nunes and Peinemann, 2006 ; ^b Qui et al., 2006)	5
Table 1.3 Thermal and structural properties of widely used polymeric membranes.	8
Table 1.4 Physical properties of gas molecules effecting transport properties (^c Matteucci, Yampolskii and Freeman, 2006; ^d NIST; ^e Enginering ToolBox).....	9
Table 2.1 Hansen solubility parameters of polymer, solvent and non-solvent. If not specified, data were taken from Guillen et al.,2011.	31
Table 2.2 Hansen solubility parameter difference between polymer-solvent, polymer-nonsolvent, nonsolvent-solvent pairs.....	31
Table 2.3 Average particle size and standard deviation of ZIF-8 prepared with different MeOH/ ZnNO ₃ .H ₂ O molar ratio based on SEM image and J-image analyzer.	45
Table 2.4 Pure PES membranes and preparation properties. The total volume of solvent was 10 ml. The coagulation bath was at room temperature and the total volume of coagulation bath was 500 ml.....	50
Table 2.5 Mixed matrix PES-ZIF-8 membranes and preparation properties. The total volume of solvent was 10 ml. The coagulation bath was at room temperature and the total volume of coagulation bath was 500 ml.	52
Table 2.6 Morphology of membranes prepared in coagulation bath with different amount of water content.	59
Table 2.7 Morphology of membranes prepared with different amount of PES concentration in DMF concentration and quenched by IPA/H ₂ O:90/10 (in %vL.) coagulation medium. Pore shape is spongy for this type of membranes.	63
Table 2.8 Morphological properties of PES/ZIF-8 mixed matrix membranes containing ZIF-8 with average particle size of 15, 25 and 65 nm. Pure IPA was used as coagulation medium. PES concentration of membrane solution was 17.4%....	72
Table 2.9 Permeance and selectivity values of membranes prepared in coagulation bath with different amount of water content in IPA.....	77
Table 2.10 Permeance and selectivity values of membranes prepared in coagulation bath with different amount of DMF content in IPA coagulation medium. Membrane casting solution made up of pure DMF and PES with 17.4 polymer concentration.	79
Table 2.11 Permeance and ideal selectivity values of membranes prepared in casting solution with different amount of PES concentration. Membranes were quenched in coagulation medium composed of IPA/H ₂ O:90/10 (in %vL.)	80

Table 2.12 Effect of non-solvent in membrane solution on gas permeance and ideal selectivity. Membranes quenched in coagulation medium IPA/H ₂ O:95/5 (in %v/v)	82
Table 2.13 Permeance and selectivity values of mixed matrix (PES/ZIF-8) membranes prepared with thermally annealed ZIF-8 crystals in pure IPA coagulation bath.	83
Table 2.14 Gas transport properties of Mixed Matrix (PES/ZIF-8) membranes prepared with ZIF-8 crystals (Treat-Type1) in pure IPA coagulation bath.	85
Table 3.1 Gas separation properties of asymmetric polymeric membranes and effect of preparation methods on gas transport properties.	105
Table 3.2 PI membranes produced via LIDWPI methods. Each membrane included 4 g PI.	114
Table 3.3 PI-ZIF-8 mixed matrix membranes produced via LIDWPI methods. Each casting solution was prepared from 4 gr. PI, 4 gr THF as volatile solvent, 9.5 gr DMF as non-volatile solvent.	116
Table 3.4 Hansen solubility parameter difference ($\Delta\delta$) between polymer (PES)-solvent (DMF)-co-solvent(Acetone)-quench medium(Water).....	118
Table 3.5 Effect of THF/DMF ratio on the asymmetric PI membrane morphology prepared via LIDWPI method and exposed to 120 s IL.....	120
Table 3.6 The permeance and selectivity of neat PI membranes based on THF/DMF ratio. IL exposure was 120 sec.	124
Table 3.7 Gas separation performance of neat PI membrane depending on difference in the light source. Each membrane was prepared from solution %22.9% THF-22.9%PI-54.3%DMF (42.2% THF/DMF ratio). Exposure period was 120 s.	130
Table 3.8 Effect of IR exposure period on morphological properties of the asymmetric PI membranes. Each membrane was prepared from solution %22.9% THF-22.9%PI-54.3%DMF (42.2% THF/DMF ratio).	135
Table 3.9 Effect of IR exposure period on gas separation properties of the asymmetric PI membranes. Each membrane was prepared from solution %22.9% THF-22.9%PI-54.3%DMF (42.2% THF/DMF ratio).	137
Table 3.10 Effect of IR exposure period and also humidity on gas separation properties of the asymmetric PI membranes. Each membrane was prepared from solution %22.9% THF-22.9%PI-54.3%DMF (42.2% THF/DMF ratio).....	140
Table 3.11 The effect of ZIF-8 loading on membrane gas separation properties.	145
Table 4.1 Membrane codes and preparation properties of PI, PI/ZIF-8, PI/ZIF-8/pNA membranes. Each membrane prepared from polymer solution made up of 4 gr. PI, 4 gr THF as volatile solvent, and 9.5 gr DMF as non-volatile solvent. ...	166
Table 4.2 Quantitative investigation of morphology of membranes prepared via VIPS.	173
Table 4.3 Quantitative investigation of morphology of membranes prepared via VIPS.	175

Table 4.4 Quantitative investigation of morphology of membranes prepared via VIPS	179
Table 4.5 Quantitative investigation of morphology of PI/ZIF-8 mixed matrix membranes including amount of 10% of polymer ZIF-8 with 65 nm average particle size and exposed IR light for 60, 120 and 180 seconds during prepared via VIPS.	187
Table 4.6 Quantitative investigation of morphology of PI/ZIF-8/pNA mixed matrix membranes including amount of 10% of polymer ZIF-8 with 65 nm average particle size and 4% of polymer pNA. During VIPS membranes were exposed IR light for 0, 60, 120 and 180 s.....	190
Table 4.7 Gas test results of the neat PI membranes prepared without light exposure during VIPS.....	192
Table 4.8 Gas test results of the neat PI membranes prepared with IR light exposure for 60, 120, 180 and 240 seconds prior of the VIPS.	193
Table 4.9 Gas test results of the neat PI membranes prepared with IL light exposure for 60, 120 s prior of the VIPS.	194
Table 4.10 Gas test results of PI/ZIF-8 mixed matrix membranes containing amount of 10% of polymer ZIF-8 with 65 nm average particle size and exposed IR light for 60, 120 and 180 seconds during prepared via VIPS.....	195
Table 4.11 Gas test results of PI/ZIF-8/pNA mixed matrix membranes including amount of 10% of polymer ZIF-8 with 65 nm average particle size and amount of 4% of polymer pNA as a compatibilizer and exposed IR light for 0, 60 and 180 seconds during prepared via VIPS.	196
Table 5.1 Comparison of sorption capacity of CO ₂ and CH ₄ in different kind of PI membranes at 35 °C.....	225
Table 5.2 Dual-mode sorption constants of polyimide for CO ₂ and CH ₄ . The parameters obtained from isotherm at 35 °C unless otherwise specified.	229
Table 5.3 Gas chromatography test operation condition.....	239
Table 5.4 Dense symmetric membranes prepared by solvent evaporation for sorption test. Solvent evaporation was taken place at 80 °C under vacuum and annealing was carried out 100 °C at N ₂ atm. for 1 week.....	240
Table 5.5 Dual-mode sorption constants for CO ₂ and CH ₄ based on sorption test average of PI-1 and PI-2.....	252
Table 5.6 Dual-mode sorption constants for CO ₂ and CH ₄ based on sorption test of MM-PI-1 and MM-PI-2.....	262
Table A.1 PES membranes produced via DWPI and LIDWPI methods.	278
Table A.2 Hansen solubility parameter difference ($\Delta\delta$) between polymer (PES)-solvent (DMF)-co-solvent(Acetone)-quench medium(Water).....	280
Table A.3 Morphological properties of asymmetric PES membranes prepared via DWPI method. AC content of the membrane solution was the investigated parameter. Casting film was standing 15 min free-evaporation before wet phase inversion in 500 ml water quench bath.	284

Table A.4 Comparison of gas separation performance of PDMS coated and un-coated PES asymmetric membranes prepared via DWPI method.	290
Table A.5 Morphological properties of asymmetric PES membranes prepared via LIDWPI method. AC content of the membrane solution and IL exposure period were the parameters inquired. The wet phase inversion period was performed in 500 ml water quench bath.	298
Table A.6 Gas separation performance of neat PES membranes prepared via LIDWPI method.	300

LIST OF FIGURES

FIGURES

Figure 1.1 Upper bound correlation for CO ₂ /CH ₄ separation (Robeson, 2008)....	12
Figure 2.1 Schematic presentation of three common polymeric membrane precipitation process; where S represents solvent and NS represents nonsolvent. (Ren and Wang, 2010).....	22
Figure 2.2 Schematic ternary phase diagram of polymer-solvent-nonsolvent system (Ren and Wang, 2010).....	24
Figure 2.3 Schematic representation of membrane formation for phase inversion process (figure modified from Ren and Wang, 2010).....	25
Figure 2.4 Schematic representation of skin layer, polymer rich phase and polymer poor (lean) phase of an asymmetric membrane (figure modified from Ren and Wang, 2010).	26
Figure 2.5 Repeating unit of polyethersulfone (Solvey Advanced Polymer, Radel).	37
Figure 2.6 Crystal structure of ZIF-8, Cyan, blue, and grey spheres represent Zn, N, and C atoms, respectively. H atoms are omitted for clarity (Cacho-Bailo et al., 2014).....	39
Figure 2.7 The schematic drawing of single gas permeation test system.	44
Figure 2.8 SEM mikrographs of synthesized ZIF-8s; (a) ZIF-8_1; (b) ZIF-8_2; (c) ZIF-8_3.....	45
Figure 2.9 XRD pattern of ZIF-8_3 crystals with 65-nm-size.	47
Figure 2.10 TGA curves of ZIF-8_3 crystals with average particle size 65 nm. ..	48
Figure 2.11 N ₂ adsorption/desorption isotherms of ZIF-8_3 crystals with 65 nm average particle size	49
Figure 2.12 SEM micrograph of the neat PES membranes quenched in pure IPA (PP-3), %2 water-%98 IPA (PP-7); %5 water-%95 IPA (PP-16); %7 water-%93 IPA (PP-21); %10 water-%90 IPA (PP-15) coagulation bath.....	55
Figure 2.13 SEM micrograph of the neat PES membrane quenched in %25 water-%75 IPA (PP-12); %50 water-%50 IPA (PP-10) coagulation bath.	56
Figure 2.14 SEM micrograph of the PES membrane quenched in IPA/DMF:75/25 (in %vl.) coagulation medium, left hand side, PP-13; and PES membrane quenched in IPA/DMF:70/30 (in %vl.) coagulation medium, right hand side, PP-24.....	61
Figure 2.15 SEM micrograph of the PES membrane made up of 17.4 wt% PES-DMF solution (PP-15); 24 wt% PES-DMF solution (PP-33) and 29.6 wt% PES-DMF solution quenched in IPA/H ₂ O:90/10 (in %vl.).....	62
Figure 2.16 SEM micrograph of the PES membrane (PP-22) made up of PES (17.6%)-DMF(75.4%)-IPA(7.0%) (in wt.%) solution quenched in IPA/H ₂ O:95/5 (in %vl.). (a) Total cross-sectional view, (b) upper layer of membrane, (c) upper layer view at higher magnification, (d) surface of the membrane.....	66

Figure 2.17 Cross-sectional SEM image of the PES/ZIF-8 (25 nm, %5 of PES) mixed matrix membranes quenched in pure IPA coagulation medium. Treatment method of ZIF-8 crystals was Type 1 (MMM-3); Type 2 (MMM-2); Type 3 (MMM-4).	68
Figure 2.18 Cross-sectional SEM image of the PES/ZIF-8 (%5 of PES) mixed matrix membranes quenched in pure IPA coagulation medium. Average particle size of ZIF-8 was 15 nm (MMM-5); 25 nm (MMM-9) and 65 nm (MMM-10)...	70
Figure 2.19 Cross-sectional SEM image of the PES/ZIF-8 (%10 of PES) mixed matrix membranes quenched in pure IPA coagulation medium. Average particle size of ZIF-8 was 15 nm (MMM-5); 25 nm (MMM-9) and 65 nm (MMM-10)...	71
Figure 2.20 Effects of ZIF-8 loading and ZIF-8 particle size on CO ₂ permeance and CO ₂ /CH ₄ of flat sheet asymmetric mixed matrix PES/ZIF-8 membranes.	86
Figure 3.1 Chemical structure of Matrimid ®5218 repeating monomer (Zhang et al., 2008).....	108
Figure 3.2 Schematic presentation of light exposure step in dry inversion step.	110
Figure 3.3 The appearance of the casting PI solution after the light-induced dry phase change, just prior to wet inversion step.....	110
Figure 3.4 Glow Box.....	112
Figure 3.5 SEM micrographs of PI membranes prepared from solution with different THF/DMF ratio and exposed to 120 s IL for dry inversion; PI-13 (34.3% THF-22.9%PI-42.9%DMF); PI-11 (22.9% THF-22.9%PI-54.3%DMF); PI-12 (11.4% THF-22.9%PI-65.7%DMF).....	121
Figure 3.6 Electromagnetic Spectrum ("What is Full Spectrum Lighting?," 2012)	125
Figure 3.7 SEM micrographs of PI membranes exposed to 120 s IL (PI-11), and exposed to 120 s IR (PI-63). Both of them prepared from solution with 0.42 THF/DMF ratio.	128
Figure 3.8 SEM micrographs of asymmetric PI membranes prepared via LIDWPI method and exposed to IR for 0 s (PI-58), 20 s (PI-55), 40 s (PI-69), 60 s (PI-68), 120 s (PI-63), and 240 s (PI-59) in dry inversion step at which relative humidity was 80%.	133
Figure 3.9 SEM micrographs of skin layer of asymmetric PI membranes prepared via LIDWPI method and exposed to IR for 0 s (PI-58), 20 s (PI-55), 40 seconds (PI-69), 60 s (PI-68), 120 s (PI-63), and 240 s (PI-59) in dry inversion step at which relative humidity was 80%.	134
Figure 3.10 SEM micrographs of skin layer of asymmetric mixed matrix PI membranes prepared via LIDWPI method and exposed to IR for 240 s.	143
Figure 4.1 (A) Bi-continuous structure usually detected in system following spinodal decomposition (modified from Nunes and Inoue 1996). (B) dispersed nuclei structure usually observed in system following binodal decomposition (i.e. nucleating and growth) (modified from Wang et al. 2000).....	158

Figure 4.2 (A) Scattering light intensity (I_s) with respect to wave angle (q) during spinodal decomposition. (B) Scattering light intensity (I_s) with respect to wave angle (q) during nucleation and growth (Liu and Kiran 1999).	159
Figure 4.3 Schematic representation of concentration profile across casting film (A), SEM image of membrane having hour-glassy structure (B) (Khare et al. 2005).	163
Figure 4.4 Chemical structure of p-nitroaniline (D. Şen 2008).....	164
Figure 4.5 Gas permeation test system for membranes produced via VIPS.	167
Figure 4.6 Flow diagram of test system for membranes produced by light induced-VIPS.	168
Figure 4.7 SEM micrographs of the neat PI membranes prepared via VIPS without IR exposure.....	169
Figure 4.8 SEM micrographs of the neat PI membranes exposed to IR light for 60, 120, 180, and 240 s priory beginning of VIPS.	172
Figure 4.9 SEM micrographs of the neat PI membranes exposed to incandescent lamp (abbreviated as IL) light for 60 and 120 seconds priory beginning of VIPS.	174
Figure 4.10 SEM micrographs of the surface of the neat PI membranes prepared without light exposure and with 60 second IR exposure during VIPS.	177
Figure 4.11 SEM micrographs of the surface of the neat PI membranes prepared with IL light exposure for 60 and 120 seconds during VIPS.	178
Figure 4.12 SEM micrographs of the mixed matrix PI/ZIF-8 membrane prepared without light exposure during VIPS.	181
Figure 4.13 SEM micrographs of the mixed matrix PI/ZIF-8 membrane prepared with 60 seconds IR light exposure during VIPS.	182
Figure 4.14 SEM micrographs of the surface of the mixed matrix PI/ZIF-8 membrane prepared with 120 seconds IR light exposure during VIPS.	183
Figure 4.15 SEM micrographs of the mixed matrix PI/ZIF-8 membrane prepared with 180 seconds IR light exposure during VIPS.	184
Figure 4.16 SEM micrographs of the mixed matrix including compatibilizer PI/ZIF-8/pNA membranes prepared with 0, 60, 120 and 180 s IR light exposure during VIPS.	189
Figure 4.17 Change in H_2 permeance depending on both IR exposure time, ZIF-8 and pNA.	197
Figure 4.18 Change in CO_2 permeance depending on both IR exposure time, ZIF-8 and pNA.	199
Figure 4.19 Change in CH_4 permeance depending on both IR exposure time, ZIF-8 and pNA.	200
Figure 4.20 Change in ideal selectivity of H_2/CO_2 depending on parameters of IR exposure period, ZIF-8 crystals and pNA	201
Figure 4.21 Change in ideal selectivity of CO_2/CH_4 depending on parameters of IR exposure period, ZIF-8 crystals and pNA.	202

Figure 4.22 Change in ideal selectivity of H ₂ /CH ₄ depending on parameters of IR exposure period, addition of ZIF-8 crystals and including pNA.....	203
Figure 4.23 Comparison of membranes produced by different methods.	204
Figure 5.1 Hypothetical unrelaxed excess free volume ($V_g - V_i$) of a glassy polymer as a function of temperature (where V_g is symbolized actual glassy volume and V_i is symbolized densified glassy volume) (Kanehashi and Nagai 2005).....	213
Figure 5.2 Schematic presentation of sorption mechanism (a) Henry-type sorption, (b) Langmuir-type sorption, (c) dual-mode sorption model (Tsujita 2003).....	214
Figure 5.3 CO ₂ and CH ₄ sorption isotherms of PIM-1 for different mixing ratio of these two gases at 35 °C. (Vopicka et al. 2014).	232
Figure 5.4 CO ₂ (●), CH ₄ (■) and N ₂ (▲) adsorption isotherms of ZIF-8 at 30 °C. Symbols showed simulation results and lines showed experimental results (Pérez-Pellitero et al., 2010).	233
Figure 5.5 Pressure-Decay type sorption test system.....	241
Figure 5.6 Flow diagram of sorption test system.	245
Figure 5.7 Pure methane and pure carbon dioxide sorption isotherm of neat symmetric dense PI membranes (PI-1 and PI-2) at 35 °C. ‘REF’ values were taken from Moore and Koros 2007.	250
Figure 5.8 Matrimid ®5218 repeating monomer (retrieved from Zhang et al., 2008).	251
Figure 5.9 Solubility selectivity of dense PI membranes (PI-1 and PI-2) and reference Moore and Koros 2007.	251
Figure 5.10 Pure and mixed gas solubility of CO ₂ in symmetric PI-2 membrane at 35 °C at different mole fractions of CO ₂	255
Figure 5.11 Pure and mixed gas sorption capacity of CH ₄ in symmetric PI-2 membrane at 35 °C at different mole fractions of CH ₄ in the gaseous mixture.	256
Figure 5.12 CO ₂ sorption capacity of mixed matrix PI/ZIF-8 dense symmetric membranes at 35 °C.....	259
Figure 5.13 CH ₄ sorption capacity of mixed matrix PI/ZIF-8 dense symmetric membranes at 35 °C.....	260
Figure 5.14 Pure and mixed gas sorption capacity of CO ₂ in symmetric mixed matrix MM-PI-1 membrane at 35 °C at different mole fractions of CO ₂ in the gaseous mixture.....	264
Figure 5.15 Pure and mixed gas sorption capacity of CH ₄ in symmetric mixed matrix MM-PI-1 membrane at 35 °C at different mole fractions of CH ₄ in the gaseous mixture.....	265
Figure 5.16 Pure and mixed gas sorption capacity of CO ₂ in symmetric mixed matrix MM-PI-2 membrane at 35 °C at different mole fractions of CO ₂ in the gaseous mixture.....	267
Figure 5.17 Pure and mixed gas sorption capacity of CH ₄ in symmetric mixed matrix MM-PI-2 membrane at 35 °C at different mole fractions of CH ₄ in the gaseous mixture.....	268

Figure A.1 PES asymmetric membranes prepared from PES-DMF-Acetone solution with different acetone (AC) content via DWPI method for 15 min free evaporation during dry inversion period. PP-55 with 34.3% AC.	286
Figure A.2 SEM micrographs of membrane prepared from 22.9%AC-22.9%PES-54.2%DMF solution DMF solution and exposed 15 min. incandescent lamp light for dry inversion. (A) cross-section, (B) transition layer and (C) selective skin layer.	293
Figure A.3 SEM micrographs of membrane prepared from 28.6%AC-22.9%PES-48.6%DMF solution DMF solution and exposed 15 min. incandescent lamp light for dry inversion. (A) cross-section, (B) transition layer and (C) selective skin layer.	295
Figure B.1 The calibration curve of CO ₂ for GC analysis.	302
Figure B.2 The calibration curve of CH ₄ for GC analysis.	303

LIST OF SYMBOLS AND ABBREVIATIONS

P : Permeability (Barrer)

F: Permeance (GPU)

Δp : Transmembrane pressure difference (cmHg)

T_g : Glass transition temperature (°C)

V_d : Dead volume (cm³)

V_g : Glassy volume of polymer (cm³)

(V_g-V_l) : Excess free volume of polymer (cm³)

G: steady state gas flux (cm³/(cm² s.))

A : Effective membrane area (cm²)

C: Dual mode sorption capacity (cm³ STP /cm³ Polymer)

C_D: Henry type sorption (cm³ STP /cm³ Polymer)

C_H: Langmuir Type Sorption (cm³ STP /cm³ Polymer)

k_D : Henry's law solubility constant (cm³ (STP)/(cm³ polymer atm))

C'_H: Langmuir capacity constant ((cm³ (STP)/(cm³ polymer))

b: Langmuir affinity constant (1/atm.)

s: seconds

ϕ : volumetric fraction

$\Delta\delta_{d,h,p}$: Hansen Solubility parameters (MPa^{0.5})

$\alpha_{A/B}$: Ideal selectivity

IL : Incandescent light

IR: Infrared Light

NIPS: Non-solvent induced phase separation

LIDWPI: Light Induced dry-wet phase inversion

LIDVPI: Light Induced dry-vapor phase inversion

CHAPTER 1

INTRODUCTION

Energy demand of world is increasing constantly due to population growth, technological improvement and industrial evolution (Kannan and Vakeesan, 2016). The total worldwide primary energy consumption in 1990 was reported around 350 quadrillion Btu. By the year 2014, this value reached 546 quadrillion Btu (International Energy Statistic, 2014). This primary energy demand is met by oil (33%), coal (29%), natural gas (24%), hydroelectricity (6.8%), nuclear energy (4.4%) and renewable energy (2.8%) (BP: Statistical Review of World Energy, 2015). A similar growth in energy demand can also be observed in our country. Currently, the primary energy consumption of Turkey is reported as 5 quadrillion Btu and is estimated to reach 8 quadrillion Btu by 2023. Today, primary energy demand of Turkey is provided by natural gas (35%), coal (28,5%), oil (27%), hydro (7%), and renewable energy sources like wind or solar energy (2,5%). In Turkey, the 90% of the primary energy demand was obtained from fossil fuels (Turkey's Energy Profile and Strategy, 2016).

Fossil fuel resources in the world are limited and getting depleted. World oil reserves, natural gas reserves and coal reserves in 2015 are predicted to be to supply 50 years, 53 years and 144 years of global production, respectively (BP: Statistical Review of World Energy, 2015). Limitation and fast depletion rate in fuel energy source, green-house gases emission due to fuel source consumption, catastrophic risk and expense of nuclear energy impose people to look renewable and clean energy source (Chen and Wu, 2017; Kannan and Vakeesan, 2016).

Biogas is that mainly composed of carbon dioxide (%30-40 v.) and methane (%60-70 vl.) is produced during anaerobic digestion of organic substrate. It is an alternative energy source because of its high methane content. There are several environmental advantages of biogas production and utilization. First of all, it is a renewable energy source and its production is an alternative way for management

of landfills, animal manure, wet organic waste, household garbage. A high quality digestate that is produced during anaerobic digestion can be used as fertilizer.

Biogas has calorific value in the range of 13.5-27.5 MJ/m³. Energy content of biogas which is proportional to its methane content (Kurchania et al., 2010). The energy content of biogas can be upgraded by removing carbon dioxide. Purification of biogas is also important to protect pipelines from corrosive and acidic nature of CO₂ and H₂S. The biogas purification process is anticipated to be cheap and energy efficient to keep the cost of biogas low and to make it comparable with fossil fuels. Pressure swing adsorption, water scrubbing, organic physical scrubbing, chemical scrubbing, cryogenic distillation and membrane separation are some of the processes that can be applied for CO₂ removal from biogas and natural gas. Among them membrane separation is an appealing process because of its low capital cost, low space requirements, favorable operating condition (low temperature and pressure), high energy efficiency, ease of processing and scaling up (Basu et al., 2010). Moreover, membrane separation does not require phase change during the separation process, hence energy consumption is reduced. Lack of mechanical complexity and relatively small processing unit are the other advantages of membrane separation. ("Chemical & Engineering News: Cover Story - Membranes for Gas Separation," 2005). Membrane market for purification of methane is estimated to grow \$220 million/yr by 2020 (Sanders et al., 2013).

The membrane, which is the heart of every membrane process, is a semi-permeable barrier between two phases. Separation occurs because of the ability of membrane to transport one component in a mixture more readily than the others. The driving force can be difference in temperature, concentration or pressure. Polymers, zeolite, carbon molecular sieves, ceramics (siliconiumcarbide, zirconiumoxide, titaniumoxide), glasses (Pyrex, Vycor) and even metals (palladium, silver) can be used as membrane materials (Mulder, 2010).

Recently, polymers are widely used as membrane materials in gas separation. Table 1.1 shows commercial polymeric gas separation membranes, their application and supplier. Polymeric membranes are attractive because they can be

produced easily and continuously with high surface area per unit volume. Relatively low cost of large scale production makes them appealing for industrial application ("Chemical & Engineering News: Cover Story - Membranes for Gas Separation," 2005; Chung et al. 2007; Lu et al., 2007).

Table 1.1 Commerically polymeric gas separation membranes (Basu et al., 2010).

Membrane	Supplier	Application
Polydimethyl Siloxane (PDMS)	MTR	Hydrocarbon vapor separation
Polysulfone (PSF)	Air Products	H ₂ and air separation
Polycarbonate (PC)	MG Generon (Messer)	Air separation
Polyimide (PI)	UBE, MEDAL (Air Liquide)	CO ₂ -CH ₄ , H ₂ -CH ₄ , air separation
Polyaramide (PA)	MEDAL (Air Liquide)	H ₂ separation
Cellulose Acetate (CA), Cellulose tri-Acetate (CTA)	Cynara (Natco), Saparex (UOP)	CO ₂ -CH ₄ separation

The performance of a gas separation membrane is shown by two important parameters; namely selectivity and permeability coefficient (it is called permeability, briefly) of the membrane. Permeability of a pure gas (P) through a polymeric film membrane is defined by Eqn. 1.1 where Δp is the trans-membrane pressure difference, L is thickness and G is normalized (normalized to the cross-sectional area) steady-state gas A flux. Generally, permeability coefficient is expressed in unit of Barrer which is equal to 10^{-10} STP $\text{cm}^3 \text{cm} / (\text{cmHg s. cm}^2)$ (Sanders at al. 2013).

$$P = \frac{G \times L}{\Delta p} \text{STP cm}^3 \text{cm} / \text{s. cmHg cm}^2 \quad \text{Eqn. 1.1}$$

Selectivity is the separation ability of a membrane. Ideal selectivity is defined as the ratio of pure gas permeance of two species. Membrane materials,

production methods, physical and chemical properties of species (both penetrant and membrane materials) affect the performance of membrane (Mulder, 2010). High permeance is important for large scale purification and high selectivity is important for effective separation.

A list of widely used polymeric membranes and their gas permeability performance are summarized in Table 1.2. The range of the permeability is very large. For example, CO₂ permeability in polycarbonate (PC) is 4.23 Barrer, while in polydimethyl Siloxane (PDMS) is 2700 Barrer. Table 1.3 is depicted the thermal properties and fractional free volume of dense film of various polymers and some physical properties influencing transport property of gas molecules are listed in Table 1.4.

Table 1.2 Permeability of polymeric membranes at 30 °C (^a Nunes and Peinemann, 2006 ; ^b Qui et al., 2006)

Polymer	Permeability (Barrer)					Selectivity
	H ₂	CO ₂	O ₂	N ₂	CH ₄	P _{(CO₂)/P_(CH₄)}
Cellulose Acetate (CA) ^a	15	6.3	0.59	0.21	0.21	30
Ethylcellulose (EC) ^a	87	26.5	26.5	8.4	19	1.4
Tetrabroma-BisA-Polycarbonate (PC) ^a	-	4.23	1.36	0.18	0.13	32.5
Polydimethyl Siloxane (PDMS) ^a	550	2700	500	250	800	3.4
Polyimide (PI) ^a	28.1	10.7	2.13	0.32	0.25	42.8
Polymethylpentene (PMP) ^a	125	84.6	27	6.7	14.9	5.7
Polyphenyleneoxide (PPO) ^a	113	75.8	16.8	3.81	11	6.9
Polysulfone (PSF) ^a	14	5.6	1.4	0.25	0.25	22.4
Poly(1-trimethylsilyl-1-propyne) (PTMSP) ^b	15850	31333	8120	5490	14833	2.1

Solution-diffusion model is used to explain gas transport in all nonporous polymeric gas separation membranes (Graham, 1995). In this model, gas is sorbed by the face of membrane exposed to high pressure, diffuse through the membrane and desorbed from the face of the membrane surface exposed to low pressure. In this model, gas permeability coefficient can be expressed as the product of gas

solubility coefficient (S) and diffusion coefficient (D). Permeability coefficient is directly proportional to solubility coefficient and diffusion coefficient. Solubility coefficient is in unit of $\text{cm}^3(\text{STP})/\text{cm}^3$ polymer atm and diffusion coefficient is in unit of cm^2/sec .

$$P = S \times D \quad \text{Eqn. 1.2}$$

In solution-diffusion mechanism, diffusion through the membrane is the rate limiting step and determined by the local scale segmental dynamics of the polymer chains. The local scale segmental dynamics of the polymer chains defines the free volume elements of polymer through which the gas molecules carry out Brownian motion. In other words, the local segmental motions of polymer chains and the packing of polymers are two critically variables influencing the diffusion of small gas molecules through polymers (Sanders et al.,2013). Increase in chain mobility and segmental motion leads to increase in fractional free volume, which enhances transport of gases through polymeric materials (Loat, 2001). As depicted in Table 3, PTMSPT which has the highest fractional free volume and the highest gas permeability coefficient (Table 1.2). Decrease in chain mobility and restricted segmental motion provide denser membrane materials which enhances diffusion selectivity and perm-selectivity (Loat, 2001). The higher glass transition temperature (T_g) is associated with lower chain mobility and denser polymeric materials. Thus, polyimide, which has among the highest T_g values (Table 1.3), shows the highest CO_2/CH_4 selectivity (Table 1.2). However, drawing a correlation between T_g and membrane selectivity failed because of complex nature of factors influencing gas transport through polymeric membrane (Hirayama et al., 1996; Matteucci et al., 2006). For example, low- T_g polymers (e.g. cellulose acetate, 80 °C) can show high CO_2/CH_4 selectivity or high- T_g polymer (e.g. PTMSP) can show low CO_2/CH_4 selectivity.

The other parameter which effects significantly the diffusion coefficient is the size of the penetrant. Penetrant with larger kinetic diameter has lower diffusion coefficient (Loat, 2001, Matteucci et al., 2006). For example, lowest kinetic diameter belongs to H_2 molecules (Table 1.4) which has the highest diffusion

coefficient and hence the highest permeability in glassy polymeric membrane (Table 1.2).

Solubility coefficient is the other factor which controls the permeability of gases in membrane. Solubility coefficient is a thermodynamic factor and is closely associated with the interaction between penetrant and polymer. S increases with penetrant condensability characterized with by critical temperature, Lennard-Jones potential well depth, normal boiling point. High critical temperature, high Lennard-Jones potential well depth, and high normal boiling point are an indicate of ease of condensability for gas molecules (Loat 2001, Sanders et al. 2013, Basu et al. 2010). CO_2 and CH_4 which are the most condensable gases (Table 1.4), have higher permeability in elastomeric membrane (Table 1.2) (Basu et al. 2010).

The stronger interaction between penetrant and functional group of polymer leads to greater solubility coefficient. Thus, CO_2 which has a significant quadrupole moment by comparison with other noble gases, is highly soluble in polar polymers (for example polymer containing amine group). This explains the higher permeability of CO_2 than that of O_2 despite their kinetic diameters that are closest in value (Table 1.4).

The increase in fractional free volume leads to increase in solubility coefficient (Loat 2001); however, it has a weaker effect on solubility than on diffusivity (Matteucci et al. 2006).

Table 1.3 Thermal and structural properties of widely used polymeric membranes.

Polymer	Glass Transition Temperature (T_g); °C	Fractional Free Volume (FFV)
Tetrabromo-BisA-Polycarbonate (PC)	263 (Matteucci, 2006)	0.092 (Sanders 2013)
Polydimethyl Siloxane (PDMS)	-123 (Matteucci, 2006)	0.15~0.25 (Petzetakis et al., 2015)
Polyimide (PI)	310 (Matteucci, 2006)	0.17 (Sanders 2013)
Polymethylpentene (PMP)	25-50(Wypych, 2016)	0.28 (Nunes & Peinemann, 2006)
Polyphenyleneoxide (PPO)	210 (Wypych, 2016)	0.183 (Sanders 2013)
Polysulfone (PSF)	186 (Matteucci, 2006)	0.144 (Sanders 2013) 0.159 (Morisato et al., 1996; Matteucci, 2006)
Poly(1-trimethylsilyl-1-propyne) (PTMSP)	230 (NIST)	0.343 (Morisato et al., 1996) 0.29 (Nunes & Peinemann, 2006)

Table 1.4 Physical properties of gas molecules effecting transport properties (^c Matteucci, Yampolskii and Freeman, 2006; ^d NIST; ^e Enginering ToolBox).

Gases	Kinetic Diameter^c (nm)	Critical Temperature^c (K)	Lennard-Jones Potential well depth^c (K)	Normal Boiling Point^d (K)	Enthalpy of Vaporisation (kJ/mol)
CH ₄	0.38	191.0	148.6	111.7	8.2 ^d
CO ₂	0.33	304.21	195.2	-	-
H ₂	0.289	33.24	59.7	20.4	0.9 ^e
N ₂	0.364	126.2	71.4	77.3	5.6 ^d
O ₂	0.346	154.6	106.7	90.15	6.8 ^e

Permeance is measure of how much gas permeates across the membrane per unit pressure difference. Permeance is equal to permeability coefficient divided by the thickness of the thin dense selective layer (Eqn. 1.3). This value is expressed in gas permeance unit GPU which is equal to 10^{-6} STP $\text{cm}^3 / (\text{cmHg s. cm}^2)$ (Sanders et al. 2013).

$$F = \frac{P}{L} = \frac{G}{\Delta p} \text{ STP cm}^3 / \text{s. cmHg cm}^2 \quad \text{Eqn. 1.3}$$

Permeance of the membrane is inversely proportional to the thickness of membrane. Therefore, the thickness of membrane is reduced to obtain high permeance membranes. However, a membrane must stand mechanical, thermal and chemical stresses. Two types of membrane morphology, asymmetric and composite membranes are synthesized to obtain the desired property (Zolandz and Fleming, 1992). An asymmetric membrane is made up of a thin dense layer of polymer providing gas separation supported thick porous sublayer of same polymer

providing mechanical strength. A composite membrane is made up of by combining two distinct layers of generally two different materials. The thin dense polymer layer is responsible for gas separation. Whereas the thick microporous substrate supplies mechanical stability. The thin polymer layer is coated or laminated on substrate layer (Gupta, 2009).

Today almost all polymeric commercial membranes are prepared in asymmetric structure with very thin non-porous dense selective layer (100 nm or less) on porous support layer. This morphology provides high flux and robust membranes. Asymmetric membranes can be produced both in flat sheet and hollow fibers shape.

There are several methods to produce polymeric membranes. Some of them are sintering, stretching, track-etching, phase inversion, dip-coating, vapor deposition, interfacial polymerisation. Among these methods, phase inversion covers large range of techniques such as precipitation by solvent evaporation, precipitation from vapor phase, precipitation by controlled evaporation, thermal precipitation, immersion precipitation, air casting of the dope solution (Mulder, 2010; Baker 2013).

In solvent evaporation method, polymer-solvent solution is cast on a suitable plate and solvent is evaporated. A dense membrane layer is obtained by this method. Gas permeation rate of this type of membrane is low (Tul Muntha, 2016). Despite the low permeance, this geometry is still the most frequently studied one because of simplicity of solvent evaporation process (Dong et al., 2013). This geometry supplies separation of penetrants even in similar size depending their solubility in membranes. They are also studied frequently in the laboratory for characterization of membrane separation properties (Baker, 2013).

Immersion precipitation method, introduced to literature by Loeb and Sourirajan in 1963 (Loeb and Sourirajan, 1963), is a one step process providing asymmetric membrane structure. This method is also known as dry-wet phase inversion method and the most frequently used method because of its important advantage of rapid film formation at room temperature using inexpensive solvent

such as water (Kausar, 2017). In this method, a homogeneous solution of polymer-solvent is cast into flat film or extruded in hollow fiber shape and then converted to solid state by immersion into non-solvent bath. Precipitation of polymer occurs due to exchange of solvent and non-solvent. Solvent and non-solvent must be miscible for this process. However, this process is more complicated than solvent evaporation method, since at least three components are required. Moreover, complex diffusion and mixing processes take place during process and these play an important role on membrane morphology (Van de Witte et al., 1996).

In vapor induced phase separation method, polymer film is exposed to non-solvent vapor and phase separation occurs due to absorption of non-solvent vapor. VIPS process also includes wet inversion step. After exposure to non-solvent vapor for desired time, membrane is quenched in coagulation bath. This production method provides symmetric porous structure with sponge like pore size and narrow pore size distribution. Although it is slow process, this method gives an opportunity to control pore size and morphology by controlling relative humidity, exposure time to humid air, air temperature and velocity of moving air. In academic literature, the membranes produced via VIPS are generally used for ultrafiltration (Alexowsky et al., 2016; Uragami, 2017; Chae et al. 1999).

The biggest problem of pure polymeric membrane which limits industrial applications of them is the trade-off between permeability and selectivity. The CO₂/CH₄ separation and CO₂ permeability performance of various polymeric membrane materials are shown in Figure 1.1. The upper limit of the polymeric membranes is prescribed by Robeson in 1991 and updated in 2008. It is not possible to exceeding this upper bound just by modifying the structure of polymeric membrane. Because increasing in permeability leads to sacrifice in selectivity (Robeson 2008; Chung et al. 2007)

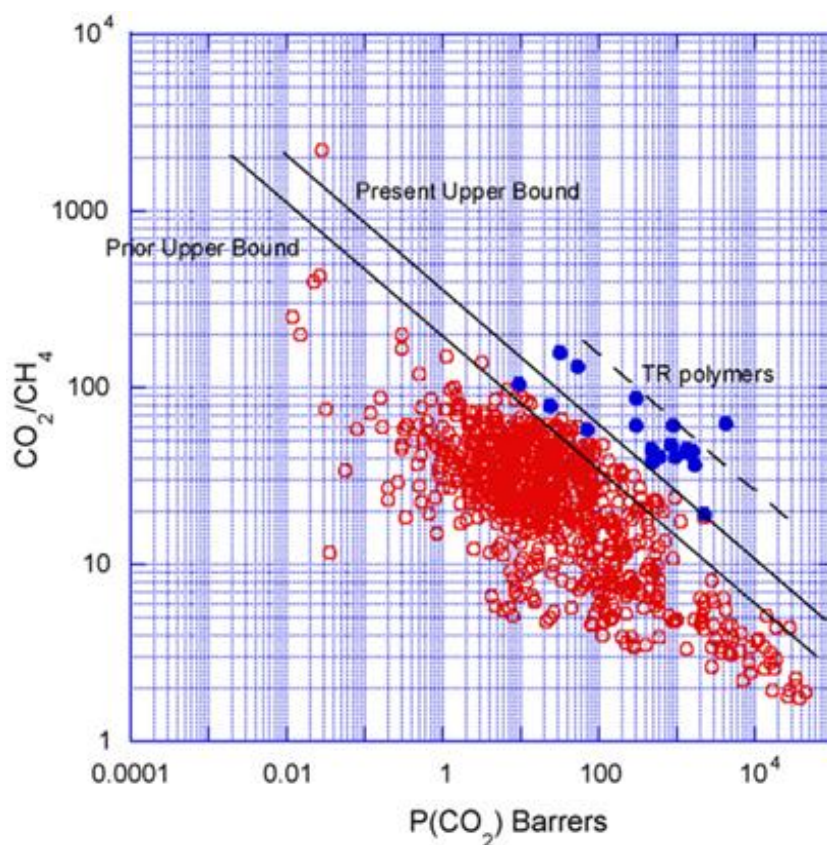


Figure 1.1 Upper bound correlation for CO₂/CH₄ separation (Robeson, 2008).

Mixed matrix membrane (MMM) is an alternative membrane morphology to improve permeability and selectivity performance of membrane. The purpose is to combine mechanical strength, ease of handling and low cost of polymeric membrane with the high gas permeability and selectivity of inorganic membrane to exceed the upper limit of Robeson plot (Chung et al. 2007; Mushtaq et al. 2013). MMM is morphology made up of organic polymer as a bulk phase and inorganic particle as a dispersed phase. Dispersed phase can be porous or non-porous. Zeolites, carbon molecular sieves, nano-sized particles, metal organic frameworks (MOFs), activated carbons, carbon nanotubes, titanosilicates, mesoporous silica are the porous type inorganic filler. Silica, titaniumdioxide, and fullerene are non-pours inorganic filler widely used in MMM production (Bastani et al. 2013).

The main challenge of MMM is poor contact between organic-inorganic interfaces which lead to non-selective voids. Therefore, selectivity of mixed matrix

membrane is effected negatively. To solve these problems; several methods have been developed such as annealing above glass transition temperature of polymers, adding plasticizer into membrane solution, modification of fillers' surface by silane coupling agent, surface initiated polymerization, low molecular weight additives and glassy polymer blends (Mahajan and Koros ,2002). Yong et al., 2001 (2,4,6-triaminopyrimidine (TAP)) and Sen et al., 2007 (p-nitroaniline (pNA)) suggested low molecular weight additives (LMWA) to enhance adhesion between zeolite and polymers. LMWAs act as an antiplasticizer, increase stiffness of polymer chains by reducing segmental motion. This type of additives is worthwhile for high pressure CO₂ separation, which leads to swelling of polymeric membrane.

1.1 Objective and Thesis Outline

The main objective of this Ph.D research was to develop asymmetric mixed matrix gas separation membranes containing zeolitic imidazole framework (ZIF-8) as a filler and para-nitro aniline (pNA) as a compatibilizer. The aim was production of CO₂/CH₄ selective membrane without additional coating.

Two different polymer, polyethersulfone (PES) and polyimide (PI) were used in this research. PES and PI are commercially available and widely used glassy polymers for gas separation purpose. Asymmetric membranes with thin dense selective layer (< 1µm) were produced. The fillers should be smaller in size to be able to disperse them in thin dense selective layer. For this purpose, ZIF-8 was selected as filler, which can be synthesized at average particle size of 60, 20 and 10 nm in our laboratory. ZIF-8 is also suitable for CO₂/CH₄ separation because of its zeolitic framework and pore size which is less than the kinetic diameter of CH₄ and bigger than the kinetic diameter of CO₂. Effect of filler loading on the membrane morphology and performance has been investigated.

Solvent evaporation method, dry-wet phase inversion method and vapor phase inversion method have been used to produce polymeric membranes. Influence of production method on membrane morphology and performance has been investigated. The production of asymmetric neat and asymmetric mixed matrix gas separation membrane and with defect-free and thin selective skin layer,

and dispersion of filler without agglomeration are very important breakthrough in the membrane research field. To provide this goal, several manipulations have been carried out in the academic literature. In the present study, we used infrared light lamp (IR) or incandescent lamp light (IL) energy in order to control the formation of dense skin layer and to fix the filler in the skin layer. This study is the first one in which light energy used in the membrane production process.

The Ph. D thesis has been written as a collection of several chapters.

First chapter provides a general background about polymeric gas separation membranes and the main objectives of the thesis and introduces the parts of the thesis.

The results of the research are presented and discussed in the following sections. Each section included an extensive literature survey and theoretical background part specific to the theme discussed in that chapter. Experimental details, chemical and physical properties of materials, details of the test set-up are also provided in each chapter.

In Chapter 2, the main focus is the gas separation performance of PES membranes produced via wet phase inversion method. Effect of coagulation bath composition, ZIF-8 loading, size of the filler, annealing type of filler on membrane morphology and gas permeability of membrane have been investigated and discussed.

In Chapter 3, the gas permeation test results of PES and PI membranes produced via dry-wet phase inversion method have been provided. During dry inversion, polymer film was exposed to lamp light or infrared light in order to control dry inversion and evaporation of volatile solvent. The volatile solvent amount in the polymer solution, lamp light or infrared time exposure during dry inversion are parameters which have been studied. The membranes are coated with PDMS and effect of coating has been discussed.

Asymmetric PI membrane have been produced with different method, dry-vapor phase inversion. Instead of water, humid air was used. In this part of the work,

humidity of air and volatile solvent amount in the polymer solution were kept constant. Time period of dry inversion and IR exposure time are parameters. The results are given in Chapter 4.

Chapter 5 includes also the study about gas sorption properties of PI membrane. For gas sorption test, symmetric dense PI membranes produced via solvent evaporation method has been used. Effects of ZIF-8 content, compatibilizer content and feed gas composition on sorption property of membrane were studied.

REFERENCES

- Alexowsky, C., Bojarska, M., & Ulbricht, M. (2016). Preparation of macroporous hydrophobic flat-sheet PVDF membranes via vapor induced phase separation. Retrieved from http://xeric.eu/wp-content/uploads/Poster_Alexowsky_EYEC_Warsaw_2016.pdf
- Baker, R. (2013). Membrane technology and applications. Hoboken, NJ: Wiley.
- Bastani, D., Esmaili, N., & Asadollahi, M. (2013). Polymeric mixed matrix membranes containing zeolites as a filler for gas separation applications: A review. *Journal of Industrial and Engineering Chemistry*, 19(2), 375-393. doi:10.1016/j.jiec.2012.09.019
- Basu, S., Khan, A. L., Cano-Odena, A., Liu, C., & Vankelecom, I. F. (2010). Membrane-Based Technologies for Biogas Separations. *ChemInform*, 41(21)
- BP: Statistical Review of World Energy. Retrieved from <http://www.bp.com/en/global/corporate/energy-economics/statistical-review-of-world-energy/2015-in-review.html>
- Chae Park, H., Po Kim, Y., Yong Kim, H., & Soo Kang, Y. (1999). Membrane formation by water vapor induced phase inversion. *Journal of Membrane Science*, 156(2), 169-178. doi:10.1016/s0376-7388(98)00359-7
- Chemical & Engineering News: Cover Story - Membranes For Gas Separation. (2005, October 3). Retrieved from <http://pubs.acs.org/cen/coverstory/83/8340membranes.html>
- Chen, G., & Wu, X. (2017). Energy overview for globalized world economy: Source, supply chain and sink. *Renewable and Sustainable Energy Reviews*, 69, 735-749. doi:10.1016/j.rser.2016.11.151
- Chung, T., Jiang, L. Y., Li, Y., & Kulprathipanja, S. (2007). Mixed matrix membranes (MMMs) comprising organic polymers with dispersed inorganic fillers for gas separation. *Progress in Polymer Science*, 32(4), 483-507. doi:10.1016/j.progpolymsci.2007.01.008
- Dong, G., Li, H., & Chen, V. (2013). Challenges and opportunities for mixed-matrix membranes for gas separation. *Journal of Materials Chemistry A*, 1(15), 4610. doi:10.1039/c3ta00927k
- Engineering ToolBox. (n.d.). Retrieved from <http://www.engineeringtoolbox.com/>
- Graham, T. (1995). On the law of the diffusion of gases. *Journal of Membrane Science*, 100(1), 27-31. doi:10.1016/0376-7388(94)00228-q
- Gupta, R. B. (2009). Hydrogen fuel: Production, transport, and storage. Boca Raton: Taylor & Francis.
- Hirayama, Y., Yoshinaga, T., Kusuki, Y., Ninomiya, K., Sakakibara, T., & Tamari, T. (1996). Relation of gas permeability with structure of aromatic polyimides I. *Journal of Membrane Science*, 111(2), 169-182. doi:10.1016/0376-7388(95)00172-7
- International Energy Statistics. (n.d.). Retrieved from <https://www.eia.gov/beta/international/data/browser/#/?vs=INTL.44-1-AFRC-QBTU.A&vo=0&v=H&start=1980&end=2014>

- Kannan, N., & Vakeesan, D. (2016). Solar energy for future world: - A review. *Renewable and Sustainable Energy Reviews*, 62, 1092-1105. doi:10.1016/j.rser.2016.05.022
- Kausar, A. (2017). Phase Inversion Technique-Based Polyamide Films and Their Applications: A Comprehensive Review. *Polymer-Plastics Technology and Engineering*, 1-17. doi:10.1080/03602559.2016.1276593
- Kurchania, A. K., Panwar, N. L., & Pagar, S. D. (2010). Design and performance evaluation of biogas stove for community cooking application. *International Journal of Sustainable Energy*, 29(2), 116-123. doi:10.1080/14786460903497391
- Loat, C. M. (2001). Gas Transport Properties In Polycarbonate: Influence Of The Cooling Rate, Physical Aging, And Orientation (Doctoral dissertation).
- Loeb, S., & Sourirajan, S. (1963). Sea Water Demineralization by Means of an Osmotic Membrane. *Advances in Chemistry*, 117-132. doi:10.1021/ba-1963-0038.ch009
- Lu, G., Diniz da Costa, J., Duke, M., Giessler, S., Socolow, R., Williams, R., & Kreutz, T. (2007). Inorganic membranes for hydrogen production and purification: A critical review and perspective. *Journal of Colloid and Interface Science*, 314(2), 589-603. doi:10.1016/j.jcis.2007.05.067
- Mahajan, R., & Koros, W. J. (2002). Mixed matrix membrane materials with glassy polymers. Part 1. *Polymer Engineering & Science*, 42(7), 1420-1431. doi:10.1002/pen.11041
- Matteucci, S., Yampolskii, Y. P., Freeman, B. D., & Pinnau, I. (2006). Transport of gases and vapors in glassy and rubbery polymers. In *Material Science of Membranes for Gas and Vapor Separation* (pp. 1-47). Chichester: John Wiley & Sons.
- Morisato, A., Shen, H. C., Sankar, S. S., Freeman, B. D., Pinnau, I., & Casillas, C. G. (1996). Polymer characterization and gas permeability of poly(1-trimethylsilyl-1-propyne) [PTMSP], poly(1-phenyl-1-propyne) [PPP], and PTMSP/PPP blends. *Journal of Polymer Science Part B: Polymer Physics*, 34(13), 2209-2222. doi:10.1002/(sici)1099-0488(19960930)34:13<2209::aid-polb10>3.0.co;2
- Mulder, M. (2010). *Basic principles of membrane technology*. Dordrecht [u.a.: Kluwer Acad. Publ.
- Mushtaq, A., Mukhtar, H. B., Shariff, A. M., & Mannan, H. A. (2013). A Review: Development of Polymeric Blend Membrane for Removal of CO₂ from Natural Gas. *International Journal of Engineering & Technology*, 13(02), 53-60.
- National Institute of Standards and Technology | NIST. (n.d.). Retrieved from <https://www.nist.gov/>
- Nunes, S. P., & Peinemann, K. V. (2006). Gas Separation with Membranes, Cp6. In *Membrane technology in the chemical industry* (pp. 39-67). Weinheim: Wiley-VCH.
- Petzetakis, N., Doherty, C. M., Thornton, A. W., Chen, X. C., Cotanda, P., Hill, A. J., & Balsara, N. P. (2015). Membranes with artificial free-volume for biofuel production. *Nature Communications*, 6, 7529. doi:10.1038/ncomms8529

- Qiu, J., Zheng, J., & Peinemann, K. (2006). Gas Transport Properties in a Novel Poly(trimethylsilylpropyne) Composite Membrane with Nanosized Organic Filler Trimethylsilylglucose. *Macromolecules*, 39(12), 4093-4100. doi:10.1021/ma0603635
- Robeson, L. M. (2008). The upper bound revisited. *Journal of Membrane Science*, 320(1-2), 390-400. doi:10.1016/j.memsci.2008.04.030
- Sanders, D. F., Smith, Z. P., Guo, R., Robeson, L. M., McGrath, J. E., Paul, D. R., & Freeman, B. D. (2013). Energy-efficient polymeric gas separation membranes for a sustainable future: A review. *Polymer*, 54(18), 4729-4761. doi:10.1016/j.polymer.2013.05.075
- Tul Muntha, S., Kausar, A., & Siddiq, M. (2016). Progress in Applications of Polymer-Based Membranes in Gas Separation Technology. *Polymer-Plastics Technology and Engineering*, 55(12), 1282-1298. doi:10.1080/03602559.2016.1163592
- TURKEY'S ENERGY PROFILE AND STRATEGY / Rep. of Turkey Ministry of Foreign Affairs. (2016, June). Retrieved from <http://www.mfa.gov.tr/turkeys-energy-strategy.en.mfa>
- Uragami, T. (2017). *Science and Technology of Separation Membranes 2 Vol Set*. Somerset: John Wiley & Sons, Incorporated.
- Van de Witte, P., Dijkstra, P., Van den Berg, J., & Feijen, J. (1996). Phase separation processes in polymer solutions in relation to membrane formation. *Journal of Membrane Science*, 117(1-2), 1-31. doi:10.1016/0376-7388(96)00088-9
- Wypych, G. (2016). *Handbook of polymers*.
- Yong, H. H., Park, H. C., Kang, Y. S., Won, J., & Kim, W. N. (2001). Zeolite-filled polyimide membrane containing 2,4,6-triaminopyrimidine. *Journal of Membrane Science*, 188(2), 151-163. doi:10.1016/s0376-7388(00)00659-1
- Zolandz, R. R., & Fleming, G. K. (1992). Gas Permeation. In *Membrane Handbook* (p. 17). New York: VanNostrand Reinhold.
- Şen, D., Kalıpçılar, H., & Yilmaz, L. (2007). Development of polycarbonate based zeolite 4A filled mixed matrix gas separation membranes. *Journal of Membrane Science*, 303(1-2), 194-203. doi:10.1016/j.memsci.2007.07.010

CHAPTER 2

ASYMMETRIC NEAT PES MEMBRANES AND ASYMMETRIC PES/ZIF-8 MIXED MATRIX MEMBRANES PRODUCED BY WET PHASE INVERSION

In this chapter, the morphological and gas transport properties of PES membranes produced by wet phase inversion method were presented. The main objective was to assess the parameters controlling the morphology and gas permeation characteristic of asymmetric PES membranes produced by wet-phase inversion.

The permeability of PES (reported permeability coefficients of PES for H₂, CO₂, and CH₄ are 8.96, 3.38 and 0.112 Barrers, respectively (Li and Chung, 2008)) is lower than several polymers such as Polymer of Intrinsic Microporosity (PIM), Poly(1-trimethylsilyl-1-propyne) (PTMSP) or Matrimid. PES was selected as polymer in this study. Because PES is cheap and commercially available, which are crucial for industrially applicable membrane materials. Despite their high permeance, PIM and PTMSP can be produced in small scale in laboratory, which is a great disadvantage for industrial application. Furthermore, PES is widely studied in literature as membrane materials. Several specific properties of PES such as ideal selectivity, Flory-Huggins interaction parameters for several solvent and non-solvent are easy to access. This feature provides an advantage in terms of controlling the accuracy of our results. Selection of solvent and nonsolvent were carried out according to affinity, interaction and miscibility of PES-solvent-nonsolvent pairs. Selection of solvent nonsolvent pairs was discussed in part Chapter 2.2 extensively.

The gas permeation test and SEM test results of neat PES and PES-ZIF-8 mixed matrix membrane prepared via wet phase inversion method are presented and discussed in this chapter. XRD, TGA, BET and SEM test results of filler, ZIF-8 crystals are provided in section 2.4.

2.1 Theoretical Background about Polymeric Membrane Formation via Phase Inversion

Polymeric membrane precipitation is induced by touching polymer solution to a vapor or liquid nonsolvent. Diffusional mass exchange between solvent and nonsolvent brings to a change in the local composition of polymer film. Polymer solution may be precipitated by different ways. Three most common are shown in Figure 2.1 (Ren and Wang, 2010);

1. Immersion Precipitation: Polymer solution is submerged into a nonsolvent bath. The nonsolvent diffuses into the casting polymer solution and the solvent diffuses from the casting solution to the coagulation bath. This is a fast precipitation beginning from top of the casting solution surface.
2. Vapor Adsorption: The casting solution is exposed to vapor involved nonsolvent and precipitation occurs due to adsorption of nonsolvent.
3. Solvent Evaporation: The casting polymer solution is precipitated by evaporation of solvent.

These three processes are shown in Figure 2.1

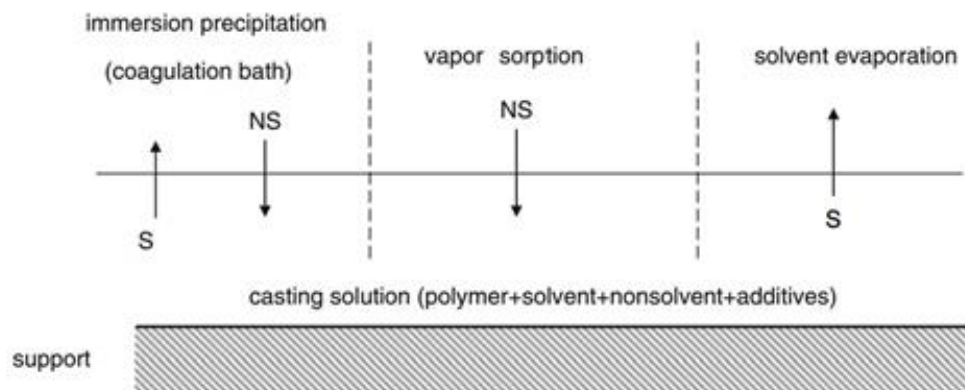


Figure 2.1 Schematic presentation of three common polymeric membrane precipitation process; where S represents solvent and NS represents nonsolvent. (Ren and Wang, 2010).

During the preparation of a membrane, these three processes may take place simultaneously. For example, in the time period between casting and immersion precipitation, the solvent in the casting solution evaporates and simultaneously

humidity in the air is adsorbed by the casting solution. Finally, immersion precipitation occurs and final structure of membrane forms (Ren and Wang, 2010).

Formation of an asymmetric membrane prepared via phase inversion is explained by both the thermodynamics of the polymer-solvent-nonsolvent system and the kinetics of transport process (Ismail and Yean, 2003; Reuvers 1987; Ren and Wang 2010). Thermodynamic behavior of the system can be described by ternary phase diagram shown in Figure 2.2. Ternary phase diagram is composed of four different regions.

Region I; one phase region: is homogeneous one phase liquid state

Region II; liquid-liquid two phase region: composed of one unstable and two metastable regions, solution will distinguish into two liquid phases; namely polymer rich and polymer lean.

Region III; liquid-solid two phase swelling: polymer will be swollen in the solvent-nonsolvent mixture. Since polymer cannot dissolve in this mixture, there is no polymer in the mixture.

Region IV; one phase glass and swelling: polymer is at its glass state.

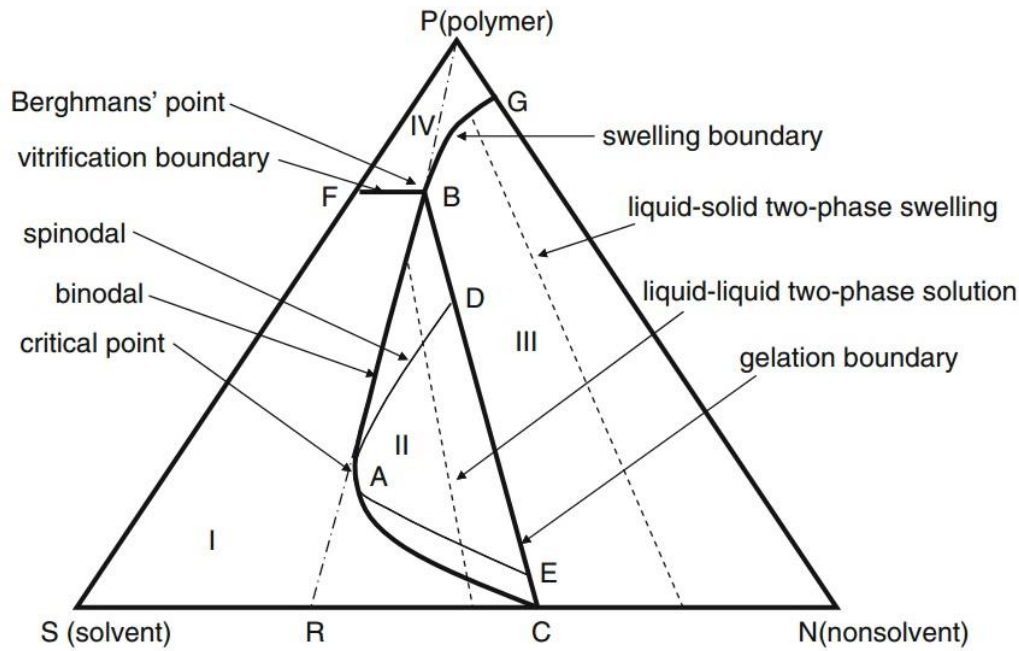


Figure 2.2 Schematic ternary phase diagram of polymer-solvent-nonsolvent system (Ren and Wang, 2010).

In Figure 2.2, binodal (BAC) and spinodal (DAE) curves show the boundary of two metastable areas; the first one BAD at high polymer concentration region, the second one CAE at low polymer concentration region. Area DAE formed by spinodal curve and gelation boundary is unstable area. The Point B, at which the porous structure of the polymer rich phase will be vitrified, named as Berghmans' point.

Figure 2.3 illustrates the membrane formation by phase inversion. Figure 2.3 includes both ternary phase diagram, the possible phase separation path and resulting membrane morphology depending on following path and gelation time. Four possible membrane morphologies are shown and black or dark grey regions represent polymer matrix, while white area represents empty pores. Point A represents the composition of casting solution. If the solution follows path 1, homogeneous glassy membrane is obtained. If the solution follows path 2, porous membrane morphology is obtained. Based on the phase separation type, pores could be formed and dispersed throughout polymer matrix (path 2-1), bi-continuous

polymer matrix could be formed (path 2-2) or polymer phase might nucleate and grow in pores (Ren and Wang 2010).

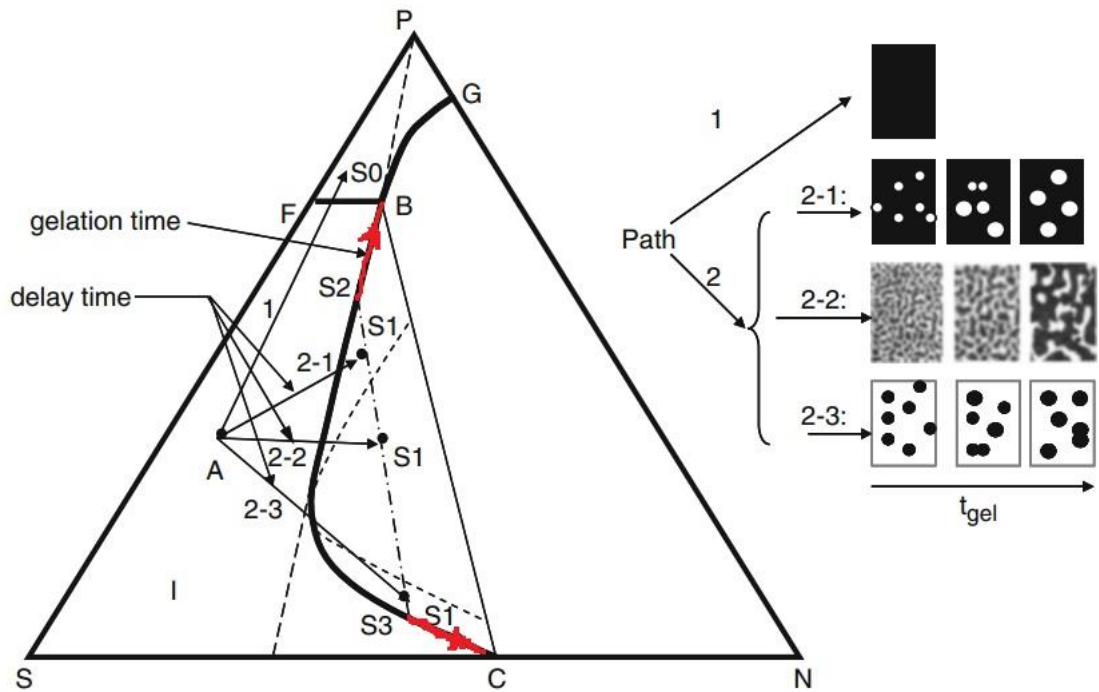


Figure 2.3 Schematic representation of membrane formation for phase inversion process (figure modified from Ren and Wang, 2010).

For the polymer-solvent-nonsolvent system following path 2, when the solution passes over the binodal curve and comes to point S1, the solution separates two phase; namely polymer rich phase (point S2) and polymer lean phase (point S3) (see Figure 2.4). Later on, polymer rich phase constitutes the polymer matrix, while polymer lean phase forms pores. This phenomenon is called liquid-liquid phase separation or liquid-liquid demixing (Ren and Wang 2010). Liquid-liquid demixing mechanism of homogenous solution is strongly based on the stability of solution. If the solution follows path 2-1 and reaches metastable region, phase separation occurs via growth of stable nuclei which can be produced by certain amount of change in concentration. This type of phase separation via nucleation and growth is called binodal decomposition. If the solution follows path 2-2 and reaches unstable region between spinodal curve and gelation boundary, the phase separation occurs rapidly by small change in the composition. This type of phase

separation called spinodal decomposition (Reuvers 1987).

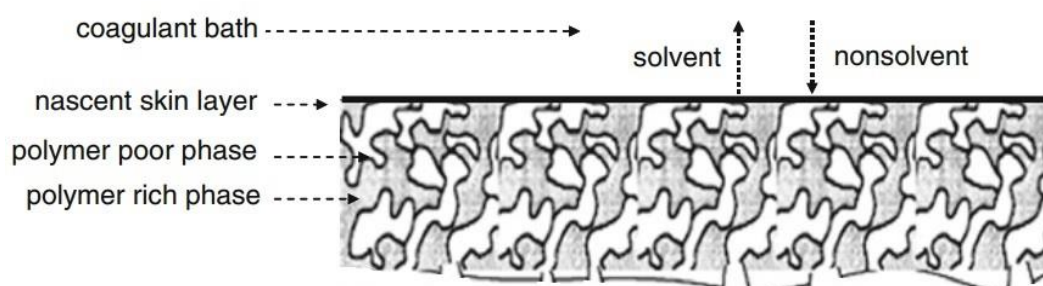


Figure 2.4 Schematic representation of skin layer, polymer rich phase and polymer poor (lean) phase of an asymmetric membrane (figure modified from Ren and Wang, 2010).

The time period between the initiation of the immersion of polymer solution into coagulant and onset of the liquid-liquid demixing (path A→S1) is named as delay time (Reng and Wang 2010). Depending on delay time, two different mechanisms will take place, which are instantaneous demixing and delayed demixing. Instantaneous demixing means phase separation starts just after immersion of solution into coagulant. In delayed demixing, the composition of polymer solution spends time in homogeneous one phase region (Region I) for a certain amount of time. Delayed demixing leads to a membrane type with relatively thick selective layer suitable for hyperfiltration or gas separation. Finger like big pores are prohibited in this type of demixing. Instantaneous demixing provides membrane with very thin selective layer shows ultrafiltration performance (Reuvers 1987).

The gelation time is defined as the time interval between the liquid-liquid phase separation and solidification of the polymer (S2→B). In other words, the time required for polymer rich phase comes to Berghmans' point B and final structure of membrane stabilizes is called gelation time (Reng and Wang 2010).

Delay time, gelation time and competition between them are three important parameters which determine the final morphology of membrane (Tanaka and Stockmayer, 1994; Li et al. 1996).

2.1.1 Formation of Membrane Surface based on Ternary System Thermodynamics

In literature, there are different approaches about the formation of asymmetric membrane structure. In this section, I listed widely accepted views about asymmetric membrane formation. General acceptance is the origin of the asymmetric membrane structure is originated from the asymmetric polymer concentration distribution of casting polymer solution. Because of this polymer concentration variation each layer follows different demixing and precipitation paths (Ismail and Yean 2003).

According to Panar et al. 1973 and Tanny 1974, asymmetric polymer concentration distribution throughout the membrane cross section is already present before contacting nonsolvent, because the surface tension leads to higher polymer concentration at the casting solution surface. Reuvers 1987, disagree with this idea and suggested that polymer distribution alters and adjust to the new thermodynamics situation just after immersion.

Loeb-Sourirajan 1963, Anderson and Ullman 1973, Kesting 1988 claimed that asymmetric polymer concentration comes from evaporation of solvent from the surface layer of casting membrane solution and final membrane structure is influenced by period of time and condition of evaporation. When the polymer solution contains volatile solvent, it is observed significant effect of evaporation time on the asymmetric structure of membrane. However, when only non-volatile solvent is used still asymmetric membrane structure is acquired. Therefore, this claim cannot solely explain asymmetric membrane formation with non-volatile solvent casting solution.

Reuvers 1987 suggested that the asymmetric structure of membrane is mainly formed and fixed by ternary diffusion taking place after immersion into coagulant. Liquid-liquid demixing process creates pores in the supporting sublayer and also determined the structure of membrane's top layer. Smolders and Reuvers 1992 shows that polymer concentration at the surface increases significantly after immersion it into coagulation bath.

Strathmann and Kock 1977; Koenhen et al, 1977 Broens et al. 1980 suggested that asymmetric polymer distribution is because of ternary diffusion process taking place during immersion precipitation. Based on this idea, high diffusion of solvent from upper surface of casting film and small amount of penetration of nonsolvent through it leads to a sharp increase in the polymer concentration of surface.

Because of solvent evaporation (Pesek and Koros, 1993) or solvent-nonsolvent exchange (Reuvers 1987; Ren and Wang 2010), the surface polymer concentration (interface of polymer solution and nonsolvent) will cross the vitrification boundary directly (path 1, Figure 2.3). Hence a dense nonporous membrane surface will be formed. The solution under the skin layer is still in fluid state and may pass the binodal line, in this case a porous membrane morphology under the skin layer will be developed. The nascent skin layer behaves as a barrier prohibiting solvent-nonsolvent counter-diffusion during wet phase inversion. Therefore, formation of sublayer is strongly influenced by the top nascent skin layer. The composite properties of top skin layer and subsequent sub-layer may manipulate the formation of a third subsequent layer and the following layer is influenced by the above layers. Because of the mass transfer resistance created by the above layers, each layer follows a different demixing path and precipitation kinetics. Hence different morphologies at each layer are formed (Young and Chen 1991; Machado et al., 1999; Ismail and Yean 2003). This type of asymmetric membrane has intrinsic polymer properties (such as permeability, selectivity...) for gas separation, reverse osmosis or pervaporation.

Sometimes, surface polymer solution moves along the binodal line, hence polymer concentration at the membrane surface is always in equilibrium with the solvent concentration of the coagulation bath at the interface. Although the surface polymer concentration changes along the binodal line, surface polymer cannot solidify since liquid-liquid phase separation does not take place. The sublayer under the polymer surface goes through liquid-liquid demixing phase separation and the formation of sublayer affects the formation of skin layer. For this case,

surface with discrete pore size distribution will be formed. This type of membrane is generally used as ultrafiltration and microfiltration (Ren and Wang 2010).

In dry-wet phase inversion process inducing forced solvent evaporation, membrane surface crosses the binodal curve follows the spinodal decomposition part (path 2-2 in Figure 2.3). Forced convective evaporation results in locally escalated polymer concentration. Outermost region of membrane will be formed instantaneously via dry-phase separation spinodal decomposition (Ismail and Yean 2003). According to Pinnau and Koros 1993; spinodal decomposition at the beginning of the evaporation step induces small scale phase separation; polymer poor and polymer rich phase. The capillary pressure force in the interstitial polymer poor phase in contact with air impels polymer rich phase and amalgamate them to form nonporous layer. This type of membrane has nascent homogeneous skin layer via highly plasticized nodule network due to the relatively long gelation time (Ren and Wang 2010).

2.1.2 Formation of Pores based on Ternary System Thermodynamics

Based on the location of the liquid-liquid separation point (S1 on Figure 2.3), three different decomposition mechanism take place (Ren and Wang 2010).

When the solution follows path 2-1 on Figure 2.3 and liquid-liquid demixing begins somewhere above the critical point between binodal line and spinodal line, polymer poor phase nucleates and grows in the polymer rich phase. Nucleating and growing phase forms pores, remaining forms polymer matrix (Ismail Yean 2003).

When the solution follows path 2-3 on Figure 2.3 and liquid-liquid demixing begins somewhere below the critical point between binodal and spinodal curves, polymer rich phase nucleates and grows in the polymer poor phase. In this type of decomposition, low integrity powdery polymer agglomerates form, which are not practical for membrane applications (Ismail Yean 2003).

For the path 2-2, spinodal decomposition will be dominant. The solution crosses directly into unstable region. In this type of phase separation, a bicontinuous interconnected polymer poor and polymer rich phase will be obtained without

nucleation and growth mechanism. This bicontinuous network provides open pores membrane support without selectivity.

2.2 Selection of Solvent and Non-Solvent Pair

Affinity and interaction between solvent-nonsolvent-polymer influences in both thermodynamic characteristics of ternary polymer solution and precipitation kinetics changing the phase inversion. The difference between Hansen solubility parameters of two components, $\Delta\delta_{x-y}$ is an indication of their affinity in terms of thermodynamics similarities. Hansen solubility parameter (Eqn. 2.1) is composed of three partial solubility parameters namely; dispersion forces, polar forces, hydrogen bonding (Soroko et al., 2011). The Hansen solubility parameters of PES, various solvents and non-solvents are shown in Table 2.1. The differences between Hansen solubility parameter of PES-Solvent, PES-Nonsolvent, Solvent-Nonsolvent pairs (Table 2.2) were calculated by Eqn. 2.2.

$$\delta = ((\delta_d)^2 + (\delta_h)^2 + (\delta_p)^2)^{0.5} \quad \text{Eqn. 2.1 (Cheng et al. 1996)}$$

$$\Delta\delta_{x-y} = ((\delta_{d,x} - \delta_{d,y})^2 + (\delta_{h,x} - \delta_{h,y})^2 + (\delta_{p,x} - \delta_{p,y})^2)^{0.5} \quad \text{Eqn. 2.2 (Cheng et al. 1996)}$$

Table 2.1 Hansen solubility parameters of polymer, solvent and non-solvent. If not specified, data were taken from Guillen et al.,2011.

Chemicals	$\delta_d(\text{MPa}^{0.5})$	$\delta_h(\text{MPa}^{0.5})$	$\delta_p(\text{MPa}^{0.5})$	$\delta(\text{MPa}^{0.5})$
Polymer				
PES (Nasir et al. 2014)	19.6	10.8	9.2	24.2
PES (Xu and Qusay 2004)	17.6	10.4	7.8	21.9
PES (average)	18.6	10.6	8.5	23.1
Solvent				
NMP	18.0	12.3	7.2	22.96
DMF	17.4	13.7	11.3	24.86
Non-Solvent				
IPA	15.8	6.1	16.4	23.6
MeOH	15.1	12.2	22.2	29.5
EtOH	15.8	8.8	19.4	26.5
Water	15.5	16	42.3	47.8

Table 2.2 Hansen solubility parameter difference between polymer-solvent, polymer-nonsolvent, nonsolvent-solvent pairs

Chemicals	Solvent		Non-Solvent			
	NMP	DMF	IPA	MeOH	EtOH	Water
Polymer	$\Delta\delta_{\text{PES-Solvent}}(\text{MPa}^{0.5})$		$\Delta\delta_{\text{PES-NonSolvent}}(\text{MPa}^{0.5})$			
PES	2.2	4.3	9.5	14.2	11.4	34.4
Solvent			$\Delta\delta_{\text{Solvent-NonSolvent}}(\text{MPa}^{0.5})$			
NMP	-	-	11.3	15.3	12.9	35.4
DMF	-	-	9.3	11.2	9.6	31.1

Chemicals with similar Hansen solubility parameters will be miscible, and polymers will dissolve in liquids with Hansen solubility parameters are close to the polymer. Small difference between Hansen solubility parameters indicates high affinity and high miscibility, whereas large difference between them shows less affinity between these chemicals (Hansen, 2007).

Table 2.2 shows the solubility parameter difference between polymer and two widely used strong solvent NMP and DMF. $\Delta\delta_{PES-NMP}$ and $\Delta\delta_{PES-DMF}$ were calculated as $2.2 \text{ (MPa)}^{0.5}$ and $4.3 \text{ (MPa)}^{0.5}$, respectively. When $\Delta\delta_{Polymer-solvent}$ is less than 8, solvent can dissolve polymer. Therefore, both of them are strong solvents for PES. NMP is stronger solvent than DMF for PES since $\Delta\delta_{PES-NMP}$ is smaller than $\Delta\delta_{PES-DMF}$. Solvent polymer affinity is highly favoured. Poor solvent induces high degree of polymer aggregation and less stable polymer-solution (Soroko et al., 2011). It is also reported that high affinity between solvent-polymer contributes to the smaller demixing gap especially lower affinity between solvent and nonsolvent (Mazinani et al., 2017).

$\Delta\delta_{Polymer-nonsolvent}$ for several nonsolvent and PES were also tabulated in Table 2.2. $\Delta\delta_{PES-IPA}$, $\Delta\delta_{PES-EtOH}$, $\Delta\delta_{PES-MeOH}$, $\Delta\delta_{PES-water}$ were calculated as 9.5, 11.4, 14.2 and $34.4 \text{ (MPa)}^{0.5}$, respectively. The largest solubility parameter difference is obtained for PES-water pair whereas the smallest one is obtained for PES-IPA pair. This means that the affinity between water and PES is very low in comparison to that between IPA and PES. Hence water is strongest non-solvent and IPA is the weakest non-solvent among the chemicals listed in Table 2.2.

Polymer nonsolvent interaction strongly influences the location and size of the demixing gap. Higher affinity between polymer-nonsolvent is characterized by binodal line lying close to the polymer/non-solvent axis. The nonsolvent which draws binodal curve closest to the polymer-solvent axis is accepted as the strongest coagulant. Since small amount of it is sufficient to precipitation. The coagulation strength which is inversely proportional to the affinity of polymer-nonsolvent characterizes the instanteneous demixing (Mazinani et al., 2017). There are several studies (Peng et al., 2012; Xu and Xu, 2002; Sukitpaneenit and Chung, 2009) insist that using a strong non-solvent such as water leads to instantaneous demixing which means fast precipitation. However, weak non-solvents such as alcohols leads to delay in liquid-liquid demixing process. This phenomenon is associated with the size of the miscibility region which decreases with increase of $\Delta\delta_{Polymer-nonsolvent}$. Instanteneous liquid-liquid demixing (fast precipitation) is enhanced by decreasing the size of miscibility gap (Mazinani et al., 2017; Soroko et al., 2011). Strathmann

et al, 1975, Soroko et al., 2011; Guillen et al., 2011; Peng et al., 2012 stated that high precipitation rate enhanced large finger like pores with thin dense skin layer whereas low precipitation rates induced sponge like porous structure with thick skin layer.

$\Delta\delta_{\text{Solvent-nonsolvent}}$ pairs are also tabulated in Table 2.2. The difference in solubility parameters between DMF-nonsolvent pairs is of the order (DMF-Water) > (DMF-MeOH) > (DMF-EtOH) > (DMF-IPA). The order of NMP-nonsolvent system is the same (NMP-Water) > (NMP-MeOH) > (NMP-EtOH) > (NMP-IPA). The difference in solubility parameter between NMP-nonsolvent and DMF-nonsolvent is in the following order (NMP-Water)>(DMF-Water); (NMP-MeOH)>(DMF-MeOH); (NMP-EtOH)>(DMF-EtOH); (NMP-IPA)>(DMF-IPA). Hence it can be concluded that miscibility between DMF and listed nonsolvents is higher than that of NMP and listed nonsolvents.

$\Delta\delta_{\text{Solvent-nonsolvent}}$ effects both solvent- nonsolvent exchange rate and location of miscibility gap. Driving force for diffusion will be detracted because of lower solvent and nonsolvent affinity (higher $\Delta\delta_{\text{Solvent-nonsolvent}}$) (Soroko et al., 2011). Skin layer formation is affected strongly from the diffusion rate ratio ($k=D_S/D_{NS}$) of solvent to nonsolvent. High k induces dense and tighter skin layer formation, whereas low k values leads to porous top layer (Young and Chen, 1995; Peng et al. 2012).

There is a contradiction between findings about influence of solvent-nonsolvent affinity in literature. Several studies (Guillen et al., 2011; Mazinani et al., 2017; Young and Chen, 1995; Reuvers 1987; von't Hof et al., 1992) declare that the ternary polymer-solvent-nonsolvent system with higher miscibility (means low $\Delta\delta_{\text{Solvent-nonsolvent}}$) between solvent and nonsolvent has a more tendency of instantaneous demixing (faster precipitation), hence finger like porous membrane structure will be formed. These researchers consider that if miscibility is high, the coagulant can easily penetrate into the casting solution and produce macro voids. They suggest that low miscibility or poor interaction leads to delay in liquid-liquid demixing which associated with sponge like pores and denser structure. On the

other hand; Chun et al., 2000 claims that smaller $\Delta\delta_{\text{Solvent-nonsolvent}}$ reinforce delayed demixing. In this study, difference between solvent-nonsolvent solubility parameter was decreased by adding solvent into nonsolvent coagulation medium. Hence the strong interaction between solvent-nonsolvent pair in the coagulation medium prevents penetration of non-solvent in the polymer solution. In other studies, Xu and Xu, 2002; Xu and Qusay, 2004; higher difference between solubility parameter of solvent and nonsolvent leads to sharp and sudden decrease of solubility of solvent to polymer associated with instantaneous demixing. These contradictions may come from complex nature of non-solvent induced phase separation and the fact that phase inversion process depends on several parameters other than thermodynamic affinity of solvent-nonsolvent.

Since the claims of different authors conflict with each other and also their own findings, I decided to investigate their findings instead of their claims and I tried to find a correlation between phase inversion characteristic and solvent-nonsolvent miscibility. For example, Mazinani et al., 2017 studied about morphological properties Extem-DMSO-water and Extem-NMP-Water systems. Extem-DMSO-water system produced dense skin layer with spongy pores on the support layer; whereas EXTEM-NMP-water system produced thinner dense skin layer with finger like big pores on the support layer. I calculated $\Delta\delta_{\text{DMSO-water}}$ as 32.23 and $\Delta\delta_{\text{NMP-water}}$ as 35.38, hence affinity between DMSO-water system is higher than that of NMP-water system. Contrary to the authors claim, high affinity solvent-nonsolvent pairs produced spongy pores with thicker selective layer. Another contradiction in this research is the position of binodal curve. Generally, higher miscible solvent-nonsolvent system provides a binodal curve closer to the polymer-nonsolvent axes. In this research, the binodal curve of Extem-DMSO-water system closer to the polymer-solvent axes, whereas Extem-NMP-water system closer to the polymer-nonsolvent axes. General belief, binodal curve closer to the polymer-solvent axes is more tend to instantaneous demixing and forming finger like pores, because small amount of nonsolvent can disturb the equilibrium of such a system. Findings of Mazinani et al 2017 is also contradict this information. Authors still are in favors of high micibility of solvent-nonsolvent pairs. When the

interaction between solvent and polymer investigated, it is obvious that NMP is stronger solvent than DMSO. Probably, for this system, the affinity between solvent-polymer pair may be more dominant in thermodynamics of the system and formation mechanism. According to the Mazinani et al.,2017, ternary phase diagram and position of binodal curve is not sufficient to explain the formation mechanism. Affinity and miscibility of solvent-nonsolvent-polymer systems, diffusivity ratio of solvent nonsolvent pairs, interfacial polymer concentration, precipitation rate should be also considered for complete definition of membrane formation mechanism.

In another research carried by Cheng et al., 1996; PMMA membranes were prepared in asymmetric membrane structure by using different solvent-nonsolvent pairs and formation mechanism was discussed. Although authors mainly focused on polymer-nonsolvent solubility parameter difference and discussed miscibility of solvent –nonsolvent pairs in terms of diffusivity instead of Hansen solubility parameter difference; their finding were very informative about the effect of solvent-nonsolvent pair affinity. Authors used PMMA-acetone-water and PMMA-acetone-nhexane as polymer-solvent-nonsolvent system. I calculated Hansen solubility parameter difference of acetone-water and acetone-nhexane solvent-nonsolvent pairs and tried to comprehend the effect of Hansen solubility parameter difference. $\Delta\delta_{Solvent-nonsolvent}$ of acetone-water and acetone-nhexane were calculated as 35.84 and 12.5 (MPa)^{0.5}, respectively. Hence it is concluded that miscibility of acetone-nhexane system is higher than that of acetone-water system. Authors reported that PMMA-acetone-water system leads to membrane with small spongy pores on support layer with dense skin layer, whereas PMMA-acetone-nhexane system leads to membrane with larger spongy pores with thicker dense skin layer. This is expected because several authors reported that higher miscibility leads larger pores on support layer. In the same research, binodal curve of PMMA-acetone-water and PMMA-NMP-water system were almost overlapped and very close to the solvent-polymer axis. On the other hand, binodal curve of PMMA-acetone-nhexane system which has the smaller Hansen solubility parameter difference was closer to polymer-nonsolvent axis. Similar trend was also observed by

Sukitpaneent and Chung, 2009. As indicated previously, it is accepted that the binodal curve closer to the polymer-solvent axes is and indicate of easy instantaneous demixing results is finger like structure. However, morphological features of PMMA-acetone-water system produced small spongy pores on the support layer. The explanation of authors was that the thermodynamics diagram is not sufficient to characterize the membrane formation. The Hansen solubility parameter differences between NMP-water and acetone-water are calculated 35.4 and 35.84, respectively. These two values are very close to each other. Highly probably the interaction between solvent and nonsolvent is a key parameter which determine the position of binodal curve on the ternary phase diagram for this polymer-solvent-nonsolvent systems. However, on the contrary of PMMA-acetone-water system; PMMA-NMP-water configuration formed finger like pores on the support layer with very thin dense skin layer. This study included also the time for precipitation by light transmission method. The required precipitation time for PMMA-NMP-water system is 18 sec., while this time took 30 sec. for PMMA-acetone-water system. From this information, it is concluded that liquid-liquid demixing time or precipitation rate is more dominant than nonsolvent-solvent miscibility in formation of morphology for this system.

Sukitpaneent and Chung et al. 2009; investigated the effect of coagulant (different nonsolvent and combination of them) on the morphology, crystallinity and pore formation of PVDF hollow fiber membrane. According to their research, binodal curve of PVDF/NMP/nonsolvent (water, MeOH, EtOH, IPA) system shift to solvent-polymer axis by increasing the difference of Hansen-solubility parameter between solvent and nonsolvent pair. Closer the binodal curve to the polymer-solvent axes is the stronger nonsolvent and small amount of strong nonsolvent is sufficient to disturb the thermodynamics equilibrium of the ternary system. Less stable system is more tend to instantaneous demixing. They explained the thermodynamic properties of the system according to the differences between polymer and nonsolvent. They insisted the importance of kinetic aspect of phase inversion. Their results concluded that higher diffusion of nonsolvent – solvent pairs cause faster precipitation.

In the light of this knowledge, the solvent and nonsolvent pairs were selected. DMF was selected as solvent. Although NMP is stronger solvent for PES, since DMF is more miscible with nonsolvents and the miscibility between solvent-nonsolvent pairs is recommended by several researchers. Moreover, boiling point of DMF is lower than NMP, hence removing solvent from membrane is anticipated to be easier. Both IPA and water were selected as nonsolvents. These two are the two ends of the nonsolvent scale, weakest and strongest nonsolvents. As explained previously, PES is very good candidate for such a research about membrane formation mechanism. Since this polymer is commercially available and cheap. Moreover, PES is widely studied in literature and its several intrinsic properties such as permeability, selectivity, Flory Huggies interaction parameters with several solvent and non-solvent pairs, Hansen solubility parameters... are available. Using such as widely studied polymer provides an opportunity to check the findings. The effects of the coagulation bath composition on morphology and separation properties of PES membranes were investigated and discussed in the following sections.

2.3 Materials and Experimental Method

2.3.1 Materials

Polyether sulfone Radel A-100 grade was supplied by Solvay Advanced Polymer, USA. The number average molecular weight is 53 000 g/mol and glass transition temperature (T_g) is about 220 °C. At 35 °C and 3.5 atm pressure difference, the reported permeability coefficients of PES for H₂, CO₂, and CH₄ are 8.96, 3.38 and 0.112 Barrers, respectively (Li and Chung, 2008). The repeating unit of PES is given in Figure 2.5.

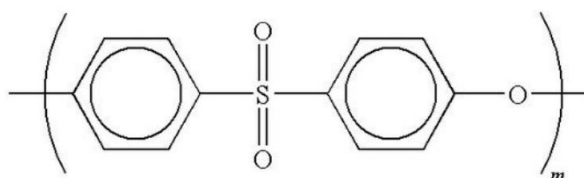


Figure 2.5 Repeating unit of polyethersulfone (Solvey Advanced Polymer, Radel).

The solvent used is N,N-Dimethylformamide (DMF), which is a polar aprotic solvent, has strong dissolving power for many polymers. DMF with high purity (>99%) was provided by Sigma-Aldrich. It has the linear chemical formula of $\text{HCON}(\text{CH}_3)_2$, normal boiling point of 153 °C, and density of 0.944 g/cm³ at 20 °C. Isopropyl alcohol (GC>%99.5) with linear chemical formula $(\text{CH}_3)_2\text{CHOH}$, normal boiling point of 82.6 °C and density of 0.786 g/cm³ at 20 °C was supplied from Sigma Aldrich and used as coagulant. DI water (H_2O) was used as coagulant additive to strengthen the non-solvent.

Zinc nitrate hexahydrate [$\text{Zn}(\text{NO}_3)_2 \cdot 6\text{H}_2\text{O}$, 98% purity] with density of 2.065 g/cm³ was purchased from Acros. 2- methylimidazole [$\text{C}_4\text{H}_6\text{N}_2$, 99% purity] with density of 1,09 g/cm³ at 20 °C, boiling point of 268 °C and melting point of 143 °C was provided by Sigma–Aldrich.

Test gases, H_2 , CO_2 , and CH_4 were purchased from Linde with purity %99.5.

2.3.2 Preparation of ZIF-8

Two solutions were prepared by dissolving 10.6 g. 2- methylimidazole in 180.8 g. MEOH and 4.8 g. zinc nitrate hexahydrate in 180.8 g. MEOH. Two solutions were mixed rapidly to obtain a mixture with a molar composition $\text{Zn}(\text{NO}_3)_2 \cdot 6\text{H}_2\text{O} \mid 7.99 \text{ C}_4\text{H}_6\text{N}_2 \mid 700.99 \text{ MeOH}$. This mixture was stirred at 300 rpm for 1 h. at room temperature. ZIF-8 crystals were collected by centrifuging at 6000 rpm for 5 minutes. The average particle size of ZIF-8 crystals was determined as 65 nm by analyzing SEM micrographs via imageJ.

Reaction medium which was separated from the ZIF-8 crystals at 65 nm by centrifuging is called mother liquor. For synthesis of ZIF-8 crystals with average particle size of 25 nm, the mother liquor obtained from the synthesis of ZIF-8 crystals with 65-nm-size was aged for a day at room temperature. The pH of the one-day aged mother liquor was adjusted by adding NaOH pellets. The new reaction medium with composition by weight 1 gr NaOH | 290 g. Mother liquor was stirred at 300 rpm for 1 hr. at room temperature. ZIF-8 crystals were collected by centrifuging at 6000 rpm for 5 minutes. The average particle size of ZIF-8 crystals was measured as 25 nm.

For synthesis of ZIF-8 crystals with average particle size of 15 nm, mother liquor obtained from the synthesis of ZIF-8 crystals with 25-nm-size was aged for a day. The consumed amount of Zn^{+2} was added into the second mother liquor (1g. Zn^{+2} | 78.2 g. Mother Liquor). After 1 h. stirring at 300 rpm and at room temperature, 15 nm ZIF-8 crystals were collected by centrifuging at 600 rpm for 5min.

Three different methods were applied to purify ZIF-8 crystals and to activate the pores. In type 1 treatment method, collected ZIF-8 crystals were washed with MeOH twice and recollected by centrifuging at 600 rpm for 25 minutes. In type 2 treatment method, after washing with MeOH, collected ZIF-8 crystals were dried overnight at 80 °C. Dried ZIF-8 crystals were grinded, then annealed overnight at 180 °C. In type 3 treatment method, after washing with MeOH, collected ZIF-8 crystals were washed with DMF one more time and recollected by centrifuging at 600 rpm for 40 minutes. The crystal structure of ZIF-8 is shown in **Figure 2.6**.

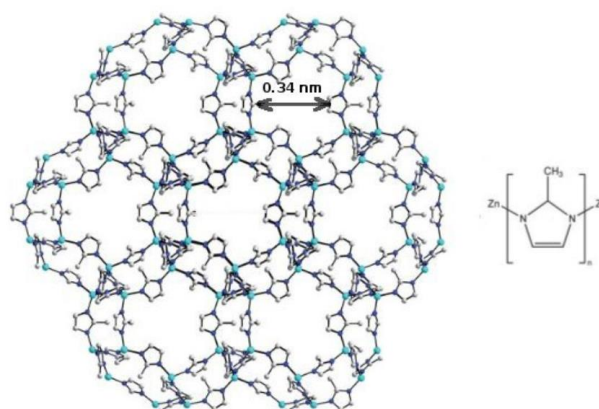


Figure 2.6 Crystal structure of ZIF-8, Cyan, blue, and grey spheres represent Zn, N, and C atoms, respectively. H atoms are omitted for clarity (Cacho-Bailo et al., 2014).

2.3.3 Characterization of ZIF-8 Crystals

ZIF-8 crystals were characterized by Philips PW 1840 X-Ray diffractometer to obtain X-ray diffraction(XRD) pattern of the crystals. The source of the X-ray was Ni filtered $Cu-K\alpha$ radiation $\lambda = 1.5406$ Å. The scan rate was 0.05 °/sec. The voltage and current were 30 kV and 24 mA, respectively. The Bragg angles were between 5

to 40 °. The crystallinity of ZIF-8 crystals was determined according to the six characteristic peak points obtained at 7.44, 10.48, 12.90, 14.87, 16.63 and 18.24 Bragg angles.

QUANTA 400F Field Emission series scanning electron microscopy (SEM) with 1.2 nm resolution was used to determine morphology and particle size of the ZIF-8 crystals. The synthesized ZIF-8 crystals were dispersed in MeOH. A few droplets of the ZIF-8-MeOH homogeneous solution were spattered at carbon strap. After evaporation of MeOH, crystals were coated Au-Pd and monitored at 30 kV voltage.

BET instrument Micromeritics TriStar II 3020 was used to determine specific surface area (m^2/gr) of synthesized ZIF-8 crystals. Before test, ZIF-8 samples were evacuated at 135 °C for 24 hr. The amount of adsorbed nitrogen volume at particle surface was measured at -196 °C (boiling point of N_2) and used to calculate surface area. The calculation is based on Brunauer-Emmett-Teller (BET) theory. N_2 adsorption-desorption isotherms were provides information about size and volume distribution of pores.

Thermal stability of ZIF-8 crystals was characterized by thermogravimetric analysis (TGA) instrument DTG-60H, Shimadzu. Samples was heated at 10 °C /min rate up to 600 °C in air. Air flow rate is 50 ml/min.

2.3.4 Membrane Preparation

Asymmetric flat sheet neat PES membranes were prepared by non-solvent induced wet phase separation (NIPS) method. The membrane solution of 17.4 wt.% concentration was prepared by dissolving 2 g. PES in 9.5 g. DMF. Before using, PES was dried at 80°C overnight in order to remove humidity. The PES-DMF solution was stirred by a magnetic stirrer at 300 rpm and at room temperature. The essential amount of PES was added in three steps to avoid agglomeration and sudden increase of viscosity. Between each steps, the solution was ultrasonicated for 10 min in order to ease the dispersion. The clear solution was cast on a clean

glass plate at 500 μm in thickness using automatic film casting machine. After casting, glass plate was immediately immersed in to isopropyl alcohol (IPA) coagulation bath. The volume of coagulation bath was 500 ml. Flat sheet membrane was washed in water bath to remove the residual solvent and non-solvent overnight. Then the membrane was dried at 120°C overnight and annealed at 180°C for two days in vacuum oven.

The effect of the water content of the coagulation medium on the membrane performance was investigated making membranes in coagulation baths with 2-5-7-10-25 vol.% water in IPA. The influence of solvent in the coagulation medium was also investigated by adding 25 and 30 vol.% DMF in IPA coagulation medium. The volume of coagulation medium was always 500 ml.

The first step in preparation of mixed matrix PES/ZIF-8 membranes was the dispersion of ZIF-8 in DMF. For this purpose, ZIF-8/DMF mixture was stirred at 300 rpm by a magnetic stirring at room temperature. The percentage of ZIF-8 loading weight was determined based on the weight of polymer utilized as expressed in Eqn. 2.3.

$$(\text{wt.\% ZIF-8 loading in membrane}) = (n \text{ wt.\%}) \times (\text{Polymer wt.}) \quad \text{Eqn. 2.3}$$

n: 0, 5 wt. %, and 10 wt. % of PES in this study.

The necessary amount of ZIF-8 was added at three or four step based on the amount. The purpose is to prevent agglomeration and provide perfect dispersion. The solution was ultrasonicated for 30 min between each step. After dispersion of necessary amount of ZIF-8 in the DMF solvent, 15 wt. % of total PES was firstly added into ZIF-8/DMF mixture. The remaining amount of PES was added in two steps; 35 wt.% of total PES, and 50 wt.% of total PES, respectively. Before each addition, membrane solution was ultrasonicated for 30 minutes. The casting and annealing methodologies of mixed matrix PES/ZIF-8 membranes were the same as those of neat PES membranes.

2.3.5 Membrane Characterization

Morphology of membrane was investigated by SEM micrograph. QUANTA 400F Field Emission series scanning electron microscopy (SEM) with 1.2 nm resolution was used to obtain SEM micrographs with magnifications between 1000x and 100 000x. For cross-sectional image, a piece of membrane was fractured in liquid N₂ and the films were mounted vertically over circular aluminum sample holder with carbon tape. Before SEM analyze, the samples were coated with Au/Pd for electrical conduction and monitored at 30 kV voltage.

Single gas permeation test was performed in the set-up depicted in Figure 2.7. This system was composed of a feed part, a permeate part and a module. Membrane module was a stainless steel Millipore filter holder (part no. XX45047 00) that holds the flat membrane with two Viton O-Rings. Before each test, whole system was kept under vacuum for 3-3.5 hours. The vacuum was supplied by a mechanical vacuum pump (Edwards). Permeate was initially 13 torr. Then, the tank was filled with the test gas. The pressure was 2 atm. Gauge pressure. The pressure difference between feed and permeate is the driving force for gas permeation. The experiment was performed by constant volume and variable pressure method. Due to driving force, the pressure of the permeate side increased with time. The rate of pressure rise was used to calculate permeability coefficient. Permeability coefficient (Eqn. 2.4) of pure gas (P_A) through a polymeric film membrane is defined as the trans-membrane pressure difference (Δp), and thickness (L) normalized steady-state gas flux, G_A (Eqn. 2.5). Generally, permeability coefficient is expressed in unit of Barrer which is equal to 10⁻¹⁰ STP cm³ cm / (cmHg s. cm²).

$$P_A = \frac{G_A \times L}{\Delta p} \text{ STP cm}^3 \text{ cm} / \text{s. cmHg cm}^2 \quad \text{Eqn. 2.4}$$

$$\text{where } G_A = \frac{\left(\frac{dP}{dt} \times V\right) \times 22400}{A_{\text{membrane}}} \text{ STP cm}^3 / \text{s. cm}^2 \quad \text{Eqn. 2.5}$$

The membrane thickness (L) is the total cross-sectional thickness of dense membrane. The membrane thickness is the thin dense skin layer of asymmetric membrane. Since measuring the thickness of thin skin layer selective of membrane is difficult and is required another characterization method (SEM), the membrane performance is defined by permeance instead of permeability coefficient. Permeance is measure of how much gas is flowing across the membrane per unit pressure difference. Permeance is equal to permeability coefficient divided by the thickness of the thin dense selective layer (Eqn. 2.6). This value is expressed in gas permeance unit GPU which is equal to 10^{-6} STP $\text{cm}^3 / (\text{cmHg s. cm}^2)$.

$$F_A = \frac{P_A}{L} = \frac{G_A}{\Delta p} \text{ STP cm}^3 / \text{s. cmHg cm}^2 \quad \text{Eqn. 2.6}$$

The ideal selectivity which is the ability of membrane to separate two gases is obtained by dividing the permeability coefficients (or permeance) of the gases (Eqn.2.7). Permeability coefficient and selectivity are two fundamental parameters characterizing membrane performance.

$$\alpha_{A/B} = \frac{P_A}{P_B} \quad \text{Eqn. 2.7}$$

The dead-volume of the permeate side is used in further calculations. To measure it, a standard volume with a known volume 119 ml was filled with nitrogen with a specific pressure. Then the standard volume was connected to dead-volume. The pressure drop of the standard volume is used to calculate the capacity of dead-volume. The calculation was carried out based on Boyle's Law ($P_1 \times V_1 = P_2 \times V_2$). The dead-end volume of permeate side was measured as 11.3 cm^3 . The test was performed at $35 \text{ }^\circ\text{C}$ constant temperature. The set-up was heated by using heating type wrapped the system and equipped with a J-type thermocouple and a PID controller to keep the temperature constant.

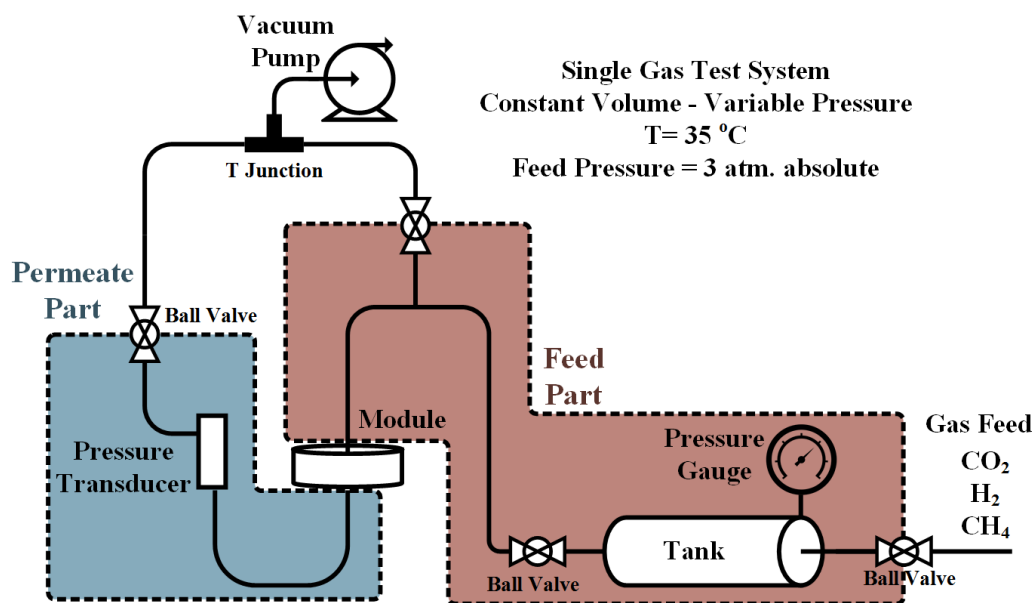


Figure 2.7 The schematic drawing of single gas permeation test system.

2.4 Characterization of ZIF-8 Crystals

In this study ZIF-8 crystals were used as fillers in the mixed matrix membranes. ZIF-8 synthesis procedure developed by Keser 2012 was followed. Details of the synthesis procedure and method to characterize ZIF-8s were given in part 2.3 Experimental Method. In this section, characterization results of ZIF-8 crystals were provided.

Figure 2.8 shows the SEM micrographs of ZIF-8s crystals produced with different MeOH/ZnNO₃.H₂O ratios. Average particle size of the ZIF-8 crystals were measured by J-image analyzer using SEM images. To determine average particle size at least 45 particles were counted for each sample. The calculated average particle size changed according to MeOH/ZnNO₃.H₂O ratio was provided in Table 2.3.

The ZIF-8 crystals with an average particle size of 65 nm has uniform and hexagonal shape (Figure 2.8(c)) By decreasing the average particle size, the structure of ZIF-8 changed from hexagonal-like to sphere-like. Moreover, aggregation becomes significant by decreasing average particle size (Keser 2012, Ayas 2014).

Table 2.3 Average particle size and standard deviation of ZIF-8 prepared with different MeOH/ ZnNO₃.H₂O molar ratio based on SEM image and J-image analyzer.

ZIF-8 Code	MeOH/ ZnNO ₃ .H ₂ O molar ratio	Average particle size based on SEM micrographs and J-image Analyzer (nm)
ZIF-8_1	1051	14.86± 3.97
ZIF-8_2	1130	27.03± 4.61
ZIF-8_3	695	64.10± 10.21

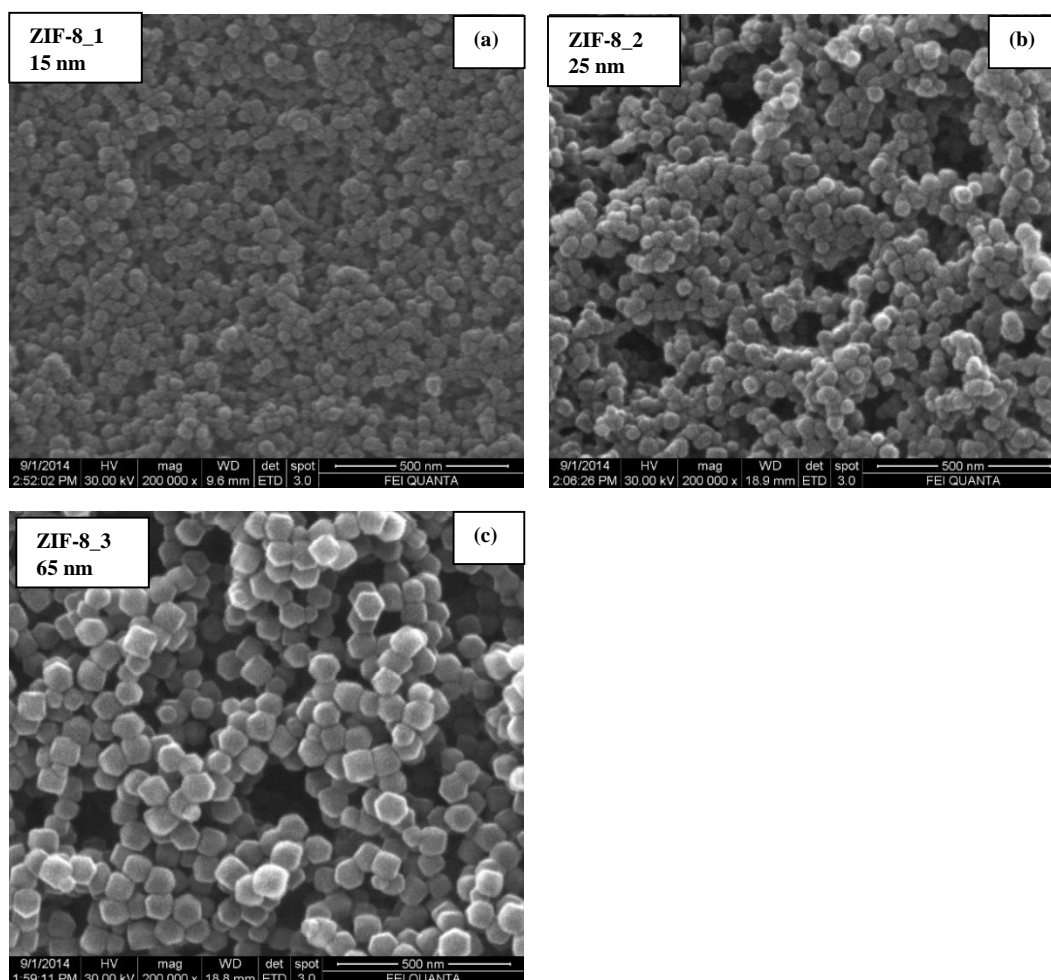


Figure 2.8 SEM micrographs of synthesized ZIF-8s; (a) ZIF-8_1; (b) ZIF-8_2; (c) ZIF-8_3

While ZIF-8 synthesis continued, preparation and testing of mixed matrix membranes continued. It was decided to continue with ZIF-8_3 (average particle size 65 nm) because it was determined that the best gas test result was obtained from mixed matrix membrane containing 65 nm ZIF-8_3. Moreover, ZIF-8_1 and ZIF-8_2 are more prone to clustering as observed by Ayas 2014 and by SEM images (Figure. 2.8). Hence, the following characterization were carried out only for ZIF-8_3 with average particle size 65 nm.

The sample ZIF-8_3 was further characterized by XRD for phase identification and semi-quantitative crystallinity (Figure. 2.9). The position of peaks and the diffraction pattern were conformed with the characteristic peak positions and diffraction pattern of ZIF-8 studied by Park et al. 2006 and Keser 2012. Pattern with well comparing with reference indicated that the high purity ZIF-8 crystals were obtained without any foreign crystalline phase. Sharp and intense peaks pointed out the high crystallinity of synthesized ZIF-8. The crystallinity of ZIF-8s was calculated by the intensity summation method using the peaks of (011), (002), (112), (022), (013), (222), (114) and (134) planes, which correspond to 7.44, 10.48, 12.90, 14.87, 16.63 and 18.24 Bragg angles. Jade Software (version 2.1) was used to calculate the areas between baseline and peaks. The area under these specific peaks were calculated as 5546 ± 623 in this study. This value was the average of five syntheses. The ZIF-8 crystals with average particle size 65 nm of Ayas 2014 study was used a reference. The total peak area of the reference ZIF-8 crystals was reported as 5855 (Ayas 2014) and it was assumed 100% crystallinity. In this study, semi-quantitative crystallinity of synthesized ZIF-8 with 65 nm average particle size was calculated as $\% 95 \pm 10$ based on the Eqn. 2.8.

$$\% \text{ cryst.} = \frac{\text{Total peak area of synthesized ZIF-8 pattern} \times 100}{\text{Total peak area of reference ZIF-8 pattern}} \quad \text{Eqn. 2.8}$$

Thermal behavior of ZIF-8 crystals at dry air atmosphere was provided in Figure 2.10. Up to 80 °C, a weight loss of almost 5% was detected. This small weight loss was attributed to loss of residual MEOH (syntheses medium) (Keser 2012). A sharp and significant weight loss (approximately 60%) was detected

between 400 and 445 °C. The 60% weight loss was ascribed to the decomposition of organic framework (Keser et al. 2014, Park et al. 2006). Upon decomposition of organic framework ZN is expected to oxidize into ZnO in air. The remaining material was nearly 40% of the initial amount of ZIF-8 which is very close to theoretical amount of residual solid ZnO (36.5%) (Zhang et al. 2012).

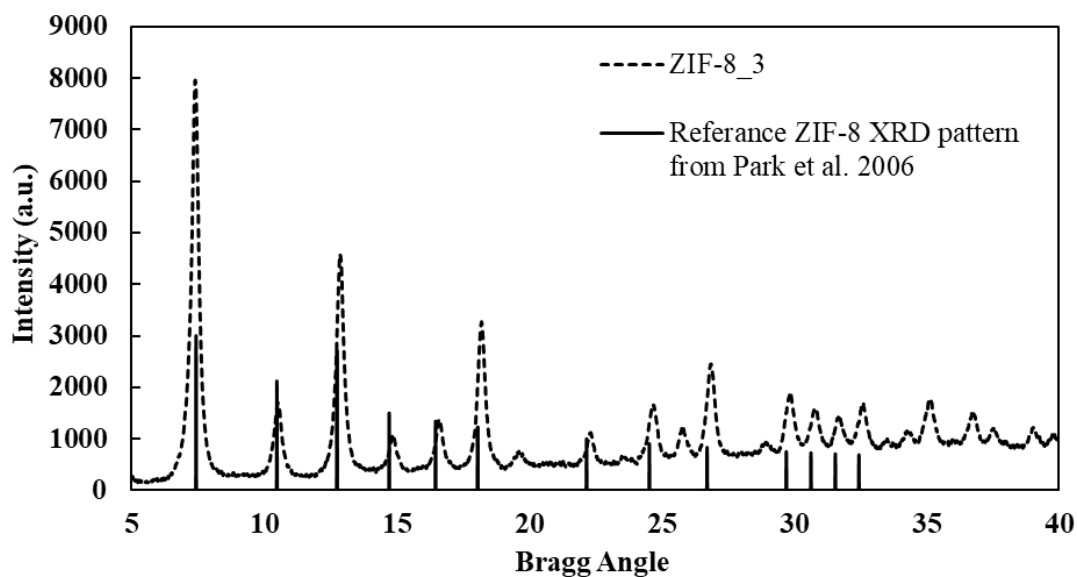


Figure 2.9 XRD pattern of ZIF-8_3 crystals with 65-nm-size.

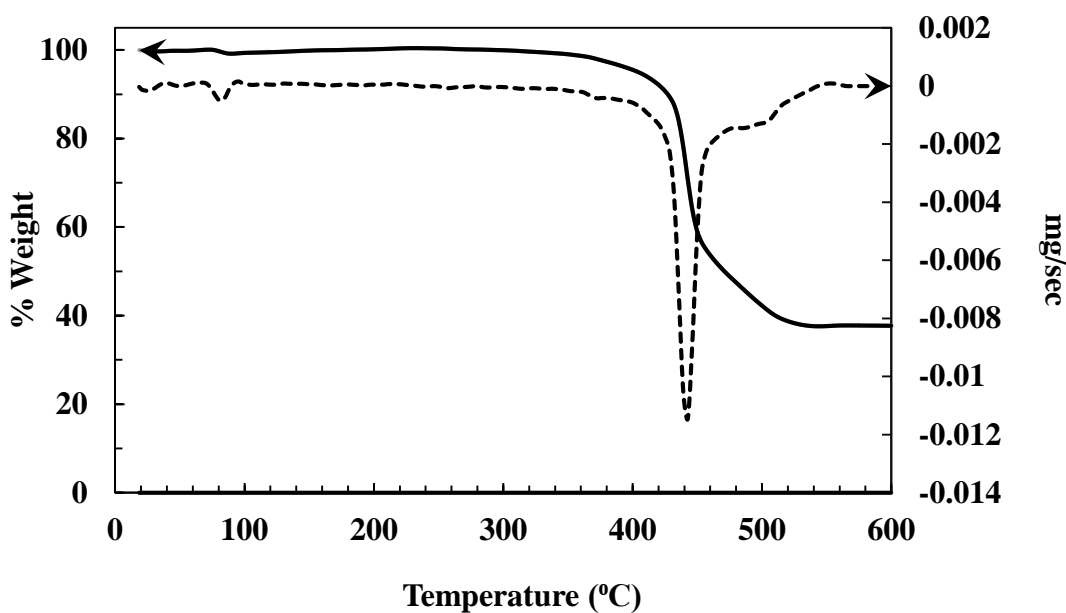


Figure 2.10 TGA curves of ZIF-8_3 crystals with average particle size 65 nm.

Figure 2.11 shows the N₂ adsorption-desorption curves at 77 °C for ZIF-8_3. For the relative pressure less than 0.1 ($P/P_0 < 0.1$), a significant amount of N₂ adsorption was observed. Further increase in relative pressure did not alter adsorption amount up to relative pressure 0.95. Up to this point, adsorption and desorption isotherm were nearly parallel to the relative pressure axis. Significant and sharp adsorption at low relative pressure and then adsorption isotherm parallel to pressure axes is a characteristic property of Type I adsorption-desorption isotherm. The N₂ adsorption shows Type I adsorption-desorption isotherm without any hysteresis, isoheating. Type I isotherm indicates the microporous structure of synthesized ZIF-8 (Keser 2012, Ayas 2014). Above the relative pressures greater than 0.95 ($P/P_0 > 0.95$), capillary condensation takes place, which is due to presence of macro-pores formed because of agglomeration. Similar trend was also observed by other researchers and explained by textural porosity (Zang et al. 2013) and intra aggregated voids (de Silva et al. 2015).

BET surface area was approximately 1320 m²/g and t-plot micropore area was calculated by computer program 1230 m²/g. This result is in agreement with

Keser 2012 and Ayas 2014 studies whose synthesis procedure was followed in this study. BET surface area of ZIF-8 reported in literature was 744 m²/g (Venna et al. 2010), 962 m²/g (Cravillon et al. 2011), 1079 m²/g (Pan et al. 2011), between 1000 m²/g and 1700 m²/g depending on particle size (Keser 2012) and 1700 m²/g (Ayas 2014).

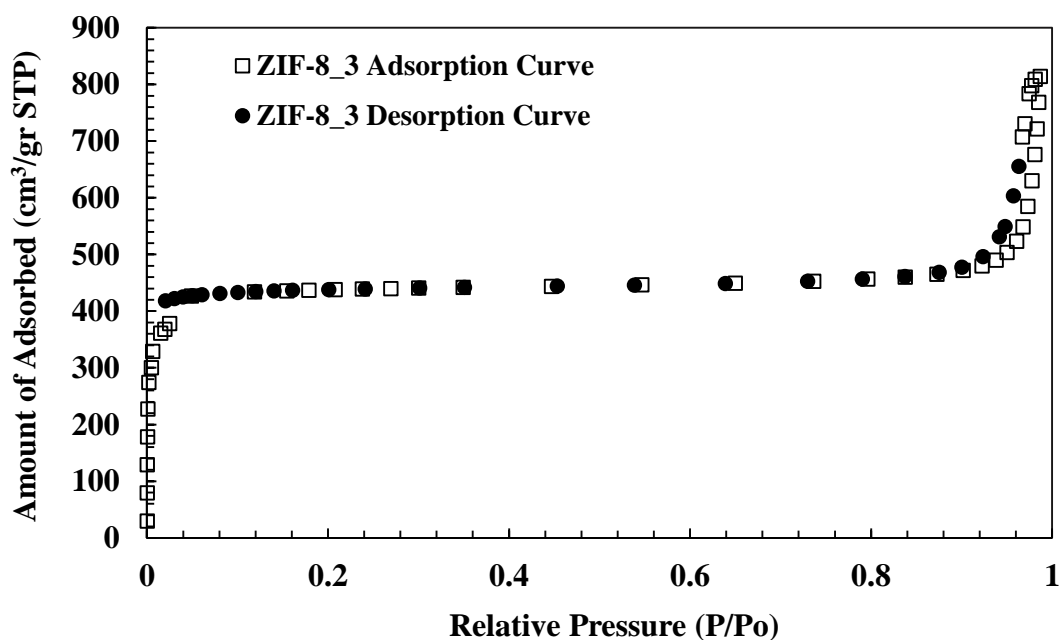


Figure 2.11 N₂ adsorption/desorption isotherms of ZIF-8_3 crystals with 65 nm average particle size

2.5 Morphology of pure PES Asymmetric Membranes (SEM Results)

The separation performance (van de Witte et al., 1996) and mechanical strength of a membrane strongly are contingent upon morphology. Hence, in this study, morphology of membrane was investigated deeply. In this section, the effect of strong non-solvent (water) or solvent (DMF) content in IPA coagulation bath on membrane morphology was studied.

The asymmetric PES membranes and PES-ZIF-8 asymmetric membranes prepared via wet phase inversion method were listed in Table 2.4 and in Table 2.5, respectively. Membrane codes and membrane preparation properties were available in these tables.

Table 2.4 Pure PES membranes and preparation properties. The total volume of solvent was 10 ml. The coagulation bath was at room temperature and the total volume of coagulation bath was 500 ml.

Membrane Code	Casting solution	Coagulation Bath (500 ml.)
PP-1	2 g PES + 10 ml DMF	Pure IPA
PP-2	2 g PES + 10 ml DMF	Pure IPA
PP-3	2 g PES + 10 ml DMF	Pure IPA
PP-4	2 g PES + 10 ml DMF	Pure IPA
PP-5	2 g PES + 10 ml DMF	Pure IPA
PP-6	2 g PES + 10 ml DMF	Pure IPA
PP-7	2 g PES + 10 ml DMF	IPA/H ₂ O:98/2 vl.%
PP-9	2 g PES + 10 ml DMF	Pure IPA
PP-10	2 g PES + 10 ml DMF	IPA/H ₂ O:50/50 vl.%
PP-11	2 g PES + 10 ml DMF	IPA/DMF:75/25 vl.%
PP-12	2 g PES + 10 ml DMF	IPA/H ₂ O:75/25 vl.%
PP-13	2 g PES + 10 ml DMF	IPA/DMF:75/25 vl.%
PP-14	2 g PES + 10 ml DMF	IPA/DMF:75/25 vl.%
PP-15	2 g PES + 10 ml DMF	IPA/H ₂ O:90/10 vl.%
PP-16	2 g PES + 10 ml DMF	IPA/H ₂ O:95/5 vl.%
PP-17	2 g PES + 10 ml DMF	IPA/H ₂ O:90/10 vl.%
PP-18	2 g PES + 10 ml DMF	IPA/H ₂ O:90/10 vl.%
PP-19	2 g PES + 10 ml DMF	IPA/H ₂ O:95/5 vl.%
PP-20	2 g PES + 10 ml DMF	IPA/H ₂ O:95/5 vl.%
PP-21	2 g PES + 10 ml DMF	IPA/H ₂ O:93/7 vl.%
PP-22	2 g PES + (10 ml) DMF/IPA:90/10	IPA/H ₂ O:95/5 vl.%
PP-23	2 g PES + (10 ml) DMF/IPA:90/10	IPA/H ₂ O:95/5 vl.%
PP-24	2 g PES + 10 ml DMF	IPA/DMF:70/30 vl.%
PP-25	2 g PES + 10 ml DMF	IPA/H ₂ O:95/5 vl.%

Table 2.4 (Cont.) Pure PES membranes and preparation properties. The total volume of solvent was 10 ml. The coagulation bath was at room temperature and the total volume of coagulation bath was 500 ml.

Membrane Code	Membrane solution	Coagulation Bath
PP-26	2 g PES + 10 ml DMF	IPA/H ₂ O:95/5 v l.%
PP-31	4 g PES + 10 ml DMF	IPA/H ₂ O:90/10 v l.%
PP-32	4 g PES + 10 ml DMF	IPA/H ₂ O:90/10 v l.%
PP-33	3 g PES + 10 ml DMF	IPA/H ₂ O:90/10 v l.%
PP-35	3 g PES + 10 ml DMF	IPA/H ₂ O:90/10 v l.%
PP-36	2 g PES + 10 ml DMF	IPA/H ₂ O:98/2 v l.%

Table 2.5 Mixed matrix PES-ZIF-8 membranes and preparation properties. The total volume of solvent was 10 ml. The coagulation bath was at room temperature and the total volume of coagulation bath was 500 ml.

Membrane Code	Casting Solution	Coagulation Bath (500 ml.)
MMM-1	2 g PES + 10 ml DMF + % 10 (type 2 treatment) 25 nm ZIF-8	Pure IPA
MMM-2	2 g PES + 10 ml DMF + % 5 (type 2 treatment) 25 nm ZIF-8	Pure IPA
MMM-3	2 g PES + 10 ml DMF + % 5 (type 1 treatment) 25 nm ZIF-8	Pure IPA
MMM-4	2 g PES + 10 ml DMF + % 5 (type 3 treatment) 25 nm ZIF-8	Pure IPA
MMM-5	2 g PES + 10 ml DMF + % 5 (type 1 treatment) 15 nm ZIF-8	Pure IPA
MMM-6	2 g PES + 10 ml DMF + % 5 (type 1 treatment) 25 nm ZIF-8	Pure IPA
MMM-7	2 g PES + 10 ml DMF + % 5 (type 1 treatment) 65 nm ZIF-8	Pure IPA
MMM-8	2 g PES + 10 ml DMF + % 5 (type 1 treatment) 25 nm ZIF-8	Pure IPA
MMM-9	2 g PES + 10 ml DMF + % 10 (type 1 treatment) 25 nm ZIF-8	Pure IPA
MMM-10	2 g PES + 10 ml DMF + % 10 (type 1 treatment) 65 nm ZIF-8	Pure IPA
MMM-11	2 g PES + 10 ml DMF + % 10 (type 2 treatment) 25 nm ZIF-8	Pure IPA
MMM-12	2 g PES + 10 ml DMF + % 10 (type 2 treatment) 65 nm ZIF-8	Pure IPA
MMM-13	2 g PES + 10 ml DMF + % 10 (type 2 treatment) 65 nm ZIF-8	IPA/H ₂ O:95/5 v.l.%

Table 2.5 (Cont.) Mixed matrix PES-ZIF-8 membranes and preparation properties. The total volume of solvent was 10 ml. The coagulation bath was at room temperature and the total volume of coagulation bath was 500 ml.

Membrane Code	Casting Solution	Coagulation Bath
MMM-15	2 g PES + 10 ml DMF + % 10 (type 2 treatment) 65 nm ZIF-8	IPA/H ₂ O:95/5 v.l.%
MMM-18	2 g PES + 10 ml DMF + % 10 (type 2 treatment) 65 nm ZIF-8	IPA/H ₂ O:90/10 v.l.%
MMM-19	2 g PES + 10 ml DMF + % 10 (type 2 treatment) 65 nm ZIF-8	IPA/H ₂ O:90/10 v.l.%
MMM-20	2 g PES + 10 ml DMF + % 10 (type 2 treatment) 65 nm ZIF-8	Pure IPA
MMM-25	2 g PES + 10 ml DMF + % 5 (type 1 treatment) 15 nm ZIF-8	Pure IPA
MMM-26	2 g PES + 10 ml DMF + % 5 (type 1 treatment) 15 nm ZIF-8	Pure IPA
MMM-27	2 g PES + 10 ml DMF + % 10 (type 1 treatment) 15 nm ZIF-8	Pure IPA
MMM-28	2 g PES + 10 ml DMF + % 10 (type 1 treatment) 15 nm ZIF-8	Pure IPA
MMM-29	2 g PES + 10 ml DMF + % 10 (type 1 treatment) 65 nm ZIF-8	Pure IPA

Figure 2.12 shows the SEM micrographs of pure PES membranes prepared in coagulation bath made up of pure IPA, IPA/H₂O:98/2 (in %v/v), IPA/H₂O:95/5 (in %v/v), IPA/H₂O:93/7 (in %v/v), IPA/H₂O:90/10 (in %v/v) mixture. According to qualitative analyze, the thickness of support layer and total membrane increased while thin selective layer thickness decreased with increasing the water content of the coagulation medium. For membranes prepared in coagulation bath including water content equal or less than 10 percent, the selective skin layer was non-porous, dense and had a thickness greater than 5 μm . The support layer of these type of membranes was made up of spongy pores and has symmetric pores structure. The pore size was uniform with approximately a diameter of 4 μm .

Figure 2.13 shows the SEM micrographs of pure PES membranes prepared in coagulation bath made up of IPA/H₂O:25/75 (in v/v %), and IPA/H₂O:50/50 (in v/v %) mixture. Since water content exceeded 20% percent, the morphology of membranes changed significantly. Existence of water in high percent (>20%), led to sharp decrease in selective skin layer thickness. For these type of membranes, the selective skin layer was thinner than 500 nm. The support layer of these type of membranes was in asymmetric shape and made up of both spongy pores and finger like pores. Pore size was not uniform and altered depending on both pore type and location on the layer. The size of the finger-like pores located just below the skin layer were smaller than that of finger-like pores located 20 μm farther from skin layer. When the water content of coagulation medium is 25%, finger like pores settle into just below the selective thin layer of membrane. By increasing water content from 25% to 50%, both size and number of finger like pores increases.

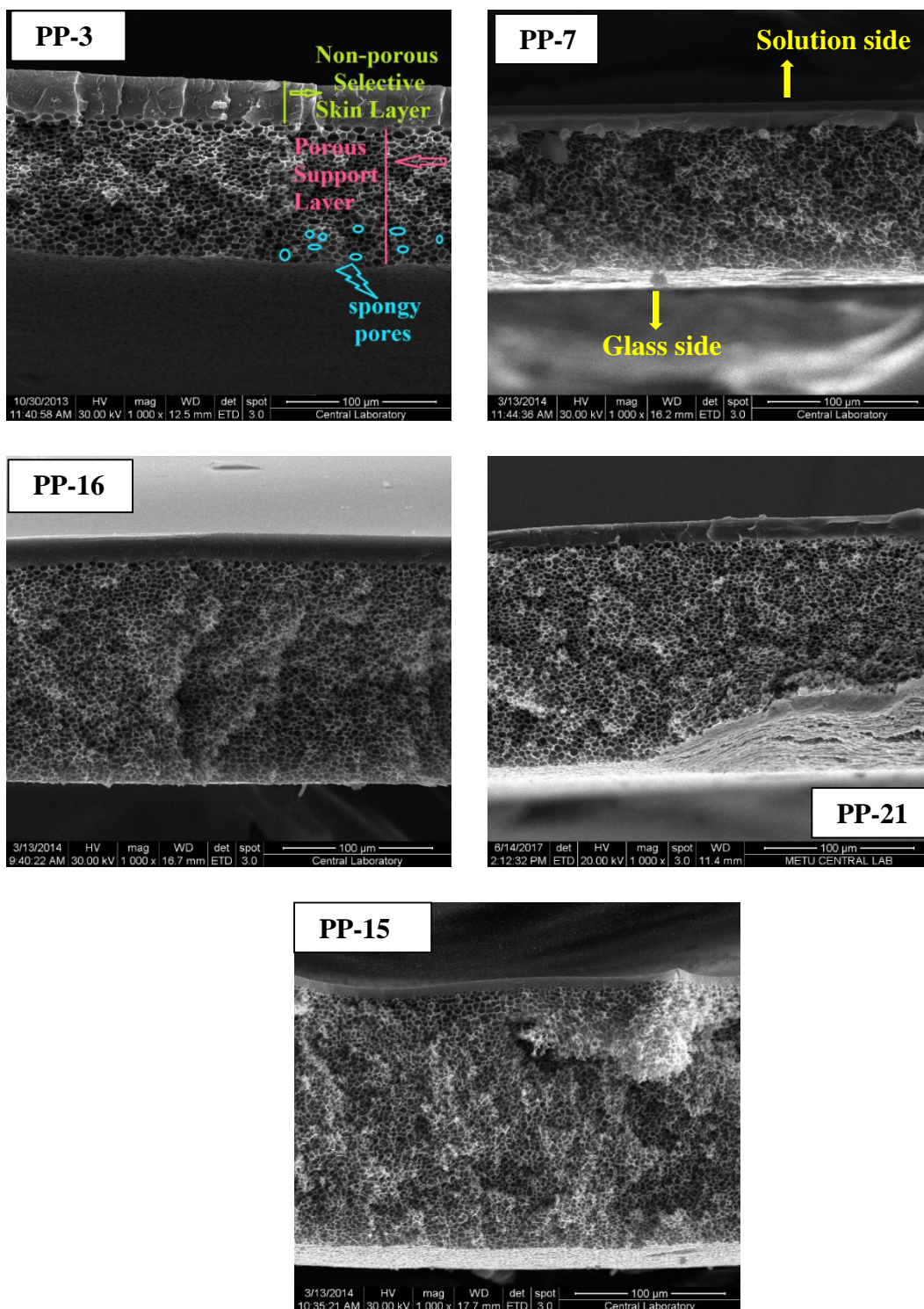


Figure 2.12 SEM micrograph of the neat PES membranes quenched in pure IPA (PP-3), %2 water-%98 IPA (PP-7); %5 water-%95 IPA (PP-16); %7 water-%93 IPA (PP-21); %10 water-%90 IPA (PP-15) coagulation bath.

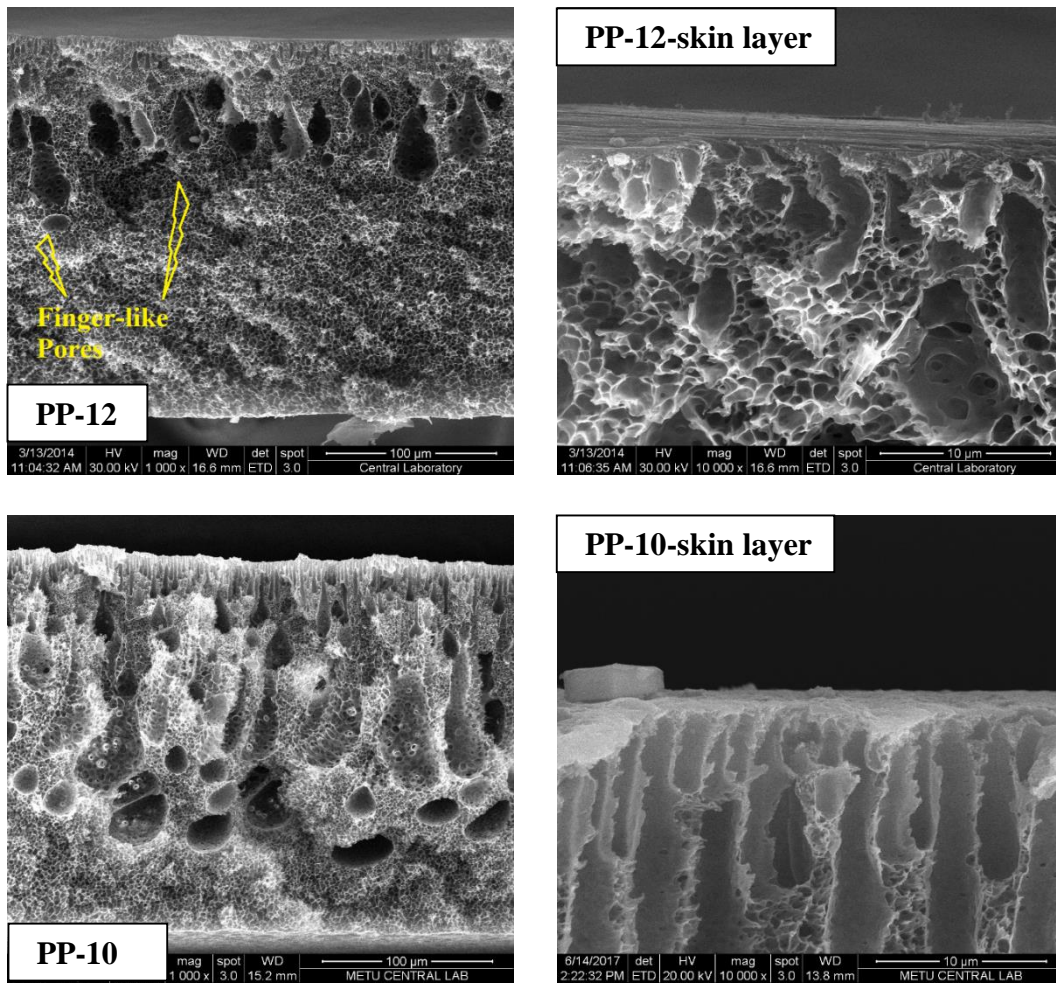


Figure 2.13 SEM micrograph of the neat PES membrane quenched in %25 water-%75 IPA (PP-12); %50 water-%50 IPA (PP-10) coagulation bath.

Table 2.6 was given the quantitative analyses of morphological properties of membranes based on SEM images. The morphological properties of membranes quenched in IPA/H₂O bath were compared to that of membranes quenched in pure IPA bath. The percent of decrease in the thickness of non-porous selective layer was 33.19%, 36.57%, 55.56%, 79.19%, 98.91%, and 99.18%; while the percent of increase in the thickness of porous support layer was 5.82%, 65.63%, 66.41%, 94.50%, 153.13%, 150.08% corresponding to the increase in the amount of H₂O content in coagulation medium with 2%, 5%, 7%, 10%, 25% and 50% respectively. As a general trend, size of the spongy like pores diminished while total thickness of membrane increased with increase of water content in coagulation medium.

I thought that total thickness of the membrane was determined by pores, because the total volume of pores in the membrane is greater than that of dense skin layer. Hence, my expectation was that as the pore sizes became smaller, the membrane had a smaller volume and a lower total thickness. Actually, increase of support layer thickness despite the diminish in pores size was out of our expectation. When the SEM images were investigated carefully, it was observed that the number of pores per unit area increased with increase of water content in IPA. For example, the number of pores per $1000 \mu\text{m}^2$ was counted as 65 for membrane PP-3 quenched in pure IPA coagulation bath. On the other hand, the number of spongy pores per $1000 \mu\text{m}^2$ of PP-12 was counted approximately 270. Probably, increase in both the thickness of support layer and total membrane was not related to the size of the pores but related to the number of pores which tends to increase with addition of water. When the water content reached to 25% percent in coagulation medium, small spongy pores merged and formed finger like pores. When the water content reached to 50%, both the number and size of the finger like pores increased. However, the uniformity in the size of the pores degenerated and standard deviation in pore size increased.

Change in morphological properties of membranes based on coagulation medium composition was explained according to the strength of coagulant. IPA is weak nonsolvent of PES ($\Delta\delta_{\text{PES-IPA}} = 9.2$; $\Delta\delta_{\text{PES-water}} = 34.4$) while water is the strongest one as explained in Chapter 2.2 deeply. Weak nonsolvents create binodal curve farther to solvent-polymer axes, whereas strongest nonsolvent produced binodal curve closer to the polymer-solvent axes (Sukitpaneemit and Chung et al. 2009; Spruck et al., 2014). Hence small amount of strong nonsolvent is sufficient to begin phase separation and system is more tend to instantaneous demixing. As explained in detail Chapter 2.1, the instantaneous demixing formed thin selective layer with large finger like pores and delayed demixing produced thicker dense selective layer with sponge like pores (Reuvers 1987). In our PES-DMF-IPA ternary system delayed demixing was dominant in phase separation because IPA is weak nonsolvent and stability region of these ternary system (Region 1; Figure 2.2)

is larger when compared PES-DMF-water system. Because of the delayed demixing, dense and thicker selective layer was obtained. By addition of water in the coagulation bath, the stability area (Region 1, See Figure 2.2) diminished and binodal line became closer to the initial polymer solution. Hence, instantaneous demixing became dominant gradually. When the water content reached %25, instantaneous demixing formed thin selective layer with finger like porous support layer. Effect of alcohol-water concentration in coagulation medium on formation of membrane morphology was studied and similar trend was also observed by several researches (Ali et al. 2007; Spruck et al., 2014, Deshmukh and Li, 1998; Sukitpaneent and Chung, 2009).

Table 2.6 Morphology of membranes prepared in coagulation bath with different amount of water content.

Membrane Code	Coagulation Bath Composition (in %v/vl.)	Skin Layer Thickness (μm)	Support Layer Thickness (μm)	Pore Shape	Pore Size (μm)
PP-3	Pure IPA	27.54 ± 1.62	87.68 ± 1.71	Spongy	5.10 ± 1.53
PP-7	IPA/H ₂ O:98/2	18.40 ± 1.58	92.78 ± 2.83	Spongy	4.77 ± 1.60
PP-16	IPA/H ₂ O:95/5	17.47 ± 1.19	145.22 ± 2.04	Spongy	3.88 ± 1.12
PP-21	IPA/H ₂ O:93/7	12.24 ± 2.35	145.91 ± 2.07	Spongy	4.13 ± 1.36
PP-15	IPA/H ₂ O:90/10	5.73 ± 0.63	170.54 ± 3.70	Spongy	3.72 ± 1.13
PP-12	IPA/H ₂ O:75/25	0.301 ± 0.095	221.94 ± 1.64	Spongy	2.93 ± 1.11
				Finger-like closer to skin layer	5.59 ± 2.50
				Finger-like located at the middle	31.54 ± 11.63
PP-10	IPA/H ₂ O:50/50	0.225 ± 0.050	219.27 ± 2.45	Spongy	2.19 ± 0.85
				Spongy located at the middle	22.28 ± 8.19
				Finger-like closer to skin layer	8.56 ± 6.41
PP-13	IPA/DMF:25/75	13.64 ± 2.05	100.01 ± 20.16	Finger-like located at the middle	53.61 ± 20.48
PP-24	IPA/DMF:30/70	8.45 ± 0.72	119.14 ± 2.48	Spongy	5.38 ± 1.79
				Spongy	4.24 ± 1.14

Figure. 2.14 shows the SEM image of membrane (PP-13) quenched in IPA/DMF:75/25 (in %v/v) and membrane (PP-24) quenched in IPA/DMF:70/30 (in %v/v) coagulation medium. When the structural properties of PP-3 (quenched in pure IPA bath) was compared to PP-13 and PP-24; at first glance, decrease in selective skin layer thickness and increase in porous support layer thickness was noticed clearly. Table 2.6 was provided the quantitative morphological analyze of PP-13 and PP-24. The percent of decrease in the thickness of non-porous selective layer was 50.47%, 69.32%; while the percent of increase in the thickness of porous support layer was 14.06%, 35.88% corresponding to the increase in the amount of DMF content in coagulation medium with 25% and 30%, respectively.

Addition of solvent in the coagulation medium shifts the binodal lines to the polymer-nonsolvent axes which implies thermodynamically more stable ternary system (Chun et al. 2000). Moreover, coagulation strength of solution diminished and the ratio of counter-diffusion rate of solvent to nonsolvent decreased. These causes delayed demixing (Groth et al. 2013; Chun et al. 2000). Results contradictory of our observations was reported by Chun et al. 2000 that addition of DMAc in water coagulation bath resulted in thicker skin layer with less porous membrane structure for PI-DMAc-water ternary system. Mansoori et al. 2011 observed that addition of DMAc into water coagulant caused to change the pore shape from finger like to sponge like, and formation of skin layer prevented due to solvent in coagulant for DMAc-PSF-THF-EtOH membrane solution. Similarly, suppression of skin layer formation in the presence of solvent in coagulant was also reported by Wijmans et al. 1983.

In our study, delayed demixing in the formation of PP-13 and PP-24 membranes was also observed. Precipitation took one night for these type of membranes. Despite the delayed demixing, the obtained skin layers were thinner than expected. The contradiction in literature and our unexpected result come from the complex nature of membrane formation. Probably, delayed demixing, position of binodal curve or counter diffusion rate of solvent-coagulant system are not sufficient to explain morphology of membrane. Moreover, the observation may

alter based on polymer-solvent-nonsolvent system or composition of the ternary system. In my opinion, for our PES-DMF-IPA system, the existence of DMF in IPA coagulant enhanced delayed demixing. However, thinner selective layer obtained despite the delayed demixing because DMF in the coagulant prevented the formation of skin layer as observed by Mansoori et al. 2011 while IPA tried to precipitate the polymer in the skin layer. These competitive precipitation dissolution process resulted in thinner selective skin layer than expected. Drastically decrease in membrane thickness and porosity were attributed to slower demixing and the slower gelation as described by Buonemenna et al. 2004.

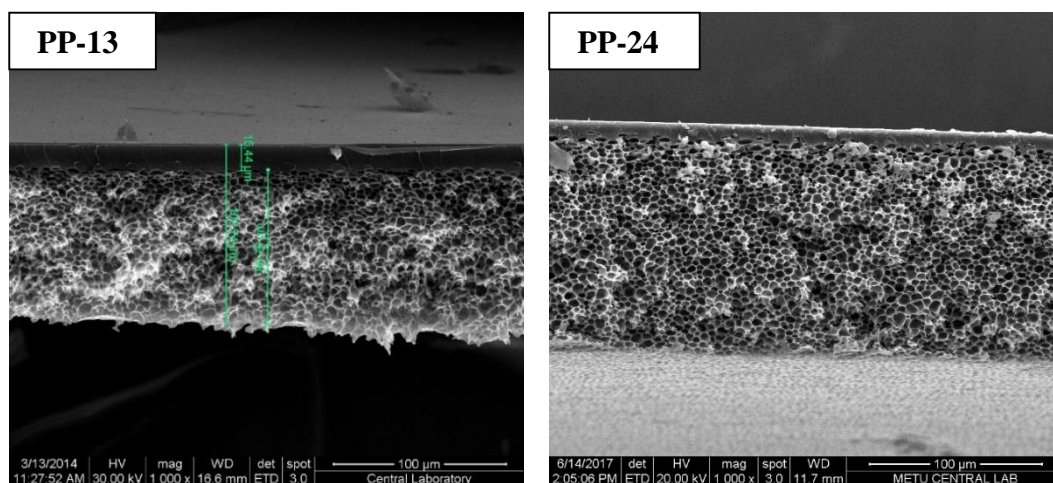


Figure 2.14 SEM micrograph of the PES membrane quenched in IPA/DMF:75/25 (in % vl.) coagulation medium, left hand side, PP-13; and PES membrane quenched in IPA/DMF:70/30 (in % vl.) coagulation medium, right hand side, PP-24.

Figure 2.15 shows SEM micrographs of membranes prepared from polymer solutions with 17.4 wt%, 24 wt% and 29.6 wt% PES-DMF mixture and quenched in IPA/H₂O:90/10 (in % vl.) coagulation medium. An increase in the porous support layer thickness and a growth in the size of the pores was observed. The quantitative analysis of SEM images was provided in Table 2.7. The percent of increase in support layer thickness was % 11.96 and %23.89 while the percent of growth in size of the pores was %57.80 and %60.48 corresponding to the increment in PES

concentration from % 17.4 to %24 and %29.6. Increment in support layer thickness may be a reason of growth in the size of the spongy-pores on the support layer.

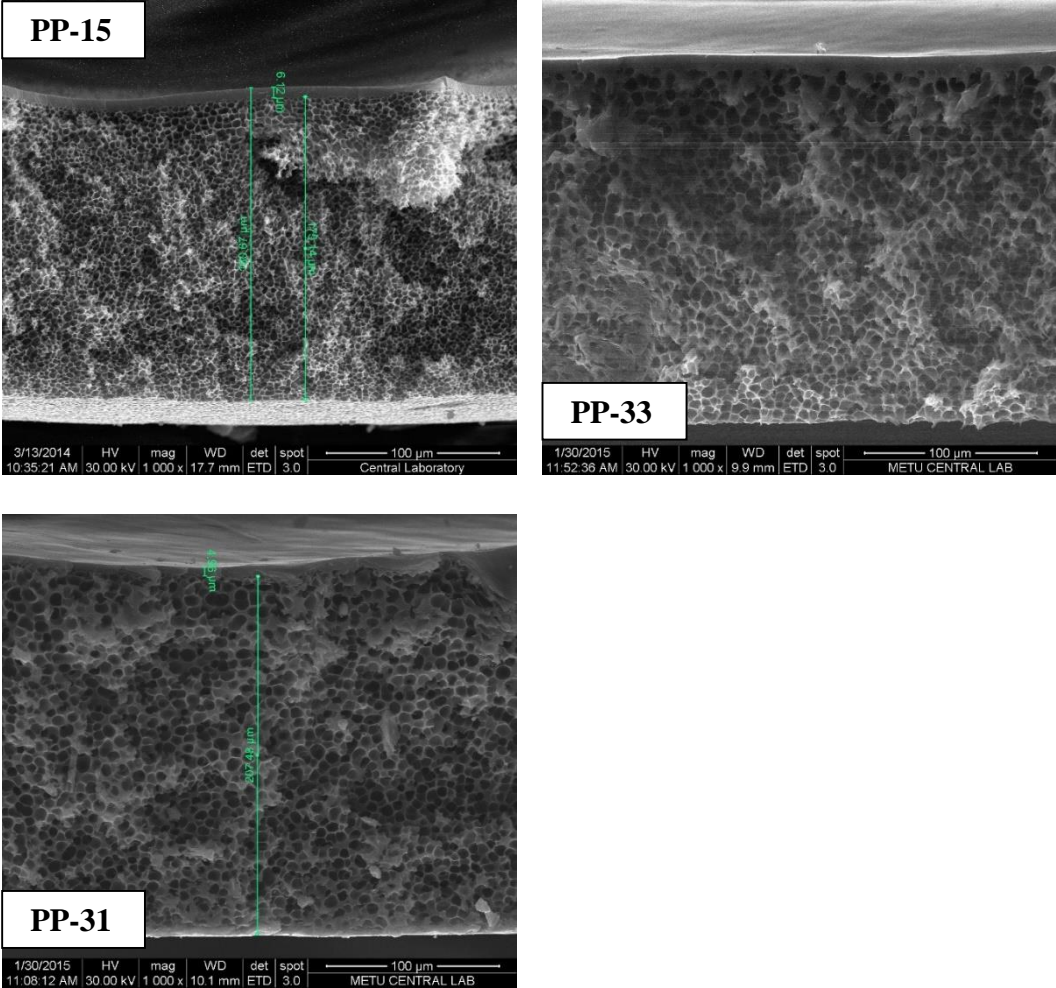


Figure 2.15 SEM micrograph of the PES membrane made up of 17.4 wt% PES-DMF solution (PP-15); 24 wt% PES-DMF solution (PP-33) and 29.6 wt% PES-DMF solution quenched in IPA/H₂O:90/10 (in % v/v.)

Table 2.7 Morphology of membranes prepared with different amount of PES concentration in DMF concentration and quenched by IPA/H₂O:90/10 (in %v/v) coagulation medium. Pore shape is spongy for this type of membranes.

Membrane Code	PES Concentration (wt.%)	Skin Layer Thickness (μm)	Support Layer Thickness (μm)	Pore Size (μm)
PP-15	17.4%	5.73 ± 0.63	170.54 ± 3.70	3.72 ± 1.13
PP-33	24%	5.70 ± 2.17	190.94 ± 13.57	5.87 ± 1.62
PP-34	29.6%	5.49 ± 0.96	211.28 ± 3.54	5.97 ± 1.65

Generally, high polymer concentration is preferred especially for gas separation membranes since high polymer concentration hinders the voids in the skin layer (Ismail and Lai 2003). Yu et al. 2014 showed that increase in PSF concentration for PSF-DMF-water ternary system resulted in increment in skin layer thickness and total membrane cross-section thickness and suppress the size of the pores. This result is contradicting to our observations about decrease in skin layer thickness and growth in pore size. Yu et al. 2014 claimed that when the polymer concentration is below the critical point, diffusion of non-solvent leads to rapid growth of polymer lean phase and hence macrovoids formation is enhanced. When the polymer concentration exceeds the critical point, since the polymer lean layer cannot locate below the critical point, macrovoids formation is prevented. Ismail and Li 2003 induced that high polymer concentration provides thick and dense skin layer with finely distributed pores on the support layer while low polymer concentration forms thin selective layer with uniform large voids on substructure. This is in good agreement with finding of Yu et al. 2014 and contradicting to our results. Van de Witte et al. 1996 claimed that increase in polymer concentration leads to increase in the thickness of top layer and size of the pores while suppress the interconnectivity of the pores and the formation of macrovoids. Assertions of Van de Witte et al. 1996 is not compatible with our observation of decrease in top layer thickness, however supports our findings of increase in size of the voids.

Increase in polymer concentration may lead delayed demixing as well as instantaneous demixing depending on solvent and nonsolvent, interaction between chemicals of the ternary system, and diffusion kinetics of solvent and nonsolvent. The required amount of non-solvent for precipitation of polymer decreased with increasing the concentration of polymer solution. Therefore, high polymer concentration results in rapid coagulation and instantaneous demixing (Ismail and Lai 2003). On the other hand, diffusional exchange rate between solvent and nonsolvent was retarded because of high polymer concentration at the interface. That slows down the precipitation promotes delayed demixing process. Hence delayed demixing creates dense and thick selective layer with finny sponge like pores (Ismail and Lai 2003; Julian and Wenten 2012; Smolders et al. 1992). Smolders et al. 1992 claimed that growth in the thickness due to extension of delay time.

In my opinion, increment of polymer concentration in our PES-DMF-(IPA/Water) system promotes instantaneous demixing. Hence thinner skin layer with larger spongy pores on support layer was obtained. One of the reasons is faster precipitation due to reduction in required amount of non-solvent at high polymer concentration.

Figure 2.16 shows SEM micrographs of membrane PP-22 prepared from polymer solutions with 17.6 wt% PES, 75.4 wt% DMF and 7 wt% IPA mixture and quenched in IPA/H₂O:95/5 (in %v/v) coagulation medium. At first glance, it was observed a skin layer thinner than that of membrane(PP-16) prepared PES-DMF casting solution quenched in IPA/H₂O:95/5 (in %v/v) coagulation medium. There are several studies showed that promotion of instantaneous demixing due to existence of non-solvent in casting solution causes thinner skin layers (Yeow et al. 2003; Mansourizadeh and Ismail 2011). In Figure 2.16 which is of a higher magnification, it was noted that skin layer composed of two-layer; namely very squashy non-dense layer, and just below it a thick dense layer. The squashy non-dense layer has defects; small voids on it. Partly, macro-voids formed at interface between dense thick layer and squashy layer. As far as our best knowledge from the

literature, such a layer-by-layer skin is not reported previously. According to my point of view, the casting polymer layer was not uniform and phase inversion began before wet quenching. During the time period between casting and wet phase inversion, liquid-liquid decomposition formed instantaneously at the surface region of the casting polymer solution. The possible reason is that outermost surface might be very close to pass two phase region due to combinational effect of high polymer concentration (due to surface tension), existence of IPA and evaporation of IPA. Since this time was very short in our case, casting polymer system entered a new thermodynamics state via wet phase inversion. This new thermodynamic state formed dense layer below pre-existent squashy non-dense layer. According to quantitative analysis of SEM images via J-image analyzer, the thickness of squashy non-dense layer, dense skin layer, porous support layer and size of the pores was determined as 1.79 ± 0.45 , 6.54 ± 0.35 , 134.53 ± 0.82 , and 2.93 ± 0.81 μm respectively.

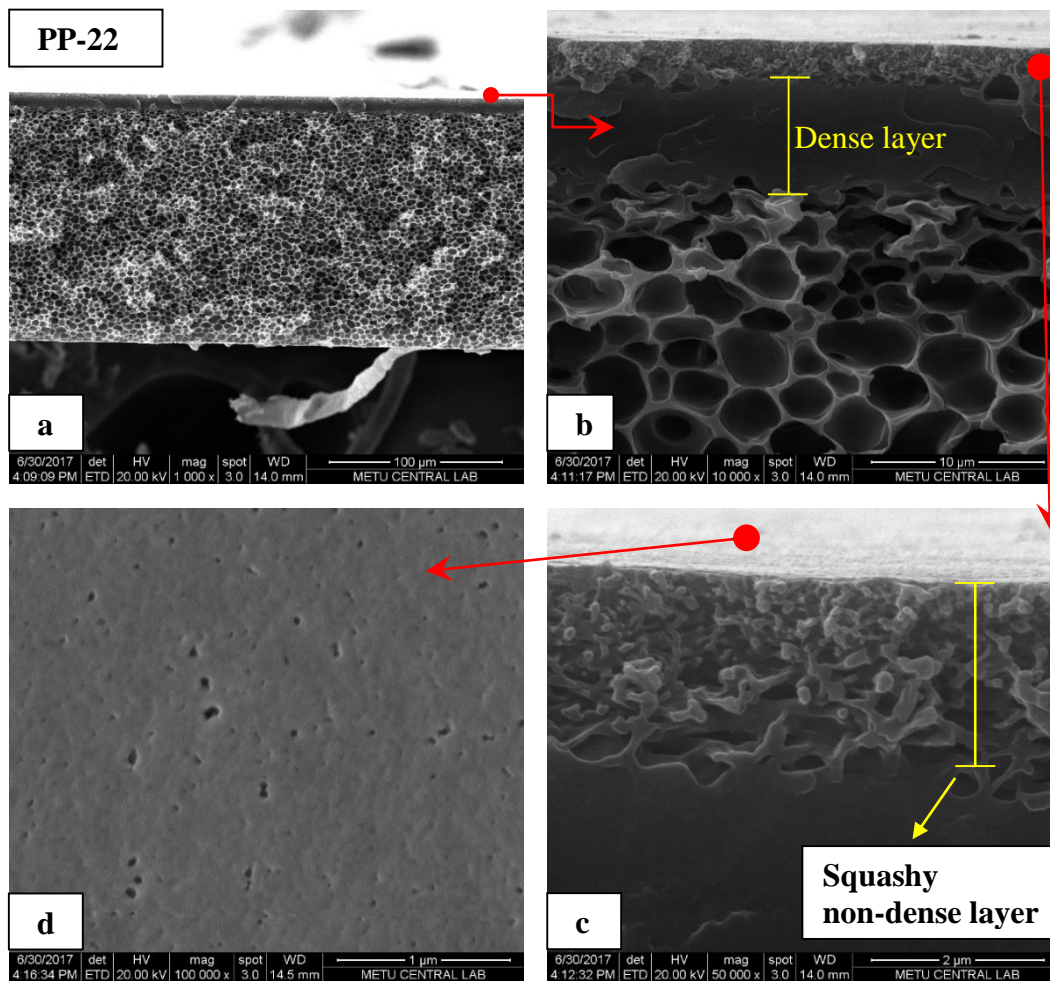


Figure 2.16 SEM micrograph of the PES membrane (PP-22) made up of PES (17.6%)-DMF(75.4%)-IPA(7.0%) (in wt.%) solution quenched in IPA/H₂O:95/5 (in % v/v). (a) Total cross-sectional view, (b) upper layer of membrane, (c) upper layer view at higher magnification, (d) surface of the membrane.

2.6 Morphology of Mixed Matrix PES-ZIF-8 Membranes

ZIF-8 crystals were treated. The purpose is to activate the pores of ZIF-8 before used as filler in mixed matrix PES membrane. Three different treatment methods were used. The details were provided in Chapter 2.3.2 in Experimental Method. Briefly, in type 1 treatment ZIF-8 was purified by washing with MeOH, in treatment 2 ZIF-8 was annealed at 180 °C and in treatment 3 ZIF-8 was purified

by washing DMF. Figure 2.17 presents the SEM micrographs of PES/ZIF-8 mixed matrix membranes; each membrane contained ZIF-8 (with 25 nm average particle size) treated by these three different methods. The amount of ZIF-8 was %5 of total PES. Since the separation performance of membrane is determined by skin layer, uniform distribution of filler throughout dense skin layer is crucial. At a closer look on skin layer, it was observed that Type 1 Treatment provided uniform distribution while Type 2 and Type 3 treatments lead to agglomeration of them. Agglomeration of fillers is associated with loss of membrane selectivity (Basu et al. 2011), hence Type 1 Treatment was preferred for mixed matrix membrane production.

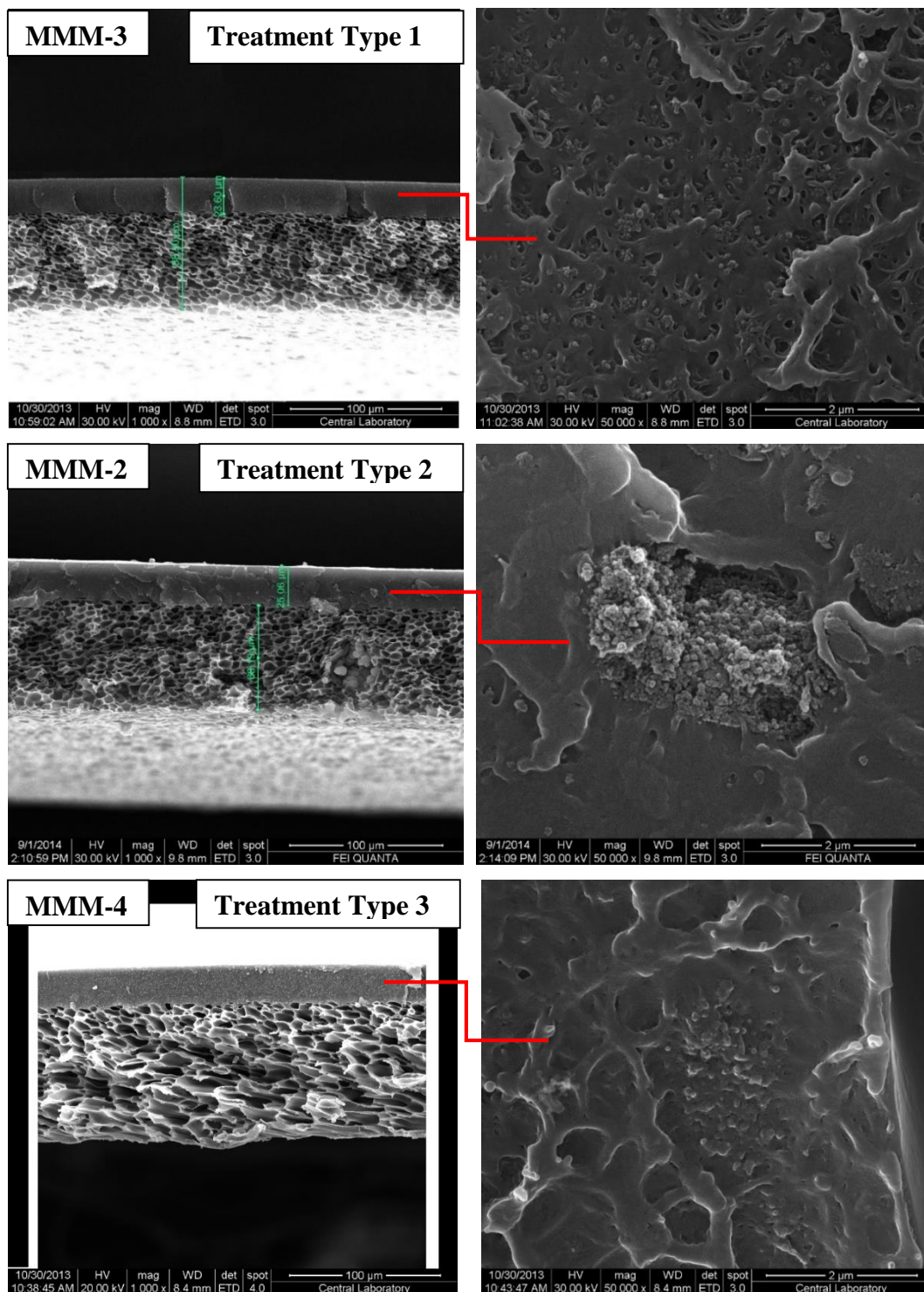


Figure 2.17 Cross-sectional SEM image of the PES/ZIF-8 (25 nm, %5 of PES) mixed matrix membranes quenched in pure IPA coagulation medium. Treatment method of ZIF-8 crystals was Type 1 (MMM-3); Type 2 (MMM-2); Type 3 (MMM-4).

Figure 2.18 presented the SEM images of PES/ZIF-8 (%5 of total PES) mixed matrix membranes with average particle size of 15 nm (MMM-5), 25 nm (MMM-3) and 65 nm (MMM-7). Since they were quenched in pure IPA coagulation medium, all have thick and distinct skin layer with spongy porous support layer. When MMMs were compared to neat PES membranes, it was noticed that addition of filler caused to decrease the support layer thickness and surprisingly increase the size of the spongy pores. When the mixed matrix membranes were compared among themselves, the enlargement in pore size of membrane MMM-5 including 15 nm ZIF-8 filler was more obvious than that of membranes including 25 nm (MMM-3) and 65 nm (MMM-7) ZIF-8. When the skin layer of MMM-5 and MMM-3 membranes were inspected at 50 000 magnifications, it was noted that the size of the filler added at 15 nm seems bigger than that of the filler added at 25 nm. As depicted in Figure 2.8, the ZIF-8 crystals were synthesized at three different size; 15 nm, 25 nm and 65 nm. However, after loading into membrane, the size of the particle enlarged. This is imputed clustering of particles of 15 nm in size. Actually, the tendency of agglomeration of particles at nano-size is the most important problem.

The SEM images of PES/ZIF-8 (%10 of total PES) mixed matrix membranes with average particle size of ZIF-8 15 nm (MMM-28), 25 nm (MMM-9) and 65 nm (MMM-10) were exhibited in Figure 2.19. The thick dense selective layer on support layer with spongy pores was the common trait. According to qualitative investigation of SEM images, the support layer thickness of membrane including 65 nm ZIF-8 at %10 percent of PES (MMM-10) decreased significantly. Increasing the amount of ZIF-8 from 5% to 10% for membranes MMM-28 (including 15 nm ZIF-8) and MMM-9 (including 25 nm ZIF-8) caused to increase in pore size and to alter in structure of the pores from spherical shape to elliptical shape. When the skin layer of MMM-28 was investigated at 50 000 magnifications, it was observed dense clustering so the boundaries of the ZIF-8 particles cannot be distinguished. On the other hand, perfect and homogeneous distribution of ZIF-8 crystals with 65 nm average particle size (MMM-10) was obtained despite the increase the loading amount.

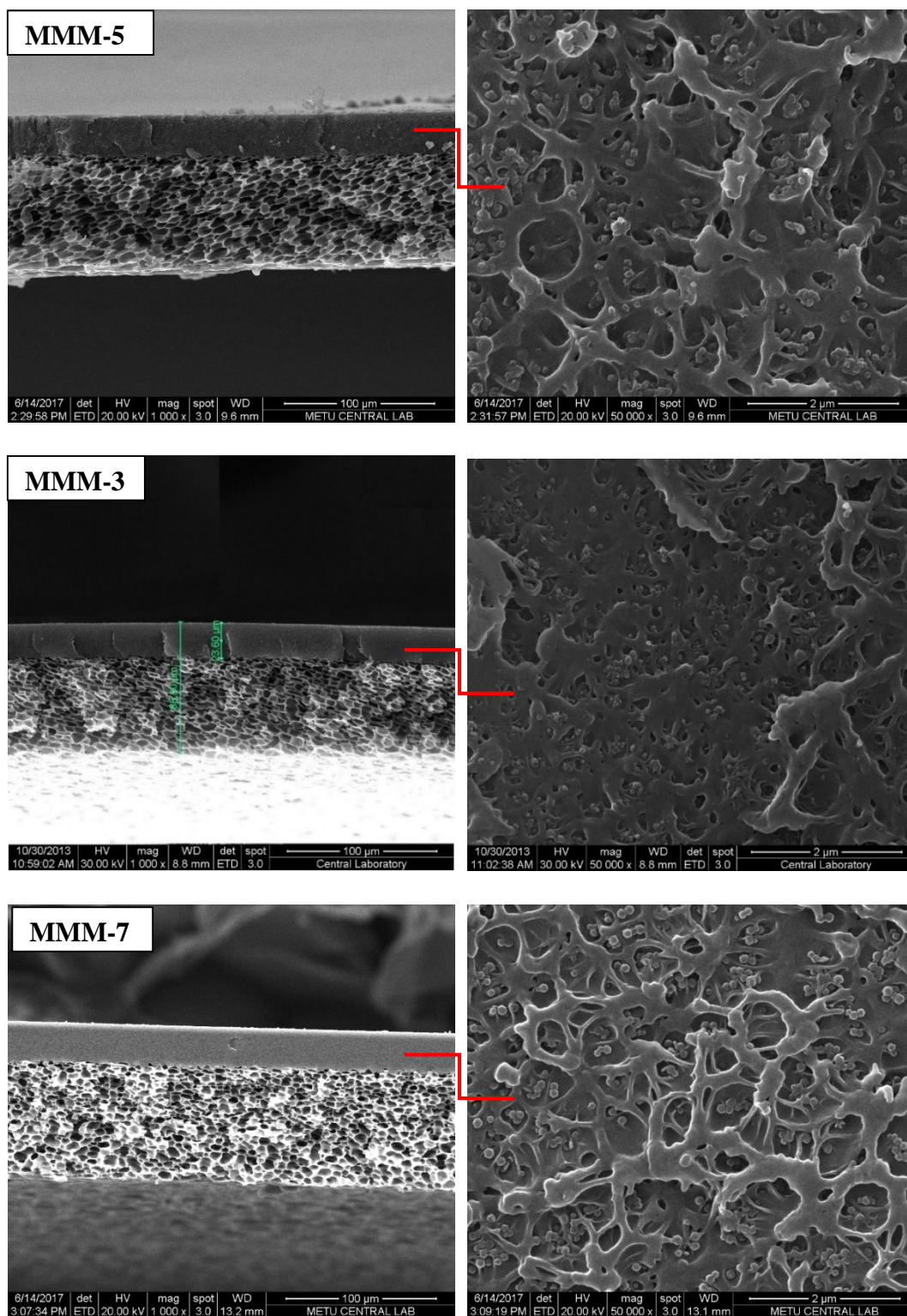


Figure 2.18 Cross-sectional SEM image of the PES/ZIF-8 (%5 of PES) mixed matrix membranes quenched in pure IPA coagulation medium. Average particle size of ZIF-8 was 15 nm (MMM-5); 25 nm (MMM-9) and 65 nm (MMM-10).

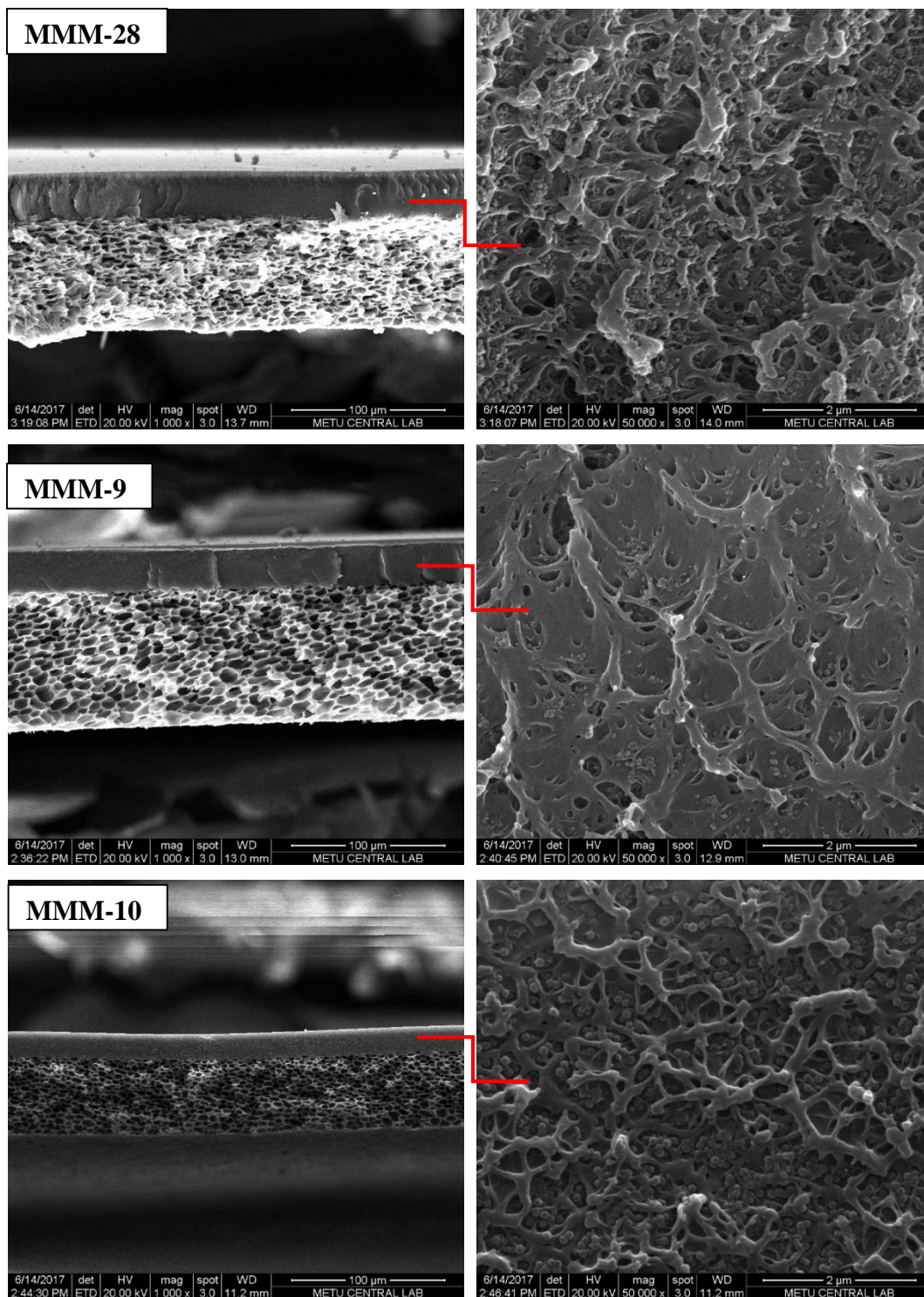


Figure 2.19 Cross-sectional SEM image of the PES/ZIF-8 (%10 of PES) mixed matrix membranes quenched in pure IPA coagulation medium. Average particle size of ZIF-8 was 15 nm (MMM-5); 25 nm (MMM-9) and 65 nm (MMM-10).

Table 2.8 Morphological properties of PES/ZIF-8 mixed matrix membranes containing ZIF-8 with average particle size of 15, 25 and 65 nm. Pure IPA was used as coagulation medium. PES concentration of membrane solution was 17.4%.

Membrane Code	ZIF-8 Content (wt.%)	Average crystal size of synthesized ZIF-8 (nm)	Average size of clustered ZIF-8 particles in membrane (nm)	Skin Layer Thickness (μm)	Support Layer Thickness (μm)	Pore Size (μm) (spongy pores)
PP-3	No	No	No	27.54 \pm 1.62	87.68 \pm 1.71	5.10 \pm 1.53
MMM-3	%5 (Type1)	25	40.4 \pm 11.82	22.62 \pm 0.71	61.37 \pm 1.91	6.03 \pm 2.02
MMM-2	%5 (Type2)	25	175 \pm 33	24.77 \pm 1.88	70.63 \pm 1.22	4.96 \pm 1.99
MMM-4	%5 (Type3)	25	69.69 \pm 28.20	24.25 \pm 0.74	87.82 \pm 2.68	12.17 \pm 5.29
MMM-9	%10 (Type1)	25	46.70 \pm 11.19	27.12 \pm 1.22	87.53 \pm 1.45	7.80 \pm 2.49
MMM-5	%5 (Type1)	15	82.67 \pm 15.93	27.04 \pm 1.12	74.15 \pm 2.19	7.71 \pm 2.68
MMM-28	%10 (Type1)	15	38.02 \pm 8.95	29.36 \pm 1.10	71.47 \pm 2.27	6.89 \pm 2.57
MMM-7	%5 (Type1)	65	86.71 \pm 15.50	25.49 \pm 0.70	75.75 \pm 1.62	5.70 \pm 2.04
MMM-10	%10 (Type1)	65	83.55 \pm 11.54	16.47 \pm 0.60	48.41 \pm 1.27	3.50 \pm 1.21

The morphological properties of PES/ZIF-8 mixed matrix membranes were listed and compared to neat PES membrane in Table 2.8. Both porous support layer, selective layer and pore size are affected from existence of ZIF-8 crystals which implies the influence of ZIF-8 crystals on the formation of membrane during non-solvent induced phase inversion. The change in morphology was strongly dependent on the amount of ZIF-8, the average particle size of ZIF-8, and the treatment methods of ZIF-8. As a general trend, existence of ZIF-8 made thinner skin and thinner support layer with larger pores with respect to neat PES membrane.

The percent of decrease in the selective layer thickness and support layer thickness depended on the pre-treatments of ZIF-8 crystals because the treatments methods effected the dispersion of crystals. The interactions and adhesion between homogeneously dispersed ZIF-8 crystals and polymer chains were stronger than those between non-homogeneous and aggregated ZIF-8 crystals and polymer chains because the homogeneously dispersed ZIF-8 particles have a larger surface area than the clustered ZIF-8 particles, and this larger surface area allows more interaction with the polymer chains. Hence stronger interaction and adhesion created thinner polymer layer. When the membranes MMM-3 (Treat. Type-1), MMM-2 (Treat. Type-2) and MMM-4 (Treat. Type-3) were compared to PP-3 neat PES membrane, the following conclusions have been drawn. The amount of decrease in the thickness of selective layer are 17.86 %, 10.00% and 11.95 % corresponding to the treatment type 1, type 2 and type 3 respectively. For treatment type 1 and treatment type 2, it was measured %30 and %19.45 decrease in support layer. For treatment type 3, no significant change observed in thickness of support layer despite striking growth in size of the pores. Because the pores extended in the horizontal plane relative to the membrane cross-sectional area, the increase in pore size was not influenced total membrane thickness. The average particle size of the filler dispersed on skin layer was increased by %61.6, %600 and %178.76 corresponding to the treatment Type 1, Type 2 and Type 3. Type 1 treatment prevented the aggregation of filler better than the other two methods. The highest homogeneous distribution of ZIF-8 crystals and minimum agglomeration are obtained by treatment type 1. By increase loading of 25 nm in size ZIF-8 from 5%

to 10%, the change in morphology of membrane diminished and the size of the skin layer and support layer became closer to that of neat PES membrane. However, the size of the pores enlarged %52.94 percent compared to the neat PES membrane due to %10 percent ZIF-8 loading.

The change in the skin layer of mixed matrix membranes including ZIF-8 of 15 nm was small and negligible, while it was observed substantial change in size of the pores and thickness of porous support layer. The percent decrease in thickness of support layer was determined as %25.43 and %18.49 compared to the neat PES membrane according to 15 nm ZIF-8 loading with %5 and %10, respectively. Despite the diminish in the thickness of support layer, enlargement in pores size was notable. Since the pores in elliptical shape extended in the horizontal plane relative to the membrane cross-sectional area, the increase in pore size was not affect the total membrane thickness.

When the average particle size of the loaded ZIF-8 crystals increased to 65 nm, especially at %10 loading, the variation in thickness of skin and support layer became more significant. %10 loading of ZIF-8 at 65 nm in size contributed to %40.20 decrease in thickness of the skin layer while %44.79 decline in thickness of support layer compared to the neat PES membrane. Unlike the general trend, the size of the pores reduced by %31.37, when the amount of ZIF-8 at 65 in size increased to %10 of PES.

Our observation about thinning of the selective skin layer in the presence of the ZIF-8 crystals is in good agreement with observations of Aroon et al. 2010 and Rezaei et al. 2015. Polymer solution including nano-sized particles enhances polymer- filler- polymer interactions which lead to tightly and densified polymer chains conformation. This makes thinner selective layer (Aroon et al. 2010). The molecular interactions caused by homogeneously dispersed ZIF-8 crystals are stronger than that created by non-homogenously dispersed ZIF-8 crystals. Hence the percent of decrease in the thickness of layer is higher for membranes including ZIF-8 crystals with Type 1 treatment. As claimed by Rezaei et al. 2015, fillers in polymer solution promotes liquid-liquid demixing rate by weaken the

thermodynamic stability, hence thinner selective layer formed. Moreover, addition of filler alters the viscosity of polymer solution which effects the solvent-nonsolvent exchange rate. High exchange rate created thinner selective layer and large porous support layer by stimulating instantaneous liquid-liquid demixing (Rezaei et al. 2015). This claim is consistent with our study. Probably, the ZIF-8 crystals alter the thermodynamic stability of polymer solution and interaction between solvent and non-solvent. As a result, polymer lean phase nucleation is enhanced. Therefore, the pore size increases and the sponge like pores turn into elliptical in shape. When the ZIF-8 with 65 nm in size loading reached % 10 of PES, probably high interaction between polymer-filler-polymer formed more stable system which hindered pore formation and smaller pores formed. Despite high stability, the obtained skin layer was thinner than expected because of the densified polymer chain conformation.

Conflicting studies with our observations have been reported by Aerts et al. 2000 part 1 and part 2. In this study, Aerts et al. reported that addition of Aerosil with average particle size of 12 nm shifted the binodal curve to solvent-polymer axes which indicated changing thermodynamic behavior of system. However, probably, the main effect of filler on membrane morphology came from the influence of fillers on phase inversion kinetics. Aerts et al. induced that a certain fillers concentration in the polymer solution slowed down the solvent-nonsolvent diffusion rate which decrease demixing rate. Hence thicker skin layer and thicker membrane layer formed.

Aerts et al 2000 and Zhang et al. 2006 reported the suppression of pore formation due to nano-sized fillers which is in agreement with our observation about decrease in pore size in the presence of % 10 of ZIF-8 crystals with 65 nm in size.

2.7 Gas Separation Test Results of neat PES Membranes

The H₂, CO₂, and CH₄ permeance of membrane quenched in IPA coagulation medium with different water content are presented in Table 2.9. The morphological properties of these membranes were available in Table 2.6. The

Table 2.9 also included the gas permeance values of dense PES membrane with $52 \pm 1 \mu\text{m}$ average thickness measured by micrometer caliper. The permeance of pure PES asymmetric membranes quenched in pure IPA bath is at least 2 times higher than that of pure PES symmetric membranes. This difference can be explained by the thickness of membrane. The thickness of selective layer of asymmetric PES membrane quenched in pure IPA was determined as $27.54 \pm 1.62 \mu\text{m}$ (Table 2.6) which was nearly half of the thickness of dense symmetric membrane. The ratio of increase in permeance is the same as the ratio of decrease in thickness of skin layer.

As a general trend, increase in water content of coagulation medium enhanced gas permeance values of membranes with small decrease in ideal selectivity. The water content lower than 7% in IPA has smaller effect on membrane permeance. 5% water content in IPA coagulation medium leads to approximately 10% increase in gas permeance of membrane. When the water content in coagulation medium increased from 0% to 10 vol. %, permeance of H_2 , CO_2 and CH_4 in the flat sheet membrane increase from 0.34 GPU to 1.095 GPU, from 0.16 GPU to 0.44 GPU, and 0.0045 GPU to 0.0312 GPU, respectively. CO_2/CH_4 ideal selectivity decreases from 35.6 to 14.1 and H_2/CH_4 ideal separation factor decreases from 75.6 to 35.1. The significant differences of gas permeance among membranes prepared from IPA coagulation medium including various water could be explained by referring to their morphologies as shown by SEM images (Figure 2.12). As indicated in SEM images, the non-porous selective skin layer thickness decreased with increase in the water content of coagulation medium. The permeance of an asymmetric membrane is inversely proportional to thickness of its skin layer. By decreasing the thickness of the skin layer, the mass transfer resistance of asymmetric membrane decreases (Ismail and Lai 2004; Kesting 1971). Hence high value of permeance can be achieved as observed in this study which was in agreement with studies carried by Deshmukh and Li 1998; and Ali et al. 2007. Selectivity of a membrane is an intrinsic property of polymer. The decrease in selectivity is attributed to variation of free-volume of the polymer layer due to production method (Kesting et al. 1990, Fritzsche et al. 1990) and variation in sorption capacity due to decrease in thickness (Punsalan and Koros 2005).

Membranes (PP12 and PP10) prepared in coagulation medium including %25 and %50 water in IPA medium were not presented in Table 2.9, because gas test of these membranes was very fast to detect data points and selectivity could not be detected. This ascribed to the porous skin layer.

Table 2.9 Permeance and selectivity values of membranes prepared in coagulation bath with different amount of water content in IPA.

Code	H ₂ O in IPA vl.%	Permeance (GPU)			Ideal Selectivity		
		H ₂	CO ₂	CH ₄	H ₂ /CO ₂	H ₂ /CH ₄	CO ₂ /CH ₄
PP0	Dense	0.17	0.07	0.0016	2.4	106.3	43.8
PP1-PP6, PP9	0	0.34	0.16	0.0045	2.1	75.6	35.6
PP7, PP36	2%	0.41	0.18	0.0042	2.4	100.1	42.5
PP16, PP19, PP20, PP25, PP26	5%	0.43	0.18	0.0050	2.4	87.9	36.4
PP21	7%	0.57	0.23	0.0102	2.5	56.3	22.8
PP15, PP17, PP18	10%	1.10	0.44	0.0312	2.5	35.1	14.1

The addition of solvent (DMF) into coagulation medium (IPA) improved both gas permeance and gas separation factor of asymmetric membrane as indicated in Table 2.10. It was observed that the polymeric membranes prepared in IPA coagulation bath with 25 vl. % DMF had CO₂ permeance 37 % higher and CH₄ permeance 24 % higher than that of prepared with pure IPA. By increasing the DMF content of the coagulation medium from 0 to 30 vl. %, H₂, CO₂ and CH₄ permeance

increased by 114 %, 94 % and 84 %, respectively. Since increment in CO₂ and H₂ permeance is higher than that in CH₄ permeance, the CO₂/CH₄ and H₂/CH₄ ideal separation factor were also improved. As investigated previously from SEM images, addition of solvent in coagulation medium formed thinner selective layer (Figure 2.14). Our gas test results and our morphological investigation were consistent, thus thinner selective layer provided higher gas permeance. The addition of solvent into non-solvent coagulation medium decreases the solubility parameter difference between the solvent and coagulant and also deteriorates the strength of coagulant. Smaller solubility parameter difference decreases the phase separation rate and induces delayed demixing which produced denser, less porous and macrovoids free selective structure (Strathmann et al. 1975; Groth et al. 2013; Chun et al. 2000). (The membrane formation took 15-20 minutes when pure IPA used as coagulant, while if took 6 hours by introducing the DMF into coagulation medium.) As a result, highly permeable membrane was obtained without sacrificing in selectivity. Our investigations about increase in permeance of membranes is compatible with several researchs in literature (Buonemenna et al. 2004; Mansoori et al. 2011). However, our investigation about enhancement in ideal selectivity could not be supported from literature. Mansoori et al 2011 claimed drastic decrease in selectivity due solvent addition in coagulation medium. Chun et al. 2000 suggested that small amount of solvent into coagulation medium led to denser membrane layer formation. Probably, similar situation is also valid for our polymer-solvent-nonsolvent system and enhancement in selectivity can be attributed to denser membrane structure. Since %25 DMF led to %10 increase in CO₂/CH₄ ideal selectivity and %23 increase in H₂/CH₄ ideal selectivity. When the DMF content of coagulation medium reached to %30, the determined ideal selectivity values were smaller than that of membranes prepared in %25 DMF-%75 IPA coagulant, but still higher than that of membranes prepared in pure IPA bath.

Table 2.10 Permeance and selectivity values of membranes prepared in coagulation bath with different amount of DMF content in IPA coagulation medium. Membrane casting solution made up of pure DMF and PES with 17.4 polymer concentration.

Code	DMF in IPA vl.%	Permeance (GPU)			Ideal Selectivity		
		H ₂	CO ₂	CH ₄	H ₂ /CO ₂	H ₂ /CH ₄	CO ₂ /CH ₄
PP1- PP6, PP9	0	0.34	0.16	0.0045	2.1	75.6	35.6
PP11, PP13, PP14	25%	0.52	0.22	0.0056	2.4	92.9	39.3
PP24	30%	0.73	0.31	0.0083	2.3	87.4	37.5
Ref.	Quench Bath Composition (vl.%)		Polymer	H ₂ (GPU)	CH ₄ (GPU)	H ₂ /CH ₄	
Mansoo- ri et al. 2011	H ₂ O (100%)		PSF	25	0.54	46.3	
	DMAc: H ₂ O; 40:60			12.1	0.36	33.6	
	DMAc: H ₂ O; 80:20			6.2	0.27	16.8	
	DMAc: H ₂ O; 90:10			3.7	0.23	16.1	

Table 2.11 presented the gas test results of membranes prepared from casting solutions with different polymer concentrations. H₂ permeance decreased from 1.095 GPU to 0.64 GPU, CO₂ permeance decreased from 0.44 GPU to 0.22 GPU and CH₄ permeance decreased from 0.0312 GPU to 0.0087 GPU by increasing the polymer concentration of casting solution from 17.4 wt.% to 29.6 wt.%. Subsequently, H₂/CH₄ and CO₂/CH₄ ideal selectivity enhanced by 100 % and 76%, respectively. Although it was not noted a significant effect of polymer concentration on membrane skin layer thickness (Figure 2.15), permeance and separation factor of membrane changed depending on polymer concentration. Because, the denser polymer solution modified the phase separation kinetics by increasing the casting solution viscosity. Effect of viscosity on polymer chain

entanglement was proved by Chung and Kafchinski 1997. Higher viscosity induced denser segmental packing and chain entanglement in the skin layer Hence lower permeance values were obtained. Moreover, more uniform skin layer was formed. This was associated to increase in the selectivity. Our observation about decrease in permeance with enhancement in selectivity with increase in polymer concentration was perfect agreement in literature (Aroon et al. 2010 (Separation and Purification Technology), Kurdi and Tremblay 1999; Ismail and Lai 2003).

Table 2.11 Permeance and ideal selectivity values of membranes prepared in casting solution with different amount of PES concentration. Membranes were quenched in coagulation medium composed of IPA/H₂O:90/10 (in % v/v.)

Code	PES in Casting Sol. wt.%	Permeance (GPU)			Ideal Selectivity		
		H ₂	CO ₂	CH ₄	H ₂ /CO ₂	H ₂ /CH ₄	CO ₂ /CH ₄
PP15, PP18	17.4%	1.095	0.44	0.0312	2.5	35.1	14.1
PP31	29.6%	0.64	0.22	0.0087	2.9	73.6	25.3
Ref.	PSF in Casting Sol. (wt.%)	Permeance (GPU)			Ideal Selectivity		
		H ₂	CO ₂	CH ₄	H ₂ /N ₂	CO ₂ /CH ₄	
Aroon et al. 2010	25%	-	9.64	4.02	-	2.29	
	30 %	-	7.26	1.64	-	4.43	
Ismail and Lai 2003	15%	130	-	-	18	-	
	19%	55	-	-	30	-	
	22%	30	-	-	45	-	
	29%	20	-	-	70	-	

The effect of IPA concentration in the polymer solution on membrane performance was depicted in Table 2.12. Addition of 10 v.l. % IPA into DMF solvent led to significant enhancement in H₂ permeance from 0.43 GPU to 1.33 GPU, in CO₂ permeance from 0.18 GPU to 0.54 GPU and in CH₄ permeance from 0.0050 GPU to 0.1220 GPU. The separation factor of membrane declined sharply from 36.4 to 4.6 for CO₂/CH₄ and from 87.9 to 11.3 for H₂/CH₄. The enhancement in permeance of membrane was attributed to the change of the phase separation behavior due to non-solvent additive. Addition of non-solvent into the polymer solution shifts the binodal curve and the spinodal curve towards the polymer/solvent axis which reduces single phase region. In other words, the casting solution becomes closer to the precipitation point. Therefore, the precipitation path shortens and precipitation process accelerates, liquid-liquid demixing enhances due to existence of nonsolvent in the polymer solution (Yeow et al. 2003; Mansourizadeh and Ismail 2011), thus thinner skin layer formed which promoted the higher permeance (Aroon et al. 2010 (Separation and Purification Technology)). The CO₂/CH₄ separation factor decreased sharply by 88 % (selectivity of 4.6 in comparison with 36.4). A possible reason was that pores or non-selective voids on the skin layer formed due to fast phase separation. As inspected from SEM images porous layer formed on dense skin layer. The pores on dense skin layer was connected to porous support layer under the skin layer. Therefore, membrane could not present its intrinsic ideal selectivity. Mansourizadeh and Ismail 2011 reported that addition of EtOH in to PVDF-NMP solution increased the surface porosity by two and a half times while doubled the N₂ permeance. This result was consistent with our observations about increase in permeance of membranes and formation of porous skin layer. Aroon et al. 2010 (Separation and Purification Technology) declared that the existence of non-solvent EtOH in PSF-NMP polymer solution enhanced both CO₂ permeance from 9.64 to 16.95 GPU and CO₂/CH₄ ideal selectivity from 2.39 to 5.09. The increment in selectivity is contradict to our finding but supported results of Wang et al 1996 and 2000. Authors associated the increase in gas permeance to instantaneous demixing and attributed the promotion of selectivity to suppression of voids

formation on the skin layer. The effects of the additives are not restricted only thermodynamic of phase inversion. The additives can also affect kinetically by altering the solvent-nonsolvent diffusion. Increase in solution viscosity due to additives retards solvent-nonsolvent diffusion, thus suppress voids formation (Aroon et al. 2010 (Separation and Purification Technology); Wang et al. 1996; and Wang et al. 2000).

To conclude, IPA in DMF-PES solution enhanced permeance by promoting instantaneous demixing but deteriorate the selectivity by promoting solvent-nonsolvent exchange rate. Highly probably, addition of IPA in casting solution decreased the viscosity of solution in our system which enhanced solvent-nonsolvent exchange rate. Decrease in viscosity of polymer solution due to alcohol additive was observed by several researchers (Mansourizadeh and Ismail 2011, Naim et al. 2012).

Table 2.12 Effect of non-solvent in membrane solution on gas permeance and ideal selectivity. Membranes quenched in coagulation medium IPA/H₂O:95/5 (in %v/v.)

Code	IPA content in casting Soln. (wt.%)	Permeance (GPU)			Ideal Selectivity		
		H ₂	CO ₂	CH ₄	H ₂ /CO ₂	H ₂ /CH ₄	CO ₂ /CH ₄
PP16, PP19, PP20, PP25, PP26	0	0.43	0.18	0.0050	2.4	87.9	36.4
P22, PP23	7%	1.33	0.54	0.1220	2.5	11.3	4.6

2.8 Gas Separation Test Results of PES/ZIF-8 Mixed Matrix Membranes

Table 2.13 shows the gas separation test results of asymmetric membrane including thermally annealed (annealing type-2) ZIF-8 crystals. The ideal selectivity values of this type of mixed matrix asymmetric PES membrane were significantly lower than that of neat PES membrane. Loss of selectivity of gas pairs with ZIF-8 loading was attributed to the cluster of ZIF-8 particles, which was observed by investigation SEM images (Figure 2.18). Since aggregated ZIF-8 particles formed non-selective voids (Moore and Koros 2005, Bae et al. 2010).

Table 2.13 Permeance and selectivity values of mixed matrix (PES/ZIF-8) membranes prepared with thermally annealed ZIF-8 crystals in pure IPA coagulation bath.

Code	ZIF-8	Permeance			Ideal Selectivity		
		H ₂	CO ₂	CH ₄	H ₂ /CO ₂	H ₂ /CH ₄	CO ₂ /CH ₄
MMM2	%5 (25 nm)	0.66	0.25	0.066	2.6	10.0	3.8
MMM1, MMM11	%10 (25 nm)	5.65	1.45	2.05	3.9	2.8	0.7
MMM12	%10 (65 nm)	10.04	1.32	2.33	7.6	4.3	0.6

In order to avoid agglomeration, ZIF-8 crystals were used without thermal annealing. Instead of thermal annealing, closed ZIF-8 pores were activated with MEOH washing (annealing type-1). Gas test results of mixed matrix membrane including type-1 annealed ZIF-8 crystals at different percentage and crystals size were depicted in Table 2.14. Loading ZIF-8 improved the permeance of membranes. Using ZIF-8 crystals with 25 and 65 nm average particle size enhanced also separation performance of membranes beside permeance. On the other hand, ZIF-8 crystals with 15 nm in size, even in small amount, led to loss in CO₂/CH₄ and H₂/CH₄ ideal selectivity values (from 35.6 to 24.6 and 75.6 to 61; respectively). A possible reason was that the non-selective voids formed due to agglomeration of

ZIF-8 crystals at 15 nm in size. Same trend was not observed at 25 nm and 65 nm ZIF-8 usage since ZIF-8s with smaller particle size are more susceptible to clustering than large ZIF-8 particles as evidence by SEM images (Figure 2.19-20, Table 2.8) and also reported by Ayas 2014.

Observations show that CO₂ permeance of membrane increases with increasing filler loading. 5% loading of ZIF-8 with 65 nm crystal size resulted in 31% increase in CO₂ permeance and 13% increase in CO₂/CH₄ selectivity as compared with neat PES membrane. On the other hand, %5 loading of ZIF-8 with smaller particle size (15 nm and 25 nm) had similar effect on permeance of membrane. Increasing 15 nm ZIF-8 content from %5 to %10, approximately %40 enhancement in H₂ and CO₂ permeance was detected with slight improvement in selectivity. By increasing in 65 nm ZIF-8 content from 5% to 10% of PES, the gas permeances fold in two without loss in selectivity. Using 65 nm ZIF-8 with %10 loading provided enhancement in both permeance and selectivity compared to the neat PES membranes, thus indicated the admirable interaction between fillers and polymer (Basu et al. 2011). To conclude, the increasing permeances with increasing ZIF-8 loadings were attributed to combinational effect of porous nature of the ZIF-8s (Basu et al. 2011; Dorosti et al. 2014) and more free volume of polymer enlarged due to ZIF-8 loading (Hashemifard et al. 2011, Gholami et al. 2017). The enhancement in selectivity is related to pore size of ZIF-8 crystals showing molecular sieving effect and tortuous path around ZIF-8 crystals. Pore size of ZIF-8 crystals (0.34 nm) is suitable to pass of CO₂ and H₂ with kinetic diameter 0.33 nm and 0.29 nm; respectively, but not suitable for pass CH₄ with kinetic diameter 0.38 nm. Moreover, specific interaction between CO₂ and ZIF-8 crystals because of high quadrupole moment of CO₂ improves CO₂ permeance larger than CH₄ permeance, this is another reason of higher CO₂/CH₄ selectivity (Gholami et al. 2017). Increasing the diffusion path length for the gas penetrants which were forced to take a more tortuous path around the ZIF-8 nanoparticles (Ordenez et al. 2010) is also a factor which improves the selectivity.

Table 2.14 Gas transport properties of Mixed Matrix (PES/ZIF-8) membranes prepared with ZIF-8 crystals (Treat-Type1) in pure IPA coagulation bath.

Code	ZIF-8 content	Permeance			Ideal Selectivity		
		H ₂	CO ₂	CH ₄	H ₂ /CO ₂	H ₂ /CH ₄	CO ₂ /CH ₄
MMM25	%5 (15 nm)	0.47	0.19	0.0077	2.5	61.0	24.7
MMM28	%10 (15 nm)	0.69	0.27	0.0098	2.6	70.4	27.6
MMM3, MMM6, MMM8	%5 (25 nm)	0.48	0.22	0.0061	2.2	78.7	36.1
MMM9	%10 (25 nm)	0.43	0.19	0.0054	2.3	79.6	35.2
MMM7	%5 (65 nm)	0.47	0.21	0.0055	2.2	85.5	38.2
MMM10, MMM29	%10 (65 nm)	0.83	0.38	0.0101	2.2	82.2	37.6
PP1-PP6, PP9	Neat PES	0.34	0.16	0.0045	2.1	75.6	35.6
Ref.	Membrane Content	CO₂		CO₂/CH₄			
Gholami et al. 2017	PU	2.5 Barrer		7.5			
	PU+30 wt.% ZIF-8	15 Barrer		13.5			
Ordonez et al. 2010	PI	10.5 Barrer		49			
	PI+40wt.% ZIF-8	26 Barrer		30			
	PI+50wt.% ZIF-8	5 Barrer		89			
Ismail et al. 2015	PES	0.94 GPU		16.94			
	PES+1wt.%Cloisite15	3.71 GPU		46.89			
Md. Nordin et al. 2015	PSF	21.27 ± 6.35 GPU		19.43			
	PSF+0.5wt.%ZIF-8	29.22 ± 3.68 GPU		23.16			
	PSF+0.75wt.%ZIF-8	33.35 ± 3.46 GPU		9.66			

Figure 2.20 showed CO₂ permeance with respect to CO₂/CH₄ selectivity of mixed matrix membranes including 25 nm and 65 nm ZIF-8 in different loading amount. It was observed proportional increase in both selectivity and permeance with 65 nm ZIF-8 loading. Effect of 25 nm ZIF-8 was not as high as that of 65 nm ZIF-8. These experiences showed that ZIF-8 with higher crystal size was more suitable than ZIF-8 in lower crystal size.

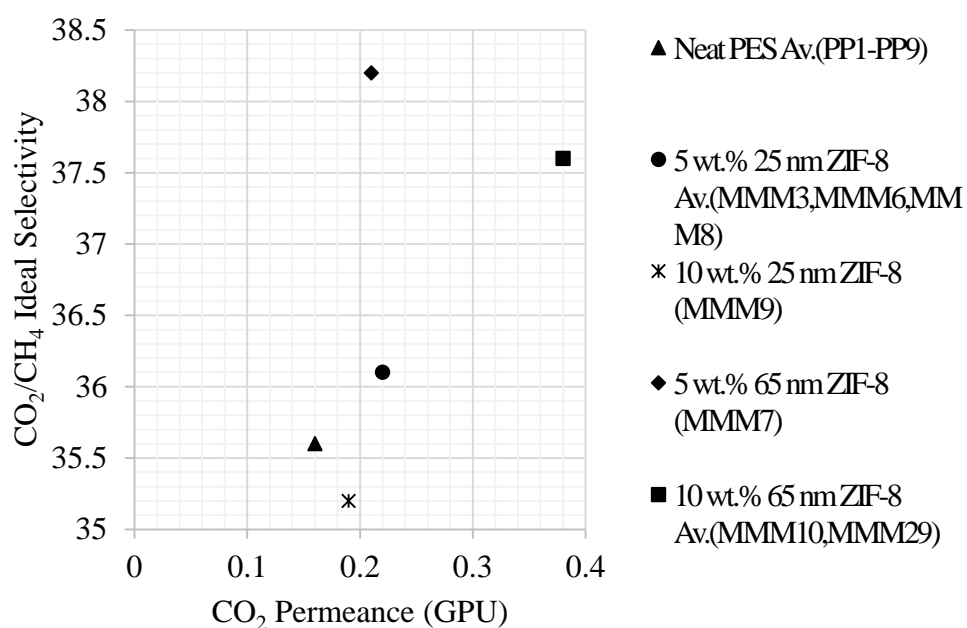


Figure 2.20 Effects of ZIF-8 loading and ZIF-8 particle size on CO₂ permeance and CO₂/CH₄ of flat sheet asymmetric mixed matrix PES/ZIF-8 membranes.

2.9 Conclusion

In Chapter 2, morphological and gas transport properties of PES membrane produced by non-solvent induced wet phase inversion method were investigated. The solvent and non-solvent content of IPA coagulation bath, loading percent of ZIF-8, and pre-treatment of ZIF-8 were parameters whose effects on both permeance and membrane structure analyzed.

The dense skin layer thickness of PES membrane quenched in pure IPA bath was 30 μm . By increasing the water content to 10 v.l. % of total coagulant, the skin layer thickness decreased to 5 μm . Further increase in water content prevented the formation of skin layer. ZIF-8 loading led to decrease in thickness of skin layer from 30 μm to 22 μm .

The polymeric membranes prepared in IPA coagulation bath with 25% DMF have CO_2 permeance 44% higher than that of prepared with pure IPA. The polymeric membranes prepared in IPA coagulation bath with 10% water have CO_2 permeance 175% higher as compared to the one prepared with pure IPA. Membranes were prepared with 5% and 10% contribution of ZIF-8 having 65, 25 and 15 nm crystal sizes. CO_2 permeance of membrane increased with increasing filler loading. 10% loading of ZIF-8 with 65 nm crystal size results in 86% increase in CO_2 permeance and 13% increase in CO_2/CH_4 selectivity of PES membrane. On the other hand, lower ZIF-8 loading with smaller particle size has smaller effect on permeance of membrane.

REFERENCES

- Aerts, P., Genne, I., Kuypers, S., Leysen, R., Vankelecom, I. J., & Jacobs, P. A. (2000). Polysulfone-aerosil composite membranes Part 2. The influence of the addition of aerosil on the skin characteristics and membrane properties. *Journal of Membrane Science*, *178*(1-2), 1-11. doi:10.1016/s0376-7388(00)00428-2
- Aerts, P., Van Hoof, E., Leysen, R., Vankelecom, I. J., & Jacobs, P. A. (2000). Polysulfone-Aerosil composite membranes Part 1. The influence of the addition of Aerosil on the formation process and membrane morphology. *Journal of Membrane Science*, *176*(1), 63-73. doi:10.1016/s0376-7388(00)00427-0
- Ali, N., Rahim, N. A., Ali, A., Sani, W., Nik, W., & Shiung, L. S. (2007). Effect of Ethanol Composition in the Coagulation Bath on Membrane Performance. *Journal of Applied Sciences*, *7*(15), 2131-2136. doi:10.3923/jas.2007.2131.2136
- Anderson, J. E., & Ullman, R. (1973). Mathematical analysis of factors influencing the skin thickness of asymmetric reverse osmosis membranes. *Journal of Applied Physics*, *44*(10), 4303-4311. doi:10.1063/1.1661955
- Aroon, M. A., Ismail, A. F., Montazer-Rahmati, M. M., & Matsuura, T. (2010). Effect of Raw Multi-Wall Carbon Nanotubes on Morphology and Separation Properties of Polyimide Membranes. *Separation Science and Technology*, *45*(16), 2287-2297. doi:10.1080/01496395.2010.484007
- Aroon, M., Ismail, A., Montazer-Rahmati, M., & Matsuura, T. (2010). Morphology and permeation properties of polysulfone membranes for gas separation: Effects of non-solvent additives and co-solvent. *Separation and Purification Technology*, *72*(2), 194-202. doi:10.1016/j.seppur.2010.02.009
- Ayas, İ. (2014). *Effect of The Particle Size of ZIF-8 on The Separation Performance of ZIF-8/PNA/PES Membranes* (Doctoral dissertation, Middle East Technical University, Ankara, Türkiye).
- Bae, T., Lee, J. S., Qiu, W., Koros, W. J., Jones, C. W., & Nair, S. (2010). A High-Performance Gas-Separation Membrane Containing Submicrometer-Sized Metal-Organic Framework Crystals. *Angewandte Chemie*, *122*(51), 10059-10062. doi:10.1002/ange.201006141
- Basu, S., Cano-Odena, A., & Vankelecom, I. F. (2011). MOF-containing mixed-matrix membranes for CO₂/CH₄ and CO₂/N₂ binary gas mixture separations. *Separation and Purification Technology*, *81*(1), 31-40. doi:10.1016/j.seppur.2011.06.037
- Broens, L., Altena, F., Smolders, C., & Koenhen, D. (1980). Asymmetric membrane structures as a result of phase separation phenomena. *Desalination*, *32*, 33-45. doi:10.1016/s0011-9164(00)86004-x
- Buonomenna, M. G., Figoli, A., Jansen, J. C., & Drioli, E. (2004). Preparation of asymmetric PEEKWC flat membranes with different microstructures by

- wet phase inversion. *Journal of Applied Polymer Science*, 92(1), 576-591. doi:10.1002/app.20042
- Cacho-Bailo, F., Seoane, B., Téllez, C., & Coronas, J. (2014). ZIF-8 continuous membrane on porous polysulfone for hydrogen separation. *Journal of Membrane Science*, 464, 119-126. doi:10.1016/j.memsci.2014.03.070
- Chung, T., & Kafchinski, E. R. (1997). The effects of spinning conditions on asymmetric 6FDA/6FDAM polyimide hollow fibers for air separation. *Journal of Applied Polymer Science*, 65(8), 1555-1569. doi:10.1002/(sici)1097-4628(19970822)65:8<1555::aid-app13>3.0.co;2-v
- Chun, K., Jang, S., Kim, H., Kim, Y., Han, H., & Joe, Y. (2000). Effects of solvent on the pore formation in asymmetric 6FDA-4,4'ODA polyimide membrane: terms of thermodynamics, precipitation kinetics, and physical factors. *Journal of Membrane Science*, 169(2), 197-214. doi:10.1016/s0376-7388(99)00336-1
- Cravillon, J., Schröder, C. A., Nayuk, R., Gummel, J., Huber, K., & Wiebcke, M. (2011). Fast Nucleation and Growth of ZIF-8 Nanocrystals Monitored by Time-Resolved In Situ Small-Angle and Wide-Angle X-Ray Scattering. *Angewandte Chemie*, 123(35), 8217-8221. doi:10.1002/ange.201102071
- Deshmukh, S., & Li, K. (1998). Effect of ethanol composition in water coagulation bath on morphology of PVDF hollow fibre membranes. *Journal of Membrane Science*, 150(1), 75-85. doi:10.1016/s0376-7388(98)00196-3
- Dorosti, F., Omidkhah, M., & Abedini, R. (2014). Fabrication and characterization of Matrimid/MIL-53 mixed matrix membrane for CO₂/CH₄ separation. *Chemical Engineering Research and Design*, 92(11), 2439-2448. doi:10.1016/j.cherd.2014.02.018
- Dos Santos Ferreira da Silva, J., López Malo, D., Anceski Bataglioni, G., Nogueira Eberlin, M., Machado Ronconi, C., Alves Júnior, S., & De Sá, G. F. (2015). Adsorption in a Fixed-Bed Column and Stability of the Antibiotic Oxytetracycline Supported on Zn(II)-[2-Methylimidazolate] Frameworks in Aqueous Media. *PLOS ONE*, 10(6), e0128436. doi:10.1371/journal.pone.0128436
- Fritzsche, A. K., Cruse, C. A., Kesting, R. E., & Murphy, M. K. (1990). Polysulfone hollow fiber membranes spun from lewis acid: Base complexes. II. The effect of lewis acid to base ratio on membrane structure. *Journal of Applied Polymer Science*, 39(9), 1949-1956. doi:10.1002/app.1990.070390910
- Gholami, M., Mohammadi, T., Mosleh, S., & Hemmati, M. (2017). CO₂/CH₄ separation using mixed matrix membrane-based polyurethane incorporated with ZIF-8 nanoparticles. *Chemical Papers*. doi:10.1007/s11696-017-0177-9
- Groth, T., Huang, X. J., & Xu, Z. K. (2013). Biomedical Applications of Membranes in Bioartificial Organs and Tissue Engineering. In *Polymeric Biomaterials, Medicinal and Pharmaceutical Applications* (3rd ed., pp. 605-635). CRC Press, Taylor and Francis Group.

- Guillen, G. R., Pan, Y., Li, M., & Hoek, E. M. (2011). Preparation and Characterization of Membranes Formed by Nonsolvent Induced Phase Separation: A Review. *Industrial & Engineering Chemistry Research*, 50(7), 3798-3817. doi:10.1021/ie101928r
- Hansen, C. M. (2007). Chapter 1: Solubility Parameters — An Introduction. In *Hansen Solubility Parameters: A User's Handbook* (2nd ed., pp. 1-22). CRC Press Taylor & Francis Group.
- Hashemifard, S., Ismail, A., & Matsuura, T. (2011). Effects of montmorillonite nano-clay fillers on PEI mixed matrix membrane for CO₂ removal. *Chemical Engineering Journal*, 170(1), 316-325. doi:10.1016/j.cej.2011.03.063
- Hong, D. H., & Suh, M. P. (2012). Selective CO₂ adsorption in a metal–organic framework constructed from an organic ligand with flexible joints. *Chemical Communications*, 48(73), 9168. doi:10.1039/c2cc34482c
- Ismail, A. F., & Yean, L. P. (2003). Review on the development of defect-free and ultrathin-skinned asymmetric membranes for gas separation through manipulation of phase inversion and rheological factors. *Journal of Applied Polymer Science*, 88(2), 442-451. doi:10.1002/app.11744
- Ismail, A., & Lai, P. (2003). Effects of phase inversion and rheological factors on formation of defect-free and ultrathin-skinned asymmetric polysulfone membranes for gas separation. *Separation and Purification Technology*, 33(2), 127-143. doi:10.1016/s1383-5866(02)00201-0
- Ismail, A., & Lai, P. (2004). Development of defect-free asymmetric polysulfone membranes for gas separation using response surface methodology. *Separation and Purification Technology*, 40(2), 191-207. doi:10.1016/j.seppur.2004.02.011
- Ismail, N., Ismail, A., Mustafa, A., Matsuura, T., Soga, T., Nagata, K., & Asaka, T. (2015). Qualitative and quantitative analysis of intercalated and exfoliated silicate layers in asymmetric polyethersulfone/cloisite15A® mixed matrix membrane for CO₂/CH₄ separation. *Chemical Engineering Journal*, 268, 371-383. doi:10.1016/j.cej.2014.11.147
- Jao-Ming Cheng, Da-Ming Wang, Fung-Ching Lin, & Juin-Yih Lai. (1996). Formation and gas flux of asymmetric PMMA membranes. *Journal of Membrane Science*, 109(1), 93-107. doi:10.1016/0376-7388(95)00187-5
- Julian, H., & Wenten, I. G. (2012). Polysulfone membranes for CO₂/CH₄ separation: State of the art. *IOSR Journal of Engineering*, 02(03), 484-495. doi:10.9790/3021-0203484495
- Keser Demir, N., Topuz, B., Yilmaz, L., & Kalipcilar, H. (2014). Synthesis of ZIF-8 from recycled mother liquors. *Microporous and Mesoporous Materials*, 198, 291-300. doi:10.1016/j.micromeso.2014.07.052
- Keser, N. (2012). *Production and Performance Evaluation of ZIF-8 Based Binary and Ternary Mixed Matrix Gas Separation Membranes* (Master's thesis, Middle East Technical University, Ankara, Turkey).
- Kesting, R. (1988). Synthetic Polymeric Membranes. *Journal of Colloidal and Interface Science*, 125(1), 312. doi:10.1016/0021-9797(88)90090-2
- Kesting, R. E. (1971). *Synthetic polymeric membranes: a structural perspective*. U.S.: McGraw-Hill. pp 117-157

- Kesting, R. E., Fritzsche, A. K., Murphy, M. K., Cruse, C. A., Handermann, A. C., Malon, R. F., Moore, M. D. (1990). The second-generation polysulfone gas-separation membrane. I. The use of lewis acid: Base complexes as transient templates to increase free volume. *Journal of Applied Polymer Science*, 40(910), 1557-1574. doi:10.1002/app.1990.070400913
- Koenhen, D. M., Mulder, M. H., & Smolders, C. A. (1977). Phase separation phenomena during the formation of asymmetric membranes. *Journal of Applied Polymer Science*, 21(1), 199-215. doi:10.1002/app.1977.070210118
- Kurdi, J., & Tremblay, A. Y. (1999). Preparation of defect-free asymmetric membranes for gas separations. *Journal of Applied Polymer Science*, 73(8), 1471-1482. doi:10.1002/(sici)1097-4628(19990822)73:8<1471::aid-app16>3.0.co;2-g
- Li, S., Van den Boomgaard, T., Smolders, C. A., & Strathmann, H. (1996). Physical Gelation of Amorphous Polymers in a Mixture of Solvent and Nonsolvent. *Macromolecules*, 29(6), 2053-2059. doi:10.1021/ma9508966
- Li, Y., & Chung, T. S. (2008). Highly selective sulfonated polyethersulfone (SPES)-based membranes with transition metal counterions for hydrogen recovery and natural gas separation. *Journal of Membrane Science*, 308(1-2), 128-135. doi:10.1016/j.memsci.2007.09.053
- Loeb, S., & Sourirajan, S. (1963). Sea Water Demineralization by Means of an Osmotic Membrane. *Advances in Chemistry*, 117-132. doi:10.1021/ba-1963-0038.ch009
- Machado, P., Habert, A., & Borges, C. (1999). Membrane formation mechanism based on precipitation kinetics and membrane morphology: flat and hollow fiber polysulfone membranes. *Journal of Membrane Science*, 155(2), 171-183. doi:10.1016/s0376-7388(98)00266-x
- Mansoori, S. A., Pakizeh, M., & Chenar, M. P. (2011). Effect of Synthesis Parameters on Structural Characteristics of Polysulfone Membrane and its Gas Separation Properties. *Journal of Membrane Science & Technology*, 01(02). doi:10.4172/2155-9589.1000103
- Mansourizadeh, A., & Ismail, A. (2011). Preparation and characterization of porous PVDF hollow fiber membranes for CO₂ absorption: Effect of different non-solvent additives in the polymer dope. *International Journal of Greenhouse Gas Control*, 5(4), 640-648. doi:10.1016/j.ijggc.2011.03.009
- Mazinani, S., Darvishmanesh, S., Ehsanzadeh, A., & Van der Bruggen, B. (2017). Phase separation analysis of Extem/solvent/non-solvent systems and relation with membrane morphology. *Journal of Membrane Science*, 526, 301-314. doi:10.1016/j.memsci.2016.12.031
- Md Nordin, N. A., Ismail, A. F., & Mustafa, A. (2014). Synthesis and Preparation of Asymmetric PSf/ZIF-8 Mixed Matrix Membrane for CO₂/CH₄ Separation. *Jurnal Teknologi*, 69(9). doi:10.11113/jt.v69.3400
- Moore, T. T., & Koros, W. J. (2005). Non-ideal effects in organic-inorganic materials for gas separation membranes. *Journal of Molecular Structure*, 739(1-3), 87-98. doi:10.1016/j.molstruc.2004.05.043

- Naim, R., Ismail, A., & Mansourizadeh, A. (2012). Effect of non-solvent additives on the structure and performance of PVDF hollow fiber membrane contactor for CO₂ stripping. *Journal of Membrane Science*, 423-424, 503-513. doi:10.1016/j.memsci.2012.08.052
- Nasir, R., Mukhtar, H., & Man, Z. (2014). Miscibility Studies of Polyethersulfone (PES), N – Methyl – 2 – Pyrrolidone (NMP) and Alkanolamines on the Basis of Hansen Solubility Parameters. *International Journal of Scientific Engineering and Technology*, 3(5), 450-453.
- Ordoñez, M. J., Balkus, K. J., Ferraris, J. P., & Musselman, I. H. (2010). Molecular sieving realized with ZIF-8/Matrimid® mixed-matrix membranes. *Journal of Membrane Science*, 361(1-2), 28-37. doi:10.1016/j.memsci.2010.06.017
- Panar, M., Hoehn, H. H., & Hebert, R. R. (1973). The Nature of Asymmetry in Reverse Osmosis Membranes. *Macromolecules*, 6(5), 777-780. doi:10.1021/ma60035a026
- Pan, Y., Liu, Y., Zeng, G., Zhao, L., & Lai, Z. (2011). Rapid synthesis of zeolitic imidazolate framework-8 (ZIF-8) nanocrystals in an aqueous system. *Chemical Communications*, 47(7), 2071. doi:10.1039/c0cc05002d
- Park, K. S., Ni, Z., Cote, A. P., Choi, J. Y., Huang, R., Uribe-Romo, F. J., ... Yaghi, O. M. (2006). Exceptional chemical and thermal stability of zeolitic imidazolate frameworks. *Proceedings of the National Academy of Sciences*, 103(27), 10186-10191. doi:10.1073/pnas.0602439103
- Peng, N., Widjojo, N., Sukitpaneinit, P., Teoh, M. M., Lipscomb, G. G., Chung, T., & Lai, J. (2012). Evolution of polymeric hollow fibers as sustainable technologies: Past, present, and future. *Progress in Polymer Science*, 37(10), 1401-1424. doi:10.1016/j.progpolymsci.2012.01.001
- Pesek, S., & Koros, W. (1993). Aqueous quenched asymmetric polysulfone membranes prepared by dry/wet phase separation. *Journal of Membrane Science*, 81(1-2), 71-88. doi:10.1016/0376-7388(93)85032-r
- Pinnau, I., & Koros, W. J. (1993). A qualitative skin layer formation mechanism for membranes made by dry/wet phase inversion. *Journal of Polymer Science Part B: Polymer Physics*, 31(4), 419-427. doi:10.1002/polb.1993.090310406
- Punsalan, D., & Koros, W. J. (2005). Thickness-dependent sorption and effects of physical aging in a polyimide sample. *Journal of Applied Polymer Science*, 96(4), 1115-1121. doi:10.1002/app.21544
- Ren, J., & Wang, R. (2010). Preparation of Polymeric Membranes. In *Membrane and Desalination Technologies* (pp. 47-100). Humana Press.
- Reuvers, A. J. (1987). *Formation-Diffusion Induced Demixing Process in Ternary Polymeric System* (Doctoral dissertation, University of Twente, Enschede, Netherlands).
- Rezaei, M., Ismail, A., Bakeri, G., Hashemifard, S., & Matsuura, T. (2015). Effect of general montmorillonite and Cloisite 15A on structural parameters and performance of mixed matrix membranes contactor for CO₂ absorption. *Chemical Engineering Journal*, 260, 875-885. doi:10.1016/j.cej.2014.09.027

- Smolders, C., Reuvers, A., Boom, R., & Wienk, I. (1992). Microstructures in phase-inversion membranes. Part 1. Formation of macrovoids. *Journal of Membrane Science*, 73(2-3), 259-275. doi:10.1016/0376-7388(92)80134-6
- Soroko, I., Lopes, M. P., & Livingston, A. (2011). The effect of membrane formation parameters on performance of polyimide membranes for organic solvent nanofiltration (OSN): Part A. Effect of polymer/solvent/non-solvent system choice. *Journal of Membrane Science*, 381(1-2), 152-162. doi:10.1016/j.memsci.2011.07.027
- Spruck, M., Stadlmayr, W., Koch, M., Mayr, L., Penner, S., & Rupprich, M. (2014). Influence of the coagulation medium on the performance of poly(ether sulfone) flat-sheet membranes. *Journal of Applied Polymer Science*, n/a-n/a. doi:10.1002/app.41645
- Strathmann, H., Kock, K., Amar, P., & Baker, R. (1975). The formation mechanism of asymmetric membranes. *Desalination*, 16(2), 179-203. doi:10.1016/s0011-9164(00)82092-5
- Sukitpaneinit, P., & Chung, T. (2009). Molecular elucidation of morphology and mechanical properties of PVDF hollow fiber membranes from aspects of phase inversion, crystallization and rheology. *Journal of Membrane Science*, 340(1-2), 192-205. doi:10.1016/j.memsci.2009.05.029
- Tanaka, F., & Stockmayer, W. H. (1994). Thermoreversible Gelation with Junctions of Variable Multiplicity. *Macromolecules*, 27(14), 3943-3954. doi:10.1021/ma00092a039
- Tanny, G. B. (1974). The surface tension of polymer solutions and asymmetric membrane formation. *Journal of Applied Polymer Science*, 18(7), 2149-2163. doi:10.1002/app.1974.070180721
- Van de Witte, P., Dijkstra, P., Van den Berg, J., & Feijen, J. (1996). Phase separation processes in polymer solutions in relation to membrane formation. *Journal of Membrane Science*, 117(1-2), 1-31. doi:10.1016/0376-7388(96)00088-9
- Van't Hof, J., Reuvers, A., Boom, R., Rolevink, H., & Smolders, C. (1992). Preparation of asymmetric gas separation membranes with high selectivity by a dual-bath coagulation method. *Journal of Membrane Science*, 70(1), 17-30. doi:10.1016/0376-7388(92)80076-v
- Venna, S. R., Jasinski, J. B., & Carreon, M. A. (2010). Structural Evolution of Zeolitic Imidazolate Framework-8. *Journal of the American Chemical Society*, 132(51), 18030-18033. doi:10.1021/ja109268m
- Wang, D., Li, K., & Teo, W. (1996). Polyethersulfone hollow fiber gas separation membranes prepared from NMP/alcohol solvent systems. *Journal of Membrane Science*, 115(1), 85-108. doi:10.1016/0376-7388(95)00312-6
- Wang, D., Li, K., & Teo, W. (2000). Highly permeable polyethersulfone hollow fiber gas separation membranes prepared using water as non-solvent additive. *Journal of Membrane Science*, 176(2), 147-158. doi:10.1016/s0376-7388(00)00419-1
- Wijmans, J., Baaij, J., & Smolders, C. (1983). The mechanism of formation of microporous or skinned membranes produced by immersion precipitation. *Journal of Membrane Science*, 14(3), 263-274. doi:10.1016/0376-7388(83)80005-2

- Xu, J., & Xu, Z. (2002). Poly(vinyl chloride) (PVC) hollow fiber ultrafiltration membranes prepared from PVC/additives/solvent. *Journal of Membrane Science*, 208(1-2), 203-212. doi:10.1016/s0376-7388(02)00261-2
- Xu, Z., & Alsahy Qusay, F. (2004). Polyethersulfone (PES) hollow fiber ultrafiltration membranes prepared by PES/non-solvent/NMP solution. *Journal of Membrane Science*, 233(1-2), 101-111. doi:10.1016/j.memsci.2004.01.005
- Yeow, M. L., Liu, Y. T., & Li, K. (2003). Isothermal phase diagrams and phase-inversion behavior of poly(vinylidene fluoride)/solvents/additives/water systems. *Journal of Applied Polymer Science*, 90(8), 2150-2155. doi:10.1002/app.12846
- Young, T., & Chen, L. (1995). Pore formation mechanism of membranes from phase inversion process. *Desalination*, 103(3), 233-247. doi:10.1016/0011-9164(95)00076-3
- Yu, L., Yang, F., & Xiang, M. (2014). Phase separation in a PSf/DMF/water system: a proposed mechanism for macrovoid formation. *RSC Adv*, 4(80), 42391-42402. doi:10.1039/c4ra06088a
- Zhang, C., Dai, Y., Johnson, J. R., Karvan, O., & Koros, W. J. (2012). High performance ZIF-8/6FDA-DAM mixed matrix membrane for propylene/propane separations. *Journal of Membrane Science*, 389, 34-42. doi:10.1016/j.memsci.2011.10.003
- Zhang, T., Zhang, X., Yan, X., Kong, L., Zhang, G., Liu, H., Yeung, K. L. (2013). Synthesis of Fe₃O₄@ZIF-8 magnetic core-shell microspheres and their potential application in a capillary microreactor. *Chemical Engineering Journal*, 228, 398-404. doi:10.1016/j.cej.2013.05.020
- Zhang, Y., Li, H., Lin, J., Li, R., & Liang, X. (2006). Preparation and characterization of zirconium oxide particles filled acrylonitrile-methyl acrylate-sodium sulfonate acrylate copolymer hybrid membranes. *Desalination*, 192(1-3), 198-206. doi:10.1016/j.desal.2005.07.036

CHAPTER 3

LIGHT INDUCED DRY-WET PHASE INVERSION METHOD FOR ASYMMETRIC NEAT PI AND PI/ZIF-8 MIXED MATRIX MEMBRANES

In this chapter, the morphological and gas separation properties of neat PI, PI/ZIF-8 MMM produced by dry-wet phase inversion method were presented and discussed.

The polymers of an industrially applicable membrane should also be commercially affordable and readily available. Hence, commercial polymers such as PI and PES are preferred for industrial membrane applications. Again, the membrane to be used in the industry must have a high gas permeance and be easily producible. The asymmetric membranes meet the requirement of high permeance. The dry-wet phase inversion method is the simplest way to obtain an asymmetric structure in a single step. The dry phase inversion is an important step to produce defect-free dense skin layer, because this step enhances the stability of polymeric solution before entering the wet phase inversion step.

In the present study, during dry phase inversion step, the polymeric solution film was exposed to lights at a certain time period. Depending on the type of light source and the duration of exposure period, the amount of volatile solvent evaporated from surface of the polymer solution film are changing. Therefore, the concentration and stability of the polymer film solution will change before entering wet phase inversion step. Hence light exposure period has significant effect on the morphological structure and also on the gas separation performance of membrane. In addition, the amount and the type of volatile solvent, its interaction with the polymer, non-volatile solvent and non-solvent, amount of filler and type of the filler influence both kinetic and thermodynamics of dry and wet phase inversion steps. Thereby morphology and gas transport properties of membrane alter significantly depending on these parameters. The light source, light exposure period, amount

and type of the volatile solvents, and ZIF-8 incorporation into casting polymer solution were the parameters those were investigated in this study. According to our current knowledge, exposure of the membrane to light energy during the dry phase change process has not been experienced and its effects has not been investigated yet.

The effects of the above mentioned parameters on membrane morphology were examined by SEM test while the effects on gas separation performance were tested by constant volume variable pressure gas test system.

3.1 Evolution and Development of Dry-Wet Phase Inversion Method for Gas Separation Asymmetric Membranes

The formation mechanism of asymmetric membrane via dry-wet phase inversion is as expressed in Chapter 2.1 Theoretical Background part. The only difference is the dry-inversion step which provides denser and more stable polymer layer at the outermost surface. This denser and stable outermost surface can resist the stress formed during wet phase separation. Furthermore, vitrification and coalescence of polymer rich region hinders the formation of defects (Aroon et al. 2010).

The major breakthrough in polymeric gas separation membrane is the production of defect-free and ultrathin skinned asymmetric membrane with high gas separation properties. The major problem is defects on the dense skin surface because of un-even packing of kinked polymer chain and deficient coalescence of polymer molecules and stress induced rupture during wet phase quenching (Kimmerle and Strathmann 1990) on the skin surface. Because the Knudsen diffusion active for non-selective pores is faster than solution-diffusion mechanism, these defects lead to significant loss in selectivity (Ismail and Yean 2003).

Several manipulations about membrane production methods are carried out to achieve a membrane with ultra-thin skinned membrane having the intrinsic selectivity of polymer. Table 3.1 has been listed gas separation and transport

properties of some of the asymmetric membranes depending on variation and manipulation in membrane preparation methods.

Henis and Tripodi 1980 suggested to plug the non-selective voids on the ultra-thin skin by non-selective and highly permeable polymers such as silicone rubber or polydimethylsiloxane. Henis and Tripodi's suggestion was widely accepted and implemented in both industry and academic researches. Henis and Tripodi 1980 entitled these coated membrane as composite membrane and indicated that the coated membranes showed the intrinsic gas separation properties of porous support membrane.

Kesting et al. 1990 propounded the Lewis acid and Lewis base complexes in the spinning dope to achieve high free volume and also ultra-thin density graded skin layer. They also hypothesized that there is a critical molar volume (~147 cc/mol for PSU) exists in dope formulation. By a small variation in dope formulation such as using propionic acid (Lewis acid) with NMP (Lewis base) instead of neat NMP as solvent, anisotropic graded skin layer was obtained which provided the fourfold increase in O₂ permeability without any scarification in O₂/N₂ selectivity. Fritzsche et al. 1990 studied systematically the effect of oxygen plasma ablation time and molar propionic acid (PA):NMP ratio on He and N₂ permeance of PSF hollow fiber membrane. He and N₂ permeance increased with increase in molar ratio of PA:NMP and also in oxygen plasma ablation period. He/N₂ selectivity increased with increase in molar ratio of PA:NMP but decreased with oxygen plasma ablation period. Existence of PA or water (non-solvent) in the solution accelerated the sol-to-gel transition. The rapid sol-to-gel transition leads to increase in the free volume. Oxygen plasma etching confined the surface of the membrane without changing its intrinsic separation properties.

Van't Hof et al. 1992 suggested dual-nonsolvent-bath for wet phase inversion in order to take the advantage of both delayed demixing and instantaneous demixing. First non-solvent bath (glycerol or 1-pentanol) was responsible to the formation of dense selective layer and the second non-solvent bath (water) provided

the polymer precipitation. This technique provided selective PES membrane without any additional solvent evaporation step prior to wet phase inversion or coating.

Hachisuka et al. 1996 produced 6FDA-BAAF polyimide membrane with ultra-thin 40-60 nm skin layer by using one type solvent and one type non-solvent systems instead of using complex solvents and non-solvents system. The formation of such a thin skin layer with almost defect-free was attributed to the dissolution properties of solvent (diethylene glycol dimethyl ether DGDE) in water (non-solvent). During phase inversion a sharp interface formed between water and DGDE and hyper-thin skin layer formed at this interface. Hachisuta et al. 1996 prepared 6FDA-BAAF membrane by using NMP instead of DGDE at the same composition and by the same preparation method. However, in this case no skin layer could be obtained. The difference between DGDE and NMP was explained via the difference between dielectric constant and dipole moment. The dielectric constant and dipole moment of DGDE are 5.97 and 1.97D, respectively which are much smaller than those of NMP (32 and 4D).

Dual-layer hollow fiber asymmetric membrane is among the recent recommendations (Jiang et al 2004). The main principle is to combine the advantages of two different materials. Dual-layer hollow fiber membranes are mainly composed of two layer made up of two different materials. The major advantage is eliminating secondary operation such as laminating or coating.

The preparation different polymers into binary or ternary blends is another way to combine advantages of polymer for membranes (Han et al. 2010). For example, PI membranes has limited industrial applications despite its good permeance and selectivity, because of its low resistance against plasticization, and relatively short lifetime compared to polysulfone. Blending Matrimid with polysulfone is a way to increase stability of the membrane (Basu et al. 2010).

Yuenyao et al. 2015 preferred plasma treatment to enhance permeance of flat polysulfone membrane. The DC plasma treatment is mainly modifying the

surface and pore properties of membrane, which leads to increase CO₂ permeance by 60% without any sacrifice in CO₂/CH₄ selectivity. (see Table 3.1)

Several authors widely preferred using additives such as polymer additives (PVP, PEG), low molecular weight additives (LiCl), acids (acetic acid, phosphoric acid, propionic acid), weak-co-solvents (acetone, ethanol), weak non-solvent (methanol, isopropanol, glycerol, ethylene glycol), strong-non-solvent (water), and volatile solvent (THF, chloroform, dichloromethane). These additives change the thermodynamics property of polymer solution, thereby the phase inversion properties alter. Since the viscosity of polymer solution changes, kinetics of phase inversion mechanism is effected also. Aroon et al. 2010 investigated the effects of several additives on separation properties of PSF asymmetric flat membranes. As indicated in Table 3.1, the CO₂ permeance and CO₂/CH₄ selectivity of PSF membrane increased due to polymer or non-solvent additives into casting polymer solution. These are attributed to the fact that additives lead to shift the binodal line towards the polymer-solvent-additive axes. Hence instantaneous demixing creates more permeable membranes. High selectivity was observed due to rapid coalescence of polymer rich phase due to additives. By addition of volatile solvent (THF), the permeance value decreased with improvement in ideal selectivity. Aroon et al. 2010 explained this phenomenon via denser and thicker skin layer due to delayed-demixing induced by THF addition.

Ismail and Lai 2003 suggested that using a primary more volatile solvent and secondary less volatile solvent provides finer adjustment of solvent evaporation and polymer coagulation. Furthermore, skin layer formation of membrane is originated from outermost surface of the casting film, because evaporation of volatile solvent creates locally elevated polymer concentration at this region. Therefore, thickness and integrity of skin layer are closely related to evaporation rate and ratio of volatile and less volatile solvent. In the present study, we used acetone for PES and THF for PI solution as co-solvent. The effects of volatile solvent / non-volatile solvent on morphological and gas transport properties of membrane were investigated systematically.

Researchers focus mainly manipulation of rheological properties and compositional properties of membrane solution or coagulation medium. There are only a few researches about dry inversion period and its effect on membrane properties (Pinnau and Koros 1991).

Pinnau and Koros 1991 produced PSF membrane by three different methods; namely solvent evaporation, wet phase inversion and dry-wet phase inversion. The optimum gas separation performance was obtained from membranes prepared via dry-wet phase inversion with convective evaporation step. These membranes have ultra-thin skin layer approximately 270 Å with tightly packed nodular transition layer. In this process, air stream with 100% RH was blown down across PSF film surface for 10 seconds and then polymer film left for free standing evaporation for 15 seconds. Then after the film was quenched with MeOH. The He/N₂ and O₂/N₂ selectivity of these membranes were approximately 85% of selectivity of dense membrane which is an indicate of defect-free layer. Lower selectivity than intrinsic value can be result of increased free-volume in the ultra-thin skin layer. Hence, the actual skin layer may be thinner than apparent skin layer. Later on Pinnau and Koros 1993 pointed out that at the initial evaporation step outermost region of polymer film undergoes spinodal decomposition. Capillary pressure occurs at the space formed by polymer-poor phase in contact with air. This force acts normal to the membrane surface and leads to coalescence of polymer rich phase, hence formation of defects will be prevented.

Ismail and Lai 2003 and Ismail et al. 2011 induced that casting polymer film content (polymer concentration, solvent ratio (ratio of volatile solvent to non-volatile solvent)) and casting conditions (evaporation time, forced convection, casting shear rate) are very important precursors for defect-free ultra-thin skin membrane production. Ismail and Lai 2003 reported that evaporation period during dry inversion step leads to the increase in the thickness of skin layer and decrease the porosity of it as suggested by Machado et al. 1999 and Huang and Feng 1995. These studied proved that skin layer properties such as thickness or porosity can be changed by manipulation in evaporation step.

Mixed matrix membranes are composed of organic polymers as continuous phase and inorganic filler as disperse phase. Recently, mixed matrix membrane is widely preferred method to improve separation and transport properties of polymeric membrane.

Zulhairun et al. 2014-a prepared mixed matrix membrane made up of PSF and Cloisite-15A (abbreviated C15A) non-porous filler. This study reported that PDMS coating was mandatory for sealing defects. Membrane solution was prepared 30 wt.% PSF, 35 wt.% DMAc (non-volatile solvent), 30 wt.% THF (volatile solvent) and 5 wt.% ethanol (non-solvent) and the amount of C15A was from 0.5 to 2.0 wt.% of PSF. The CO₂ permeance increased with C-15A loading. The optimum result observed for 1 wt.% C-15A loading which was approximately 270% increment in CO₂ permeance with slight decrease in CO₂/CH₄ selectivity. Further increase in C-15A (2 wt.%) loading led to small increase in permeance but deteriorated the selectivity, which was attributed to non-selective voids on selective layer due to particle cluster. Enhancement in permeation despite the non-porosity of filler was because of additional free volumes at the clay-polymer interface and also gallery space in the clays.

Dorosti et al. 2015 enhanced the CO₂/CH₄ separation performance of Matrimid 5218 asymmetric flat membranes by incorporating nano-porous MIL-53 and ZSM-5 particles. Even small amount of filler loading such as 6 wt.% resulted in enhancement in both permeance and selectivity as depicted in Table 3.1. When the ZSM-5 loading exceeded 6 wt.%, the CO₂/CH₄ selectivity began to decrease which was attributed to creation of interfacial voids due to higher loading. This optimum loading value was higher for MIL-53 compared to ZSM-5. The deterioration of selectivity began for Matrimid/MIL-53 when MIL-53 loading was higher than 15 wt.%. The better performance of mixed matrix membrane incorporated with MIL-53 was ascribed the organic linkers of MIL-53 which provide better interaction between polymer and MIL-53. Hence formation probability of interfacial voids decreased. The highest CO₂/CH₄ selectivity was observed when Matrimid incorporated with 15 wt.% MIL-53. The detected CO₂

permeance was 19 GPU with 23.6 CO₂/CH₄ selectivity. The permeance was 3.8 times of the CO₂ permeance of neat Matrimid and the selectivity was 59% higher than CO₂/CH₄ selectivity of neat Matrimid. Although Dorosti et al. 2015 was not used volatile solvent, they kept casting solution at 50 °C for 2 min. to facilitate partially evaporation of NMP. The skin layer thickness of Matrimid mixed matrix membrane was reported approximately 3-5 μm. It was observed also agglomeration of MIL-53 and ZSM-5 particles especially 30% loading. But the agglomeration has any negative effect on permeance values. On the other hand, agglomeration of filler promoted the formation of interfacial voids which decreased the selectivity. Enhancement in permeance was attributed to increased free-volume of polymer due to ZSM-5 and MIL-53 loading. The improvement in ideal selectivity was explained by size selectivity characteristic of filler.

Ismail et al. 2015 studied about PES/Cloisite15A asymmetric flat sheet mixed matrix membrane. 1 wt.% exfoliated Cloisite15A resulted in increment of CO₂ permeance from 0.94 to 3.77 and CO₂/CH₄ selectivity from 16.94 to 46.89. On the other hand, the CO₂ permeance increased from 0.94 to 3.44 and CO₂/CH₄ selectivity increased from 16.94 to 22.57 due to 5 wt.% intercalated Cloisite15A loading. The difference arisen from the dispersion properties of filler. The improvements in permeance was ascribed to silicate galleries.

Md-Nordin et al. 2014 investigated the effect of ZIF-8 loading into PSF asymmetric flat membrane and reported that 1 wt.% ZIF-8 of PSF resulted in 51% and 47% increment in CO₂ permeance and CO₂/CH₄ selectivity, respectively.

Table 3.1 Gas separation properties of asymmetric polymeric membranes and effect of preparation methods on gas transport properties.

Membrane materials	Novelty in Membrane Preparation	Content	CO ₂ (GPU)	CO ₂ /CH ₄	Selective Layer Thickness	Reference
6FDA-BAAF	Using solvent with low dielectric constant and dipole moment		580	35	40-60 nm	Hachisuka et al. 1996
PES	Dual-nonsolvent bath				1.6- 2 μm	Van't Hof et al. 1992
	water		8.2	4		
	1-pentanol		5	55		
	glycerol		3.7	56		
	1-pentanol		1.9	56		
PSF	Non-porous filler Cloisite-15A	Neat PSF	19.88	23.12	250 nm	Zulhairun et al. 2014
	Using non-solvent additive	PSF-Cloisite15A (0.5%)	46.92	19.63		
	PDMS coating	PSF-Cloisite15A (1%)	74.91	20.98		
	Using volatile and non-volatile solvent together	PSF-Cloisite15A (2%)	75.4	4.20		

Table 3.1 (Cont.) Gas separation properties of asymmetric polymeric membranes and effect of preparation methods on gas transport properties.

Membrane materials	Novelty in Membrane Preparation	Content	CO ₂ (GPU)	CO ₂ /CH ₄	Reference
PSF	DC plasma treatment	No treatment	0.93	40	Yuenyao et al. 2015
		treatment	1.56		
PSF	ZIF-8 loading	PSF	4.97	7.52	Md-Nordin 2014
		PSF + %1 ZIF-8	7.50	11.03	
PSF	Using additives into casting solution	30% PSF - 70% NMP	7.26	4.43	Aroon et al. 2010
		30% PSF, 10%PEG, 60%NMP	16	5.93	
		30% PSF, 10%EtOH, 60%NMP	14.35	8.86	
		30% PSF, 10%PVP, 60%NMP	13.71	8.90	
		30% PSF, 10% glycerol, 60%NMP	17.64	15.07	
		30% PSF, 52.5% NMP, 17.5% THF	3.53	7.67	
		30% PSF, 10% PEG400, 45% NMP, 15% THF	5.36	10.31	
		30% PSF, 10% EtOH, 45% NMP, 15% THF	4.11	12.45	
		30% PSF, 10% PVPK15, 45% NMP, 15% THF	7.71	16.40	
		30% PSF, 10% glycerol, 45% NMP, 15% THF	8.23	32.65	

Table 3.1 (Cont.) Gas separation properties of asymmetric polymeric membranes and effect of preparation methods on gas transport properties.

Membrane materials	Novelty in Membrane Preparation	Content	CO₂ (GPU)	CO₂/CH₄	Reference
PES	Mixing with Cloisite15A	Neat PES	0.94	16.94	Ismail et al. 2015
		PES + 1 wt.% exfoliated Cloisite15A	3.71	46.89	
		PES + 5 w.% intercalated Cloisite15A	3.44	22.57	
Matrimid 5218	Using nano-porous filler ZSM-5 and MIL-53	Neat Matrimid	5.1	14.8	Dorosti et al. 2015
		Matrimid + 6 wt.% ZSM-5	6.6	15.6	
		Matrimid + 15 wt.% ZSM-5	11.1	7.2	
		Matrimid + 24 wt.% ZSM-5	14.5	4.8	
		Matrimid + 30 wt.% ZSM-5	21.0	3.6	
		Matrimid + 6 wt.% MIL-53	9	20.6	
		Matrimid + 15 wt.% MIL-53	19	23.6	
		Matrimid + 24 wt.% MIL-53	30	11.2	
		Matrimid + 30 wt.% MIL-53	46	7.5	

3.2 Experimental Method and Materials

3.2.1 Materials

Polyimide resin, Matrimid[®]5218 with 1.2 g/cm³ density, 588,000 g/mol molecular weight and 300°C glass transition temperature (T_g) was purchased from Alfa Easer. Polyimide resin was dried at least for one night at 80 °C before use. At 35 °C and 4 bar upstream pressure, the reported permeability coefficients of Matrimid[®]5218 membrane for H₂, CO₂, and CH₄ are 17.50, 7.29 and 0.21 Barrers, respectively (Zhang et al., 2008). The open chemical formula of Matrimid[®]5218 polymer monolayer is depicted in Figure 3.1.

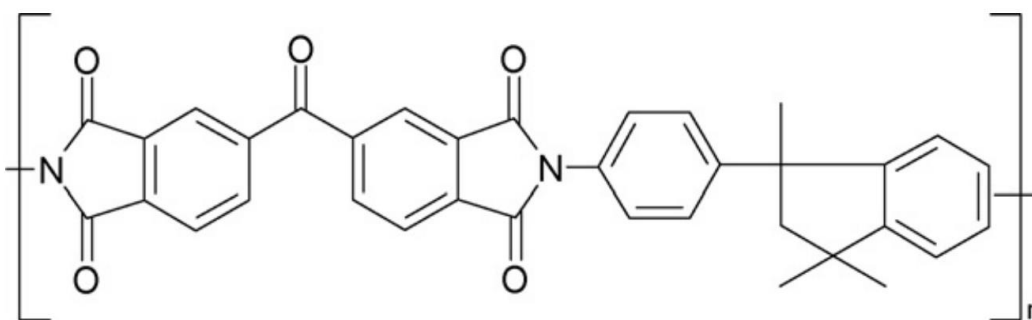


Figure 3.1 Chemical structure of Matrimid[®]5218 repeating monomer (Zhang et al., 2008).

Two solvents were used, one of them was high boiling point and the other one was low boiling point. The high boiling point solvent was N,N-Dimethylformamide (DMF) with high purity (>99%) was provided by Sigma-Aldrich. It has the linear chemical formula of HCON(CH₃)₂, normal boiling point of 153 °C, and density of 0.944 g/cm³ at 20 °C. The low boiling point solvent was Tetrahydrofuran EMPLURA[®] from Merk with purity higher than 99% and stabilized with 2,6-Di-tert-butyl-4-methylphenol (BHT). It has the chemical formula of C₄H₈O, normal boiling point of 65 °C, molecular weight of 72.11 g/mol and density of 0.89 g/cm³ at 20 °C.

ZIF-8 with 65 nm average particle size was used as MOFs based filler. The details of ZIF-8 synthesis and pre-treatment procedures were already expressed in

Chapter 2. In PI, unlike wet phase inversion of PES-ZIF-8 MMM production method, ZIF-8 crystals were used after thermal annealing (Treatment Type-3).

3.2.2 Light Induced Dry-Wet Phase Inversion Method

During this PhD. work, four different membranes production method were studied. These were solvent evaporation, vapor phase inversion, non-solvent induced phase inversion and dry-wet phase inversion. By solvent evaporation method, solvent is removed from polymer solution at high temperature under vacuum condition. By this method, non-selective, non-defected, symmetric thick membrane layer is obtained. The selectivity of these membranes is quite high while their permeance is low.

By dry-wet phase inversion method, asymmetric membrane with thin skin layer and thick porous support layer is obtained. Membranes with high permeance are produced by this method. Despite its convenience and advantage in terms of permeance, this method has also some problems. One of common problems is defective skin layer. The non-porous selective layer is formed during dry inversion step. However, this step is quite sensitive to environmental condition such as temperature or humidity. Moreover, during the wet inversion method strong non-solvent may lead to defects on selective layer. Similar problems are not observed in solvent evaporation method. Because of this reason, it was planned to combine these two methods; solvent evaporation and dry-wet phase inversion.

For this purpose, casted polymer solution was subjected to heating by exposing light source for a while. For light sources, infrared light bulb (IR-light) or incandescent lamp light (IL-light) was used. The main aim was obtaining more rigidified, homogeneous and defect-free polymeric layer by enhancing evaporation from surface. This method has not been tried before in literature and it has been innovated during this work. In this chapter, this method is abbreviated as LIDWPI. Dorosti et al. 2015 prepared by dry-wet phase inversion method and they used vacuum oven at 50 °C for two minutes during dry inversion. However, in this process evaporation step was controlled by convective heat transfer method. We preferred using light as a heat source because by light especially by IR-light heating

was provided via electromagnetic radiation which is more effective method for heating. Figure 3.2 shows the schematic presentation of light exposure step in dry inversion period. The appearance of the casting solution just after IR-light exposure can be seen in Figure 3.3.

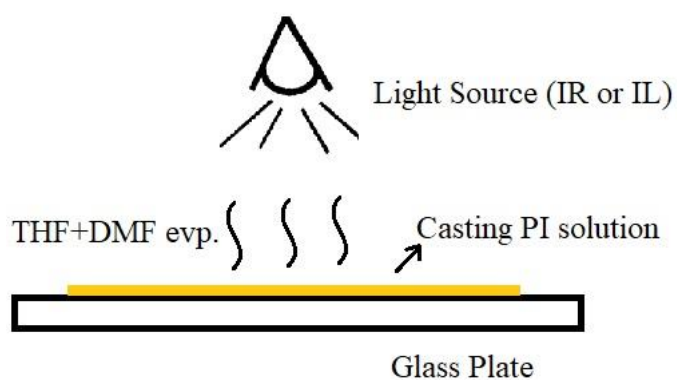


Figure 3.2 Schematic presentation of light exposure step in dry inversion step.



Figure 3.3 The appearance of the casting PI solution after the light-induced dry phase change, just prior to wet inversion step.

3.2.3 Light Induced Dry-Wet Phase Inversion (LIDWPI) for neat PI, PI/ZIF-8 Membranes

A homogeneous polymer solution consisting of 4 g of THF, 9.5 g of DMF and 4 g of PI was prepared. First, 4 g of THF and 9.5 g of DMF were mixed and then 4 grams of PI was added to this solvent mixture in three steps for priming purposes. The solution was mixed in a magnetic stirrer at 300 rpm at room temperature to dissolve the polymer. Before and after each PI addition, the polymer solution was sonicated in ultrasonic sound wave bath for ten minutes to accelerate the dispersion of the agglomerated polymer. After the polymer was completely dissolved and a homogeneous solution was obtained, the solution was allowed to stand overnight for degassing. The content of THF, which was another parameter, increased to 34 wt. % and decreased to 11 wt.% of the solution and the effects of the volatile solvent contents were examined.

The air conditioning cabinet (a home-made Glow Box) shown in Figure 3.4 was used to stabilize membrane casting conditions such as humidity and temperature. The membrane cabinet is about 40 liters in volume. It has an automatic film applicator and an infrared bulb at 250 Watt power. There are three discharge outlets on the cover and are numbered 1, 2, and 3 in Figure 3.4. The first discharge outlet is used to evacuate the solvent vapor in the cabinet. The other two outputs are designed to adjust the humidity of the air inside the cabin. The air inside the cabin is sucked by a fan through the outlet of the number 3 and humidified by passing through a column containing 700 ml of water at 100 °C then fed back to the cabin from the outlet of the number 2 by the help of the fan.

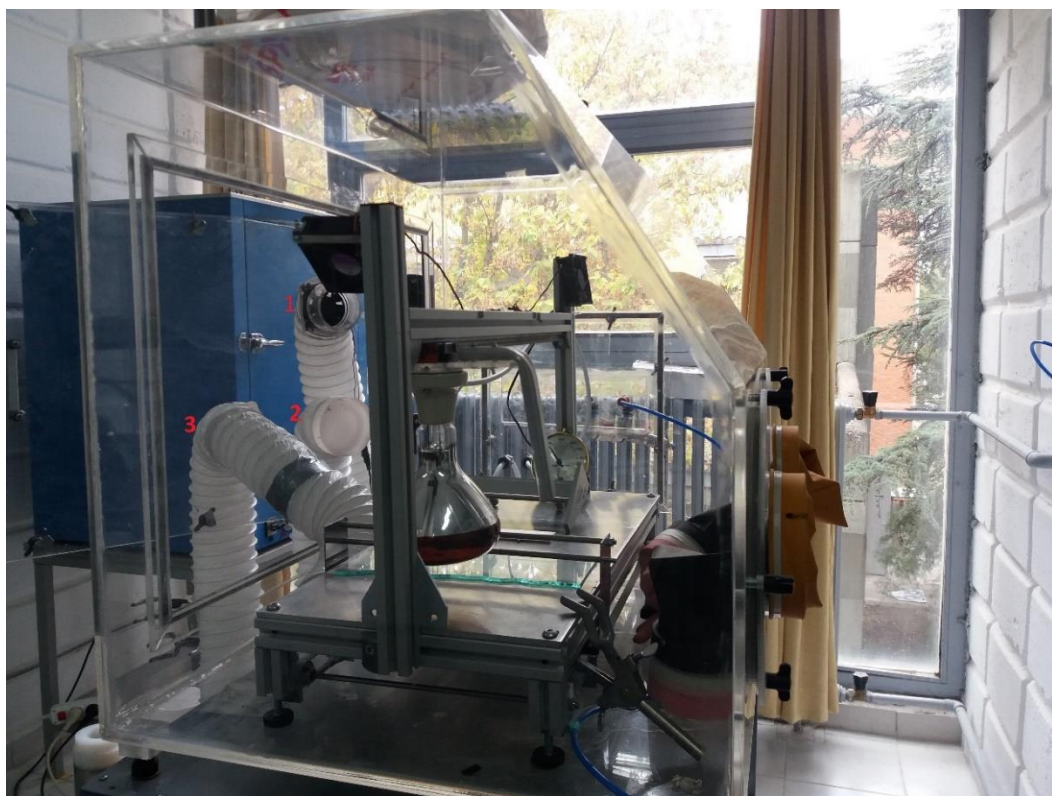


Figure 3.4 Glow Box

After bringing the humidity cabinet to the desired moisture value, the membrane solution was poured onto the glass surface with a thickness of 500 μm with the aid of an automatic film applicator. The polymer film was then exposed to infrared light during the dry phase change. Infrared light source is a General Electric bulb with 250 Watt power. In some experiment, incandescent light with 75 Watt was used instead of infrared light. During the dry phase change, the purpose of exposing the membrane to the infrared light is to accelerate the evaporation of the volatile solvent, thereby controlling the thickness of the selective non-porous skin layer and producing it in a non-destructive manner. After dry inversion step, casting film was quenched in 500 ml DI water. To remove the residual solvent, the solidified membrane was dried overnight in a 120 ° C vacuum oven.

In order to prepare PI/ZIF-8 mixed matrix membrane, ZIF-8 at 10% by mass of the polyimide was dispersed in 9.5 g DMF solvent. The ZIF-8/DMF solution was stirred at 300 rpm and at room temperature. The necessary amount of ZIF-8 was added at three or four step based on the amount. The solution was ultrasonicated

for 30 min between each step. After dispersion of necessary amount of ZIF-8 in the 9.5 g DMF solvent, 4 g THF was added to DMF/ZIF-8 solution. The 4 g of PI was added in three steps; 15 wt.% of total PI, 35 wt.% of total PI, and 50 wt.% of total PI, respectively. Before each addition, membrane solution was ultrasonicated for 10 minutes. The casting and annealing methodologies of mixed matrix PI/ZIF-8 membranes were the same as those of neat PI membranes.

PI membranes prepared by LIDWPI method were listed in Table 3.2 with their production specifications and their codes. The mixed matrix membranes were listed in Table 3.3 with production conditions.

Membrane Characterization: Morphological properties and gas separation performance of membranes were investigated by SEM and constant volume variable pressure gas test system, respectively. The details of these test method and system were already available in Chapter 2.3.5 experimental part.

Table 3.2 PI membranes produced via LIDWPI methods. Each membrane included 4 g PI.

Membrane Code	THF (g)	DMF (g)	Light Source	Dry-inversion (s)	Humidity
PI-8	4	9.5	IL	120	No control
PI-10	4	9.5	IL	120	No control
PI-11	4	9.5	IL	120	No control
PI-12	2	11.5	IL	120	No control
PI-13	6	7.5	IL	120	No control
PI-14	4	9.5	IR	6.5	No control
PI-15	4	9.5	IR	120	No control
PI-16	2	11.5	IL	120	No control
PI-17	6	7.5	IL	120	No control
PI-19	4	9.5	IR	120	No control
PI-20	4	9.5	IR	40	No control
PI-21	4	9.5	IR	6.5	No control
PI-22	4	9.5	No light	0	No control
PI-24	4	9.5	IR	40	No control
PI-25	4	9.5	IR	40	No control
PI-26	4	9.5	IR	20	No control
PI-28	4	9.5	No light	0	No control
PI-29	4	9.5	No light	0	No control
PI-30	4	9.5	No light	0	No control
PI-31	4	9.5	IR	60	No control
PI-32	4	9.5	IR	20	No control
PI-33	4	9.5	IR	120	No control
PI-34	4	9.5	No light	0	No control
PI-35	4	9.5	No light	0	No control
PI-36	4	9.5	No light	0	No control

Table 3.2 (Cont.) PI membranes produced via LIDWPI methods. Each membrane included 4 g PI.

Membrane Code	THF (g)	DMF (g)	Light Source	Dry-inversion (s.)	Humidity
PI-37	4	9.5	No light	0	No control
PI-38	4	9.5	IR	240	No control
PI-39	4	9.5	IR	240	No control
PI-40	4	9.5	IR	240	No control
PI-41	4	9.5	IR	240	No control
PI-42	4	9.5	IR	60	No control
PI-43	4	9.5	IR	120	No control
PI-48	4	9.5	IR	60	35 % RH
PI-49	4	9.5	IR	60	80 % RH
PI-52	4	9.5	IR	60	80 % RH
PI-53	4	9.5	IR	60	50 % RH
PI-54	4	9.5	IR	20	50 % RH
PI-55	4	9.5	IR	20	80 % RH
PI-57	4	9.5	IR	20	25 % RH
PI-58	4	9.5	No light	0	80 % RH
PI-59	4	9.5	IR	240	80 % RH
PI-60	4	9.5	No light	0	20 % RH
PI-61	4	9.5	IR	60	20 % RH
PI-63	4	9.5	IR	120	80 % RH
PI-64	4	9.5	IR	60	80 % RH
PI-66	4	9.5	IR	60	80 % RH
PI-68	4	9.5	IR	60	80 % RH
PI-69	4	9.5	IR	40	80 % RH
PI-70	4	9.5	No light	0	50 % RH
PI-71	4	9.5	IR	180	80 % RH
PI-72	4	9.5	IR	180	

Table 3.3 PI-ZIF-8 mixed matrix membranes produced via LIDWPI methods. Each casting solution was prepared from 4 gr. PI, 4 gr THF as volatile solvent, 9.5 gr DMF as non-volatile solvent.

Membrane Code	ZIF-8 Filler (65 nm in size)	Light Source	Dry-inversion (s)	Humidity
M-PI-1	%3 annealed	No Light	0	No control
M-PI-2	%3 annealed	No Light	0	No control
M-PI-3	%3 annealed	No Light	0	No control
M-PI-4	%3 annealed	IR	240	No control
M-PI-5	%5 annealed	IR	240	No control
M-PI-8	%5 non-annealed	IR	10	No control
M-PI-10	%10 non-annealed	IR	20	80% RH
M-PI-11	10% annealed	IR	20	80% RH
M-PI-12	10% annealed	IR	240	80% RH
M-PI-13	10% annealed	IR	120	80% RH
M-PI-14	10% annealed	IR	180	80% RH
M-PI-15	10% annealed	No Light	0	80% RH
M-PI-16	10% annealed	No Light	60	80% RH

3.3 Experimental Results of PI Membranes Produced via LWDPI Method

Polymer used in this PHD work was changed because of several reasons listed below;

- Despite all efforts the permeance of PES membranes could not exceed 60 GPU for H₂, 25 GPU for CO₂ and 15 GPU for CH₄.
- The selectivity values could not exceed 2 unless PDMS coating. (The experimental results were provided in Appendix A)
- Polyimide is more suitable and widely used polymer for high flux asymmetric gas separation membrane fabrication especially commercially available Matrimid (Clausi and Koros 2000).

Based on the Hansen Solubility of Matrimid with common solvents listed in Table 5.9, DMF is a solvent for Matrimid but at the limit of solubility, because $\Delta\delta_{\text{Matrimid-DMF}}=7.3$. Moreover, the miscibility THF-DMF is also at the limit since $\Delta\delta_{\text{THF-DMF}} = 8$. $\Delta\delta_{\text{THF-water}}$ and $\Delta\delta_{\text{water-DMF}}$ values are quite high showing low interaction between solvent and non-solvent, that property increases the coagulation and phase separation rate (Chung and Kafchinski 1997). Nevertheless, the system of Matrimid-THF-DMF-water was preferred instead of Matrimid-Acetone-NMP-water system for membrane casting. Because this system is near its limit of solubility or thermodynamic instability and closer position to phase separation which provides a membrane layer with open pores and a thin selective layer. Several authors (Aroon et al. 2010, Ismail et al. 2011, Clausi and Koros 2000) added non-solvent into the casting polymer solution for this purpose. Furthermore, low dissolving power promotes polymer-polymer interaction which leads to more-tightly coiled conformation (Aroon et al. 2010).

Table 3.4 Hansen solubility parameter difference ($\Delta\delta$) between polymer (PES)-solvent (DMF)-co-solvent(Acetone)-quench medium(Water).

Chemicals	$\delta_d(\text{MPa}^{0.5})$	$\delta_h(\text{MPa}^{0.5})$	$\delta_p(\text{MPa}^{0.5})$	$\delta(\text{MPa}^{0.5})$	
Matrimid (Dong et al. 2010)	18.7	6.7	9.5	22.01	
THF (Dong et al. 2010)	16.8	8	5.7	19.46	
Acetone	15.5	6.9	10.4	19.9	
$\Delta\delta$					
	Matrimid	THF	Acetone	DMF	Water
Matrimid	-	4.44	3.3	7.3	34.24
THF	4.44	-	4.99	8.0	37.49
DMF	7.3	8.0	7.12	-	31.1
Water	34.24	37.49	33.2	31.1	-
Acetone	3.3	4.99	-	7.12	33.2
NMP	6.1	4.71	6.38	4.37	35.4

3.3.1 Effect of THF/DMF Ratio on Membrane Morphology

SEM micrographs of asymmetric PI membrane prepared from solution with different THF/DMF ratio have been given in Figure 3.5 and the quantitative analyze based on SEM images can be seen in Table 3.5. The dense skin layer and also finger type pores of asymmetric PI membrane were more distinctive compared to those of asymmetric PES membranes prepared via LIDWPI method. The total PI membrane thickness varied in inversely proportional to the THF/DMF ratio in the casting solution. The total membrane thickness increased from 160 μm to 240 μm corresponding to the decrease in the THF/DMF ratio from 80% to 17.4%. The percent increase in THF/DMF ratio from 17.4% to 42.2% led to increase in skin layer thickness from 114 nm to 275 nm. When the THF/DMF ratio was 80% in the casting solution, the detected skin layer thickness was nearly 656 nm. Change in solvent ratio affected membrane performance and morphology by changing the kinetics of phase change. The thermodynamic interaction between DMF and PI is weaker than that between THF and PI, while the miscibility of THF-water is weaker than that of DMF-water. As the THF ratio in the solvent increased, the diffusion of solvent into non-solvent slowed down, hence phase change delayed. As a result, denser and thinner membrane layer was obtained. There are several researches which support our findings and theory. Similar observation was also reported by Aroon et al. 2010 whose suggested that the skin layer of PSF membrane increased from 560 nm to 800 nm due to addition of THF into NMP-PSF solution with 15%. Aroon et al. 2010 and Ismail and Lai 2003 attributed the thicker skin layer to induction of the delayed liquid-liquid demixing due to existence of THF. Ismail and Lai 2003 studied about properties of PSF membrane depending on THF/DMAC/EtOH ratio in the casting solution. Since boiling point of THF is considerably lower than both DMAC and EtOH, they assumed that only THF removed from outermost region of casting film during dry inversion. Their experience was perfectly match with our findings. The skin layer thickness of PSF membrane increased with increase the amount of THF in the casting solution. According to Ismail and Lai 2003, higher amount of THF led to high evaporation rate which enlarged the region of elevated polymer concentration, thereby denser

and thicker skin layer was acquired. Clausi and Koros 2000 documented that the skin layer of hollow fiber Matrimid extended from 760 Å to 1430 Å by increasing THF content of the Matrimid/NMP solution from 5% to 10 % of the solution.

Table 3.5 Effect of THF/DMF ratio on the asymmetric PI membrane morphology prepared via LIDWPI method and exposed to 120 s IL.

Membrane Code	Casting Solution Composition (wt.%)	Total Thickness (µm)	Skin layer Thickness (nm)	Pore Shape
PI-13	34.3% THF- 22.9% PI- 42.9% DMF (0.80 THF/DMF)	162.15±3.87	656±113	Spongy + Finger like
PI-11	22.9% THF- 22.9% PI- 54.3% DMF (0.42 THF/DMF)	201.33±1.41	275±9.55	
PI-12	11.4% THF- 22.9% PI- 65.7% DMF (0.17 THF/DMF)	240.47±1.91	114±2.79	

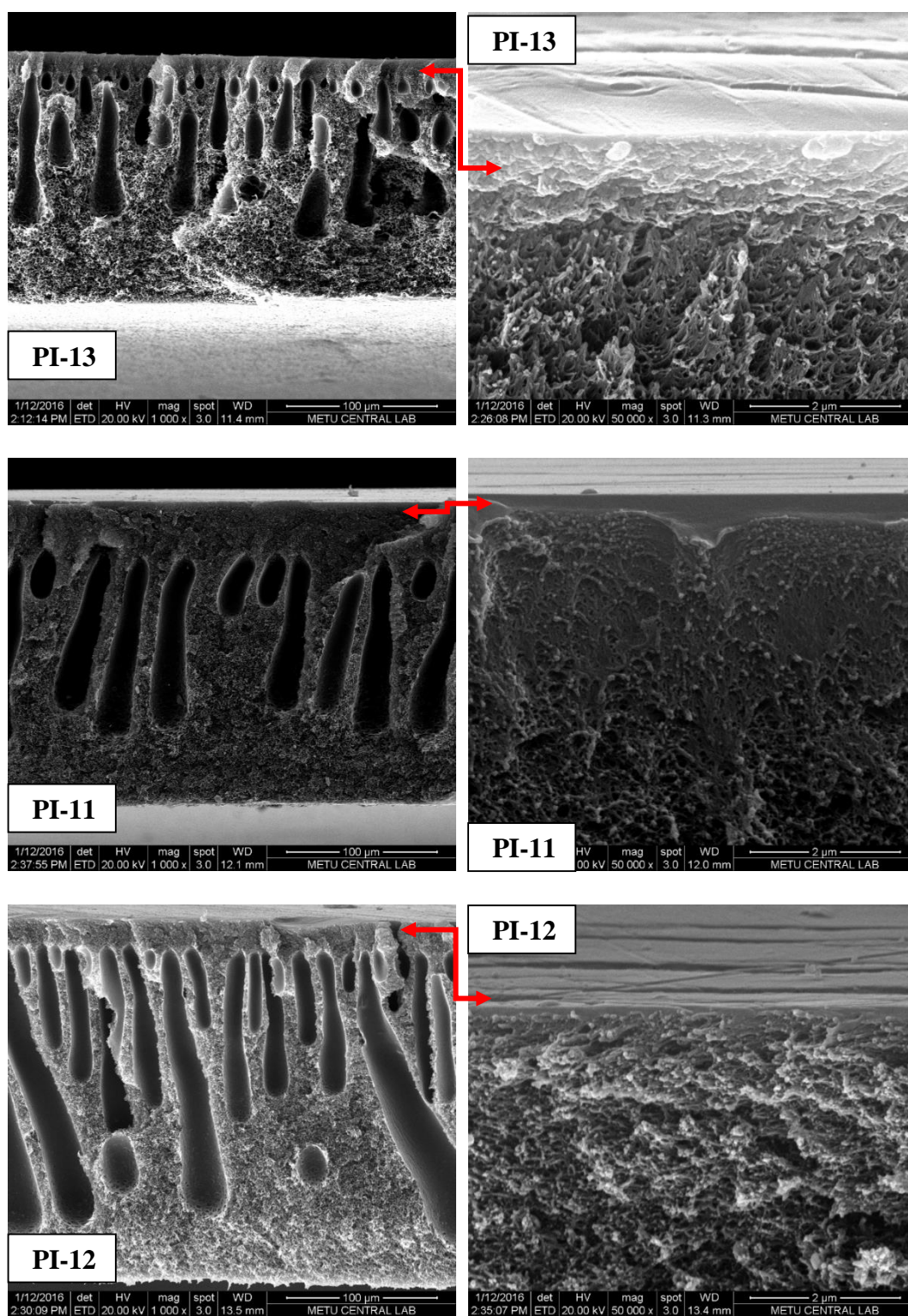


Figure 3.5 SEM micrographs of PI membranes prepared from solution with different THF/DMF ratio and exposed to 120 s IL for dry inversion; PI-13 (34.3%THF-22.9%PI-42.9%DMF); PI-11 (22.9% THF-22.9%PI-54.3%DMF); PI-12 (11.4% THF-22.9%PI-65.7%DMF)

3.3.2 Effect of THF/DMF Ratio on Membrane Gas Separation Properties

The gas separation properties of asymmetric PI membranes, which have been given in Table 3.6, were changed depending on THF/DMF ratio of casting solution. The gas permeance of membrane decreased with increase in THF/DMF ratio. Both CO₂/CH₄ and H₂/CH₄ ideal selectivity values increased with increase in THF/DMF ratio, while H₂/CO₂ ideal selectivity decreased slightly with increase in THF/DMF ratio from 42.2% to 80%.

The morphological properties of membrane were compatible with gas permeance properties of them. The membrane with largest skin layer thickness (PI-13) has the lowest gas permeance and highest ideal selectivity values of H₂/CH₄ and CO₂/CH₄. As the thickness of the selective skin layer increases, the resistance against mass transfer also increases, hence lower permeance value is obtained. CO₂ permeance of PI membranes were measured 0.81 GPU, 2.55 GPU and 6.65 GPU corresponding to the 80%, 42.2%, 17.4% THF/DMF ratio of casting solution, respectively. Although the highest CO₂ permeance was detected as 6.65 GPU belonging to membrane PI-12 and PI-16, the 17.4% THF/DMF ratio for casting solution was not preferred in further research, since the corresponding CO₂/CH₄ ideal selectivity was only 3.43. 80% THF/DMF ratio (PI-13) was also eliminated despite 42.63 CO₂/CH₄ selectivity, because of low permeance values. It was decided to use solutions with a THF / DMF ratio of 42.4% in the further experiments. Although Aroon et al. 2010 did not studied about THF/NMP ratio systematically, but they also argued the decrease in CO₂ permeance with enhancement in CO₂/CH₄ selectivity of PSF membrane. When adding THF with (1/3 = THF/NMP) ratio, the CO₂ permeance of PSF membrane decreased from 7.26 to 3.53 GPU while CO₂/CH₄ ideal selectivity was enhanced from 4.43 to 7.67 compared to the membrane casted from neat NMP/PSF solution. According to Aroon et al. 2010, THF effects the gas transport properties of membrane by three ways. Firstly, THF hinders the formation of macro-voids. Secondly, THF induces delay in liquid-liquid demixing which leads to denser selectivity layer. Finally, evaporation of highly volatile THF results in rapid vitrification of polymer rich

phase hence defect-free skin layer is formed. In our case, by increasing THF/DMF ratio in the PI solution, we enhanced the effects of THF. Shieh and Chung 1998 inquired the effect of THF content of solution on O₂ permeance of cellulose acetate membrane, it was reported that the highest O₂ permeance observed at 20 wt.% THF, then the permeance decreased gradually due to increase in THF content. This result is compatible with our findings. Furthermore, Ismail and Lai 2003 detected lower H₂ and O₂ permeance of PSF membrane with increment in volatile solvent THF amount in the casting solution. This is attributed to the inhibition of mass transfer due to extra resistance of enlarged and densified skin layer by evaporation of THF. Clausi and Koros 2000 corroborates both our findings and the other studies. They induced that the O₂ permeance of Matrimid hollow fiber reduced from 19.9 to 9.2 GPU while O₂/N₂ enhanced from 5.6 to 7.4 corresponding to increase in the THF content from 5% to 10% of the dope solution.

Table 3.6 The permeance and selectivity of neat PI membranes based on THF/DMF ratio. IL exposure was 120 sec.

THF/DMF	Content of Membrane Solution	Membrane Code	Permeance (GPU)			Ideal Selectivity		
			H ₂	CO ₂	CH ₄	H ₂ /CO ₂	H ₂ /CH ₄	CO ₂ /CH ₄
80%	34.3%THF- 22.9%PI- 42.9%DMF	PI-13-p1	2.96	0.81	0.019	3.65	155.79	42.63
		PI-13-p2	2.91	0.81	0.019	3.59	153.16	42.63
		Average	2.94	0.81	0.019	3.62	154.5	42.63
42.2%	22.9%THF- 22.9%PI- 54.3%DMF	PI-8-p1	10.31	2.21	0.143	4.67	72.10	15.45
		PI-8-p2	11.98	2.48	0.167	4.83	71.74	14.85
		PI-8-p3	12.77	2.64	0.29	4.84	44.03	9.10
		PI-10-p1	12.29	2.85	0.138	4.31	89.06	20.65
		PI-10-p2	12.17	2.72	0.14	4.47	86.93	19.43
		PI-11-p1	9.41	2.32	0.088	4.05	106.9	26.36
		PI-11-p2	12.24	2.63	0.21	4.65	58.29	12.52
17.4%	11.4%THF- 22.9%PI- 65.7%DMF	Average	11.60	2.55	0.17	4.55	75.58	16.91
		PI-12-p1	29.4	5.69	2.57	5.17	11.44	2.21
		PI-16-p1	30.08	7.36	2.21	4.09	13.61	3.33
		PI-16-p2	27.23	6.9	1.45	3.95	18.78	4.76
		Average	28.90	6.65	2.08	4.4	14.61	3.43

3.3.3 Importance of Light Source

Two different light sources were used in LIDWPI method. One of them was 70 Watt incandescent lamp with 300-700 nm wave length. The other was the 250 Watt infrared light lamp with 750-1400 nm (Near Infrared range) wave length. The electromagnetic spectrum range was provided in Figure 3.6. The differences in light sources resulted in different amount of heat transfer to the casting film, hence the amount of evaporated THF or increase in temperature of the casting polymer film will be changed based on light source.

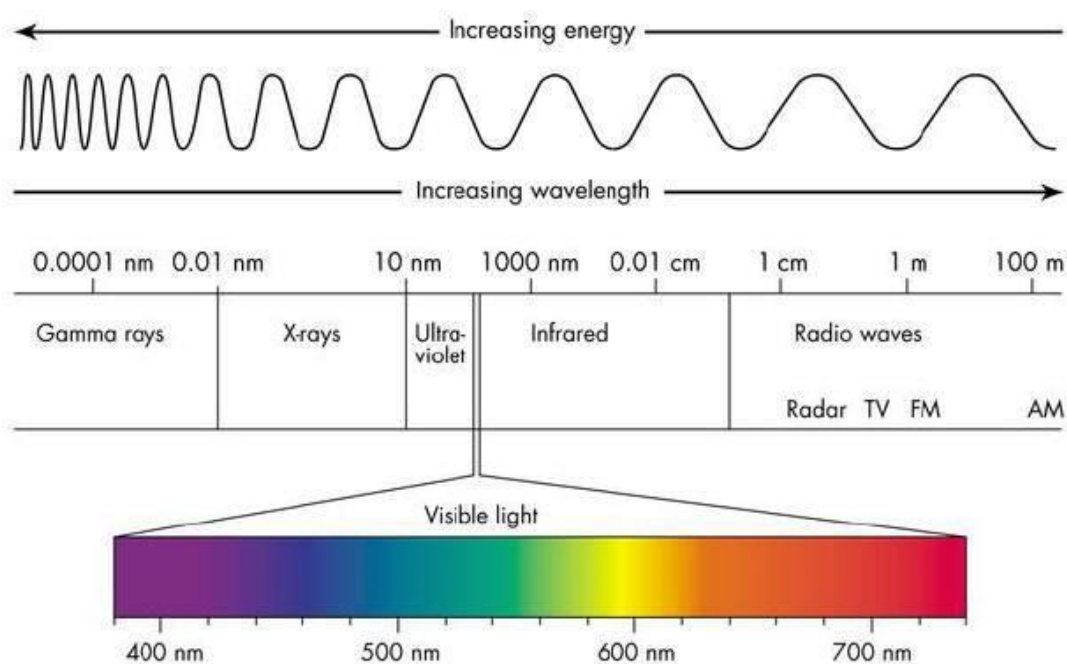


Figure 3.6 Electromagnetic Spectrum ("What is Full Spectrum Lighting?," 2012)

The Amount of Heat from Lamps

$$\Delta H_{\text{vap-THF}} = 443.77 \text{ j/g (Flick, 1998)}$$

$$\Delta H_{\text{vap-DMF}} = 641.59 \text{ j/g (Flick, 1998)}$$

Assumption;

- All electrical energy given to the lamps was used in perfect efficiency.

The Amount of Heat from Incandescent Lamp

The Luminous efficiency of incandescent lamp is not more than 2.6% ("Luminous efficacy," 2017). For 70-watt incandescent lamp produced

$$70 \times 0.02 = 1.4 \text{ Watts of light}$$

$$70 \times 0.98 = 68.6 \text{ Watts of heat}$$

Since the percent of visible light is small its effect on heating was omitted. The other assumption is that 68.6 J/s is transferred to the casting solution without loss.

The Amount of Heat from IR-Lamp

The IR-lamp provided heat to the object through electromagnetic radiation.

Assumption;

- Casting polymer solution behaves as blackbody.

Wien's Displacement Law and Stefan-Boltzman Law can be used to estimate transferred energy (Bergman, Dewit, Lavine, and A. S., Incropera, 2005).

$$\text{Wien's Law} \quad \lambda^{\max} T = C \quad \text{where } C \text{ is } 2898 \text{ } \mu\text{m.K}$$

$$T = 2898 \text{ } \mu\text{m.K} / 1.4 \text{ } \mu\text{m} = 2070 \text{ K}$$

$$\text{Stefan-Boltzman Law} \quad E_b = \sigma T^4 \quad \text{where } \sigma \text{ is } 5.670 \times 10^{-8} \text{ W/m}^2\text{K}^4$$

$$E_b = 5.670 \times 10^{-8} \text{ (W/m}^2\text{K}^4) \times (2070)^4 = 1041033 \text{ W/m}^2$$

The exposed surface area of casting solution;

$$= \pi \times (10 \text{ cm})^2 / 4 = 78.54 \text{ cm}^2 = 7.85 \times 10^{-3}$$

The obtained heat energy per second;

$$= 1041033 \text{ W/m}^2 \times 7.85 \times 10^{-3} \text{ m}^2 = 8176.25 \text{ J/s}$$

Based on these rough estimation; for a few seconds IR exposure is sufficient to evaporate all THF and DMF, whereas the heat of incandescent light can increase the temperature of casting solution slightly.

It is essential to note that calculations made in this section are very simple and are based on several rough assumptions. However, it can be interpreted that the energy obtained from infrared radiation is significantly higher than that of incandescent light.

3.3.4 Effect of Light Source on Membrane Morphology

The SEM micrographs of asymmetric PI membranes exposed different light source during dry inversion have been provided in Figure 3.7. The thickness of total membrane layer and skin layer of PI-11 were measured as $201.33 \pm 1.41 \mu\text{m}$ and $275 \pm 9.55 \text{ nm}$, respectively, while those of PI-63 were measured as $190.22 \pm 1.1 \mu\text{m}$ and $322 \pm 4.24 \text{ nm}$. Based on SEM investigation, using IR instead of IL resulted in $10 \mu\text{m}$ decrease in total membrane thickness while 50 nm increase in the thickness of dense skin layer. In fact, such thickness differences can be seen even in different region of the same membrane due to the complex nature of the dry-wet phase inversion. However, according to my experience, this was not a coincidence. IR exposure instead of IL promoted THF evaporation because of higher amount of heat energy provided by IR. After IR exposure, denser polymer layer was introduced to wet phase inversion, hence thinner and denser membrane layer was obtained. The thickness of the selective dense skin layer increased proportionally to the amount of THF evaporated.

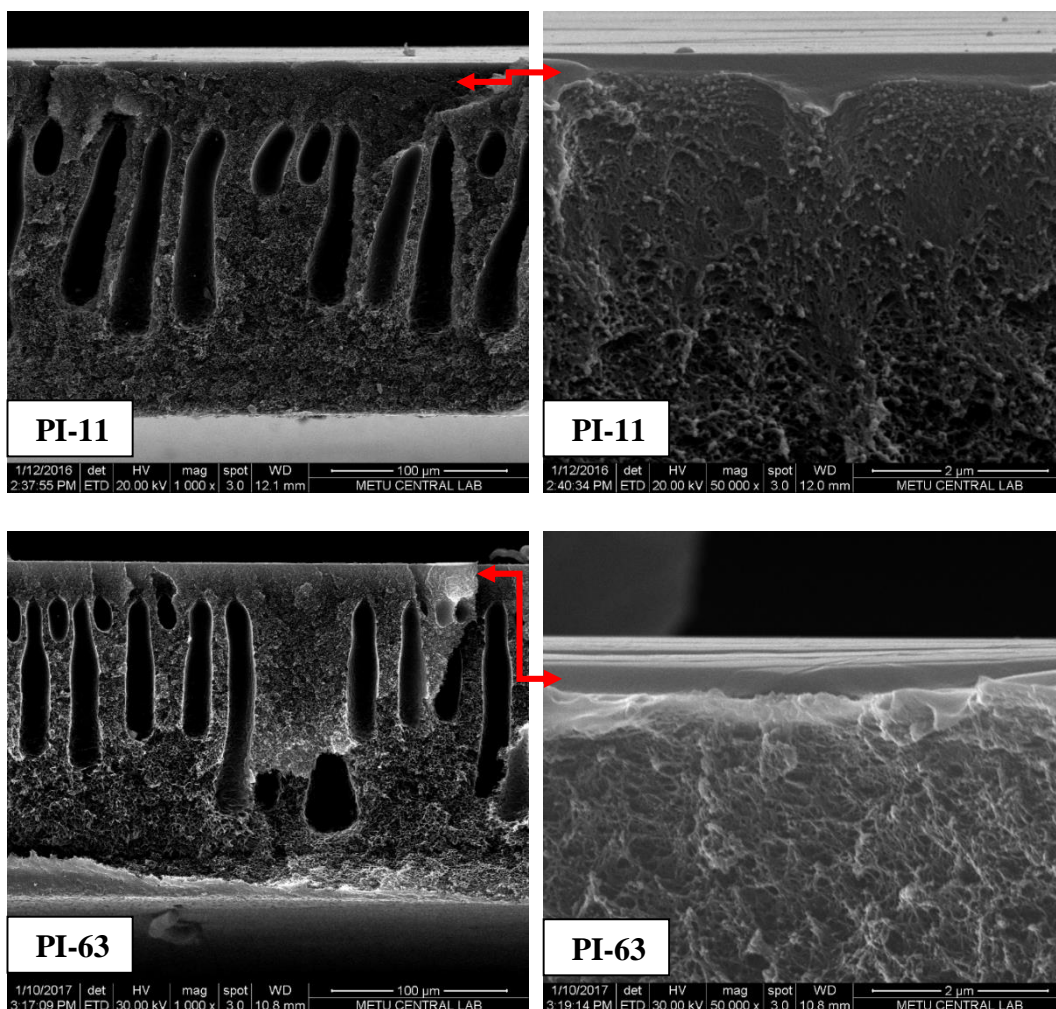


Figure 3.7 SEM micrographs of PI membranes exposed to 120 s IL (PI-11), and exposed to 120 s IR (PI-63). Both of them prepared from solution with 0.42 THF/DMF ratio.

3.3.5 Effect of Light Source on Membrane Gas Separation Properties

Table 3.7 has been shown the gas separation performance of asymmetric PI membranes exposed to 120 s IL or IR during dry inversion. Preference of IR instead of IL led to percent decrease of 61%, 49% and 61% in H_2 , CO_2 , CH_4 permeance, respectively while resulting in slightly enhancement in ideal selectivity values. The reduction in permeance was attributed to the increase in the thickness of skin layer of membrane approximately 50 nm (the percent increase was 17%) due to IR exposure. The percent of increase in skin layer was significantly lower than that of

decrease in permeance. This reinforced the prediction that the membrane probably had the transition layer with closed pores, which showed additional resistance against gas permeance. IR exposure enhanced the enlargement of this transition layer.

In literature, there are no studies about accelerated dry phase change using different light sources. However, many authors have reported that as the evaporation rate of the volatile solvent increases, the skin layer thickness increases and gas transfer values decrease (Ismail and Lai 2003, Zulhairun et al. 2014-b). For example, Zulhairun et al. 2014-b flushed non-reactive gases such as N₂ or He along the surface of membrane with a certain period of time (dry-inversion period) and with a certain flow rate. The purpose and the logic are the same; to promote evaporation rate of solvent. They observed enlargement in skin layer, decrease in CO₂ permeance and enhancement in CO₂/CH₄ selectivity for membranes exposed to higher convection flow rates. These findings are in harmony with our observations, since the influence of the flow rate is similar to the effect of light source or difference in the energy obtained from different light source.

Table 3.7 Gas separation performance of neat PI membrane depending on difference in the light source. Each membrane was prepared from solution %22.9% THF-22.9%PI-54.3%DMF (42.2% THF/DMF ratio). Exposure period was 120 s.

Light Source	Membrane Code	Permeance (GPU)			Ideal Selectivity		
		H ₂	CO ₂	CH ₄	H ₂ /CO ₂	H ₂ /CH ₄	CO ₂ /CH ₄
IL (120 s)	PI-8-p1	10.31	2.21	0.143	4.67	72.10	15.45
	PI-8-p2	11.98	2.48	0.167	4.83	71.74	14.85
	PI-8-p3	12.77	2.64	0.29	4.84	44.03	9.10
	PI-10-p1	12.29	2.85	0.138	4.31	89.06	20.65
	PI-10-p2	12.17	2.72	0.14	4.47	86.93	19.43
	PI-11-p1	9.41	2.32	0.088	4.05	106.9	26.36
	PI-11-p2	12.24	2.63	0.21	4.65	58.29	12.52
	Average	11.60	2.55	0.17	4.55	75.58	16.91
IR (120 s)	PI-15-p1	4.24	1.23	0.038	3.45	111.58	32.37
	PI-15-p2	4.53	1.2	0.042	3.78	107.86	28.57
	PI-19-p1	5.77	1.87	0.068	3.09	84.85	27.5
	PI-19-p2	5.16	1.54	0.068	3.35	75.88	22.65
	PI-33-p1	4.35	1.21	0.1	3.60	43.5	12.1
	PI-33-p2	3.88	1.14	0.06	3.40	64.67	19
	PI-43-p1	4.24	1.15	0.040	3.69	107.34	29.11
	PI-63-p1	4.19	1.16	0.094	3.61	44.57	12.34
	Average	4.55	1.31	0.064	3.49	80.03	22.96

3.3.6 Effect of IR Exposure Period on Membrane Morphology

Figure 3.8 has been showing cross-sectional view of asymmetric PI membrane exposed to IR for 0, 20, 40, 60, 120 and 240 s in dry inversion at which relative humidity was 80%. At first glance, the membranes exposed to IR for 0, 20, 40, 60 and 120 s had several common traits. The membranes were composed of two types of pore types, namely finger like and spongy. The spongy pores became smaller as they get closer to the dense skin layer. The finger type pores located just behind the spongy pores under the dense skin layer. When the IR exposure period reached 240 s, the finger type pores disappeared and the skin layer extended significantly.

The closer view of skin layers of these membranes have been given in Figure 3.9. The thickness of skin layer extended with increasing IR exposure period. The pores of the transition layer were so small that they cannot be measured even at 50 000 magnifications. These pores were out of focus because of their nodular and reticulated form. With the prolonged period of IR exposure, this transition layer almost meshed with the skin layer.

The quantitative analyze based on these SEM micrographs has been provided in Table 3.8. The thickness of skin layer was measured as approximately 70.5 nm for the membrane prepared without IR exposure. With increase in IR exposure period, the skin layer thickness increased and exceeded 10 μm for membrane exposed to 240 s IR in dry inversion. The observation was compatible with my expectation. Since the skin layer formation was associated with dry inversion step and the amount of evaporated volatile solvent, by increasing the period of dry inversion and enhancement of THF evaporation with IR exposure thicker skin layer was obtained. This observation is also in agreement with the results reported by Yuenyao et al. 2015 and Ismail et al. 2011. Yuenyao et al. 2015 suggested that by increasing evaporation time from 0 to 60 s, the skin layer thickness of polysulfone membrane increased from 0.33 μm to 8.5 μm . The total thickness of membrane increased, spongy pores increased, number of finger like and macro-pores were lowered due to longer evaporation time. Ismail et al. 2011 observed that the skin layer of membrane increased from 495.35 \AA to 709.16 \AA and surface porosity decreased from $0.754 \times 10^{-4} \text{ cm}^2/\text{cm}^2$ to $0.346 \times 10^{-4} \text{ cm}^2/\text{cm}^2$ due to increment in evaporation time from 8 seconds to 20 seconds. Both Yuenyao et al. 2015, Ismail et al. 2011, and Ismail and Lai 2003 observed transition layer formation. Both Koros and Ismail groups investigated effects of forced-evaporation time interval. The prolonged evaporation time might remove plenty of volatile solvent, thereby densified polymer region enlarged which led to nascent and thick skin layer. This densified layer shows resistance against solvent-nonsolvent exchange during wet phase inversion. Consequently, delayed liquid-liquid demixing arises. Hence, thicker skin layer, reduction in porosity, closed pores are observed. Probably, the reason of this transition zone with closed and tiny pores

arises from the resistance of solvent-nonsolvent exchange applied by densified polymer region.

For our membranes, the thickness of transition layer oscillated between 10 and 15 μm , and it was not possible to establish a relationship between transition layer thickness and IR exposure period. When the IR exposure period reached 240 s, the transition layer meshed with the skin layer. The total thickness of membrane increased with IR exposure period up to 60 s and then decreased with further increase in the IR exposure time. When the IR exposure period reached to 240 seconds, the measured total membrane thickness was approximately 127 μm . The decrease in the total membrane thickness with IR exposure is expected, because evaporation of solvent resulted in denser polymer layer. In addition, denser polymer layer led to thicker skin layer and support layer with small pores. Nevertheless, the increase in total membrane thickness up to 60 s IR exposure indicated that there are several factors other than IR exposure that influence membrane morphology. When the IR exposure period is short, these factors cannot dominate each other and fluctuation in thickness was observed. The temperature differences between polymer and quenching bath can be given as an example for factors affecting morphology other than IR exposure period. Because of temperature difference between DMF and quench medium, higher diffusion might take place during wet quenching and larger pores might lead to larger membrane layer. In addition, thermally expanded polymer film may have formed volumetrically larger membrane layer. When the IR exposure period exceeded to 60 seconds, IR effect became dominant and expected result for example larger skin layer and thinner total layer can be observed.

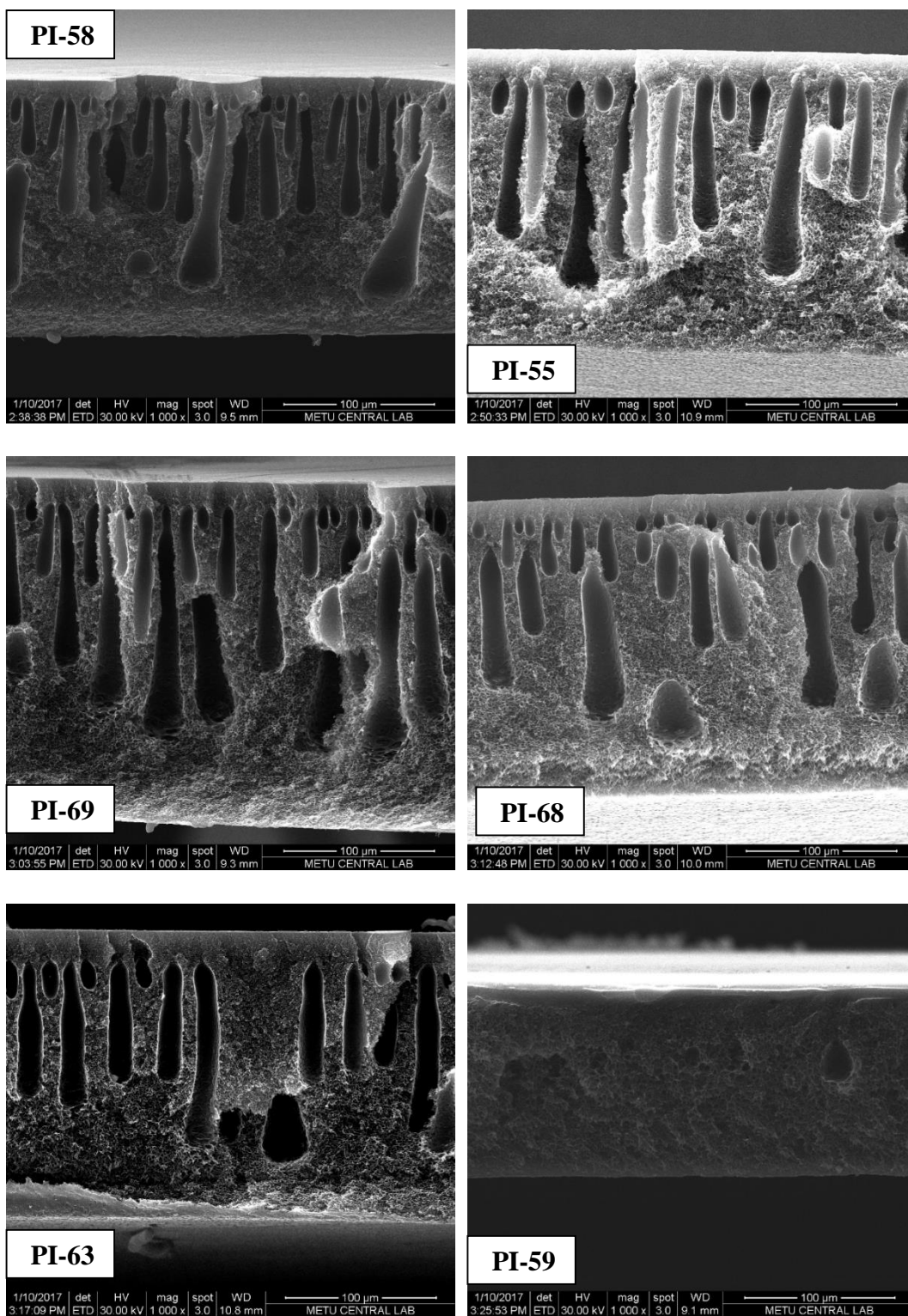


Figure 3.8 SEM micrographs of asymmetric PI membranes prepared via LIDWPI method and exposed to IR for 0 s (PI-58), 20 s (PI-55), 40 s (PI-69), 60 s (PI-68), 120 s (PI-63), and 240 s (PI-59) in dry inversion step at which relative humidity was 80%.

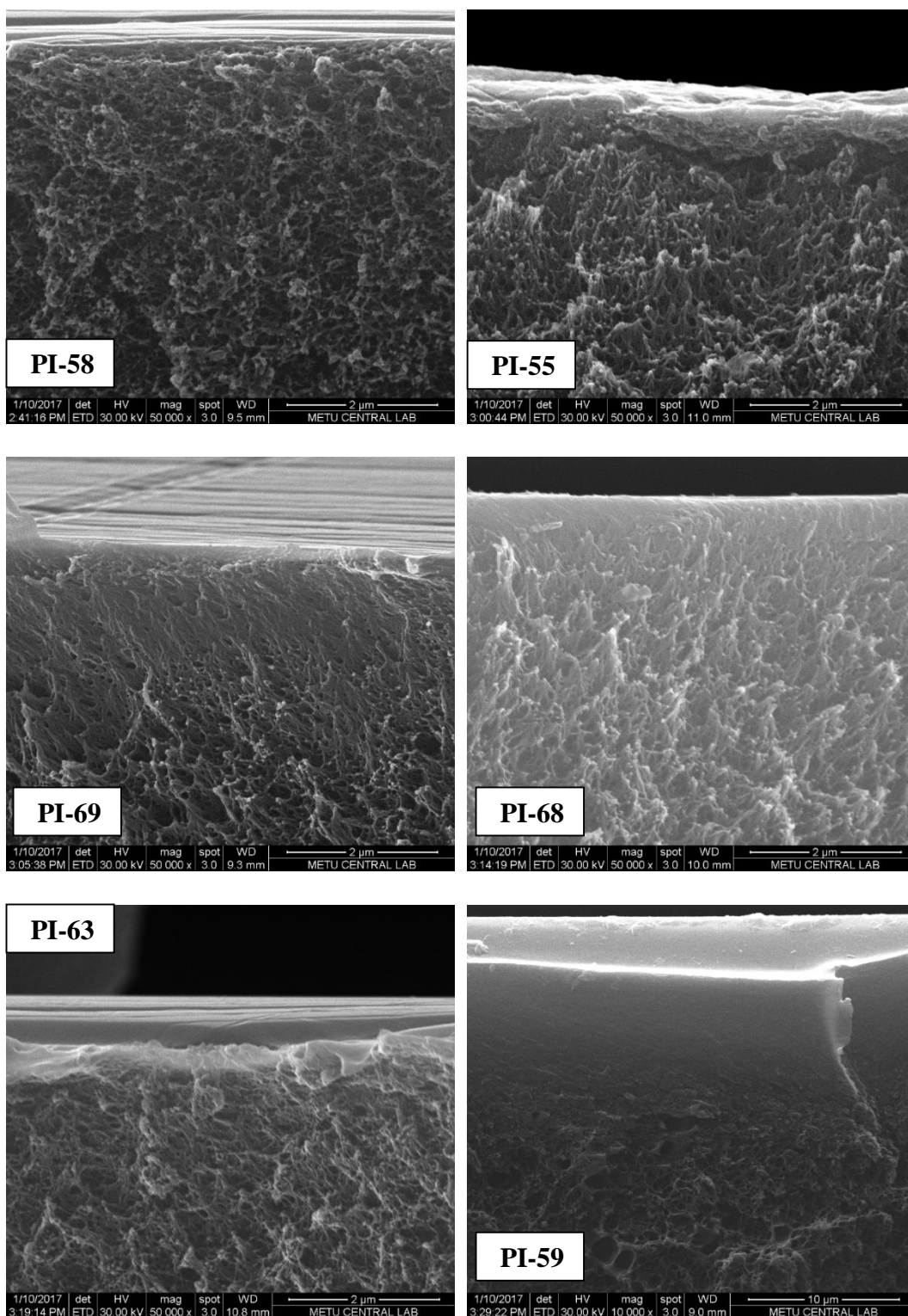


Figure 3.9 SEM micrographs of skin layer of asymmetric PI membranes prepared via LIDWPI method and exposed to IR for 0 s (PI-58), 20 s (PI-55), 40 seconds (PI-69), 60 s (PI-68), 120 s (PI-63), and 240 s (PI-59) in dry inversion step at which relative humidity was 80%.

Table 3.8 Effect of IR exposure period on morphological properties of the asymmetric PI membranes. Each membrane was prepared from solution %22.9% THF-22.9% PI-54.3% DMF (42.2% THF/DMF ratio).

Membrane Code	IR exposure period (s)	Total Thickness (μm)	Transition Layer Thickness (μm)	Skin layer Thickness (nm)	Pore Shape
PI-58	0	169.48 \pm 1.85	9.65 \pm 1.33	70.5 \pm 8.5	Spongy
PI-55	20	198.12 \pm 1.45	15.20 \pm 1.92	247.9 \pm 48.9	+
PI-69	40	227.12 \pm 1.47	14.12 \pm 1.17	195.5 \pm 21.5	Finger
PI-68	60	198.16 \pm 1.63	10.12 \pm 1.26	289.9 \pm 50.3	like
PI-63	120	190.22 \pm 1.10	15.37 \pm 3.58	322 \pm 4.24	
PI-59	240	127.26 \pm 1.49	-	10000 \pm 579	Spongy

3.3.7 Effect of IR Exposure Period on Membrane Gas Separation Properties

The gas test performances of the neat PI membranes depending on IR exposure period are listed in Table 3.9. In literature dry inversion step does not took more than 2 minutes. However, we elongated the dry-inversion step up to 240 s. The main aim is to rigidified the skin layer and fix ZIF-8 particles prior to wet inversion step which can be achieved solely longer IR exposure. When IR exposure period exceeded 60 s, the gas permeance values decreased with prolonged IR exposure. On the other hand, when the IR exposure was less than 60 s, the membrane permeance sharply increased with IR exposure and then decreased slightly. For the case that IR exposure period was less than 10 seconds, the H₂ permeance increased from 3.70 GPU to 8.51 GPU, CO₂ permeance increased from 1.08 GPU to 2.44 GPU and CH₄ permeance increased from 0.038 GPU to 0.13 GPU with slight decline in CO₂/CH₄ and H₂/CH₄ ideal selectivity from 30.66 to 20.74 and from 104.56 to 72.16, respectively.

The oscillation in gas permeance for the membranes exposed to IR between 0 and 60 s may arise from the fact that there are more than one parameter affecting

on phase inversion. Temperature, humidity, dry inversion period, volatile solvent evaporation amount and rate, interaction between chemicals are some of the parameters. When exposed to IR, the THF in the membrane solution evaporated to form a denser skin layer, thereby low permeance membranes formation have been enhanced. On the other hand, the temperature of the casting solution increased due to IR exposure. The temperature difference between non-solvent bath and solvent (DMF and THF) in the polymer solution contributed to faster solvent-nonsolvent exchange, which enhanced formation of highly permeable membrane and also open and larger pore formation. In the literature, it has been reported by many studies about effect of higher external coagulation medium on membrane properties. Chou and Yang 2005 suggested that higher temperature promoted molecular mobility, increased the solvent-nonsolvent exchange rate, thereby phase separation accelerated. Finally, higher permeance, larger and open pores structure were obtained. Chung and Kafchinski 1997 argued that the temperature of coagulation which is higher than room temperature results in increase in both solubility and diffusivity. Since the enhanced solubility, the decomposition line shifts to the polymer-coagulant axes in the ternary phase diagram and delayed decomposition will be promoted. On the other hand, higher bath temperature facilitates rapid phase separation by lowering the viscosity, chain rigidity and surface tension. There is no study about membrane formation with casting polymer solution at higher temperature. However, I think that since the positive effect of temperature on molecular mobility is still valid, faster phase separation may create highly permeable membrane with open pores as suggested by Chou and Yang 2005. When the IR exposure was less than 60 seconds, these parameters may not surpass to each other and may lead to oscillation in permeance of membrane.

Table 3.9 Effect of IR exposure period on gas separation properties of the asymmetric PI membranes. Each membrane was prepared from solution %22.9% THF-22.9%PI-54.3%DMF (42.2% THF/DMF ratio).

IR (s)	Membrane Code	Permeance (GPU)			Ideal Selectivity		
		H ₂	CO ₂	CH ₄	H ₂ /CO ₂	CO ₂ /CH ₄	H ₂ /CH ₄
0	PI-22-p1	4.51	1.32	0.061	3.42	21.64	73.93
	PI-22-p2	4.86	1.41	0.051	3.45	27.65	95.29
	PI-28-p1	2.82	0.83	0.02	3.40	41.5	141
	PI-28-p2	2.12	0.62	0.022	3.42	28.18	96.36
	PI-29-p1	2.62	0.77	0.019	3.40	40.53	137.90
	PI-29-p2	2.4	0.72	0.02	3.33	36	120
	PI-30-p1	3.15	0.93	0.059	3.39	15.76	53.39
	PI-30-p2	3.21	0.94	0.041	3.41	22.93	78.29
	PI-34-p1	4.79	1.36	0.065	3.52	20.92	73.69
	PI-34-p2	4.11	1.2	0.031	3.43	38.71	132.58
	PI-35-p1	4.38	1.3	0.044	3.37	29.55	99.55
	PI-35-p1	4.06	1.17	0.033	3.47	35.45	123.03
	PI-36-p1	3.59	1.1	0.03	3.26	36.67	119.67
	PI-36-p2	4.38	1.29	0.038	3.40	33.95	115.26
	PI-37-p1	4.45	1.25	0.041	3.56	30.49	108.54
Average	3.70	1.08	0.038	3.41	30.66	104.56	
6.5	PI-14-p1	8.45	2.46	0.14	3.43	17.57	60.36
	PI-14-p2	9.27	2.58	0.19	3.59	13.58	48.79
	PI-21-p1	9.37	2.75	0.1	3.41	27.5	93.7
	PI-21-p2	6.95	1.97	0.081	3.53	24.32	85.80
	Average	8.51	2.44	0.13	3.49	20.74	72.16
20	PI-26-p1	4.34	1.26	0.044	3.44	28.64	98.64
	PI-26-p3	6.48	1.85	0.12	3.50	15.42	54
	PI-32-p1	3.78	1.09	0.03	3.47	36.33	126
	Average	4.87	1.4	0.065	3.47	26.80	92.88
40	PI-20-p1	6.45	2	0.088	3.225	22.73	73.30
	PI-20-p2	7.62	2.21	0.32	3.45	6.91	23.81
	PI-24-p2	6.55	1.85	0.063	3.54	29.37	103.97
	PI-25-p1	8.2	2.27	0.22	3.61	10.32	37.27
	PI-25-p2	7.5	2.19	0.17	3.42	12.88	44.12
	Average	7.26	2.10	0.17	3.45	16.44	56.49

Table 3.9 (Cont.) Effect of IR exposure period on gas separation properties of the asymmetric PI membranes. Each membrane was prepared from solution %22.9% THF-22.9%PI-54.3%DMF (42.2% THF/DMF ratio).

IR (s)	Membrane Code	Permeance (GPU)			Ideal Selectivity		
		H ₂	CO ₂	CH ₄	H ₂ /CO ₂	CO ₂ /CH ₄	H ₂ /CH ₄
60	PI-31-p1	6.92	1.98	0.1	3.50	19.8	69.2
	PI-31-p2	7.19	1.99	0.15	3.61	13.27	47.93
	PI-42-p1	5.93	1.67	0.09	3.55	18.56	65.89
	PI-42-p2	6.72	1.88	0.096	3.57	19.58	70
	Average	6.69	1.88	0.109	3.56	17.80	63.26
120	Average of PI-15, PI-19, PI-33, PI-43, PI-63 see Table 3.9	4.55	1.31	0.064	3.49	22.96	80.03
240	PI-38-p1	1.55	0.42	0.015	3.69	28	103.33
	PI-38-p2	1.37	0.37	0.0096	3.70	38.54	142.71
	PI-39-p1	2.95	0.99	0.034	2.98	29.12	86.76
	PI-39-p2	1.21	0.3	0.0096	4.03	31.25	126.04
	PI-40-p1	1.53	0.42	0.02	3.64	21	76.5
	PI-41-p1	1.2	0.3	0.0096	4	31.25	125
	Average	1.635	0.47	0.0163	3.67	29.86	110.06

With exceeding the 60 seconds in IR exposure period, the gas permeance decreased gradually. The longer evaporation with IR contributed to thicker membrane layer formation and dominated the other parameters affecting membrane permeance. By increasing exposure time from 60 s to 240 s, H₂ permeance decreased from 6.69 GPU to 1.64 GPU, CO₂ permeance decreased from 1.88 GPU to 0.47 GPU and CH₄ permeance decreased from 0.109 GPU to 0.0163 GPU. The percent of decrease in permeance was 75% for CO₂ and H₂ and 85% for CH₄. The determination about decrease in permeance due to elongated IR exposure period is compatible with findings about decrease in permeance with longer evaporation time reported in literature. Ismail et al. 2011 observed that the O₂ permeance of polyethersulfone asymmetric membrane decreased from 10.32 to 7.30 GPU while O₂/N₂ selectivity increased from 5.12 to 11.79 when the evaporation time in dry

inversion step was prolonged from 8 s to 20 s. According to Ismail et al. 2011, by increasing the evaporation time the most of the volatile solvent will evaporate and more nascent skin layer will be formed. The higher amount of loss of solvent shifts the solution from phase boundary to the miscible region which tends to form denser and thicker skin layer. This claim is perfectly agreement with our findings about change of the morphological and permeance properties of our PI membranes. Zuhairun et al. 2014-b documented that reduction in CO₂ permeance from 71.13 to 20.02 GPU due to increase in the evaporation period from 1.02 seconds to 2.54 seconds.

3.3.8 Effect of IR Exposure Period with Humidity Control Membrane Gas Separation Properties

The effect of relative humidity of environment during dry inversion period has been examined and two different trends have been observed. The gas test results have been listed in Table. 3.10.

When the membrane prepared without IR exposure and dry inversion period was very short (0 second PI-60, PI-70 and PI-58), the membrane permeance increased with increasing relative humidity. By increasing the relative humidity from 20% to 80%, the H₂ permeance increased from 3.72 to 8.34 GPU, CO₂ permeance increased from 1.1 to 2.75 GPU and CH₄ permeance increased from 0.048 to 0.12 GPU. There are two possible explanations of this trend. Firstly, because these membranes were not exposed to dry phase inversion, the polymer layer forming the selective skin layer was not yet able to densify sufficiently. Thereby, thinner and elastic skin layer formed which enhanced the permeance. Secondly, at high relative humidity, the condensed water vapor on the casting film caused to phase separation of the skin layer before wet phase inversion step, hence thinner or even porous skin layer was obtained.

Table 3.10 Effect of IR exposure period and also humidity on gas separation properties of the asymmetric PI membranes. Each membrane was prepared from solution %22.9% THF-22.9%PI-54.3%DMF (42.2% THF/DMF ratio).

humidity	IR (s)	Code	Permeance (GPU)			Ideal Selectivity		
			H ₂	CO ₂	CH ₄	H ₂ /CO ₂	CO ₂ /CH ₄	H ₂ /CH ₄
20%	0	PI-60-p1	3.73	1.1	0.048	3.39	22.92	77.71
		PI-60-p2	3.71	1.1	0.033	3.37	33.33	112.42
	20	PI-57-p1	6.42	1.89	0.056	3.40	33.75	114.64
	60	PI-61-p1	13.44	2.81	0.45	4.78	6.24	29.87
50%	0	PI-70-p1	2.78	0.81	0.095	3.43	8.53	29.26
	20	PI-54-p1	5.4	1.44	0.1	3.75	14.47	54.27
	60	PI-53-p1	5.17	1.42	0.066	3.64	21.52	78.33
80%	0	PI-58-p1	8.34	2.75	0.12	3.03	22.92	69.5
		PI-58-p2	9.69	2.72	0.31	3.56	8.77	31.26
	20	PI-55-p1	4.05	1.15	0.047	3.52	24.47	86.17
	60	PI-49-p1	5.75	1.62	0.19	3.55	8.53	30.26
		PI-68-p1	7.79	2.39	0.11	3.26	21.73	70.82
	90	PI-72-p1	4.33	1.16	0.047	3.73	24.68	92.13
	120	PI-63-p1	4.19	1.16	0.094	3.61	12.34	44.57
	180	PI-71-p1	2.12	0.55	0.018	3.85	30.56	117.78
240	PI-59-p1	1.29	0.37	0.012	3.49	30.83	107.5	

When the IR exposure period 20 s, by increasing the relative humidity from 29% to 80%, the H₂ permeance decreased from 6.42 to 4.05 GPU, CO₂ permeance decreased from 1.89 to 1.15 GPU and CH₄ permeance decreased from 0.056 to 0.047 GPU. Similar observation was also carried out by Clausi and Koros 2000. By increasing the air gap humidity from 15% to 65-70%, the O₂ permeance decreased from 16.4 to 15.7 GPU and He permeance decreased from 231.8 to 197.3 GPU.

The experiment of Gao et al. 2009 is conflicted with Clausi and Koros 2000. On the other hand, their suggestion is perfectly interpretive for our observation about humidity effect at 0 s IR exposure. When the initial casting solution exposed to humid atmosphere during dry inversion, the driving force for net diffusion of non-solvent water into polymer film and accumulation of water in the polymer solution would be promoted, thereby fast phase inversion and thin skin layer would

be obtained. The water flux of the produced membrane at higher relative humidity would be higher than that of membrane produced at lower relative humidity. Kapantaidakis and Koops 2002, is the other authors who observed increase in permeance of membrane due to exposure of higher humidity during evaporation period. They are also ascribed this phenomenon via fast phase separation due to water penetration into polymer solution.

The opposite trends for 0 s and 20 s IR exposure would be originated from IR exposure and evaporation period. For 20 seconds IR exposure, high relative humidity led to diminish both evaporation rate and the amount of evaporated THF. This enhanced the delay in dry-phase inversion. Moreover, because of hindered evaporation of THF, the casting solution run into wet phase inversion step with higher amount of THF than estimated. It is known that the co-solvent such as THF enhanced delayed demixing phase separation which created denser and low permeability membrane. The higher relative humidity in the casting environment may contribute the formation of larger and flexible pores structure resulting in decrease in selectivity. According to our experience, closed and small pores affect the selectivity of membranes (see Chapter 4).

When the IR exposure period reached to 240 seconds, the permeance of membranes prepared at 80% relative humidity and prepared without humidity control were very close to each other. Hence it was suggested that longer IR exposure duration suppressed the effect of humidity. The difficulty in drawing a conclusion about effect of humidity when the IR exposure period was short arisen from the competition of evaporation period and relative humidity factors which is also argued by Gao et al. 2009.

3.3.9 Effect of ZIF-8 loading on Membrane Morphology

Figure 3.10 showed the SEM micrographs of mixed matrix PI membranes prepared with 10% ZIF-8 loading. The incorporation of ZIF-8 resulted in thicker skin layer. Moreover, skin layer and transition layer merged, hence it was not possible to measure a distinct skin layer thickness. By incorporation of ZIF-8, formation of finger like pores were suppressed. For MM-PI-12, the total thickness

of membrane was measured as $128.65 \pm 1.11 \mu\text{m}$ while the skin layer was measured approximately $17.25 \pm 2.23 \mu\text{m}$. For 240 seconds IR exposure, the total membrane thickness was the same for both mixed matrix PI and neat PI. However, the existence of 10% ZIF-8 in the casting solution contributed to increase in skin layer thickness from $10 \mu\text{m}$ to $17 \mu\text{m}$. The reason might be the higher viscosity of casting solution due to existence of ZIF-8s. According to my experience, the addition of ZIF-8s into casting polymer solution led to higher viscosity. Increase in viscosity due to addition of fillers into polymer solution and probable effects of higher viscosity on membrane formation kinetics were investigated by several researchers (Majeed et al. 2012, Mollahosseini et al. 2012, Yang et al. 2007, Li et al. 2009). The additional effects of ZIF-8 loading are the rigidification of polymer chain and increasing in packing density of polymer. The casting solution with higher viscosity and denser polymer reinforced delayed-demixing during wet phase inversion, thereby thicker and denser membrane layer was obtained.

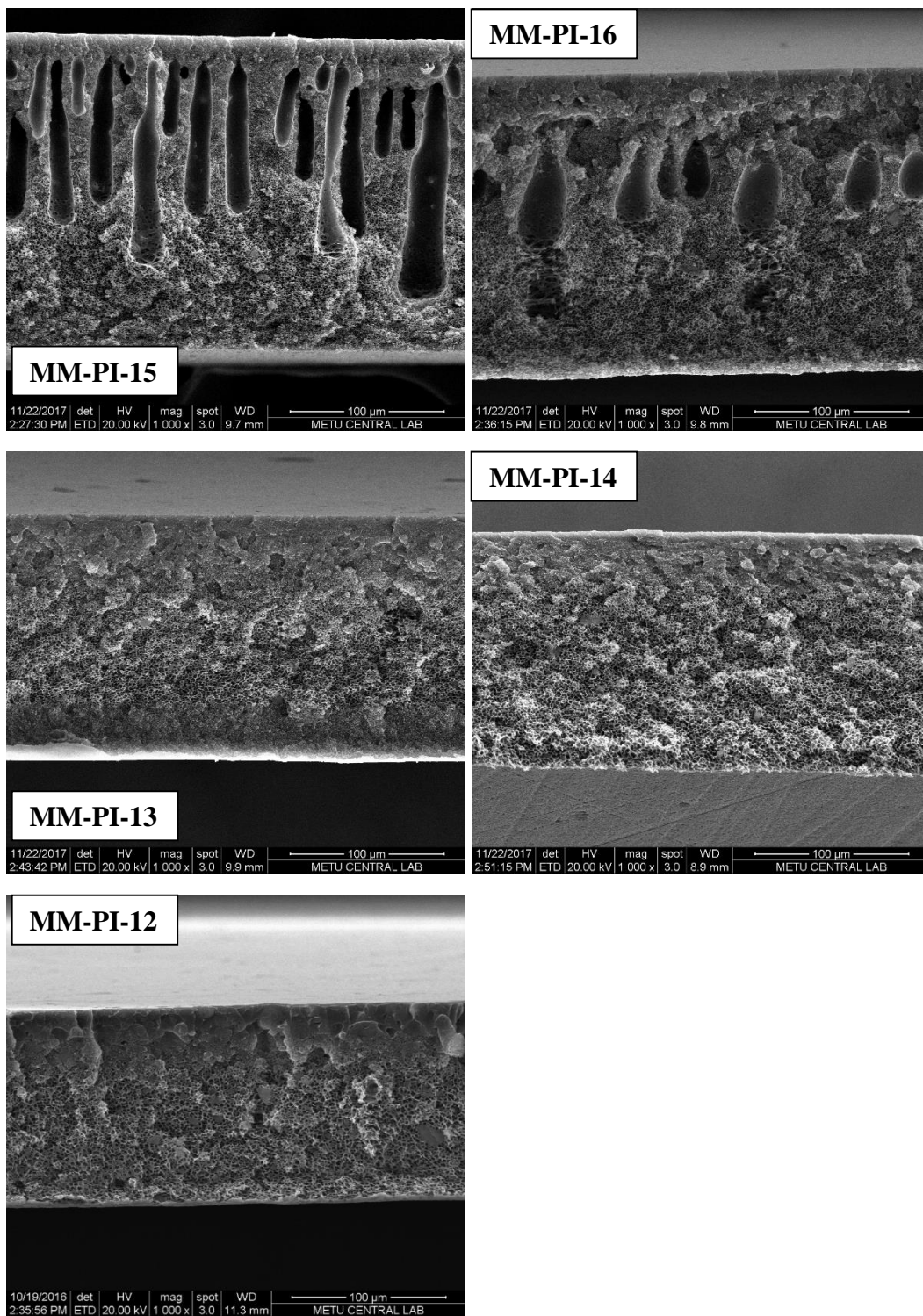


Figure 3.10 SEM micrographs of skin layer of asymmetric mixed matrix PI membranes prepared via LIDWPI method and exposed to IR for 240 s.

3.3.10 Effect of ZIF-8 loading on Membrane Gas Separation Performance

The gas separation performance of mixed matrix-PI membranes has been given in Table 3.11. The percent of decrease in gas permeance for each gas was more than 60% in mixed matrix PI membranes including 10% ZIF-8 compared to the neat PI membranes prepared with the same casting condition. Since the ZIF-8 permeability is higher than that of PI, the expectation was the improving in gas permeance due to ZIF-8 loading. However, the morphological variation due to ZIF-8 loading is compatible with diminishment in permeance. ZIF-8 loading led to decrease in permeance by several ways. Firstly, ZIF-8 loading created thicker selective layer which is the strong resistance against mass transfer. Secondly polymer chain rigidification and denser packing because of existence of ZIF-8 reduced the permeance. As reported in Chapter 5, ZIF-8 loading in PI also led to decrease in the free-volume of polymer which is known as an important factor enhance permeance. The ideal selectivity of H_2/CO_2 and H_2/CH_4 were detected larger than the intrinsic ideal selectivity of PI which is a strong evidence of that the mixed matrix membrane has different intrinsic gas separation properties than neat PI. Another factor effecting selectivity is the increased tortuosity because of porous nature of ZIF-8. The tortuous path has hindered the transfer of larger molecules (for example CH_4 and CO_2) more than the transfer of smaller molecules (for example H_2).

Our experimental results are inconsistent with both our expectations and findings in the literature. Since the CO_2 and CH_4 permeance of ZIF-8 are higher than PI, materials of incorporation of ZIF-8 and PI should have permeance higher than that of PI and lower than that of ZIF-8. Furthermore, Ordenez et al. 2011 prepared ZIF-8/Matrimid dense mixed matrix membrane. For 40 wt.% ZIF-8 loading, permeability of CO_2 rised from 9.52 to 24.55 Barrer, while CO_2/CH_4 selectivity decreased from 40 to 28. According to this study, 40 wt.% ZIF-8 addition to Matrimid increased the distance between polymer chain and free volume, thus promoted the permeability of gases. For 50 wt.% ZIF-8 loading, permeability of CO_2 decreased from 9.52 to 4.72 Barrer, while CO_2/CH_4 selectivity increased from

40 to 94. In this case, loading of ZIF-8 higher than %40 reduced the available polymers which constrains gases pass through tortuous path of around ZIF-8.

Table 3.11 The effect of ZIF-8 loading on membrane gas separation properties.

Humidity	IR (sec.)	Membrane Code	ZIF-8 Content	Permeance (GPU)			Ideal Selectivity			
				H ₂	CO ₂	CH ₄	H ₂ /CO ₂	CO ₂ /CH ₄	H ₂ /CH ₄	
No Control	0	MM-PI-1-p1	%3	3.89	1.04	0.03	3.74	34.67	129.67	
		MM-PI-1-p2		4.12	1.12	0.037	3.68	30.27	111.35	
		MM-PI-2-p1		3	1.08	0.031	2.78	34.84	96.77	
		MM-PI-2-p2		4.05	1.05	0.031	3.86	33.87	130.65	
	240	MM-PI-4-p1	%3	1.16	0.27	0.009	4.30	30	128.89	
		MM-PI-5-p1		%5	1.26	0.29	0.01	4.34	29	126
		MM-PI-5-p2			0.68	0.16	0.004	4.25	40	170
%80	0	MM-PI-15	10%	2.84	0.83	0.03	3.42	27.67	94.67	
	60	MM-PI-16		4.25	0.78	0.3	5.45	2.6	14.17	
	120	MM-PI-13		2.72	0.54	0.017	5.04	31.76	160	
	180	MM-PI-14		1.03	0.21	0.0072	4.90	29.17	143.06	
	240	MM-PI-12		0.62	0.14	0.0033	4.43	42.42	187.88	

3.4 Conclusion

The effect of electromagnetic radiation heating during dry-inversion, THF/DMF ratio in the casting solution and ZIF-8 loading on the properties of asymmetric PI membranes have been demonstrated. The following conclusions can be drawn.

- By increasing THF/DMF ratio from 0.17 to 0.82, the thickness of skin layer enlarged from 114 nm to 656 nm.
- CO₂ permeance of PI membranes were measured 0.81 GPU, 2.55 GPU and 6.65 GPU corresponding to the 0.80, 0.42, 0.17 THF/DMF ratio of casting solution, respectively. Although the highest CO₂ permeance was detected as 6.65 GPU when the THF/DMF ratio was 0.17, this composition was not preferred in further research, since the corresponding CO₂/CH₄ ideal selectivity was only 3.43.
- Heat for evaporation in dry inversion was supplied from two different light source and the difference in light source has a significant effect on membrane gas transport properties. The effect on morphology is significantly lower, hence using IR instead of IL led to increase in skin layer thickness only 50 nm. On the other hand, IR instead of IL resulted in 61%, 49% and 61% percent of decrease in H₂, CO₂, CH₄ permeance, respectively with slightly improvement in ideal selectivity values.
- By increasing IR exposure period from 0 to 240 seconds, the skin layer thickness increased from 70 nm to 10000 nm. When the IR exposure period reached 240 seconds, all finger-like pores disappeared and only spongy pores were observed in support layer.
- When the IR exposure period was less than 10 seconds, the membrane permeance sharply increased from 3.70 to 8.51 GPU for H₂, from 1.08 to 2.44 for CO₂, and from 0.038 to 0.13 GPU for CH₄, with respect to that of membrane prepared without IR exposure. Further increase in IR exposure led to lower gas permeance.
- The humidity of the dry-inversion environment promoted higher permeance values when the IR exposure period less than 10 seconds. At higher IR

exposure period, increasing in relative humidity led to lower permeance. When the IR exposure period exceeded 120 seconds, the effect of humidity went down.

- ZIF-8 loading promoted the formation of thicker skin layer. The gas permeance values decreased more than 60% corresponding to 10% ZIF-8 loading.

REFERENCES

- Ahmed, I., Idris, A., Hussain, A., Yusof, Z. A., & Saad Khan, M. (2013). Influence of Co-Solvent Concentration on the Properties of Dope Solution and Performance of Polyethersulfone Membranes. *Chemical Engineering & Technology*, n/a-n/a. doi:10.1002/ceat.201300235
- Ahmed, I., Idris, A., Khan, M. S., Chowdhury, S., & Akhtar, J. (2014). Effect of Acetone on Physical Properties of PES Membrane. *Applied Mechanics and Materials*, 625, 545-548. doi:10.4028/www.scientific.net/amm.625.545
- Aroon, M., Ismail, A., Montazer-Rahmati, M., & Matsuura, T. (2010). Morphology and permeation properties of polysulfone membranes for gas separation: Effects of non-solvent additives and co-solvent. *Separation and Purification Technology*, 72(2), 194-202. doi:10.1016/j.seppur.2010.02.009
- Barth, C., Gonçalves, M., Pires, A., Roeder, J., & Wolf, B. (2000). Asymmetric polysulfone and polyethersulfone membranes: effects of thermodynamic conditions during formation on their performance. *Journal of Membrane Science*, 169(2), 287-299. doi:10.1016/s0376-7388(99)00344-0
- Basu, S., Khan, A. L., Cano-Odena, A., Liu, C., & Vankelecom, I. F. (2010). ChemInform Abstract: Membrane-Based Technologies for Biogas Separations. *ChemInform*, 41(21), no-no. doi:10.1002/chin.201021273
- Bergman, T. L., Dewit, D. P., Lavine, & A. S., Incropera, F. P. (2005). Radiation: Processes and Properties. In *Fundamentals of heat and mass transfer* (6th ed., pp. 736-739). New Jersey: John Wiley & Sons.
- Chabot, S., Roy, C., Chowdhury, G., & Matsuura, T. (1997). Development of poly(vinylidene fluoride) hollow-fiber membranes for the treatment of water/organic vapor mixtures. *Journal of Applied Polymer Science*, 65(7), 1263-1270. doi:10.1002/(sici)1097-4628(19970815)65:7<1263::aid-app4>3.0.co;2-g
- Chou, W., & Yang, M. (2005). Effect of coagulant temperature and composition on surface morphology and mass transfer properties of cellulose acetate hollow fiber membranes. *Polymers for Advanced Technologies*, 16(7), 524-532. doi:10.1002/pat.617
- Chung, T., & Kafchinski, E. R. (1997). The effects of spinning conditions on asymmetric 6FDA/6FDAM polyimide hollow fibers for air separation. *Journal of Applied Polymer Science*, 65(8), 1555-1569. doi:10.1002/(sici)1097-4628(19970822)65:8<1555::aid-app13>3.0.co;2-v
- Clausi, D. T., & Koros, W. J. (2000). Formation of defect-free polyimide hollow fiber membranes for gas separations. *Journal of Membrane Science*, 167(1), 79-89. doi:10.1016/s0376-7388(99)00276-8
- Dong, G., Li, H., & Chen, V. (2010). Factors affect defect-free Matrimid® hollow fiber gas separation performance in natural gas purification. *Journal of Membrane Science*, 353(1-2), 17-27. doi:10.1016/j.memsci.2010.02.012
- Dorosti, F., Omidkhah, M., & Abedini, R. (2015). Enhanced CO₂/CH₄ separation properties of asymmetric mixed matrix membrane by incorporating nano-

- porous ZSM-5 and MIL-53 particles into Matrimid®5218. *Journal of Natural Gas Science and Engineering*, 25, 88-102.
doi:10.1016/j.jngse.2015.04.033
- Flick, E. W. (1998). *Industrial solvents handbook*. Westwood, NJ: Noyes Data Corporation.
- Fritzsche, A. K., Cruse, C. A., Kesting, R. E., & Murphy, M. K. (1990). Polysulfone hollow fiber membranes spun from lewis acid: Base complexes. II. The effect of lewis acid to base ratio on membrane structure. *Journal of Applied Polymer Science*, 39(9), 1949-1956. doi:10.1002/app.1990.070390910
- Gao, L., Tang, B., & Wu, P. (2009). An experimental investigation of evaporation time and the relative humidity on a novel positively charged ultrafiltration membrane via dry-wet phase inversion. *Journal of Membrane Science*, 326(1), 168-177. doi:10.1016/j.memsci.2008.09.048
- Hachisuka, H., Ohara, T., & Ikeda, K. (1996). New type asymmetric membranes having almost defect free hyper-thin skin layer and sponge-like porous matrix. *Journal of Membrane Science*, 116(2), 265-272. doi:10.1016/0376-7388(96)00048-8
- Han, J., Lee, W., Choi, J. M., Patel, R., & Min, B. (2010). Characterization of polyethersulfone/polyimide blend membranes prepared by a dry/wet phase inversion: Precipitation kinetics, morphology and gas separation. *Journal of Membrane Science*, 351(1-2), 141-148. doi:10.1016/j.memsci.2010.01.038
- Henis, J. M., & Tripodi, M. K. (1980). A Novel Approach to Gas Separations Using Composite Hollow Fiber Membranes. *Separation Science and Technology*, 15(4), 1059-1068. doi:10.1080/01496398008076287
- Huang, R. Y., & Feng, X. (1995). Studies on solvent evaporation and polymer precipitation pertinent to the formation of asymmetric polyetherimide membranes. *Journal of Applied Polymer Science*, 57(5), 613-621. doi:10.1002/app.1995.070570511
- Hussain, M., & König, A. (2012). Mixed-Matrix Membrane for Gas Separation: Polydimethylsiloxane Filled with Zeolite. *Chemical Engineering & Technology*, 35(3), 561-569. doi:10.1002/ceat.201100419
- Ismail, A. F., & Yean, L. P. (2003). Review on the development of defect-free and ultrathin-skinned asymmetric membranes for gas separation through manipulation of phase inversion and rheological factors. *Journal of Applied Polymer Science*, 88(2), 442-451. doi:10.1002/app.11744
- Ismail, A., & Lai, P. (2003). Effects of phase inversion and rheological factors on formation of defect-free and ultrathin-skinned asymmetric polysulfone membranes for gas separation. *Separation and Purification Technology*, 33(2), 127-143. doi:10.1016/s1383-5866(02)00201-0
- Ismail, A., Norida, R., Rahman, W. A., Matsuura, T., & Hashemifard, S. (2011). Preparation and characterization of hyperthin-skinned and high performances asymmetric polyethersulfone membrane for gas separation. *Desalination*, 273(1), 93-104. doi:10.1016/j.desal.2010.10.015
- Ismail, N., Ismail, A., Mustafa, A., Matsuura, T., Soga, T., Nagata, K., & Asaka, T. (2015). Qualitative and quantitative analysis of intercalated and

- exfoliated silicate layers in asymmetric polyethersulfone/cloisite15A® mixed matrix membrane for CO₂/CH₄ separation. *Chemical Engineering Journal*, 268, 371-383. doi:10.1016/j.cej.2014.11.147
- Jiang, L., Chung, T. S., Li, D. F., Cao, C., & Kulprathipanja, S. (2004). Fabrication of Matrimid/polyethersulfone dual-layer hollow fiber membranes for gas separation. *Journal of Membrane Science*, 240(1-2), 91-103. doi:10.1016/j.memsci.2004.04.015
- Kapantaidakis, G., & Koops, G. (2002). High flux polyethersulfone–polyimide blend hollow fiber membranes for gas separation. *Journal of Membrane Science*, 204(1-2), 153-171. doi:10.1016/s0376-7388(02)00030-3
- Kesting, R. E., Fritzsche, A. K., Murphy, M. K., Cruse, C. A., Handermann, A.C., Malon, R. F., & Moore, M. D. (1990). The second-generation polysulfone gas-separation membrane. I. The use of lewis acid: Base complexes as transient templates to increase free volume. *Journal of Applied Polymer Science*, 40(910), 1557-1574. doi:10.1002/app.1990.070400913
- Kimmerle, K., & Strathmann, H. (1990). Analysis of the structure-determining process of phase inversion membranes. *Desalination*, 79(2-3), 283-302. doi:10.1016/0011-9164(90)85012-y
- Krol, J., Boerrigter, M., & Koops, G. (2001). Polyimide hollow fiber gas separation membranes: preparation and the suppression of plasticization in propane/propylene environments. *Journal of Membrane Science*, 184(2), 275-286. doi:10.1016/s0376-7388(00)00640-2
- Li, Y., & Chung, T. S. (2008). Highly selective sulfonated polyethersulfone (SPES)-based membranes with transition metal counterions for hydrogen recovery and natural gas separation. *Journal of Membrane Science*, 308(1-2), 128-135. doi:10.1016/j.memsci.2007.09.053
- Lua, A. C., & Shen, Y. (2013). Preparation and characterization of asymmetric membranes based on nonsolvent/NMP/P84 for gas separation. *Journal of Membrane Science*, 429, 155-167. doi:10.1016/j.memsci.2012.11.018
- Luminous efficacy. (2017, November 7). Retrieved from https://en.wikipedia.org/wiki/Luminous_efficacy
- Machado, P., Habert, A., & Borges, C. (1999). Membrane formation mechanism based on precipitation kinetics and membrane morphology: flat and hollow fiber polysulfone membranes. *Journal of Membrane Science*, 155(2), 171-183. doi:10.1016/s0376-7388(98)00266-x
- Madaeni, S. S., Rahimpour, A., & Barzin, J. (2005). Iranian Polymer Journal. *Preparation of Polysulphone Ultrafiltration Membranes for Milk Concentration: Effect of Additives on Morphology and Performance*, 14(5), 421-428.
- Majeed, S., Fierro, D., Buhr, K., Wind, J., Du, B., Boschetti-de-Fierro, A., & Abetz, V. (2012). Multi-walled carbon nanotubes (MWCNTs) mixed polyacrylonitrile (PAN) ultrafiltration membranes. *Journal of Membrane Science*, 403-404, 101-109. doi:10.1016/j.memsci.2012.02.029
- Md Nordin, N. A., Ismail, A. F., & Mustafa, A. (2014). Synthesis and Preparation of Asymmetric PSf/ZIF-8 Mixed Matrix Membrane for CO₂/CH₄ Separation. *Jurnal Teknologi*, 69(9). doi:10.11113/jt.v69.3400

- Mollahosseini, A., Rahimpour, A., Jahamshahi, M., Peyravi, M., Khavarpour, M. (2012). The effect of silver nanoparticle size on performance and antibacteriability of polysulfone ultrafiltration membrane. *Desalination*, 306, 41-50. doi:10.1016/j.desal.2012.08.035
- Ordoñez, M. J., Balkus, K. J., Ferraris, J. P., & Musselman, I. H. (2010). Molecular sieving realized with ZIF-8/Matrimid® mixed-matrix membranes. *Journal of Membrane Science*, 361(1-2), 28-37. doi:10.1016/j.memsci.2010.06.017
- Orme, C. J., Stone, M. L., Benson, M. T., & Peterson, E. S. (2003). Testing Of Polymer Membranes For The Selective Permeability Of Hydrogen. *Separation Science and Technology*, 38(12-13), 3225-3238. doi:10.1081/ss-120022595
- Pinnau, I., & Koros, W. J. (1991). Structures and gas separation properties of asymmetric polysulfone membranes made by dry, wet, and dry/wet phase inversion. *Journal of Applied Polymer Science*, 43(8), 1491-1502. doi:10.1002/app.1991.070430811
- Pinnau, I., & Koros, W. J. (1993). A qualitative skin layer formation mechanism for membranes made by dry/wet phase inversion. *Journal of Polymer Science Part B: Polymer Physics*, 31(4), 419-427. doi:10.1002/polb.1993.090310406
- Saedi, S., Madaeni, S., Arabi Shamsabadi, A., & Mottaghi, F. (2012). The effect of surfactants on the structure and performance of PES membrane for separation of carbon dioxide from methane. *Separation and Purification Technology*, 99, 104-119. doi:10.1016/j.seppur.2012.08.028
- Saedi, S., Madaeni, S. S., Hassanzadeh, K., Shamsabadi, A. A., & Laki, S. (2014). The effect of polyurethane on the structure and performance of PES membrane for separation of carbon dioxide from methane. *Journal of Industrial and Engineering Chemistry*, 20(4), 1916-1929. doi:10.1016/j.jiec.2013.09.012
- Shieh, J., & Chung, T. S. (1998). Effect of liquid-liquid demixing on the membrane morphology, gas permeation, thermal and mechanical properties of cellulose acetate hollow fibers. *Journal of Membrane Science*, 140(1), 67-79. doi:10.1016/s0376-7388(97)00267-6
- Sridhar, S., Smitha, B., & Aminabhavi, T. M. (2007). Separation of Carbon Dioxide from Natural Gas Mixtures through Polymeric Membranes—A Review. *Separation & Purification Reviews*, 36(2), 113-174. doi:10.1080/15422110601165967
- Van't Hof, J., Reuvers, A., Boom, R., Rolevink, H., & Smolders, C. (1992). Preparation of asymmetric gas separation membranes with high selectivity by a dual-bath coagulation method. *Journal of Membrane Science*, 70(1), 17-30. doi:10.1016/0376-7388(92)80076-v
- Visser, T., Masetto, N., & Wessling, M. (2007). Materials dependence of mixed gas plasticization behavior in asymmetric membranes. *Journal of Membrane Science*, 306(1-2), 16-28. doi:10.1016/j.memsci.2007.07.048
- Vogrin, N., Stropnik, Č., Musil, V., & Brumen, M. (2002). The wet phase separation: the effect of cast solution thickness on the appearance of macrovoids in the membrane forming ternary cellulose

- acetate/acetone/water system. *Journal of Membrane Science*, 207(1), 139-141. doi:10.1016/s0376-7388(02)00119-9
- What is Full Spectrum Lighting? (2012, March 19). Retrieved from <http://lumenistics.com/what-is-full-spectrum-lighting/>
- What is light intensity? Shining a light on intensity measurement. (2016, November 28). Retrieved from <https://www.omega.co.uk/technical-learning/shining-a-light-on-intensity-measurement.html>
- Yuenyao, C., Tirawanichakul, Y., & Chittrakarn, T. (2015). Asymmetric polysulfone gas separation membranes treated by low pressure DC glow discharge plasmas. *Journal of Applied Polymer Science*, 132(24), n/a-n/a. doi:10.1002/app.42116
- Zhang, Y., Musselman, I. H., Ferraris, J. P., & Balkus, K. J. (2008). Gas permeability properties of Matrimid® membranes containing the metal-organic framework Cu-BPY-HFS. *Journal of Membrane Science*, 313(1-2), 170-181. doi:10.1016/j.memsci.2008.01.005
- Zulhairun, A., Ismail, A., Matsuura, T., Abdullah, M., & Mustafa, A. (2014). Asymmetric mixed matrix membrane incorporating organically modified clay particle for gas separation. *Chemical Engineering Journal*, 241, 495-503. doi:10.1016/j.cej.2013.10.042
- Zulhairun, A., Ng, B., Ismail, A., Surya Murali, R., & Abdullah, M. (2014). Production of mixed matrix hollow fiber membrane for CO₂/CH₄ separation. *Separation and Purification Technology*, 137, 1-12. doi:10.1016/j.seppur.2014.09.014

CHAPTER 4

ASYMMETRIC NEAT PI MEMBRANES AND ASYMMETRIC PI/ZIF-8/PNA MIXED MATRIX MEMBRANES BY LIGHT INDUCED DRY-VAPOR-PHASE INVERSION

The main focus of this chapter was analysing the morphological and gas transport properties of PI membranes prepared by IR and IL light induced dry-vapor phase inversion method. Effect of pNA and ZIF-8 loading on membrane properties were also investigated besides the effects of IR exposure period and vapor phase inversion method (VIPS). This chapter of the study is a work that will be the pioneer in the literature in many ways;

- The PI membranes produced in this study are the first gas separation membranes prepared by vapor phase inversion method.
- Unlike the other studies about VIPS, the VIPS period was not followed by wet quenching step, in this study. Therefore, the effects of the VIPS method could be examined without the shadow of the possible effects of the wet quenching method.
- This is the first study, in which mixed matrix membrane made up of ternary PI/ZIF-8/pNA component was produced by VIPS in asymmetric structure.
- This is the first study in literature in which light induced dry inversion step was used prior to VIPS.

4.1 Theoretical Background about Vapor Phase Inversion

Vapor induced phase separation (VIPS) is a way to initiate phase separation and involves dry and wet phase inversion steps. In this method, casting polymer solution is exposed to water (or non-solvent) vapor for a certain period of time prior to wet phase inversion step. Generally, researchers preferred high boiling point solvent to suppress evaporation of nonsolvent and to preference non-solvent inflow during VIPS. Since transfer of non-solvent vapor into casting polymer solution is

slow this process is a very slow process compared to NIPS. Thus, VIPS provides an opportunity to control membrane morphology and porosity by manipulating the relative humidity, air flow rate, air temperature, non-solvent vapor exposure period (Khare et al. 2005) and also to prepare super-hydrophobic surface (Su et al. 2009). On the other hand, phase inversion by NIPS is very fast process and generally membrane formation occurs in a few second. This fast process makes impossible to observation of phase separation kinetics. Besides it is possible to monitor the phase separation (Lee et al. 2004).

The differences from the thermodynamics point of view between VIPS and NIPS are not being interpreted clearly yet because thermodynamic status of all the components are the same in both VIPS and NIPS methods. Besides, the activity of water in vapor phase is similar to that in liquid phase. The divergence in structure of membranes produced by these two different methods was attributed to kinetic factors rather than differences in thermodynamics (Caquineau et al. 2003, Park et al. 1999), for example time required to increase non-solvent content of casting solution. Caquineau et al. 2003; Su et al. 2009; Menut et al. 2008; Tsai et al. 2006 and Lee et al. 2004 claimed that increase in water (non-solvent) content of polymer film is mainly because of the hygroscopicity of NMP (solvent). With acceptance of this claim, I have another idea based on my experience and observation. In our laboratory, two different polymer PES and PI were dissolved by using same solvent. It was observed that formation duration of PES membrane was shorter than that of PI membrane despite using the same solvent, relative humidity, temperature and production method, VIPS. Besides, another research carried out in our laboratory, it was observed a decrease in phase change period with an increase in the PES content of PI-PES blend casting solution. This is related to higher hygroscopicity of PES compared to PI polymer. Since PES has sulfonated group. Hence, hygroscopicity of polymer is also important.

Wang et al. 2000 is another research group who support the idea that non-solvent inflow into casting solution is mainly due to hygroscopicity of solvent. They

produced PS membrane with cellular surface pores via VIPS. Hydrophilic additive such as acetic acid was added to cyclohexane-PS polymer solution to promote water vapor non-solvent inflow since hydrophobic solvent cyclohexane does not let water diffusion into casting solution. However, addition of acetic acid for toluene-acetic acid- PS system was not sufficient to form cellular surface pores. Authors explained this phenomenon by water tolerance of toluene-PSF solution. Wang et al. 2000 determined binodal curve of the water-solvent-additive-polymer system by titrating polymer solution with water. According to their observations, systems with less water tolerance (small amount of water required to reach cloud point) are easy to phase separate resulting in cellular surface pores and surface emulsion drops. In light of this knowledge, it is possible to interpret that position of binodal curve, stability or demixing gap of the polymer-solvent-nonsolvent system influence initiation of VIPS in addition to the hygroscopicity of solvent or additive.

Typical morphology (polymer-lean + polymer rich phase) of VIPS membrane indicates the liquid-liquid phase separation (Caquineau et al. 2003). As explained in Chapter 4 part 4.0, there are two possible ways of phase separation of polymer solution; namely spinodal decomposition (Figure 2.5 path 2-2) and nucleation-and-growth (Figure 2.5 path 2-1 or path 2-3). When the polymer solution follows path 2-2, phase separation occurs in un-stable region which is specified by spinodal curve. This type of phase separation is called spinodal decomposition and results in bi-continuous interconnected pores. Spinodal decomposition may also observed even if polymer-solvent-nonsolvent system crosses slowly metastable region near the critical point. In spinodal decomposition, phase separation occurs via concentration fluctuation rather than nucleation-and-growth and two continuous phase with a characteristic periodic interphase distance obtained as depicted in Figure 4.1-A (Nunes and Inoue 1996, Ren and Wang 2010). When the polymer solution follows path 2-1 or 2-3, phase separation occurs in metastable regions which are the area between spinodal curve and binodal curve. This type of phase separation is called nucleation-and growth and results in cellular isolated pores embedded in polymer matrix as depicted in Figure 4.1-B. NG, which is a slow process, leads to formation of dispersed nuclei and these dispersed nuclei become

stable as long as activation energy of nucleation formation is higher than their surface free energy (Nunes and Inoue 1996, Ren and Wang 2010).

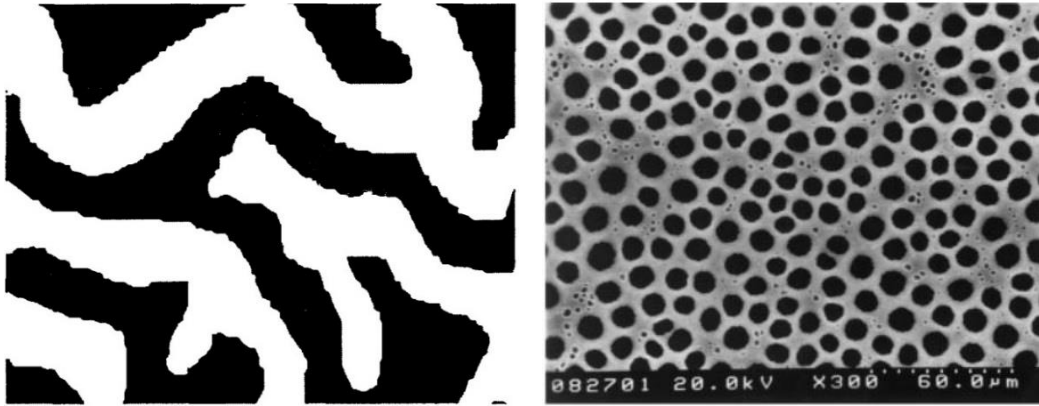


Figure 4.1 (A) Bi-continuous structure usually detected in system following spinodal decomposition (modified from Nunes and Inoue 1996). (B) dispersed nuclei structure usually observed in system following binodal decomposition (i.e. nucleating and growth) (modified from Wang et al. 2000).

In general admission, the interconnected porous structure is formed by spinodal decomposition and the closed pores are formed by the nucleation and growth mechanism. Nevertheless, open porous structure can be formed due to the coalescence of droplets of the polymer-lean phase in nucleation and growth mechanism. On the other hand, loss of interconnectivity in spinodal decomposition is observed when coarsening happens because of the interfacial tension between the polymer-rich and polymer-lean phases (Chae Park et al. 1999, Nunes and Inoue 1996, Su et al. 2009). Thus, it is not possible to distinct these two mechanism just based on morphological analysis. Hence, researchers used different procedures to differentiate of phase separation mechanisms, one of them is measurements by dynamic light scattering intensity. The characteristic fingerprints of light scattering patterns of spinodal decomposition and nucleation-and-growth mechanism are presented in Figure 4.2-A and 4.2-B, respectively. Spinodal decomposition is identified with a maximum in the angular variation, while the feature of nucleation-

and-growth is continual decline of scattered light intensities with increasing angles (Liu and Kiran 1999).

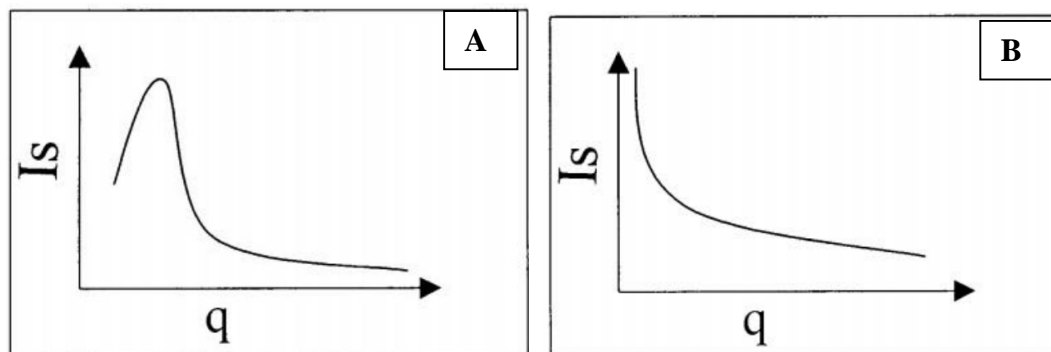


Figure 4.2 (A) Scattering light intensity (I_s) with respect to wave angle (q) during spinodal decomposition. (B) Scattering light intensity (I_s) with respect to wave angle (q) during nucleation and growth (Liu and Kiran 1999).

There are two different opinions in the literature as to what is the phase separation mechanism during VIPS. According to Caquineau et al. 2003; Menut et al. 2008; Han and Bhattacharyya, 1995; Chae Park et al. 1999; characteristic morphological properties of membranes via VIPS, which is cell-like structure, is attributed to nucleation-and-growth mechanism by coalescence coarsening. Because nucleation-and-growth mechanism is coherent with the slowness of non-solvent diffusion into casting polymer solution. Besides, isolates polymer-lean phase spheres are another characteristic of nucleation and growth mechanism.

Lee et al. 2004 is the first research group who proved that the phase separation could occur via spinodal decomposition in VIPS. Authors supported their claim with a mathematical model and also small angle light scattering data. There are two criteria of being in unstable region in which spinodal decomposition is likely to occur. First of all, free energy of mixing should be positive and second derivative of free energy of mixing should be negative (Favvas and Mitropoulos 2008; Lee et al. 2004). The Flory–Huggins form of the free energy of mixing and the second derivative of this term were calculated as positive and negative respectively in this research. Hence authors proved that spinodal decomposition mathematically. Lee et al. 2004 proved the spinodal decomposition by measured scattered light intensity. Polymer solution exposed to nonsolvent vapor presented

scattered light intensity which go through maximum and show a typical diffraction halo pattern with respect to angle. This type of behavior is a typical characteristic of spinodal decomposition according to Cahn Linear theory (Lin and Kiran 1999). Despite their proof, the morphology of membranes is consistent with characteristic structure of nucleation-and-growth phase separation rather than spinodal decomposition. The incompatibility between morphology and phase separation mechanism is explained by Kuo et al. 2005. According to their assertion, due to coarsening, bi-continuous structure turns into cellular pores. (As explained previously, coarsening may occur after spinodal decomposition to reduce the interfacial energy between polymer rich and polymer lean phases (Nunes and Inoue 1996; Chae Park et al. 1999; Su et al. 2009)).

Su et al. 2009 and Peng et al. 2013 who showed that VIPS was capable to bring the solution to spinodal decomposition, which leads to transient bi-continuous structure later turn into cellular pores. In their studies, VIPS period or exposure duration of non-solvent vapor is very short (less than 1 min for Peng et al. 2013). After short period of non-solvent vapor exposure was followed by wet quenching. In my opinion, such a short vapor-exposure duration is sufficient to begin phase separation at the upper surface and to densify a polymer layer at upper part, but not sufficient to designate the final membrane structure. During quenching, fast solvent-nonsolvent interchange and strong activity of nonsolvent determine the final structure of membrane. Spinodal decomposition and its characteristic membrane morphology is a natural result of wet quenching. Han and Bhattacharyya, 1995 also asserted that when non-solvent vapor exposure followed by wet quenching, preformed morphology of membrane changed due to fast demixing during wet quenching and nodular structure might be observed.

Tsai et al. 2006 are another authors who observed spinodal decomposition. Tsai et al. 2006 was also used liquid water to obtain final membrane structure. But for some experiment, unlike the other researchers, Tsai et al 2006 used liquid nitrogen to fix the structure of membrane just after water vapor exposure. They observed both bicontinuous structure and cellular structure depending on relative

humidity and exposure time of humidity. When the humid air exposure time was long enough, cellular structure was observed and this phenomenon was explained by coarsening of bicontinuous structure. Tsai et al 2006 also approved that the structure formed in the air gap would then further develop into its final form in the coagulation bath. Gelation of polymer rich phase after VIPS effects membrane morphology with different ways. Gelation of polymer rich layer hinders the fast solvent-nonsolvent exchange rate during wet quenching. Hence macrovoids suppression is observed. Bicontinuous pore structure is another effect of gelation. Gelation of polymer rich phase inhibits coarsening in the coagulation bath, hence bicontinuous structure formed during VIPS are preserved. Further increase in humidity exposure period leads to reoccurrence of macrovoids because gel layer is disappearing due to relaxation of polymer for longer time period and cannot inhibit coarsening anymore.

Generally, membranes produced via VIPS have symmetric cellular porous structure. The sharp concentration and activity gradient of nonsolvent, solvent and polymer across the polymer solution creates asymmetric structure, as in the case of NIPS. On the other hand, in VIPS, the concentration gradient of the three components are smooth across the polymer cross-section due to slow diffusion of water vapor (Chae Park et al. 1999). Yip and McHugh 2006 showed that the concentration profiles of the nonsolvent, solvent and polymer across the casting film are relatively flat especially polymer solution prepared with high boiling point solvent. Matsuyama et al. 1999-I, proved flat polymer concentration profile mathematically. According to their calculations, the polymer fractions near the top surface increases at the beginning, with time the flat polymer concentration profile is formed. Hence symmetric membrane structure is expected and obtained for phase separation via VIPS rather than asymmetric morphology.

Unlike the general characteristic symmetric morphology of VIPS membranes, Menut et al. 2008, Khare et al. 2005 and Wang et al. 2000 reported asymmetric membrane morphology via VIPS. Wang et al. 2000 attributed the asymmetric membrane morphology to lower polymer concentration near air-polymer solution interface than that in the bulk casting solution. Menut et al. 2008

induced that the surface liquid layer formed on top of the casting solution after the phase separation and then disappeared. After the phase separation, due to gelation of polymer layer water diffusion into casting polymer layer is retarded, this leads to accumulation of water layer on top of casting film. The solvent NMP is extracted from polymer layer by the accumulated water layer due to affinity between NMP and water. Polymer concentration decreased because of the intake of water and NMP in the surface liquid layer. Anisotropic membrane morphology with larger pores near the membrane surface and smaller pores near the bottom surface is emerged. Since the solvent moves toward the membrane surface due to affinity to the surface liquid layer, polymer concentration and viscosity in the top layer of membrane is lower than that of bottom layer. As a result, coarsening of droplets takes place more easily in the top layer of membrane due to lower viscosity. Due to low polymer concentration, the continuous polymer rich phase reaches the glass transition concentration later than in the bulk of the membrane, this delay provides more time for cell growth and coalescence. Decrease in polymer concentration due to increase in solvent and water content on top layer was also reported by Khare et al. 2005. The variant concentration profile as depicted in Figure 4.3-A leads to asymmetric membrane morphology as shown in Figure 4.3-B is called hour-glassy structure by Khare et al. 2005.

Finally, there is no gas separation membranes produced by VIPS method, in the literature. Barth et al. 2000 used the PS and PES membranes prepared by VIPS in order to separate PEG/water solution and PVA/water solution. Han and Bhattacharyya, 1995 studied PEG/water solution separation by PS membranes prepared by VIPS and wet phase inversion. They reported that decrease in water flux and increase in PEG rejection when membranes were produced by VIPS.

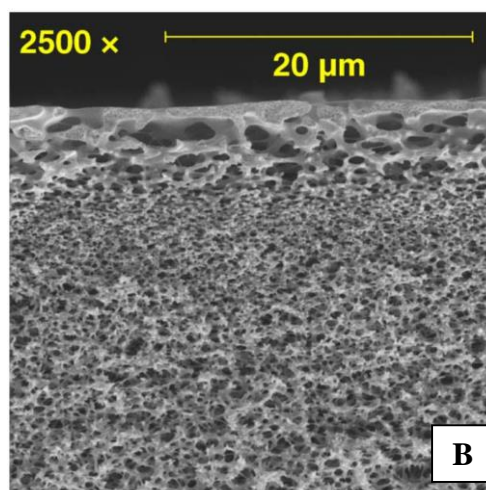
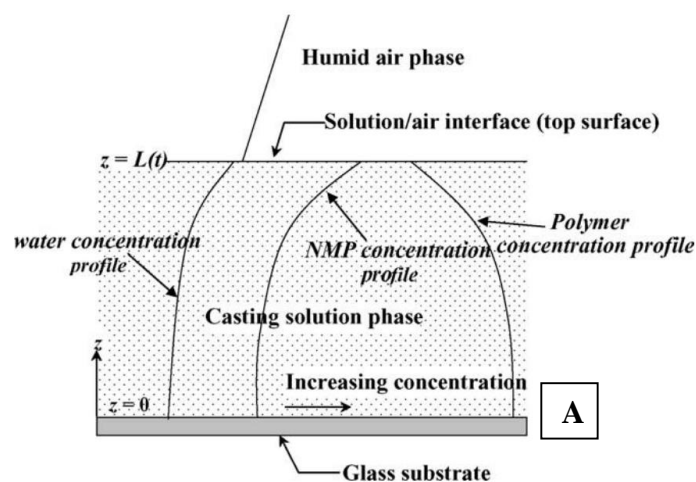


Figure 4.3 Schematic representation of concentration profile across casting film (A), SEM image of membrane having hour-glassy structure (B) (Khare et al. 2005).

4.2 Materials and Experimental Method of PI Membrane Production via Light Induced Dry-VIPS

4.2.1 Materials

Polyimide resin, Matrimid[®] 5218, THF, DMF and ZIF-8 were used. The properties of these materials were given in **Chapter 3.2**. The ZIF-8s preferred in this part of the study have 65 nm crystal size and were thermally annealed (Treatment-Type3). The reason of thermal annealing was the deteriorating effect of

residual MeOH in the pores of ZIF-8 in the treatment type 1. Furthermore, 65 nm crystals size was preferred because of higher tendency of 25 and 15 nm of ZIF-8 to clustering. In this part of the study, different from other parts, pNA was used. p-nitroaniline, pNA, which has amine and nitro functional group, was used as compatibilizer and anti-plasticizer and purchased from Across. It has a chemical formula of $C_6H_4(NH_2)(NO_2)$, molecular weight of 138.1 g/mol and density of 1.44 g/cm³. The solubility of pNA in DMF was 1200 g/L (Phatak and Gaikar 1996). The chemical structure of pNA is presented in Figure 4.4.

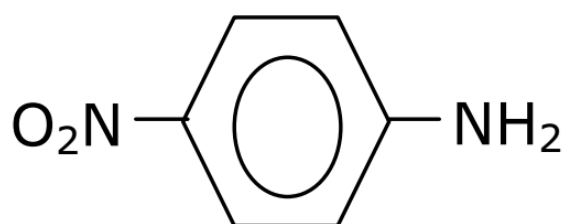


Figure 4.4 Chemical structure of p-nitroaniline (D. Şen 2008).

4.2.2 Preparation of neat PI, PI/ZIF-8 and pNA/PI/ZIF-8 Membranes via VIPS

The homogeneous PI and PI/ZIF-8 membrane solution was prepared and as narrated in Chapter 3.2. In order to prepare PI/ZIF-8/pNA mixed matrix membrane, after dispersion of ZIF-8 in 9.5 g DMF and addition of THF, pNA at 10% by mass of the polyimide was dispersed in THF/DMF/ZIF-8 solution. at 10% by mass of the polyimide was dispersed in 9.5 g DMF solvent. The addition of PI, casting of membrane and annealing procedures were the same as those of neat PI membranes.

VIPS was carried out at 80% relative humidity. After bringing the humidity in the home-made Glow Box shown in Figure 3.2 the membrane solution was poured onto the glass surface with a thickness of 500 µm with the aid of an automatic film applicator. The polymer film was then exposed to infrared light or incandescent light during the dry phase change. After dry inversion step, casting film was left in the glow box at 80% relative humidity until the film until it was self-peeled off from the glass. This period took approximately 5 hours. To remove

the residual solvent, the solidified membrane was dried overnight in a 120 °C vacuum oven.

Morphological properties of membranes were investigated via SEM. The details of it was already provided in Chapter 2.3.

4.2.3 Gas Separation Test of neat PI, PI/ZIF-8 and pNA/PI/ZIF-8 Membranes

Single gas permeation test of the membranes produced via VIPS was performed in the set-up depicted in Figure 4.5 and flow diagram can be seen in Figure 4.6. This system has an oven to keep the temperature constant during gas permeation test, and a manifold to connect the feed and permeate with purge, vacuum and pure gases. Membrane modules were fixed in oven. The oven temperature was kept at 35 °C. Heating of the oven was provided by resistance heater. Homogeneous distribution of heat throughout the oven was provided by a fan. Heating and temperature were monitored and controlled by a thermocouple equipped with PID controller (GEMO TD107A). Two stainless steel membrane modules were placed in oven. These modules held the flat membranes with two o-rings. Modules connected to the manifold via copper tubing and brass valve and fittings from the top. Bottom part of the modules were connected to pressure transmitter by copper tubing and brass valves and fittings. The line between module bottom side and pressure transducer was called permeate. The pressure increment in permeate side under vacuum with respect to time was monitored by pressure transmitter (with part no. KELLER-PAA-21Y-81554.33) with 0-4 bar range and 0.25% full scale linearity. The volume of the permeate side was measured 13.6 cm³ for each module. The permeate also was connected to the manifold by a brass on-off valve. The pressure of the feed part was monitored by pressure transmitter (with part no. KELLER-PA-23SEI-81155.10) with 0-25 bar range and 0.25% full scale linearity. Before each test, whole system was kept under vacuum for 3-3.5 hours via manifold. The vacuum was supplied by a mechanical vacuum pump (Edwards). Then, the pure single gas (H₂, CO₂ or CH₄ for this system) was fed to module upper part via manifold when the valves provided convection with manifold and permeate

were closed. The feed pressure was 2 atm. Gauge pressure. The pressure difference between feed and permeate is the driving force for gas permeation. The experiment was performed by constant volume and variable pressure method. Due to driving force, the pressure of the permeate side increased with time. The rate of pressure rise was used to calculate permeability coefficient. The details about these calculations was already provided in Chapter 2.3.

Table 4.1 provided the codes of the membranes produced via VIPS. Membrane content and membrane casting parameters were also available in this table.

Table 4.1 Membrane codes and preparation properties of PI, PI/ZIF-8, PI/ZIF-8/pNA membranes. Each membrane prepared from polymer solution made up of 4 gr. PI, 4 gr THF as volatile solvent, and 9.5 gr DMF as non-volatile solvent.

Membrane Code	ZIF-8	pNA	Dry inversion
VIPS_PI_0_Ex_1	No	No	No Light
VIPS_PI_0_IR_2			No Light
VIPS_PI_60_IR_1			60 s IR
VIPS_PI_120_IR_1			120 s IR
VIPS_PI_120_IR_2			120 s IR
VIPS_PI_180_IR_1			180 s IR
VIPS_PI_240_IR_1			240 s IR
VIPS_PI_240_IR_2			240 s IR
VIPS_PI_60_IL_1			60 s IL
VIPS_PI_120_IL_1			120 s IL
VIPS_M-PI_0_Ex_1			0.4 g (10% of PI)
VIPS_M-PI_60_IR_1	60 s IR		
VIPS_M-PI_120_IR_1	120 s IR		
VIPS_M-PI_120_IR_2	120 s IR		
VIPS_M-PI_180_IR_1	180 s IR		
VIPS_M-PI-C_0_Ex_1	0.4 g (10% of PI)	0.16 g (4% of PI)	No Light
VIPS_M-PI-C_60_IR_1			60 s IR
VIPS_M-PI-C_120_IR_1			120 s IR
VIPS_M-PI-C_120_IR_2			180 s IR

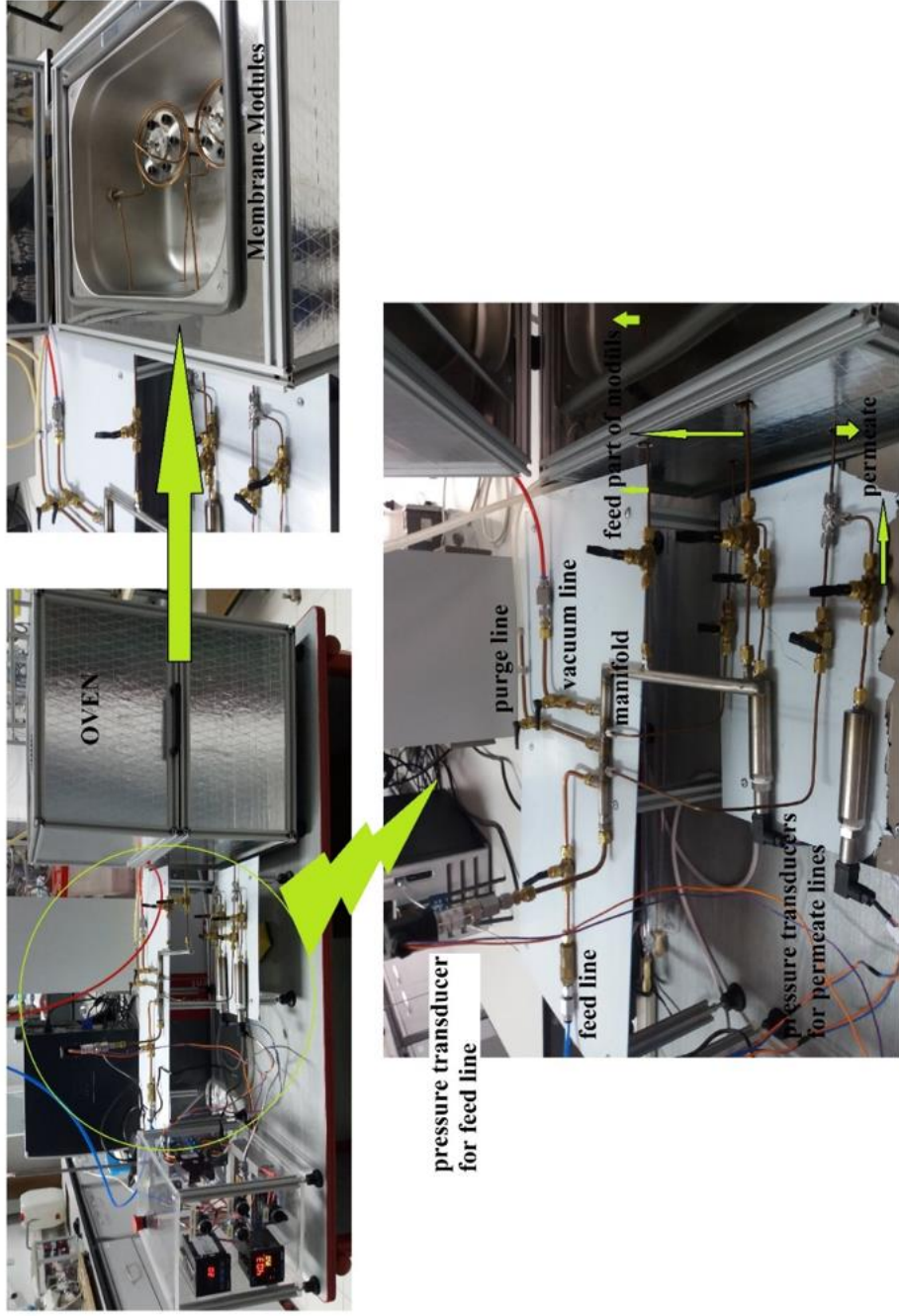


Figure 4.5 Gas permeation test system for membranes produced via VIPS.

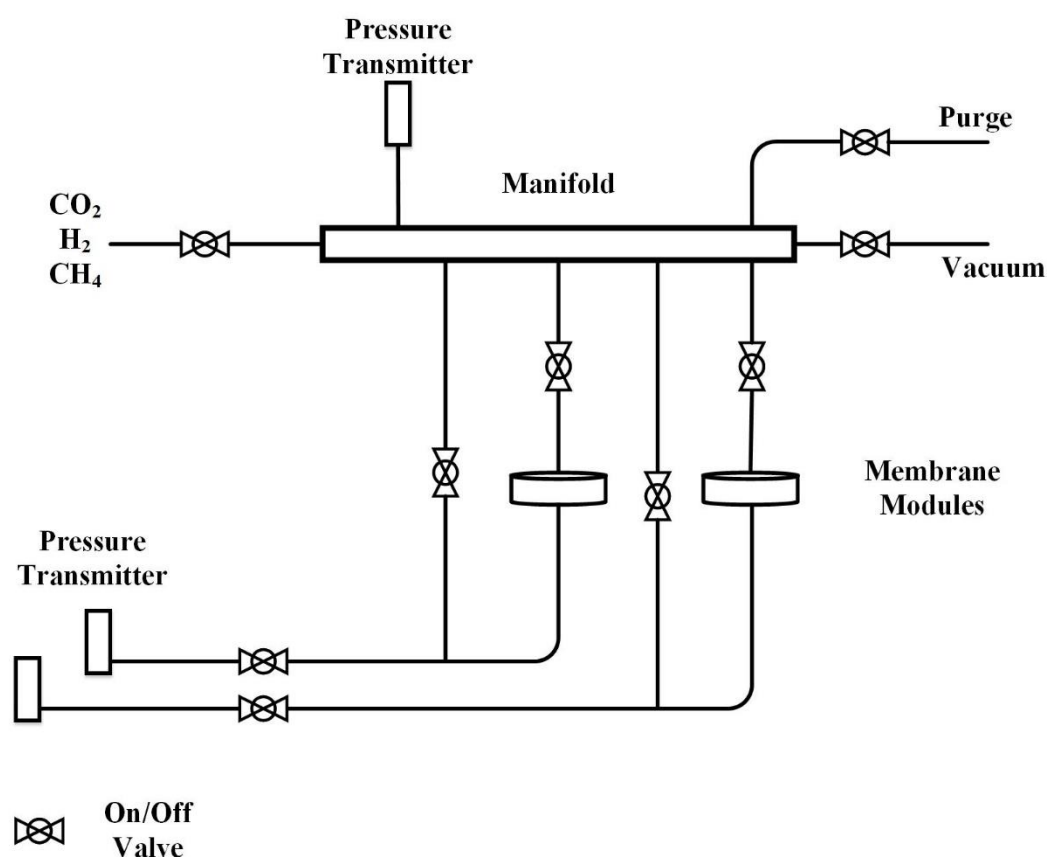


Figure 4.6 Flow diagram of test system for membranes produced by light induced-VIPS.

4.3 Morphological Investigation of VIPS Membranes

4.3.1 IR Exposure Effect on Membrane Morphology

Figure 4.7 shows the SEM micrograph of cross-section of pure PI membrane produced by VIPS without IR exposure. Based on the qualitative analysis, membrane was made up of cellular pores with uniform shape and completely symmetric. At a closer look on both top and bottom layer of the membrane, no skin layer could be detected. This type of symmetric morphology was also reported by Caquineau et al. 2003, Han and Bhattacharya 1995, Chae Park et al. 1999 and the reason of such symmetric morphology is associated with the smooth concentration gradient of solvent-nonsolvent and polymer because of the slow intake of non-solvent into casting film and also limited loss of the high boiling point solvent in

VIPS (Chae Park et al. 1999, Yip and McHugh 2006, Matsuyama et al. 1999 D). Moreover, isolated cellular pores was an evidence of that phase separation occurred via nucleation-and-growth mechanism as observed by Caquineau et al. 2003 and Menut et al. 2008.

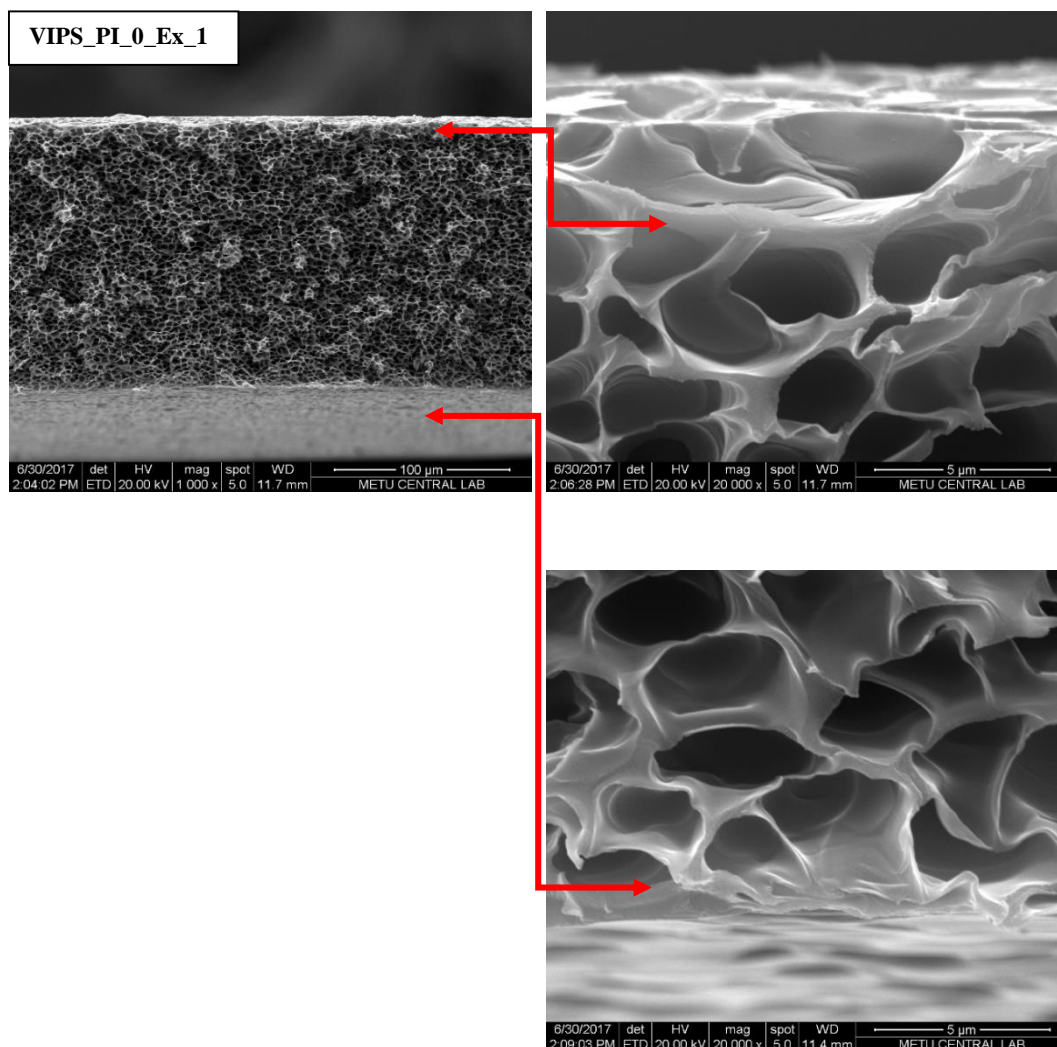


Figure 4.7 SEM micrographs of the neat PI membranes prepared via VIPS without IR exposure.

Figure 4.8 presented the SEM micrographs of the neat PI membranes exposed to IR light for 60, 120, 180 and 240 seconds during dry inversion period. When their morphology was compared to the that of non IR exposed membrane, the first and most striking feature was existence of a skin layer which thickened with IR exposure time. The total thickness of membranes decreased when the IR

exposure period exceeded 120 second. There is no doubt that the reason of the asymmetric structure was the rapid evaporation of THF (low boiling point solvent) and DMF (high boiling point solvent) which led to increase of the polymer fraction at the top layer of the casting solution. Hence concentration profile across casting solution results in different phase separation dynamics and asymmetric morphology in the precipitated casting polymer film (Yip and McHugh 2006). Probably, in our system, exposure of IR led to increase in polymer fraction on top layer via evaporation of solvents. This high polymer fraction layer may have followed path 1 as depicted in Figure 2.5 and after passing vitrification boundary dense skin layer formed. The layer below this high polymer fraction layer has followed path 2-1 as depicted in Figure 2.5 and nucleation-and-growth of the polymer lean phase creates isolated uniformly distributed porous cells. There are several studies reported asymmetric membrane morphology after VIPS precipitation (Menuet et al. 2008, Wang et al. 2000, Khare et al. 2005). In these studies, membranes had large pores on top layer, and smaller pores below these large pores due to solvent accumulation near the top layer as a result of affinity between solvent and nonsolvent. The difference in asymmetric structure obtained in our study and other studies come from difference in precipitation process. To the best of our knowledge, this study is the first in literature in which dry inversion step is promoted by IR exposure and precipitation of polymer film finalized via VIPS.

The total polymer film thickness decreased when the IR exposure time exceed 120 second. When the IR exposure time reached 240 seconds, dense symmetric polymer film was obtained. 240 second IR exposure might be sufficient to increase the polymer fraction at the bottom layer of casting film as in the top layer. This high polymer fraction promoted the vitrification of polymer film by following path 1 (see Figure 2.5) and smooth polymer concentration gradient led to symmetric dense polymer film. The second possible reason of dense symmetric polymer film formation might be limited in-diffusion of nonsolvent vapors due to low solvent fraction in the polymer layer. As suggested by several researchers, initiation of nonsolvent in-diffusion in VIPS is mainly because of affinity between

solvent and nonsolvent vapors (Caquineau et al. 2003; Su et al. 2009; Menut et al. 2008; Tsai et al. 2006). 240 second IR exposure significantly diminished solvent amount in the casting film and the remaining amount of solvent might be not sufficient to draw required amount of nonsolvent into casting polymer film. Therefore, phase separation due to non-solvent vapor in-diffusion could not occur.

When the IR exposure time was 180 second, a strange morphology was obtained. This membrane contained two dense layer one of them was at top of the membrane and the other was on the bottom. Between these two dense non-porous layers, spongy porous layer was located. In my opinion, the remaining solvent in the casting polymer film after 180 second IR exposure might be still sufficient to draw non-solvent vapor from humid air atmosphere which led to phase separation and porous morphology formed under the dense top layer. Since the drawn of non-solvent occurred from the top layer, the in-taking non-solvent vapor could not reach the bottom layer, hence non-porous dense bottom layer obtained via vitrification. The other possible explanation might be incomplete vitrification of casting film for 180 second IR exposure. Probably, 240 second IR exposure was sufficient to vitrify the casting polymer film. Further non-solvent vapor exposure of it could not change its thermodynamic stability. However, after 180 second IR exposure, phase inversion was not completed and further non-solvent vapor exposure brought a new thermodynamic state for sublayer at which vitrification was not finalized yet.

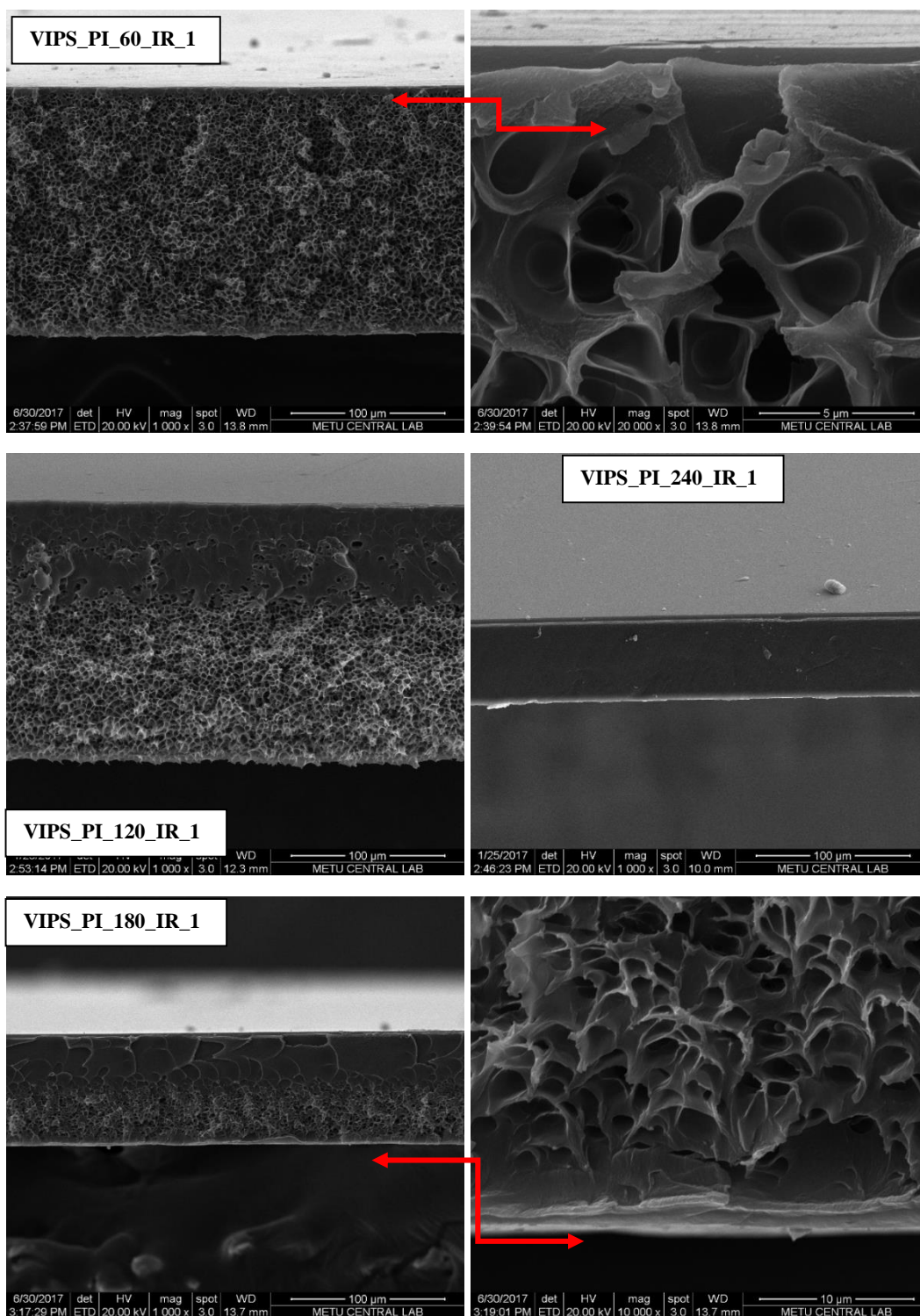


Figure 4.8 SEM micrographs of the neat PI membranes exposed to IR light for 60, 120, 180, and 240 s priory beginning of VIPS.

Table 4.2 presented the quantitative analyses of morphological properties of membranes based on SEM images. The IR exposure for 60 seconds allowed the formation of a non-porous dense skin layer with a thickness of about 4.56 ± 1.09 μm , while increasing the thickness of the porous layer by 4.5%. The increase in the thickness of the porous layer was ascribed the thermal expansion of polymer casting film during IR exposure period. Due to resistance provided this dense skin layer non-solvent vapor diffusion into casting polymer film was decelerated. This slowed down diffusion process resulted in slow growing of pores (Young and Chen 1995), hence the pore size diminished approximately by 15% due to 60 seconds IR exposure. When the IR exposure period reached to 120 seconds, the dense layer thickness increased to 42.76 ± 16.66 μm and porous layer thickness decreased from 154.50 ± 1.35 μm to 102.12 ± 5.00 μm . The increase in thickness of dense skin layer was a result of increment in the thickness of densified polymer layer of casting solution film. Further increase in IR exposure decreased both pores size, porous layer thickness. Finally, dense non-porous polymer film with 53.68 ± 0.72 μm was obtained after 240 second IR exposure. The reason of the polymer film shrinkage was increased polymer fraction in the casting film.

Table 4.2 Quantitative investigation of morphology of membranes prepared via VIPS.

Membrane Code	IR exposure time (s)	Dense Layer Thickness (μm)	Porous Layer Thickness (μm)	Pore Shape	Pore Size (μm)
VIPS_PI_0_Ex_1	0	No dense	149.77 ± 1.33	spongy	3.15 ± 0.88
VIPS_PI_60_IR_1	60	4.56 ± 1.09	154.50 ± 1.35	spongy	2.68 ± 0.75
VIPS_PI_120_IR_1	120	42.76 ± 16.66	102.12 ± 5.00	spongy	2.79 ± 0.65
VIPS_PI_180_IR_1	180	Top = 37.25 ± 1.52	27.65 ± 2.21	spongy	1.65 ± 0.49
		Bottom = 5.87 ± 1.48			
VIPS_PI_240_IR_1	240	53.68 ± 0.72	No pores	-	-

4.3.2 Incandescent Lamp Light Exposure Effect on Membrane Morphology

Figure 4.9 shows the SEM micrograph of cross-section of pure PI membrane exposed to incandescent lamp light for 60 and 120 seconds prior to VIPS. At first glance, no difference could be detected between the morphological structure of these membranes and the that of the prepared membrane (VIPS_PI_0_IR_1) without being exposed to the light at all. A closer look at the upper layer of the membrane, a separate dense skin layer could not be detected since the thickness is not more than the wall thickness of the isolated pores.

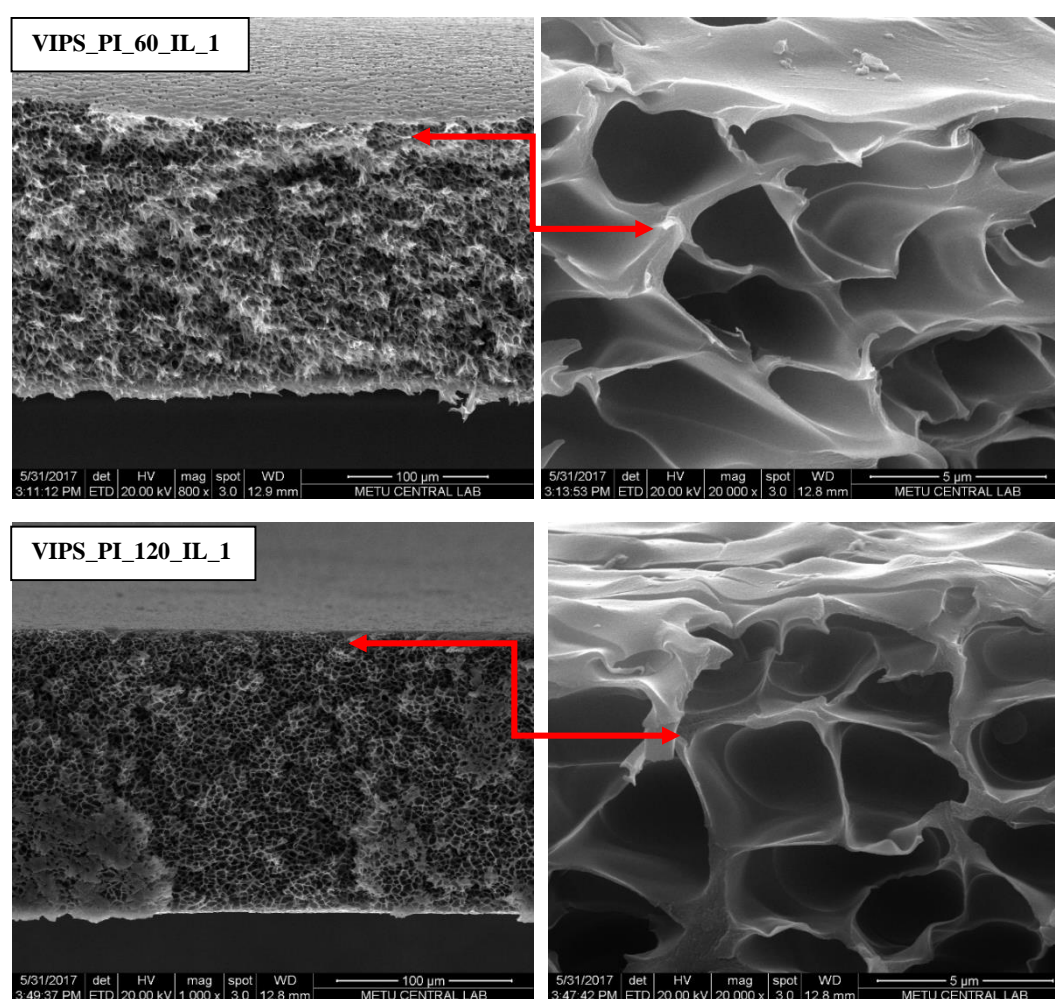


Figure 4.9 SEM micrographs of the neat PI membranes exposed to incandescent lamp (abbreviated as IL) light for 60 and 120 seconds prior to beginning of VIPS.

Table 4.3 are listed the morphological properties of membranes prepared via IL explosion following VIPS. Although IL exposure was not sufficient to create a dense skin layer in a conventional manner, 60 seconds IL led to increase 31.2 % in thickness of porous layer and 20% in the size of the pores. When the IL exposure period increased from 60 seconds to 120 seconds, the increment in the thickness of porous layer was reduced. However, still the thickness of porous layer of membrane exposed to 120 seconds IL was approximately 7% higher than that of membrane prepared without light exposure. Light exposure led to increase the temperature of the casting film and thermal expansion of casting film formed thicker membrane. As the exposure time to the light increased, the thermal expansion was still active and however the increase in the polymer fraction due to the amount of evaporated solvent tended to denser membrane layer. Therefore, effectiveness of thermal expansion reduced and the percent of increase in membrane thickness diminished.

Table 4.3 Quantitative investigation of morphology of membranes prepared via VIPS.

Membrane Code	IL exposure time (s)	Dense Layer Thickness (μm)	Porous Layer Thickness (μm)	Pore Size (μm)
VIPS_PI_0_Ex_1	0	Not in a conventional manner	149.77 ± 1.33	3.15 ± 0.88
VIPS_PI_60_IL_1	60		196.50 ± 8.15	3.78 ± 1.28
VIPS_PI_120_IL_1	120		160.05 ± 1.09	2.90 ± 0.95

4.3.3 Effect of Light Exposure on Membrane Surface

Figure 4.10 presented the SEM images of surface of the membranes prepared without light exposure and 60 second IR exposure, respectively. On the surface skin of the membrane (VIPS_PI_0_Ex_1) prepared without light exposure, pin holes were detected. Similar observation was also reported by Menut et al. 2008, Han and Bhattacharyya 1995 and Wang et al. 2000. According to Menut et al. 2008, incomplete closure of the polymer phase during coalescence was the reason of such pinholes. Han and Bhattacharyya 1995 induced that the membrane immersed water bath after 3 minutes VIPS and membrane prepared by 3-days VIPS both had

spherical voids on the skin layer. It was assumed that these voids were originated from surface tension and stress during liquid-liquid phase separation. Formation of surface pores and also increase the size of these pores with increase in relative humidity were experienced by Wang et al. 2000 who attributed to spontaneous emulsification induced by the contact of casting solution with water vapor. To prepare functional membranes for antibacterial activity or protein adsorption, honeycomb film surface was fabricated with breath figure method (Dou et al. 2015). In this method, formation of holes in honeycomb shape on the polymer layer was also provided by condensation water droplets on the polymer film. The observation about surface pinholes of Peng et al. 2013 and Su et al. 2009 provided different perspective. In the method of Peng et al. 2013 and Su et al 2009, VIPS was followed by wet phase inversion. They suggested that increasing the period of VIPS inhibited the formation of surface pores. They suggested that with longer non-solvent water vapor exposure promoted coarsening of the polymer rich phase formed dense skin layer. In light of thin knowledge, in our method, condensation of non-solvent water droplets on casting PI film initiated nucleating-and-growth type phase separation and polymer poor phase created these pinholes or voids. Although in our case VIPS duration was very long (at least 3 hours), the coarsening of polymer rich phase could not create dense surface layer for membrane prepared without light exposure. Probably, surface tension which is assumed the origin of coarsening was not strong enough to complete the coarsening of polymer rich phase on our casting polymer film surface. Smaller pinholes were assumed as an indicate of coarsening of polymer rich phase. However, large voids showed that membrane phase separation was completed before coarsening of polymer rich phase finalized.

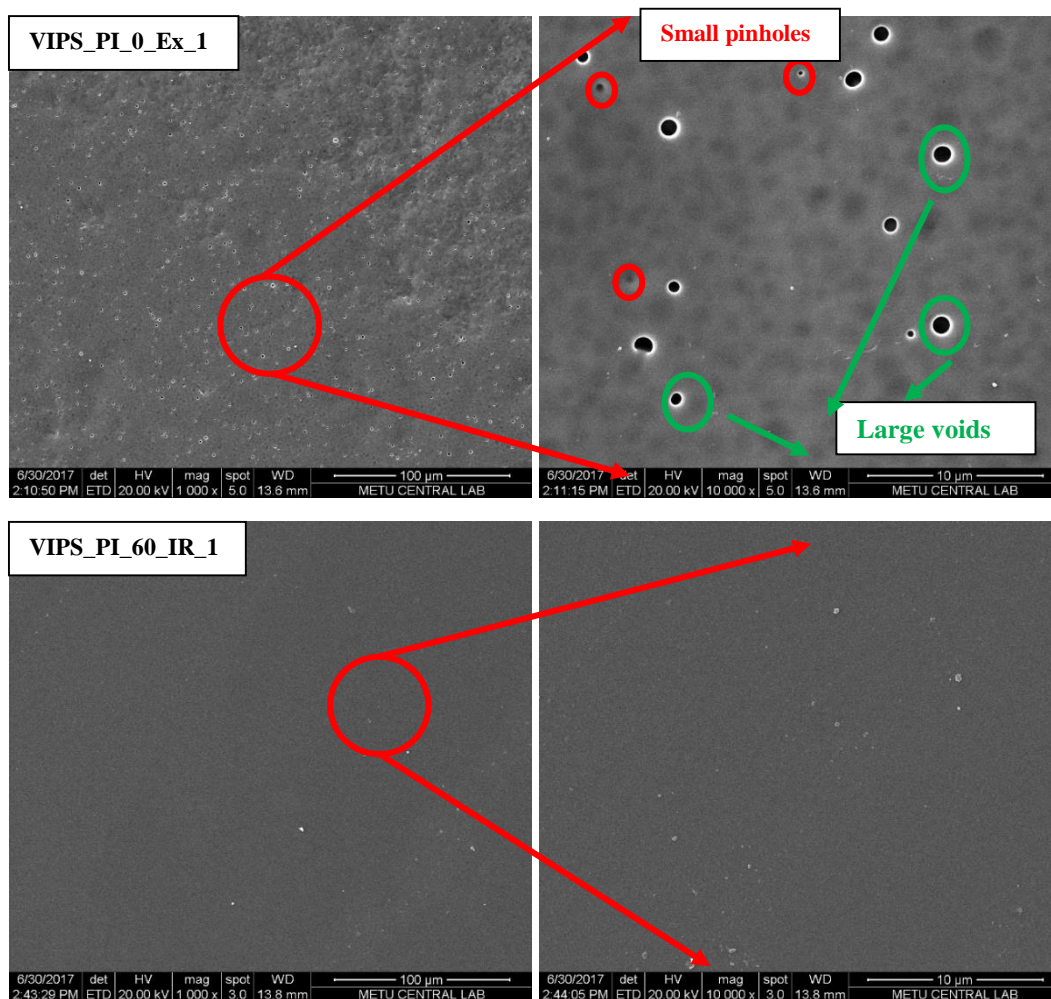


Figure 4.10 SEM micrographs of the surface of the neat PI membranes prepared without light exposure and with 60 second IR exposure during VIPS.

When the membrane exposed to 60 seconds IR light during VIPS, it was observed that surface pinholes or large voids completely disappeared as shown in Figure 4.10. One of the possible reasons was the vitrification of the surface layer of the casting polymer film due to high radiative energy of IR. Since the surface layer vitrified before water vapor condensation further phase separation could not take place on the surface layer. However, this vitrified layer still allowed the water vapor diffusion into the casting film and phase separation could take place in the sublayer. The increased temperature on the casting film because of IR light might be the other reason of dense surface layer. High polymer film surface temperature prevented the condensation of water droplets on the surface or fast evaporation of condensed

water droplets. Therefore, phase separation on the surface due to water vapor condensation hindered.

The SEM micrographs of surface of the neat PI membranes exposed 60 (VIPS_PI_60_IL_1) and 120 (VIPS_PI_60_IL_1) seconds IL light during VIPS were depicted in Figure 4.11. 60 seconds IL exposure increased both quantity and size of the voids. Further increase the IL exposure period from 60 seconds to 120 seconds induced shrinkage in the size of the voids when compared the size of the voids on the VIPS_PI_60_IL_1. The quantitative analysis of surface voids based on SEM images was presented in Table 4.4.

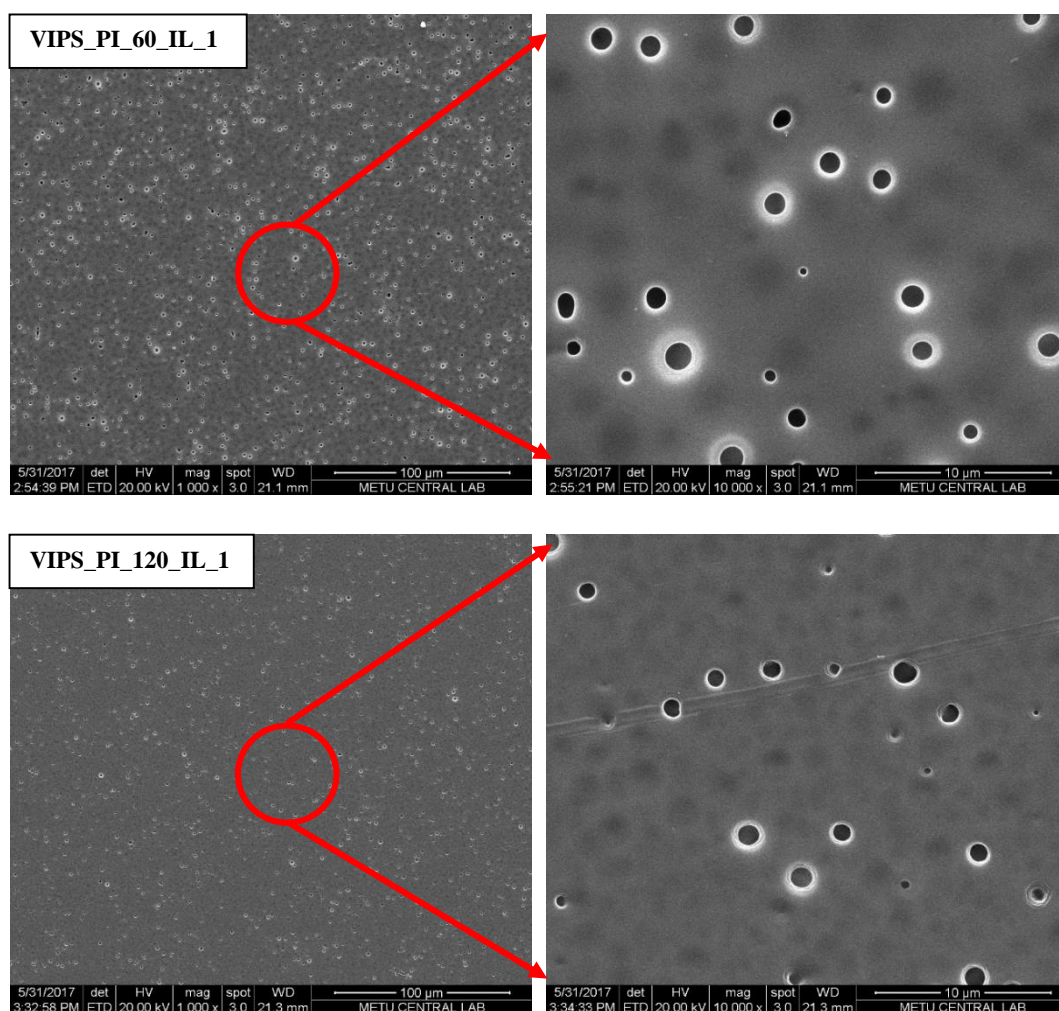


Figure 4.11 SEM micrographs of the surface of the neat PI membranes prepared with IL light exposure for 60 and 120 seconds during VIPS.

Table 4.4 Quantitative investigation of morphology of membranes prepared via VIPS

Membrane Code	Light exposure time (s)	Number of voids per 3050 μm^2	Average size of the voids (μm)
VIPS_PI_0_Ex_1	0	50	0.65 ± 0.30
VIPS_PI_60_IL_1	60	84	1.12 ± 0.46
VIPS_PI_120_IL_1	120	100	0.75 ± 0.26
VIPS_PI_60_IR_1	60	No voids	-

The temperature increment caused by the fluorescent light exposure was not high enough to prevent water vapor condensation of film surface or evaporate the water droplets which were condensed already. For this reason, the fluorescent light could not prevent formation of surface voids as it was infrared light. However, the temperature increment because of the fluorescent light promoted and accelerated the evaporation of THF and DMF solvents. Hence, the solvents that proceed toward the casting polymer film surface and increment in fraction of solvents near the surface attracted more water vapor and enhanced formation of polymer poor phase. Therefore, both fraction and size of the voids were increased as depicted in Table 4.4.

4.3.4 Morphological Properties of PI/ZIF-8 Mixed Matrix Membrane prepared via IR Exposure during VIPS

Figure 4.12 showed the SEM micrograph of PI/ZIF-8 mixed matrix membrane (VIPS_M-PI_0_Ex_1) prepared without light exposure during VIPS. VIPS_M-PI_0_Ex_1 membrane had completely symmetric porous structure as VIPS_PI_0_Ex_1. VIPS_M-PI_0_Ex_1 had no skin layer and membrane was composed of spongy closed. In some places, ZIF-8 crystals agglomerated within closed spongy pores.

SEM micrographs depicted in Figure 4.13 belongs to PI/ZIF-8 mixed matrix membrane (VIPS_M-PI_60_IR_1) prepared with 60 seconds IR light exposure during VIPS. The morphological properties of VIPS_M-PI_60_IR_1 was

completely similar to that of VIPS_M-PI_0_Ex_1. 60 seconds IR exposure led to formation of a skin layer with approximately 5 μm thick for pure PI membrane as shown in Figure 4.8. However, 60 seconds IR exposure might be not sufficient for skin layer formation in the presence of ZIF-8 crystals. Agglomeration of ZIF-8 particles was observed also in some pores near the upper surface as in the total membrane cross sections.

SEM images of membrane VIPS_M-PI_120_IR_1 (exposed 120 seconds IR light during VIPS) was shown in Figure 4.14. The dense and non-porous skin layer formation was observed as in the case of neat PI membrane exposed 120 seconds IR (VIPS_PI_120_IR_1, see Figure 4.8). However, the thickness of skin layer belongs to VIPS_M-PI_120_IR_1 was lower than that of VIPS_PI_120_IR_1. ZIF-8 crystals were distributed within this dense non-porous skin layer. On the other hand, agglomeration of the ZIF-8 crystals within some pores was observed. In light of this observation, it was deduced that the ZIF-8 crystals were distributed homogeneously and without clustering within the polymer-solvent solution. When the membrane was exposed to 120 seconds IR, the upper surface of the casting polymer film was densified quickly because of fast solvent evaporation. The densified polymer layer inhibited the movement of ZIF-8 crystals, hence homogeneously distributed ZIF-8 crystals within casting polymer solution were fixed without clustering in the non-porous skin layer. However, in the sublayer casting film densification was not enough to fix the crystals or prevent to movement of them. Hence nano-sized ZIF-8 crystals moved and agglomerated to become more stable form. Another phenomenon that supported my theory about that densified polymer phase prevented aggregation of ZIF-8 crystals was the fact that the ZIF-8 clusters were mostly seen in the pores which were region formed by polymer poor phase.

The cross-sectional view of VIPS_M-PI_180_IR_1 membrane prepared with 180 seconds IR exposure during VIPS was presented in Figure 4.15. Formation of non-porous skin layer with homogeneously distributed ZIF-8 crystals and closed spongy pores including agglomerated ZIF-8 crystals were noted at first

glance as investigated for membrane VIPS_M-PI_120_IR_1. Just as neat PI membrane (VIPS_PI_180_IR_1) exposed to 180 s IR, this membrane had also sandwich type morphology; namely thick dense skin layer on top surface, porous sublayer, and thinner dense layer on the bottom.

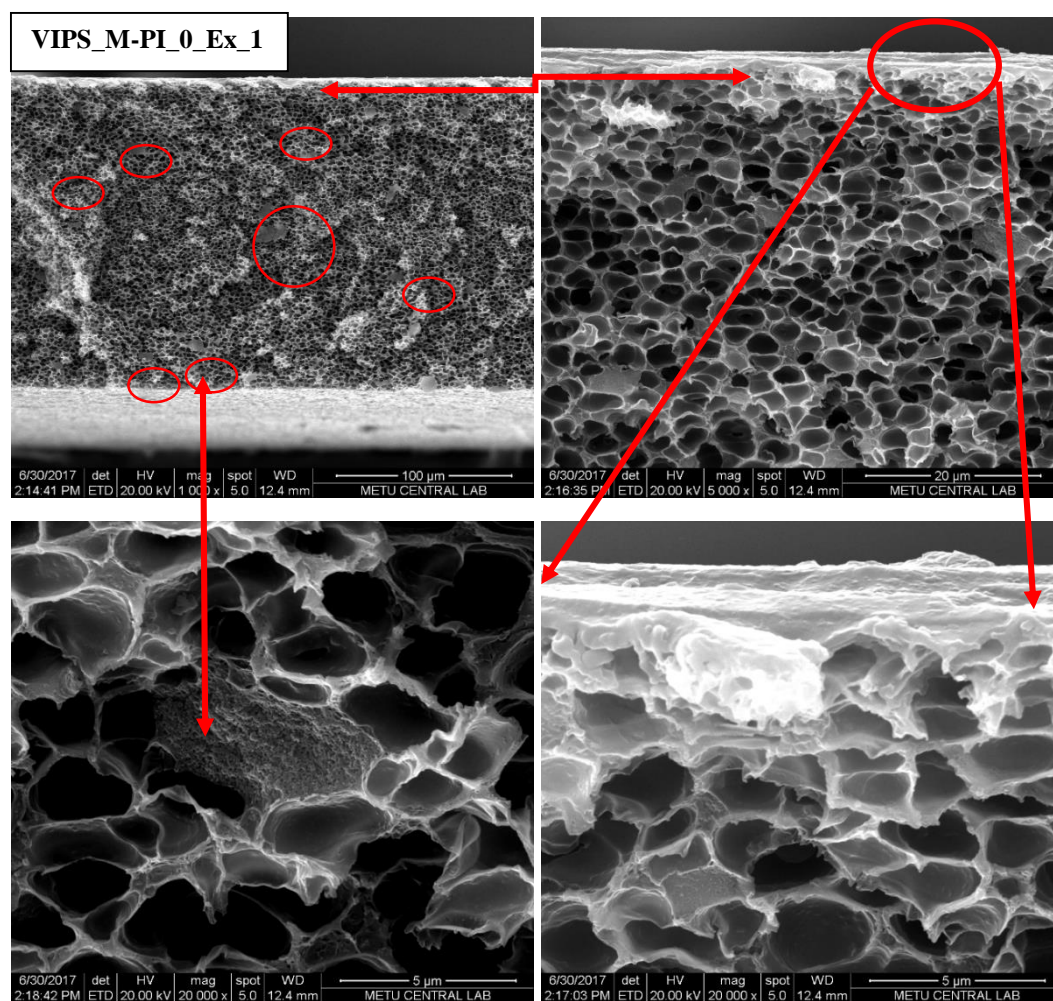


Figure 4.12 SEM micrographs of the mixed matrix PI/ZIF-8 membrane prepared without light exposure during VIPS.

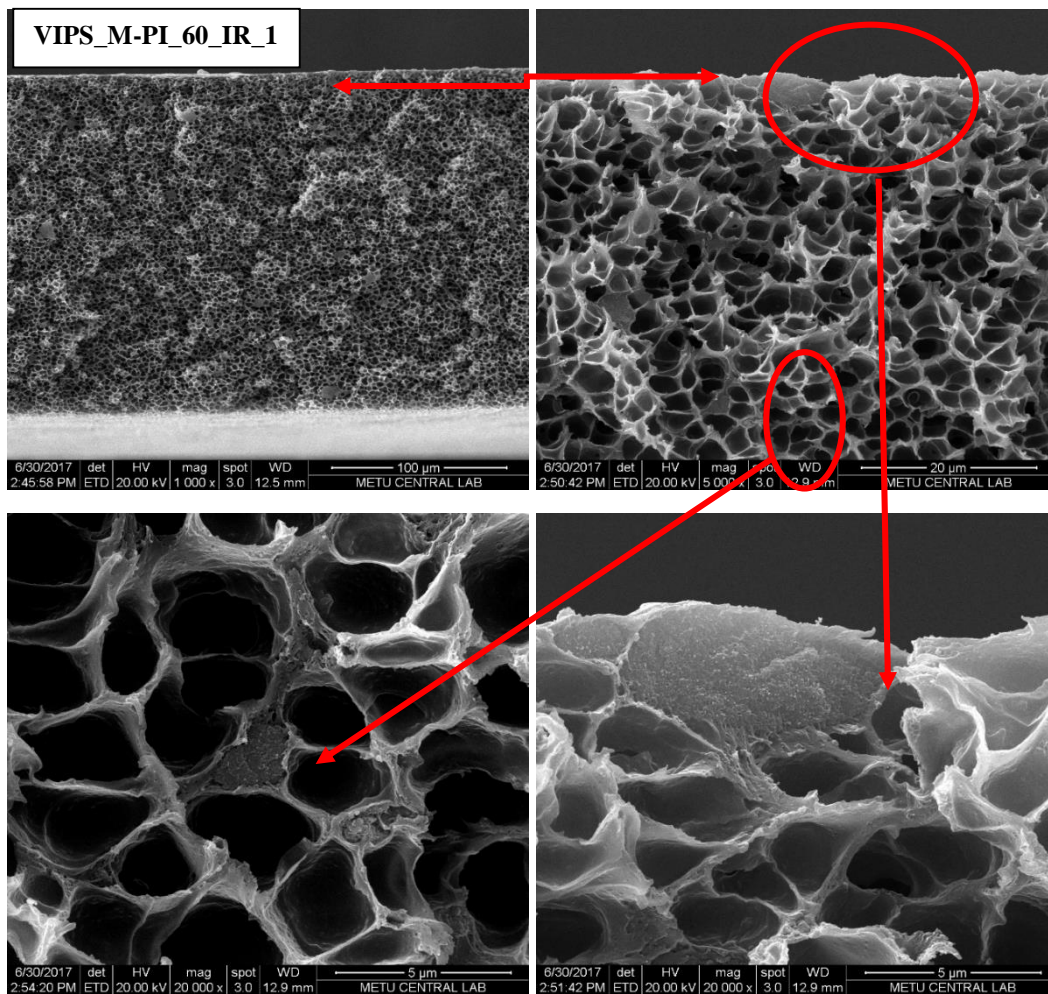


Figure 4.13 SEM micrographs of the mixed matrix PI/ZIF-8 membrane prepared with 60 seconds IR light exposure during VIPS.

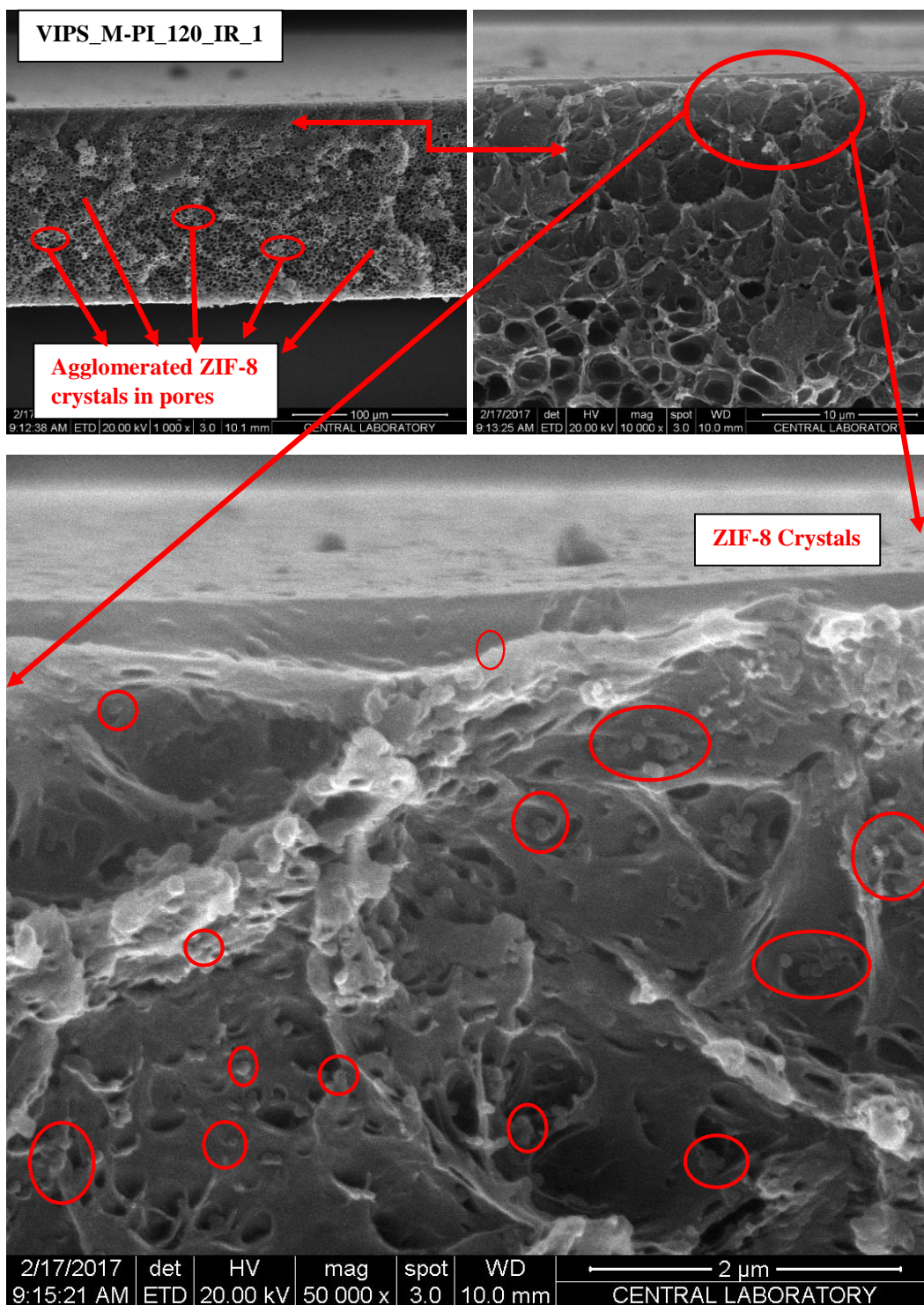


Figure 4.14 SEM micrographs of the surface of the mixed matrix PI/ZIF-8 membrane prepared with 120 seconds IR light exposure during VIPS.

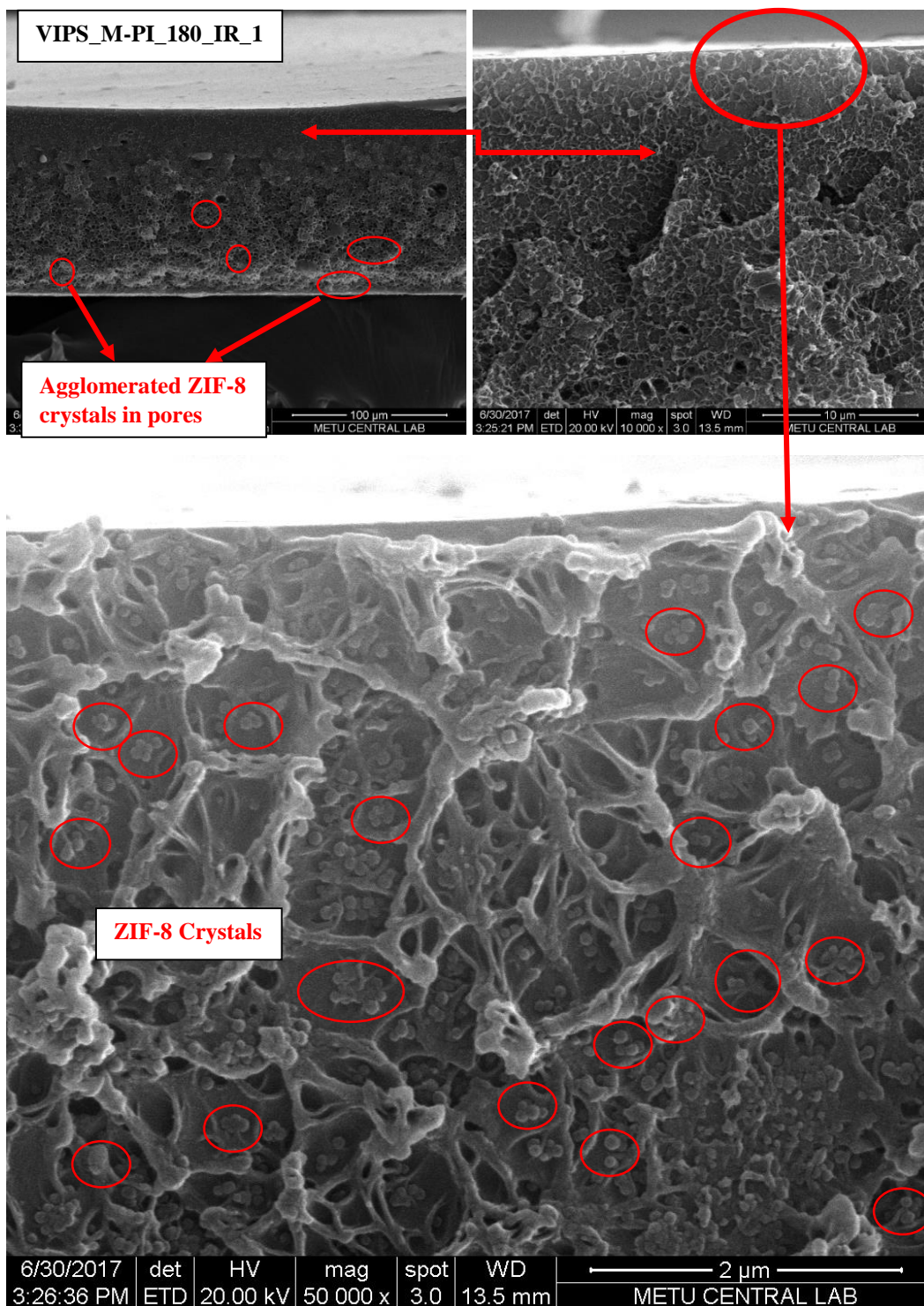


Figure 4.15 SEM micrographs of the mixed matrix PI/ZIF-8 membrane prepared with 180 seconds IR light exposure during VIPS.

The quantitative analysis of morphological properties of mixed matrix PI/ZIF-8 membranes exposed to IR during VIPS was listed in Table 4.5. As a general trend, IR exposure led to decrease in the thickness of porous layer, and in the size of the pores. Moreover, it promoted the formation of skin layer. In order to understand the effect of ZIF-8 on membrane morphology, membranes containing ZIF-8 were compared with pure PI membranes exposed to IR at the same time period during VIPS. It was investigated that the thickness of porous layer of membranes including ZIF-8 crystals was significantly higher than that of neat PI membranes, whereas the non-porous dense layer thickness of mixed matrix membranes was thinner than that of neat PI membranes. (The values listed in Table 4.2 was compared the values listed in Table 4.5). For example, due to addition of ZIF-8 crystals; the percent increase in the thickness of the porous layer was 17.89%, 24.61%, 9.23%, 160.9% corresponding to IR exposure time 0, 60, 120 and 180 seconds period. On the other hand, a 60 seconds IR exposure period in mixed matrix membrane (VIPS_M-PI_60_IR) was not sufficient to form a non-porous surface layer, which resulted in the formation of a non-porous skin layer of about 5 μm in pure PI membrane (VIPS_PI_60_IR_1). When the exposure time to IR was increased to 120 seconds (VIPS_M-PI_120_IR_1), a non-porous skin layer having an average thickness of 13.15 μm was obtained. However, this thickness was 69.25% smaller than the skin layer thickness of pure PI membrane exposing 120 seconds IR (VIPS_PI_120_IR_1).

In the mixed matrix membrane exposed to 180 seconds IR during VIPS (VIPS_M-PI_180_IR_1), the non-porous surface layer thickness was measured approximately 42.31 μm , which was about 13.58 percent thicker than that of neat PI membrane (VIPS_PI_180_IR_1) prepared under same casting conditions. Despite the increase in non-porous skin layer thickness, the ratio of dense layer thickness to the total membrane thickness decreased. In VIPS_M-PI_180_IR_1, the non-porous layer was 39.40 percent of the total membrane thickness. On the other hand, this value was approximately 60.93 percent for neat PI membrane (VIPS_PI_180_IR_1).

The reduction of the thickness of nonporous layer or its ratio in the total membrane thickness and the increase in the thickness of the porous layer have been associated with the amount of evaporated solvent and evaporation rate (or solvent removing rate). According to my experience, amount of evaporated solvents was high and the evaporation rate was fast enough, the thickness of dense layer increased while the thickness of porous layer decreased hence porous layer disappeared finally and symmetric dense membrane was obtained. When the amount of evaporated solvents was smaller and evaporation rate was slower, phase separation and formation of polymer poor phase promoted, hence thinner dense layer with porous morphology was obtained. In my opinion, the presence of ZIF-8 crystals hindered and slowed down the evaporation of solvents during VIPS. The reason might be the additional interaction between solvents and ZIF-8s or higher viscosity of casting solution due to existence of ZIF-8s. According to my experience, the addition of ZIF-8s into casting polymer solution led to higher viscosity. Increase in viscosity due to addition of fillers into polymer solution and probable effects of higher viscosity on membrane formation kinetics were investigated by several researchers (Majeed et al. 2012, Mollahosseini et al. 2012, Yang et al. 2007, Li et al. 2009). In our polymer-solvent-filler system, the viscosity of casting film increased with ZIF-8 loading and higher viscosity hindered movement of solvents (Dong et al. 2013), decreased their evaporation rate (Paula 2012, Munekata et al. 2013). Therefore, higher fraction of solvent in the casting solution promoted the formation polymer poor phase, porous structure and inhibited denser layer formation.

Table 4.5 Quantitative investigation of morphology of PI/ZIF-8 mixed matrix membranes including amount of 10% of polymer ZIF-8 with 65 nm average particle size and exposed IR light for 60, 120 and 180 seconds during prepared via VIPS.

Membrane Code	IR (s)	Dense Layer Thickness (μm)	Porous Layer Thickness (μm)	Pore Size (μm)
VIPS_M-PI_0_Ex_1	0	No dense	176.56 ± 0.73	2.39 ± 0.55
VIPS_M-PI_60_IR_1	60	No dense	192.53 ± 0.54	2.41 ± 0.67
VIPS_M-PI_120_IR_1	120	13.15 ± 2.85	111.55 ± 2.69	2.28 ± 0.59
VIPS_M-PI_180_IR_1	180	Top = 42.31 ± 4.03	72.14 ± 4.16	1.98 ± 0.46
		Bottom = 4.60 ± 1.28		

4.3.5 Morphological Properties of PI/ZIF-8/pNA Mixed Matrix Membrane including Compatibilizer prepared via IR Exposure during VIPS

Figure 4.16 presented SEM micrographs of mixed matrix membranes including 65 nm ZIF-8 at 10% of the PI and pNA at 4% of the PI exposed 0, 60, 120 and 180 seconds IR light beginning of the VIPS. The quantitative investigation of membrane morphology based on SEM images was listed in Table 4.6. In mixed matrix membranes including pNA, skin layer formation could not be observed without IR exposure, with increasing the IR exposure time the thickness of non-porous dense skin layer increased while porous layer thickness decreased, and with reaching 180 seconds of IR exposure period non-porous dense skin layer formation was observed at both upper and bottom layer of the porous membrane as observed in pure PI and mixed matrix PI membranes.

The total porous layer thickness of PI/ZIF-8/pNA membrane prepared without light exposure (VIPS_M-PI-C_0_Ex_1) was higher 12.21% and 25.53% than that of VIPS_M-PI_0_Ex_1 and VIPS_PI_0_Ex_1, respectively. This increase in thickness was attributed to the inhibition of solvent evaporation due to the molecular interaction resulting from the presence of pNA. As explained in previous section, when the solvent evaporation rate was high and fast, the thickness of the porous shell layer decreased while the thickness of the nonporous dense skin layer

increased or vice versa. The dense skin layer thickness of VIPS_M-PI-C_60_IR_1 was approximately 40.24% higher than that of VIPS_PI_60_IR_1. It was surprising that the thickness of dense skin layer of pNA containing mixed matrix membrane was measured higher than that of pure PI membrane while no dense skin layer formation was observed in mixed matrix PI membrane exposing 60 seconds IR (VIPS_M-PI_60_IR_1). The reason might be changed relaxation period of polymer due to existence of pNA.

When IR exposure period increased to 120 seconds, the obtained dense skin layer thickness was measured as 19.80 μm , this value was 33.59% higher than that of mixed matrix membrane without pNA. The change in porous layer thickness was not significant on the other hand.

When the IR exposure period reached 180 seconds, the dense upper layer thickness was measured as 27.02 μm , which was 56.59% lower than that of VIPS_M-PI_180_IR_1. On the other hand, the porous layer thickness decreased by 12.90% with respect to VIPS_M-PI_180_IR_1. Hence total membrane thickness was not change.

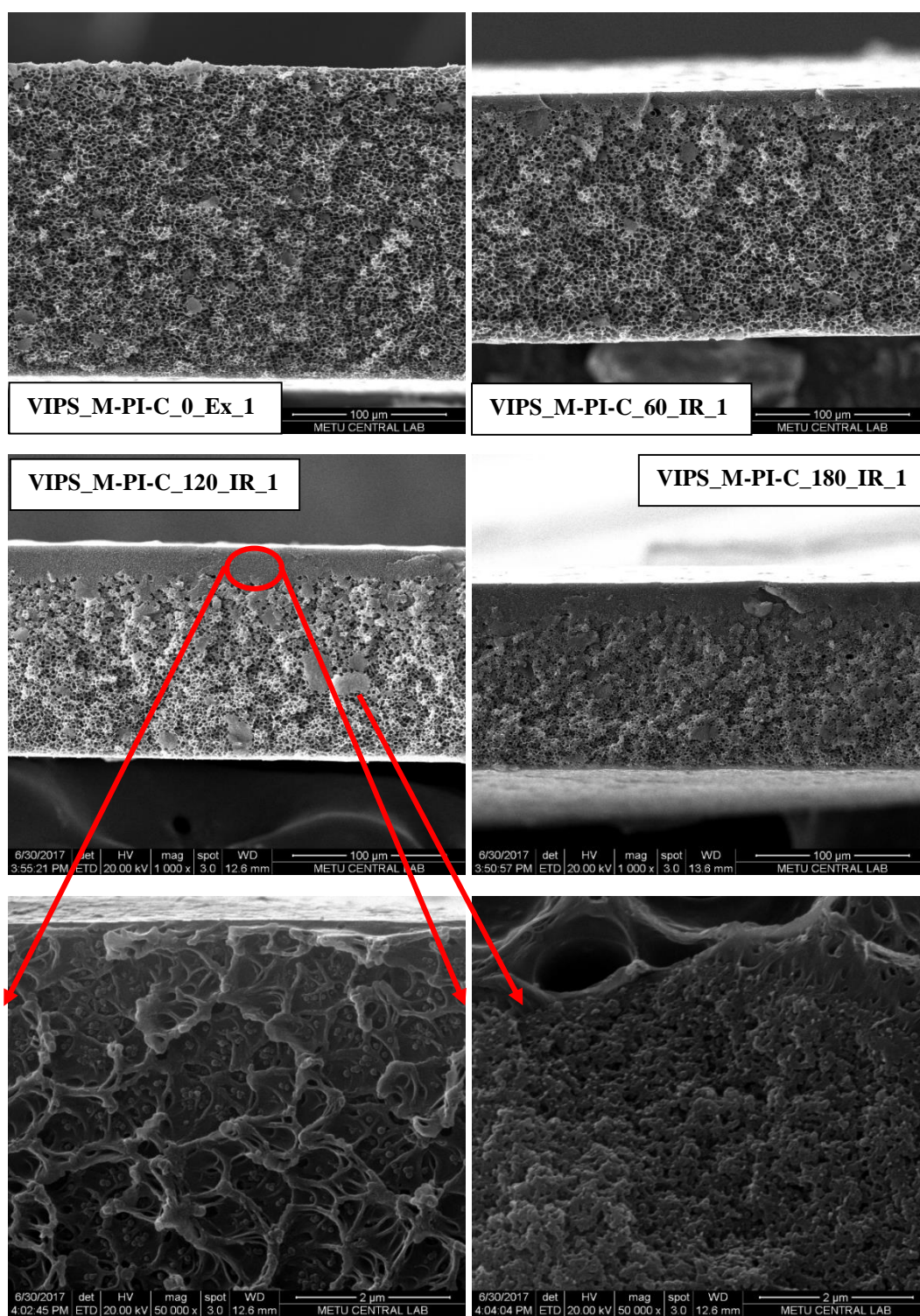


Figure 4.16 SEM micrographs of the mixed matrix including compatibilizer PI/ZIF-8/pNA membranes prepared with 0, 60, 120 and 180 s IR light exposure during VIPS.

The presence of pNA is expected to cause the polymer chain to harden and reduce its flexibility due to its antiplasticizer effect (Şen 2008). Therefore, it was expected that the formation of dense skin layer was enhanced in the presence of PNA. However, the presence of ZIF-8 and PNA also prevented solvent evaporation. The solvents presence showed plasticizer effect (Oral 2011) and also promoted the formation of porous layer. During formation of membrane, competition of these two factors determined the final morphology of membranes. When the IR exposure time was less than 180 seconds, the antiplasticizer effect of pNA was dominant. This is why mixed matrix membranes including pNA had a thicker non-porous dense skin layer with compared to mixed matrix membranes without pNA. If the IR exposure time exceeded 180 seconds, higher solvents fraction in the casting solution during VIPS became dominant hence thinner dense skin layer obtained than expected.

Table 4.6 Quantitative investigation of morphology of PI/ZIF-8/pNA mixed matrix membranes including amount of 10% of polymer ZIF-8 with 65 nm average particle size and 4% of polymer pNA. During VIPS membranes were exposed IR light for 0, 60, 120 and 180 s.

Membrane Code	IR (s)	Dense Layer Thickness (μm)	Porous Layer Thickness (μm)	Pore Size (μm)
VIPS_M-PI-C_0_Ex_1	0	No dense	201.11 \pm 0.82	2.39 \pm 0.63
VIPS_M-PI-C_60_IR_1	60	7.63 \pm 1.66	150.13 \pm 1.34	2.61 \pm 0.54
VIPS_M-PI-C_120_IR_1	120	19.80 \pm 5.17	109.55 \pm 3.73	2.22 \pm 0.44
VIPS_M-PI-C_180_IR_1	180	Top = 27.02 \pm 4.14	82.82 \pm 4.56	1.54 \pm 0.41
		Bottom= 4.39 \pm 1.17		

4.4 Gas Separation Performance of VIPS Membranes

Neat PI membranes, mixed matrix PI/ZIF-8 membranes and mixed matrix PI/ZIF-8/pNA membranes were tested in terms of gas separation performance in the test system presented in Figure 4.5. The gas test results were presented and discussed in this section.

Table 4.7 presented the gas test results of the neat PI membranes prepared without light exposure. Hence only the effect of VIPS formation could be investigated based on gas test results. Two different membranes were prepared in the same relative humidity on different days. Two parts from each membrane were tested. Although the test results of two different parts of the same membrane gave the same gas flux value, there was a difference of about 45% for each type of gas between the test results of two different membranes. In our membrane casting system, management of the humidity was possible but temperature was not. The difference in gas permeance might be the result of temperature difference between the membrane casting days. The ideal selectivity values were constant despite the variance in permeance values. Therefore, the characteristic permeance values and ideal selectivity of non-light exposed neat PI VIPS membrane were taken the average values of test results of these two membranes.

The most important point was the very high ideal selectivity values. As depicted in previous Chapter 4.3, the dense skin layer formation could not be observed in VIPS membranes unless IR light exposure. In addition, as described in Chapter 4.3.3, there were holes about 1 μm in size on the surface layers of the membranes that were not exposed to IR. This high ideal selectivity despite the existence of surface holes and the absence of dense skin layer was the most important evidence that all pores in the membranes were closed and isolated. Therefore, the wall of each pore in the membrane cross-section exhibited a resistance to gas flow resulting in high selectivity and a lower gas permeance than expected value. Reduction or interruption of water permeate flux (these studied were about ultrafiltration membranes) due to VIPS type of membrane formation

were also reported in literature and reason was assumed the closed pores (Han and Bhattacharyya 1995; Chae Park et al. 1999).

Table 4.7 Gas test results of the neat PI membranes prepared without light exposure during VIPS.

Membran Code	Permeance (GPU)			Ideal Selectivity		
	H ₂	CO ₂	CH ₄	H ₂ /CO ₂	H ₂ /CH ₄	CO ₂ /CH ₄
VIPS_PI_0_Ex_1_p1	3.40	1.15	0.033	2.95	100.6	34.11
VIPS_PI_0_Ex_1_p2	3.70	1.23	0.036	3.0	107.78	34.16
VIPS_PI_0_Ex_2_p1	1.96	0.61	0.018	3.2	108.89	33.88
	1.98	0.64	0.019	3.1	104.21	33.68
VIPS_PI_0_Ex_2_p1	1.89	0.56	0.017	3.4	111.17	33.94
	1.91	0.59	0.017	3.3	112.35	33.71
Average	2.47	0.80	0.023	3.16	107.5	33.91
Standard Deviation	0.84	0.31	0.009	0.17	4.41	0.20

4.4.1 Effect of IR Exposure on Neat PI Membranes prepared via VIPS

The neat PI membranes exposed IR light at the beginning of VIPS process have lower gas permeance than membrane prepared without IR exposure. The permeance and ideal selectivity values of IR exposed neat PI membranes were listed in Table 4.8. With increasing IR exposure time, the gas permeance values decreased gradually because of increase in the thickness of non-porous dense skin layer as shown in Figure 4.8.

The percent of decrease in the CO₂ permeance was 41.25%, 83.75%, 90% and 90%; while the percent of decrease in the H₂ permeance was 51.42%, 83.40%, 90.69%, and 94.33% corresponding to the increase in the IR exposure time with 60, 120, 180 and 240 seconds, respectively. There could not be measured a significant change in methane permeance (just only 4.35% decrease) due to increase in the IR exposure period from 0 to 60 seconds. The methane permeance decreased from 0.022 to 0.0044 GPU by increasing the IR exposure time from 60 seconds to 120 seconds. Further increase in IR exposure time (from 120 seconds to 180 seconds) led to 41.73% decrease in CH₄ permeance. When the IR exposure period increased from 180 seconds to 240 seconds, there could not be detected any significant change in CO₂ and CH₄ permeance but 39.13% decrease in H₂ permeance (from 0.23 to

0.14 GPU) was detected. The reason might be the precision of our pressure transmitter which is not quite high or sensitive to detect the change in the permeance of CO₂ or CH₄ when the change was quite small or permeance was very low.

There was no significant deviation in H₂/CO₂ selectivity due to IR exposure. On the other hand, H₂/CH₄ selectivity and CO₂/CH₄ selectivity reduced from 107.5 to 54.54 and from 33.91 to 21.36, respectively due to increase in IR exposure period from 0 to 60 seconds. Further increase in IR exposure time, the H₂/CH₄ selectivity and CO₂/CH₄ selectivity values increased gradually and reached the selectivity values obtained membranes prepared without IR exposure when the IR exposure raised to 180 seconds.

Table 4.8 Gas test results of the neat PI membranes prepared with IR light exposure for 60, 120, 180 and 240 seconds prior of the VIPS.

Membrane Code	Permeance (GPU)			Ideal Selectivity		
	H ₂	CO ₂	CH ₄	H ₂ /CO ₂	H ₂ /CH ₄	CO ₂ /CH ₄
VIPS_PI_60_IR_1_p1	1.20	0.47	0.022	2.55	54.54	21.36
VIPS_PI_120_IR_2_p1	0.41	0.13	0.0044	3.15	93.18	29.54
VIPS_PI_180_IR_1_p1	0.23	0.08	0.0023	2.88	100	34.78
VISP_PI_240_IR_2_p1	0.14	0.08	0.0026	2.54	53.85	31.15

4.4.2 Effect of IL Exposure on Neat PI Membranes prepared via VIPS

Table 4.9 listed the gas test results of membranes prepared using fluorescence light for dry inversion step instead of infrared light. When the gas test results of membranes prepared without light exposure and membranes exposed IL light were compared, small diminish in gas permeance with small increment in ideal selectivity values were investigated.

The percent of decrease in the CO₂ permeance was 8.75%, 12.50; the percent of decrease in the H₂ permeance was 8.91%, 10.12%; and the percent of decrease in CH₄ permeance was 8.70%, %20.43 corresponding to the increase in the IL exposure period from 0 to 60 and 120 seconds, respectively. Since the percent of decrease in CH₄ permeance was higher than that of decrease in CO₂ and H₂

permeance of membrane VIPS_PI_120_IL_1, the ideal selectivity of H₂/CH₄ and CO₂/CH₄ enhanced by 11.38% and 10.60%, respectively. The enhancement in selectivity values of VIPS_PI_60_IL_1 membrane was smaller.

The effect of the IL light on membrane gas separation performance was significantly less than that of the IR light. The diminish in gas permeance with enhancement in selectivity due to IL exposure while IL exposure could not form a dense skin layer was attributed to the higher polymer fraction. IL light induction led to higher solvent evaporation when compared without light induction VIPS process, hence membrane formation occurred with higher polymer fraction and denser membrane layer obtained, which means higher mass transfer resistance.

Table 4.9 Gas test results of the neat PI membranes prepared with IL light exposure for 60, 120 s prior of the VIPS.

Membran Code	Permeance (GPU)			Ideal Selectivity		
	H ₂	CO ₂	CH ₄	H ₂ /CO ₂	H ₂ /CH ₄	CO ₂ /CH ₄
VIPS_PI_60_IL_1_p1	2.09	0.69	0.019	3.02	110	36.32
VIPS_PI_60_IL_1_p2	2.41	0.76	0.022	3.17	109.54	34.55
Average	2.25	0.73	0.021	3.10	109.77	35.44
Standard Deviation	0.23	0.050	0.0021	0.11	0.33	1.25
VIPS_PI_120_IL_1_p1 (test1)	2.10	0.65	0.0176	3.23	123.52	38.23
VIPS_PI_120_IL_1_p2 (test1)	2.40	0.75	0.0196	3.20	120	37.5
VIPS_PI_120_IL_1_p1 (test2)	1.98	0.63	0.017	3.14	116.47	37.05
VIPS_PI_120_IL_1_p2 (test2)	2.38	0.74	0.019	3.22	125.26	38.95
Average	2.22	0.70	0.0183	3.20	121.31	37.93
Standard Deviation	0.21	0.061	0.0012	0.04	3.90	0.83

4.4.3 Effect of Containing ZIF-8 and Containing ZIF-8 with pNA on Gas Separation Performance

Table 4.10 introduced gas test results of PI/ZIF-8 mixed matrix membranes prepared via VIPS. At the first glance, the most prominent point was that the membrane prepared without exposure to IR has lower H₂ permeance, H₂/CO₂ (should be 2.5-3) and H₂/CH₄ (should be higher than 75) ideal selectivity values

than that of expected. On the other hand, CO₂/CH₄ ideal selectivity value was very close to the intrinsic CO₂/CH₄ ideal selectivity value of neat PI membrane (CO₂/CH₄~35; Zhang et al. 2008). Moreover, the H₂ gas permeation test repeated two times for each part of the membrane. These eliminated the possibility of membrane fracture or testing method failure. Diminish in H₂ permeance despite enhancement in CO₂ and CH₄ permeance in the existence of ZIF-8 in the membrane content was an unexpected result since H₂ permeance of neat ZIF-8 membrane was six times higher than CO₂ permeance and 11 times higher than that of CH₄ permeance (Zhang et al. 2014). This problem could not be understanding and explained yet. When the results listed in Table 4.8 and Table 4.10 compared except the H₂ permeance of VIPS_M-PI_0_Ex_1, it was noticed that the addition of ZIF-8 into membrane enhanced the permeance of H₂, CO₂, and CH₄. Similar positive effect of ZIF-8 loading was also reported in literature (Basu et al. 2011; Gholami et al. 2017). The improvements were related porous nature of ZIF-8.

Table 4.10 Gas test results of PI/ZIF-8 mixed matrix membranes containing amount of 10% of polymer ZIF-8 with 65 nm average particle size and exposed IR light for 60, 120 and 180 seconds during prepared via VIPS.

Membran Code	Permeance (GPU)			Ideal Selectivity		
	H ₂	CO ₂	CH ₄	H ₂ /CO ₂	H ₂ /CH ₄	CO ₂ /CH ₄
VIPS_M-PI_0_Ex_1_p1	1.14	0.67	0.022	1.70	51.82	30.45
	1.31	0.74	0.024	1.78	54.58	30.83
VIPS_M-PI_0_Ex_1_p2	1.36	0.88	0.030	1.54	45.33	29.33
	1.61	0.96	0.035	1.68	46	27.43
Average	1.36	0.81	0.028	1.68	49.43	29.51
Standard deviation	0.19	0.13	0.0059	0.0998	4.50	1.53
VIPS_M-PI_60_IR_1_p1	1.47	0.54	0.02	2.72	73.5	27
VIPS_M-PI_120_IR_2_p1	0.48	0.17	0.005	2.82	96	34
VIPS_M-PI_120_IR_2_p2	0.52	0.18	0.0053	2.89	98	34.6
Average	0.5	0.175	0.0052	2.86	97	34.3
Standard deviation	0.028	0.007	0.00021	0.050	1.41	0.42
VIPS_M-PI_180_IR_1_p1	0.28	0.11	0.0033	2.54	84.85	33.3

Table 4.11 showed gas test results of PI/ZIF-8/pNA mixed matrix with compatibilizer membranes prepared via VIPS. At the first glance, it was noticed that the gas permeance values decreased with pNA addition compared to mixed matrix membranes (Table 4.10). Sharp decrease in gas permeance and enhancement in selectivity values due to pNA including are expected since pNA was known with its antiplasticization effect. Addition of antiplasticizer into polymer reduced the segmental motion and free volume of the polymer (Yong et al. 2001; Şen 2003; Şen 2008).

Table 4.11 Gas test results of PI/ZIF-8/pNA mixed matrix membranes including amount of 10% of polymer ZIF-8 with 65 nm average particle size and amount of 4% of polymer pNA as a compatibilizer and exposed IR light for 0, 60 and 180 seconds during prepared via VIPS.

Membran Code	Permeance(GPU)			Ideal Selectivity		
	H ₂	CO ₂	CH ₄	H ₂ /CO ₂	H ₂ /CH ₄	CO ₂ /CH ₄
VIPS_M-PI-C_0_Ex_1_p1	1.79	0.55	0.014	3.25	127.86	39.29
VIPS_M-PI-C_0_Ex_1_p2	1.65	0.51	0.012	3.23	137.5	42.5
Average	1.72	0.53	0.013	3.24	132.68	40.90
Standard Deviation	0.1	0.03	0.0014	0.014	6.82	2.27
VIPS_M-PI-C_60_IR_1_p1	0.56	0.19	0.0054	2.95	103.7	35.2
VIPS_M-PI-C_180_IR_1_p1	0.156	0.065	0.0018	2.4	86.7	36.11

Figure 4.17 illustrated the change in H₂ permeance depending on both ZIF-8 loading, ZIF-8 with pNA addition and also IR exposure time. The existence of ZIF-8 at 10% of PI in the membrane led to 22.5%, 21.95%, and 21.75% increase in H₂ permeance, corresponding to 60, 120, and 180 seconds IR exposure, respectively. Despite the change IR exposure period, the percent increment in H₂ permeance did not change. The positive impact of ZIF-8 on H₂ permeance came into insight with IR induction. Because ZIF-8 crystals aggregated into pores could not show their impact. In order to obtain a sensible effect of the filler, they should be homogeneously dispersed into skin layer. In this study, the most important achievement with IR exposure was that homogeneously dispersed ZIF-8 crystals

were fixed in a non-porous dense skin layer of the casting film without clustering. The H₂ permeance of VISP_M-PI-C_0_Ex_1 membrane was 43.60 percent lower than that of VIPS_PI_0_Ex (average) and 23.25 percent higher than that of VIPS_M-PI_0_Ex_1. The H₂ permeance of the mixed matrix membrane including PNA exposed 60 seconds IR (VIPS_M-PI-C_60_IR_1) was lower than the half of the neat PI membrane (VIPS_PI_60_IR_1) and even lower than the half value of the mixed matrix membrane (VIPS_M-PI_60_IR_1) produced by the same exposing time. With 180 seconds IR induction, the percentage reduction in H₂ permeance due to PNA was calculated to be 70 percent when compared to the VIPS_M-PI_180_IR_1 and 40 percent compared to VIPS_PI_180_IR_1.

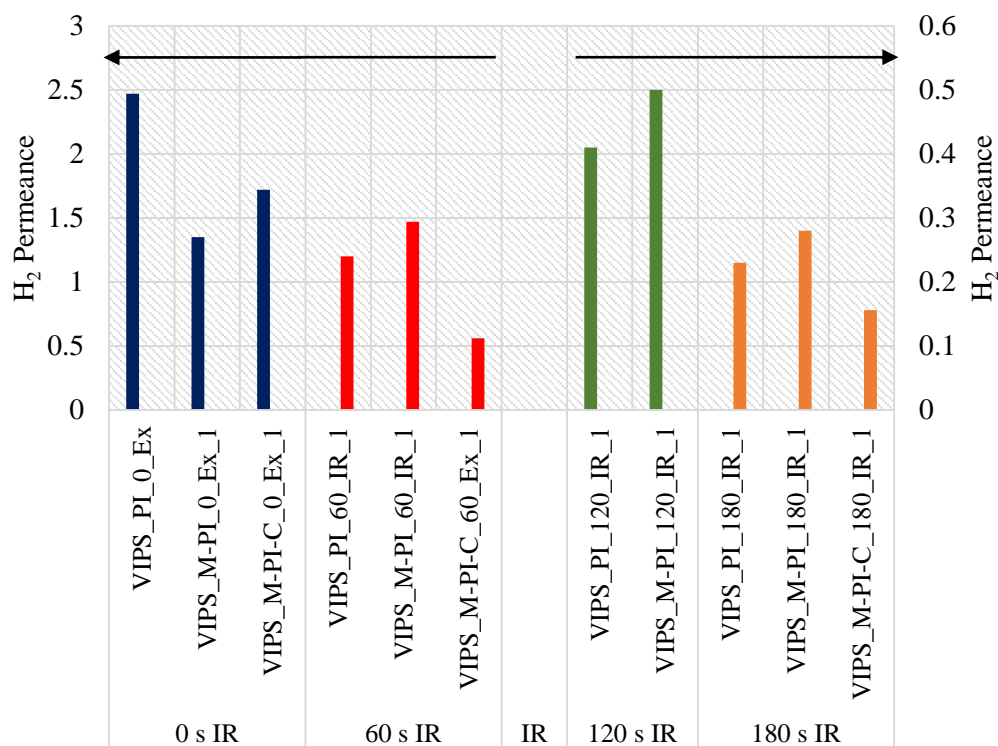


Figure 4.17 Change in H₂ permeance depending on both IR exposure time, ZIF-8 and pNA.

Figure 4.18 showed the variation in CO₂ permeance based on both ZIF-8 loading, ZIF-8 with pNA addition and also IR exposure time. When the mixed matrix membrane casting solution did not exposed IR, the observed change in CO₂ permeance was negligibly small. The existence of ZIF-8 at 10% of PI in the membrane led to 14.89%, 34.61%, and 37.5% increase in CO₂ permeance, corresponding to 60, 120, and 180 seconds IR exposure, respectively. Unlike the change in the H₂ permeance, the percent of increment in CO₂ permeance increased with IR exposure. Actually, this phenomenon was unexpected for me. As discussed previously, the thickness of skin layer increased with IR exposure, hence concerning the increased skin layer, the permeance decreased. I expected that the increase in skin layer thickness with IR exposure obscured the percent of enhancement in permeance due to ZIF-8 addition. Contrary to my expectation, the percent increment in CO₂ permeance was also increased with increase in the IR exposure period. The fraction or amount of ZIF-8 dispersed and fixed in skin layer might be increased with increase in skin layer thickness. Therefore, the percent increment also enhanced due to higher ZIF-8 amount in the skin layer. pNA led to approximately 30 percent decrease in CO₂ permeance when the membranes prepared without IR exposure. 60 seconds IR exposure upgraded the effect of the pNA and the percent decrease in CO₂ permeance was calculated almost 65 percent when compared to VIPS_M-PI_60_IR_1 and nearly 60 percent when compared to neat PI (VIPS_PI_60_IR_1). Further enhancement in IR exposure period to 180 seconds diminished the effect of pNA. The percent decrease in CO₂ permeance of VIPS_M-PI-C_180_1 was calculated as 18.75% and 40.91% compared to neat PI (VIPS_PI_180_1) and mixed matrix PI (VIPS_M-PI_180_1), respectively.

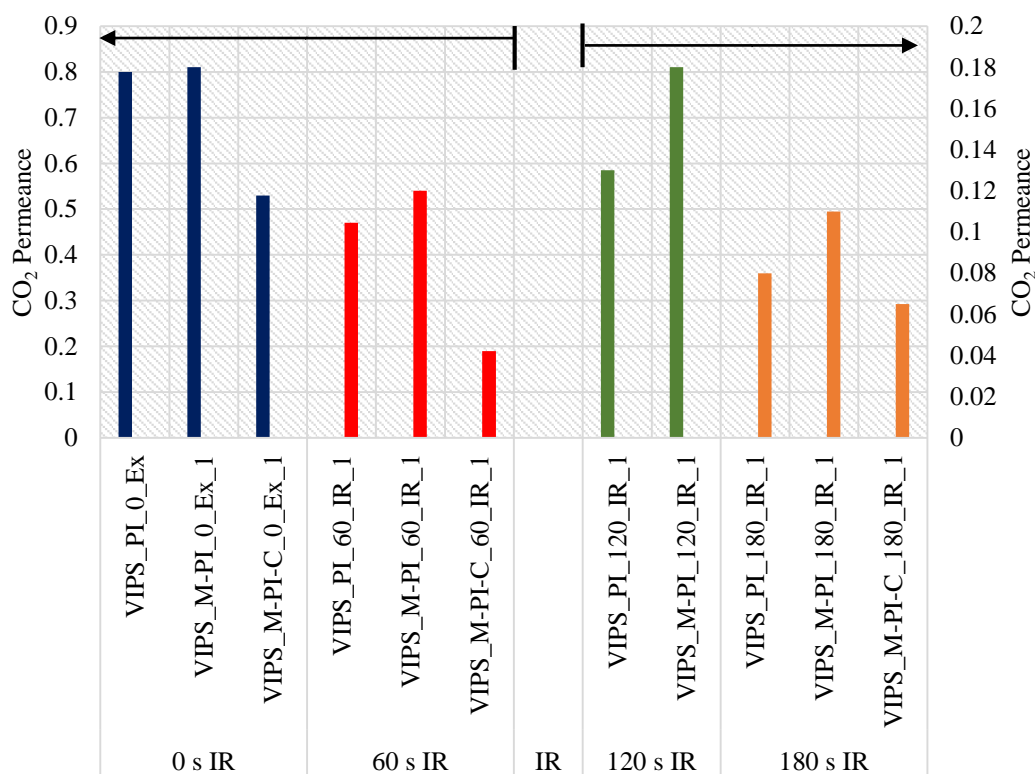


Figure 4.18 Change in CO₂ permeance depending on both IR exposure time, ZIF-8 and pNA.

Figure 4.19 illustrated the CH₄ permeance according to our parameters IR exposure time, ZIF-8 loading and ZIF-8 with pNA loading. The CH₄ permeance of VISP_M-PI_0_Ex_1 membrane was 27.27% percent higher than that of VIPS_PI_0_Ex (average). When the exposure period increased 60 seconds, the measured CH₄ permeance of VIPS_PI_60_IR_1 (neat PI) membrane was 10% higher than that of VIPS_M-PI_60_IR_1. This founding was incompatible with the general trend. The existence of ZIF-8 at 10% of PI in the membrane led to 18.18%, and 43.47% increase in CH₄ permeance, corresponding to 120, and 180 seconds IR exposure, respectively. For membranes prepared without IR exposure, pNA resulted in approximately 40 percent and 50 percent decrease in CH₄ permeance compared to neat PI and mixed matrix PI, respectively. The percent of decrease was calculated as nearly 73 percent compared to both neat PI and mixed matrix PI when the membranes induced to 60 seconds IR (CH₄ permeance of

VIPS_PI_60_IR_1 and VIPS_M-PI_60_IR_1 are very close to each other). Finally, CH₄ permeance of VIPS_M-PI-C_180_IR_1 was lower approximately 21.74 percent and 45.45 percent than that of VIPS_PI_180_IR_1 and VIPS_M-PI_180_IR, respectively.

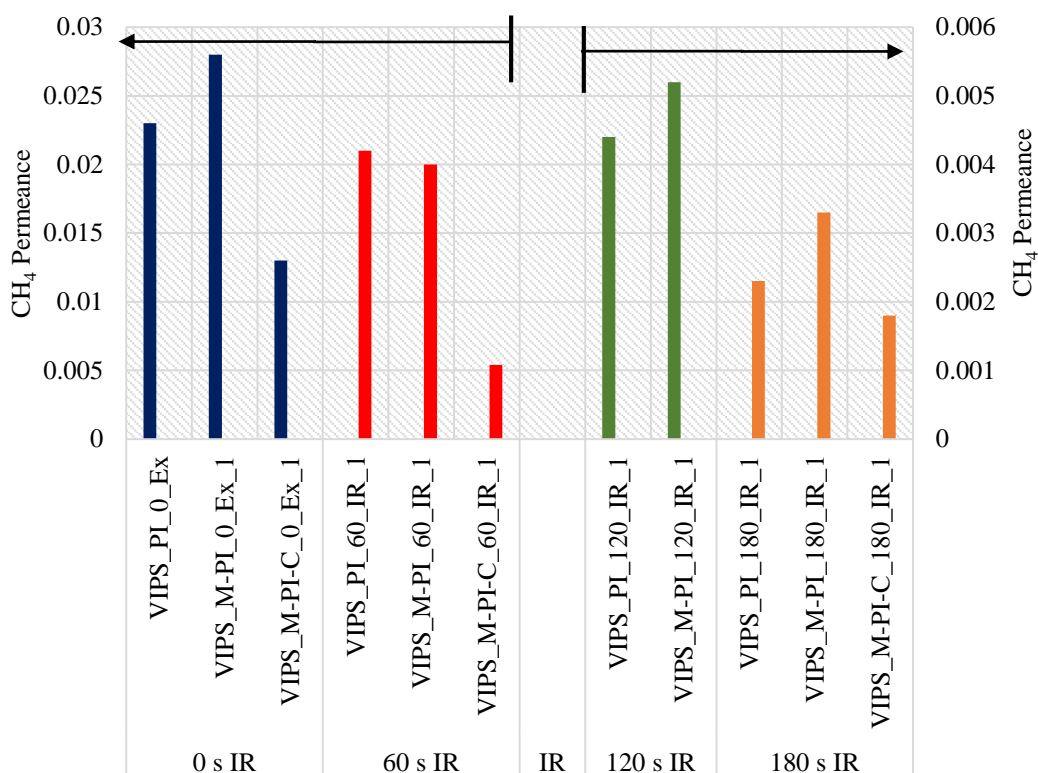


Figure 4.19 Change in CH₄ permeance depending on both IR exposure time, ZIF-8 and pNA.

Figure 4.20, Figure 4.21 and Figure 4.22 showed the alteration in ideal selectivity of H₂/CO₂, CO₂/CH₄ and H₂/CH₄, respectively. The alteration was based on the parameters of IR induction, ZIF-8 and pNA addition.

At a closer look on Figure 4.20, it was noticed that the ideal selectivity of H₂/CO₂ fluctuated between 2.5 and 3.3. The only exception to this the ideal selectivity value of VIPS_M-PI_0_Ex_1. The membranes exposed 60 seconds IR during VIPS have ideal H₂/CO₂ selectivity increasing gradually with addition of

ZIF-8 and pNA. On the other hand, membranes exposed 180 seconds IR showed opposite trend and H_2/CO_2 selectivity of these membranes decreased gradually with addition of ZIF-8 and pNA.

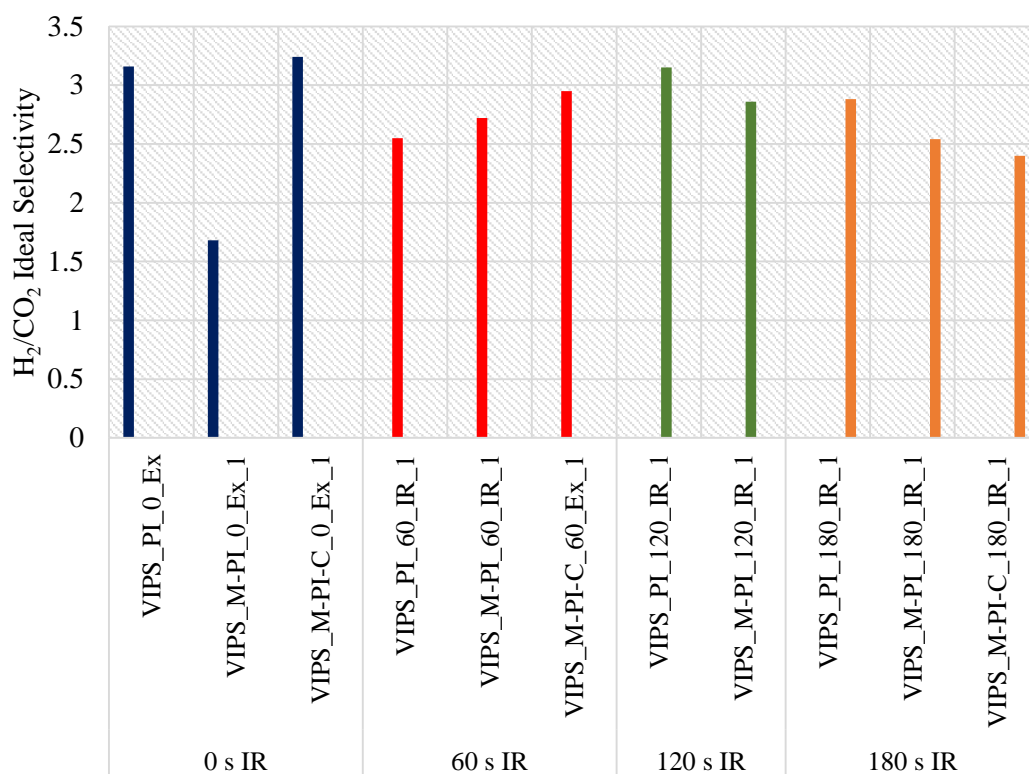


Figure 4.20 Change in ideal selectivity of H_2/CO_2 depending on parameters of IR exposure period, ZIF-8 crystals and pNA

As shown in Figure 4.21, at each four different IR exposing group, the highest CO_2/CH_4 selectivity was belonged to the membranes containing pNA. The CO_2/CH_4 ideal selectivity values oscillated between 20 and 40. The highest one (40.9) was belonged to the membrane VIPS_M-PI-C_0_Ex_1 containing ZIF-8 and pNA and prepared without IR exposure. For membranes exposed to 60 seconds IR, the percent of increase in ideal selectivity of CO_2/CH_4 was calculated as 20.88 percent and 39.32 percent corresponding to the addition of ZIF-8 and ZIF-8 with pNA, respectively. When the IR exposure time was 120 seconds, addition of ZIF-8 led to 13.88 percent increment in CO_2/CH_4 ideal selectivity. The oscillation in

CO₂/CH₄ ideal selectivity diminished when the IR exposure period reached 180 seconds.

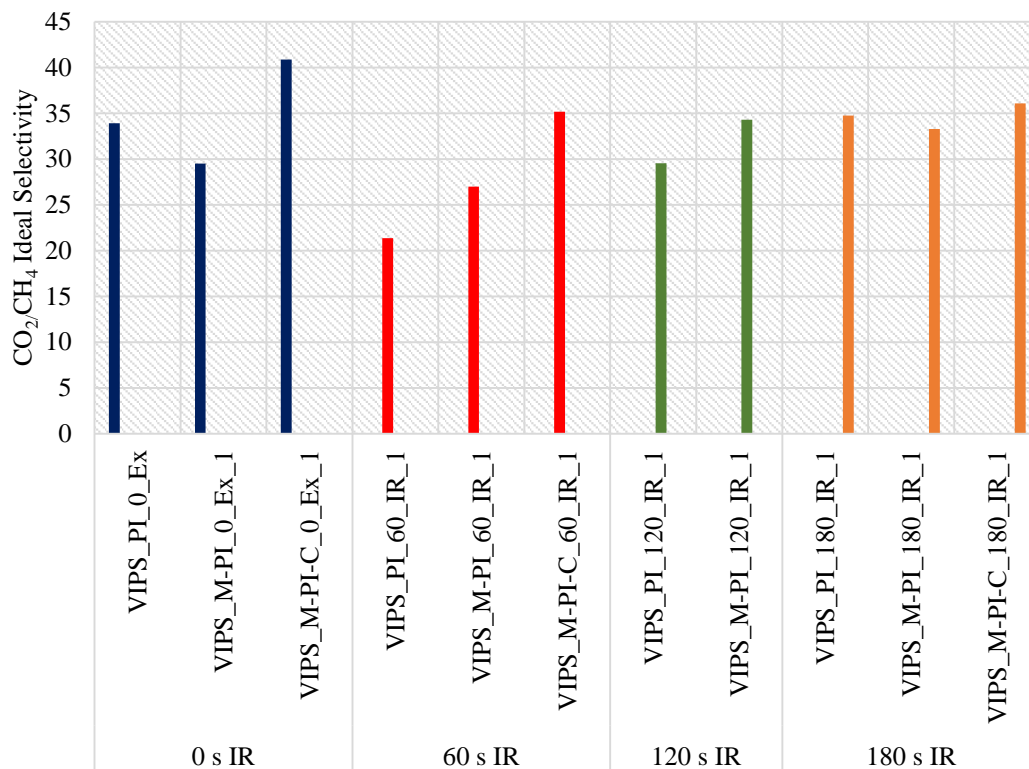


Figure 4.21 Change in ideal selectivity of CO₂/CH₄ depending on parameters of IR exposure period, ZIF-8 crystals and pNA.

The H₂/CH₄ ideal selectivity of membranes was depicted in Figure 4.22. The highest one (132.68) was belonged to the membrane VIPS_M-PI-C_0_Ex_1 containing ZIF-8 and pNA and prepared without IR exposure. This value approximately 43.47 percent higher than the intrinsic H₂/CH₄ ideal selectivity value of neat PI membrane. The highest fluctuation in H₂/CH₄ selectivity value was observed from the test results of the membranes exposed 60 seconds IR during VIPS. For the case of 60 seconds IR exposure, the percent of increase in ideal selectivity of H₂/CH₄ was calculated as 25.80 percent and 47.41 percent corresponding to the addition of ZIF-8 and addition of ZIF-8 with pNA, respectively. When the IR exposure time was 120 seconds, the observed selectivity of H₂/CH₄ was not change depending on ZIF-8 content. Opposing to the general

trend, IR exposure 180 seconds led to 15.15 percent decrease in H₂/CH₄ selectivity despite the existence of ZIF-8. Addition of pNA could not provide further enhancement in H₂/CH₄ selectivity.

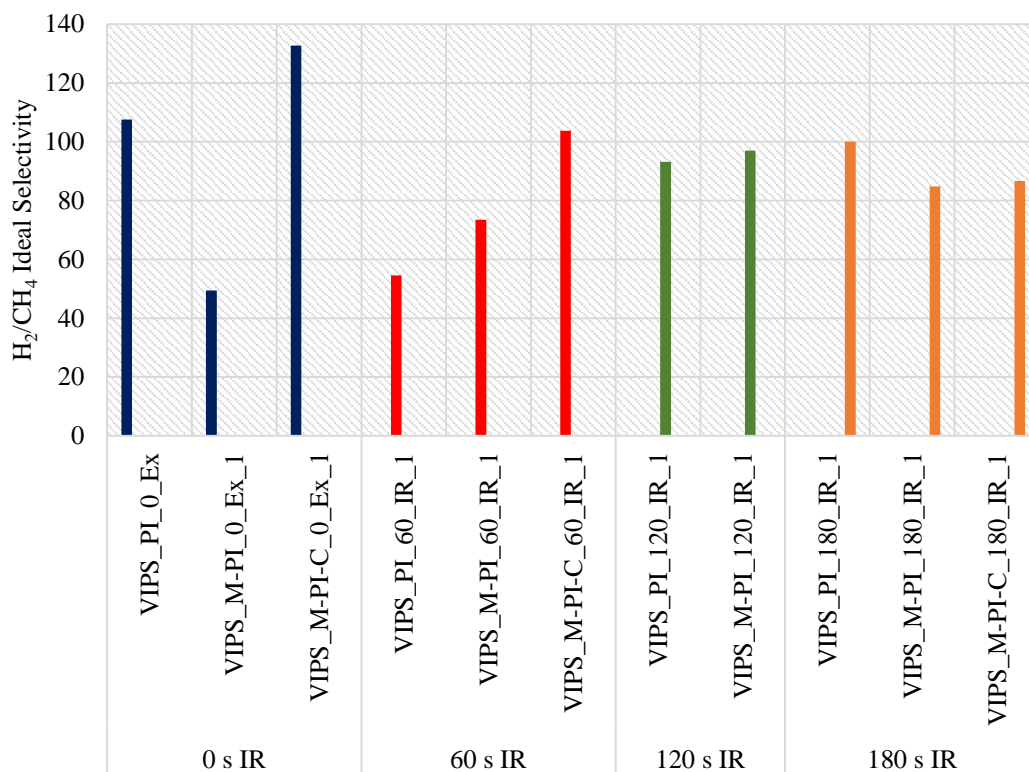


Figure 4.22 Change in ideal selectivity of H₂/CH₄ depending on parameters of IR exposure period, addition of ZIF-8 crystals and including pNA.

4.5 Comparison of The Membranes

Figure 4.23 showed the PI and PES membranes produced by different methods. The non-solvent induced phase separation is abbreviated to the NIPS. The light induced dry-wet phase inversion is abbreviated to the LIDWPI. The LIDVPI is the abbreviation of the light induced dry-vapor phase inversion. The lines on the Robeson plot depicted the Robeson upper bound based on imaginary membrane with different dense layer thickness.

The PES and PI membranes have very high CO_2/CH_4 ideal selectivity. The reason of low permeance of PES membranes is thick dense selective layer. The permeance of PI membranes is low despite the thin dense skin layer. The reason is the closed pores formed because of IR exposure.

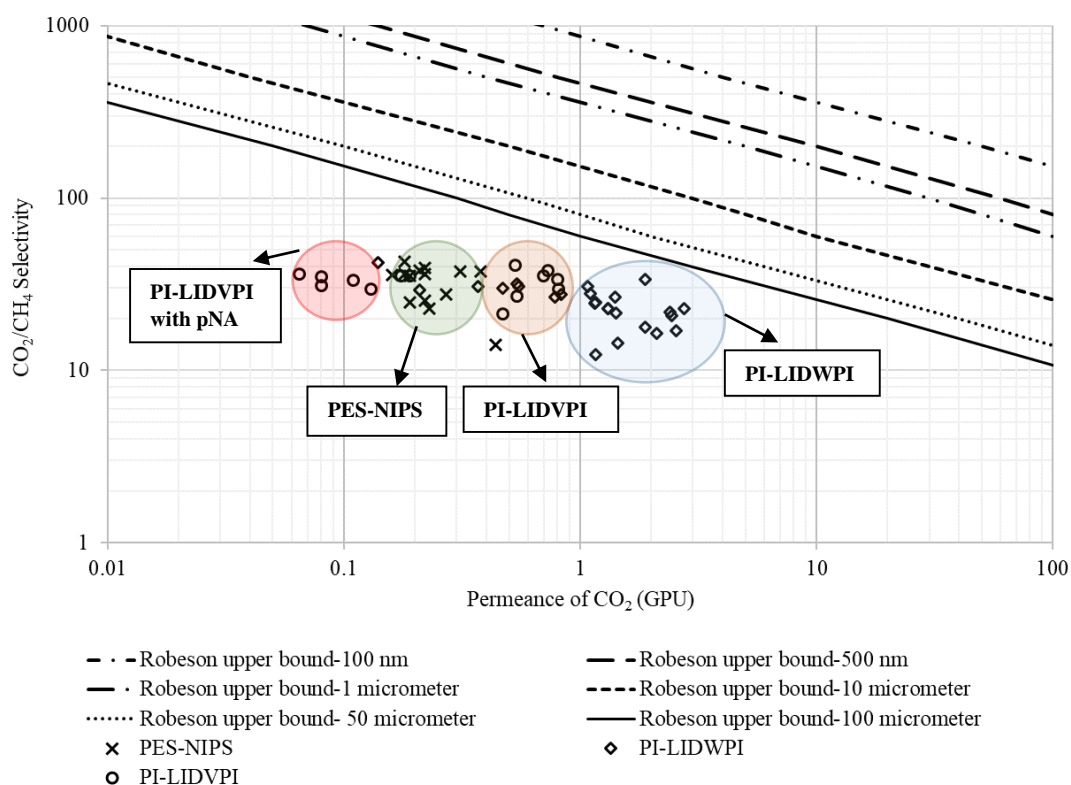


Figure 4.23 Comparison of membranes produced by different methods.

4.6 Conclusions

The membranes were produced by light-exposed dry-vapor phase inversion method. The effect of heating source, dry inversion period, loading pNA and ZIF-8 on membrane morphology and gas transport properties were analysed systematically and following conclusions have been drawn.

- VIPS method led to formation of spongy pores symmetric membrane. Formation of dense skin layer cannot be detected.
- IR exposure during dry inversion step promoted formation of dense skin layer. The thickness of skin layer increased by increasing the IR exposure period. When the IR exposure period reached 240 seconds, the dense symmetric membrane was obtained.
- Despite the absence of skin layer, membranes prepared without IR exposure via VIPS showed the intrinsic ideal selectivity of neat dense PI membranes. This is attributed to the mass transfer resistance because of closed pores.
- The permeance values decreased with increasing IR exposure. The highest permeance was obtained when the membrane prepared without IR exposure. The observed permeance values were 2.47, 0.80 and 0.023 GPU for H₂, CO₂ and CH₄, respectively.
- The effect of incandescent lamp light exposure was significantly lower compared to the effect of IR exposure.
- There are two important opportunities of light induced dry-VIPS method.
- Firstly, IR exposure provided fixing the ZIF-8 particles within dense skin layer without clustering.
- Secondly, VIPS method provided incorporation of pNA into membrane.
- The loading ZIF-8 at 10% of PI led to increase in gas permeance.

REFERENCES

- Barth, C., Gonçalves, M., Pires, A., Roeder, J., & Wolf, B. (2000). Asymmetric polysulfone and polyethersulfone membranes: effects of thermodynamic conditions during formation on their performance. *Journal of Membrane Science*, *169*(2), 287-299. doi:10.1016/s0376-7388(99)00344-0
- Basu, S., Cano-Odena, A., & Vankelecom, I. F. (2011). MOF-containing mixed-matrix membranes for CO₂/CH₄ and CO₂/N₂ binary gas mixture separations. *Separation and Purification Technology*, *81*(1), 31-40. doi:10.1016/j.seppur.2011.06.037
- Caquineau, H., Menut, P., Deratani, A., & Dupuy, C. (2003). Influence of the relative humidity on film formation by vapor induced phase separation. *Polymer Engineering & Science*, *43*(4), 798-808. doi:10.1002/pen.10066
- Chae Park, H., Po Kim, Y., Yong Kim, H., & Soo Kang, Y. (1999). Membrane formation by water vapor induced phase inversion. *Journal of Membrane Science*, *156*(2), 169-178. doi:10.1016/s0376-7388(98)00359-7
- Dong, G., Li, H., & Chen, V. (2013). Challenges and opportunities for mixed-matrix membranes for gas separation. *Journal of Materials Chemistry A*, *1*(15), 4610. doi:10.1039/c3ta00927k
- Dou, Y., Jin, M., Zhou, G., & Shui, L. (2015). Breath Figure Method for Construction of Honeycomb Films. *Membranes*, *5*(3), 399-424. doi:10.3390/membranes5030399
- Favvas, E. P., & Mitropoulos, A. C. (2008). What is spinodal decomposition? *Journal of Engineering Science and Technology Review*, *1*, 25-27.
- Gholami, M., Mohammadi, T., Mosleh, S., & Hemmati, M. (2017). CO₂/CH₄ separation using mixed matrix membrane-based polyurethane incorporated with ZIF-8 nanoparticles. *Chemical Papers*. doi:10.1007/s11696-017-0177-9
- Han, M., & Bhattacharyya, D. (1995). Changes in morphology and transport characteristics of polysulfone membranes prepared by different demixing conditions. *Journal of Membrane Science*, *98*(3), 191-200. doi:10.1016/0376-7388(94)00181-w
- Khare, V., Greenberg, A., & Krantz, W. (2005). Vapor-induced phase separation—effect of the humid air exposure step on membrane morphology Part I. Insights from mathematical modeling. *Journal of Membrane Science*, *258*(1-2), 140-156. doi:10.1016/j.memsci.2005.03.015
- Kuo, C. Y., Tsai, H. A., Lai, J. Y., Wang, D. M., Deratani, A., Pochat-Bohatier, C., & Matsuyama, H. (2005). ICOM, Seoul, South Korea. *Mechanism of Water Induced Phase Separation—nucleation and Growth or Spinodal Decomposition*.
- Lee, H. J., Jung, B., Kang, Y. S., & Lee, H. (2004). Phase separation of polymer casting solution by nonsolvent vapor. *Journal of Membrane Science*, *245*(1-2), 103-112. doi:10.1016/j.memsci.2004.08.006

- Li, J., Xu, Z., Yang, H., Yu, L., & Liu, M. (2009). Effect of TiO₂ nanoparticles on the surface morphology and performance of microporous PES membrane. *Applied Surface Science*, 255(9), 4725-4732. doi:10.1016/j.apsusc.2008.07.139
- Liu, K., & Kiran, E. (1999). Kinetics of pressure-induced phase separation (PIPS) in solutions of polydimethylsiloxane in supercritical carbon dioxide: crossover from nucleation and growth to spinodal decomposition mechanism. *The Journal of Supercritical Fluids*, 16(1), 59-79. doi:10.1016/s0896-8446(99)00016-9
- Majeed, S., Fierro, D., Buhr, K., Wind, J., Du, B., Boschetti-de-Fierro, A., & Abetz, V. (2012). Multi-walled carbon nanotubes (MWCNTs) mixed polyacrylonitrile (PAN) ultrafiltration membranes. *Journal of Membrane Science*, 403-404, 101-109. doi:10.1016/j.memsci.2012.02.029
- Matsuyama, H., Teramoto, M., Nakatani, R., & Maki, T. (1999). Membrane formation via phase separation induced by penetration of nonsolvent from vapor phase. I. Phase diagram and mass transfer process. *Journal of Applied Polymer Science*, 74(1), 159-170. doi:10.1002/(sici)1097-4628(19991003)74:1<159::aid-app20>3.0.co;2-s
- Menut, P., Pochat-Bohatier, C., Deratani, A., Dupuy, C., & Guilbert, S. (2002). Structure formation of poly (ether-imide) films using non-solvent vapor induced phase separation: relationship between mass transfer and relative humidity. *Desalination*, 145(1-3), 11-16. doi:10.1016/s0011-9164(02)00323-5
- Mollahosseini, A., Rahimpour, A., Jahamshahi, M., Peyravi, M., & Khavarpour, M. (2012). The effect of silver nanoparticle size on performance and antibacteriability of polysulfone ultrafiltration membrane. *Desalination*, 306, 41-50. doi:10.1016/j.desal.2012.08.035
- Munekata, T., Suzuki, T., Yamakawa, S., & Asahi, R. (2013). Effects of viscosity, surface tension, and evaporation rate of solvent on dry colloidal structures: A lattice Boltzmann study. *Physical Review E*, 88(5). doi:10.1103/physreve.88.052314
- Nunes, S. P., & Inoue, T. (1996). Evidence for spinodal decomposition and nucleation and growth mechanisms during membrane formation. *Journal of Membrane Science*, 111(1), 93-103. doi:10.1016/0376-7388(95)00281-2
- Oral, E. E. (2011). *Effect of Operating Parameters on Performance of Additive/Zeolite/Polymer Mixed Matrix Membranes* (Master's thesis, Middle East Technical University, Ankara, Türkiye).
- Paula, F. (2012, October 4). Viscosity and Evaporation. Retrieved from <https://stab-iitb.org/newton-mirror/askasci/chem03/chem03017.htm>
- Peng, Y., Dong, Y., Fan, H., Chen, P., Li, Z., & Jiang, Q. (2013). Preparation of polysulfone membranes via vapor-induced phase separation and simulation of direct-contact membrane distillation by measuring hydrophobic layer thickness. *Desalination*, 316, 53-66. doi:10.1016/j.desal.2013.01.021
- Phatak, P. V., & Gaikar, V. G. (1996). Solubilities of *o*- and *p*-Chlorobenzoic Acids and *o*- and *p*-Nitroanilines in *N,N*-Dimethylformamide + Water. *Journal of Chemical & Engineering Data*, 41(5), 1052-1054. doi:10.1021/je9600820

- Ren, J., & Wang, R. (2010). Preparation of Polymeric Membranes. In *Membranes and Desalination Technologies* (pp. 47-100). Humana Press.
- Su, Y., Kuo, C., Wang, D., Lai, J., Deratani, A., Pochat, C., & Bouyer, D. (2009). Interplay of mass transfer, phase separation, and membrane morphology in vapor-induced phase separation. *Journal of Membrane Science*, 338(1-2), 17-28. doi:10.1016/j.memsci.2009.03.050
- Tsai, H., Kuo, C., Lin, J., Wang, D., Deratani, A., Pochat-Bohatier, C., Lai, J. (2006). Morphology control of polysulfone hollow fiber membranes via water vapor induced phase separation. *Journal of Membrane Science*, 278(1-2), 390-400. doi:10.1016/j.memsci.2005.11.029
- Wang, D., Wu, T., Lin, F., Hou, J., & Lai, J. (2000). A novel method for controlling the surface morphology of polymeric membranes. *Journal of Membrane Science*, 169(1), 39-51. doi:10.1016/s0376-7388(99)00330-0
- Yang, Y., Zhang, H., Wang, P., Zheng, Q., & Li, J. (2007). The influence of nano-sized TiO₂ fillers on the morphologies and properties of PSF UF membrane. *Journal of Membrane Science*, 288(1-2), 231-238. doi:10.1016/j.memsci.2006.11.019
- Yip, Y., & McHugh, A. (2006). Modeling and simulation of nonsolvent vapor-induced phase separation. *Journal of Membrane Science*, 271(1-2), 163-176. doi:10.1016/j.memsci.2005.06.063
- Yong, H. H., Park, H. C., Kang, Y. S., Won, J., & Kim, W. N. (2001). Zeolite-filled polyimide membrane containing 2,4,6-triaminopyrimidine. *Journal of Membrane Science*, 188(2), 151-163. doi:10.1016/s0376-7388(00)00659-1
- Young, T., & Chen, L. (1995). Pore formation mechanism of membranes from phase inversion process. *Desalination*, 103(3), 233-247. doi:10.1016/0011-9164(95)00076-3
- Zhang, X., Liu, Y., Li, S., Kong, L., Liu, H., Li, Y., ... Qiu, J. (2014). New Membrane Architecture with High Performance: ZIF-8 Membrane Supported on Vertically Aligned ZnO Nanorods for Gas Permeation and Separation. *Chemistry of Materials*, 26(5), 1975-1981. doi:10.1021/cm500269e
- Zhang, Y., Musselman, I. H., Ferraris, J. P., & Balkus, K. J. (2008). Gas permeability properties of Matrimid® membranes containing the metal-organic framework Cu-BPY-HFS. *Journal of Membrane Science*, 313(1-2), 170-181. doi:10.1016/j.memsci.2008.01.005
- Şen, D. (2003). *Effect of Compatibilizers on the Gas Separation Performance of Polycarbonate Membranes* (Master's thesis, Middle East Technical University, Ankara, Türkiye).
- Şen, D. (2008). *Polycarbonate Based Zeolite 4A Filled Mixed Matrix Membranes: Preparation, Characterization and Gas Separation Performances* (Doctoral dissertation, Middle East Technical University, Ankara, Türkiye).

CHAPTER 5

SORPTION CAPACITY OF DENSE-SYMMETRIC NEAT PI AND PI/ZIF-8 MIXED MATRIX MEMBRANES PRODUCED BY SOLVENT EVAPORATION

In this chapter, sorption capacity of symmetric dense PI membrane and the symmetric PI/ZIF-8 membrane have been presented. Pure CO₂, pure CH₄ and mixture of these two gases at three different compositions namely 30% CO₂-70% CH₄, 50% CO₂-50% CH₄, 70% CO₂-30% CH₄ were selected as sorption feed. The ZIF-8 content of the membrane and the mixture composition of sorption feed are two important parameters whose influence on sorption capacity have been investigated.

The sorption capacity is very important to make sense of the selectivity of the polymeric membrane. The gas separation performance of a polymer is related to the selectivity of that polymer. In the formation of the permeability selectivity, the selectivity of the diffusion and the selectivity of the solubility are equally important. Furthermore, gas transport through a membrane begins with sorption of gases by the surface of membrane exposed to high pressure of penetrant gases. Thus, sorption is initiation step for gas transport.

This study is the first in which the effect of ZIF-8 content on sorption capacity of Matrimid membrane has been examined.

5.1 Theoretical Background about Sorption Mechanism of Polymers

The amount of gas molecules permeated into a polymer is referred as “sorption” (Loat 2001). There are several different sorption models studied in the literature. Among them free volume theory (Zielinski and Duda 1996) is suitable for rubbery polymers while macroscopic and lattice theory (Baschetti, Doghieri and Sarti, 1996; Conforti et al. 1991; Lipscomb 1990; Boudouris and Panayiotou 1998, Rein et al. 1992) have been developed to explain sorption mechanism in glassy

polymers. The dual mode sorption theory has been the most preferred and widely used model because of both its simplicity and constancy with experimental sorption data of glassy polymers up to 30 bars for several gases (Loat 2001). The most important reason of widely acceptance of dual model in glassy polymers is that the unrelaxed volume also takes part in this model (Koros et al., 1981). This model is also very successful to explain the sorption mechanism in our PI/ZIF-8/CO₂/CH₄ system, because Matrimid is a kind of glassy polymer and test pressure is below 10 bar. Therefore, only dual-mode sorption theory was discussed and studied in this study.

5.1.1 Dual Mode Sorption Model

A homogeneous glassy polymer is consisting of two different volumes. The dense polymer packing region constitutes the Henry- type sorption region which is smaller than Langmuir sites. Lower density region or unrelaxed gap originated from fixed microvoids during restriction of chain mobility. This region constitutes the Langmuir sites which are larger and variable in size. The small-scale inhomogeneity in the polymer matrix determines the non-equilibrium characteristic of materials (Loat 2001, Koros and Paul 1978).

In Figure 5.1, the unrelaxed volume change of the glassy polymer as a function of the temperature was given. As indicated, the non-equilibrium excess-free volume increases with T_g at a given temperature. Generally, the gas sorption capacity of glassy polymer is higher than that of rubbery polymer. This is attributed to additional excess-free volume in the glassy polymer (Kanehashi and Nagai 2005). In glassy polymers, the reason for the absorption curves extending concave to the pressure axis originates from this variable volume state of the glassy polymers. As the pressure increases to a certain pressure level, this variable volume that is not in equilibrium begins to saturate and the solubility decreases. The permeability, which is the product of the solubility and the diffusion, decreases as the pressure increases. When the glass transition temperature is exceeded, all chains have sufficient mobility and the sorption isotherms are obtained as straight line, which is a characteristic to the Henry-type absorption model. Thus permeability

becomes independent of pressure (Koros et al., 1981). The polymer structure and thermal history are two important factors determine the amount of unrelaxed free volume in a glassy polymer (Wind et al. 2003).

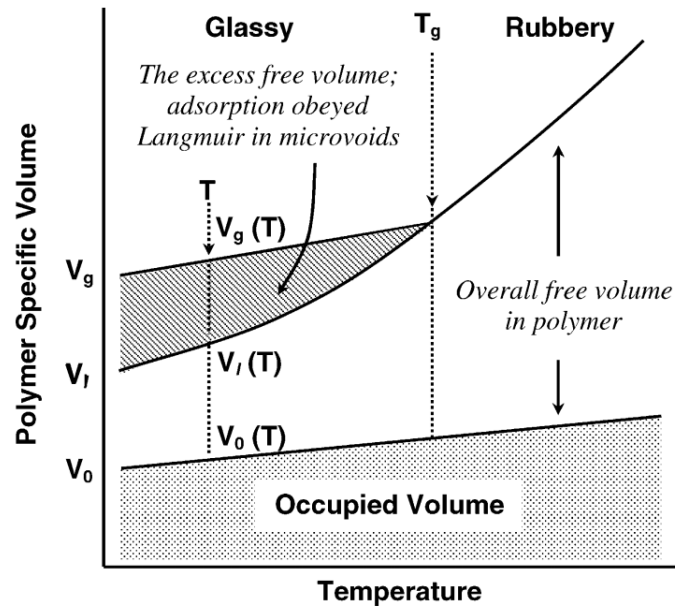


Figure 5.1 Hypothetical unrelaxed excess free volume ($V_g - V_l$) of a glassy polymer as a function of temperature (where V_g is symbolized actual glassy volume and V_l is symbolized densified glassy volume) (Kanehashi and Nagai 2005).

In dual mode sorption model, Henry type sorption is active in polymer matrix. Henry-type gas sorption is resembled to gas dissolution in a liquid where solubility or sorption concentration linearly increases with pressure (Li, Chung and Paul 2013, Punsalan and Koros 2004). Langmuir type sorption is dominated in excess free volume of polymer and Langmuir-type sorption is resembled a hole-filling process, hence it has a capacity limit (means no further increase in sorption capacity despite increase in pressure) (Li, Chung and Paul 2013, Punsalan and Koros 2004). A schematic representation of the dual-mode absorption mechanism is given in Figure 5.2. In this model, isotherms extend concave to the pressure axis. The dual mode sorption mechanism model successfully explains the change in gas permeability to a wide range of glassy polymers (Chen et al. 1997; Tsujita 2003) in the absence of plasticization or swelling at moderate pressure (Chern et al. 1984).

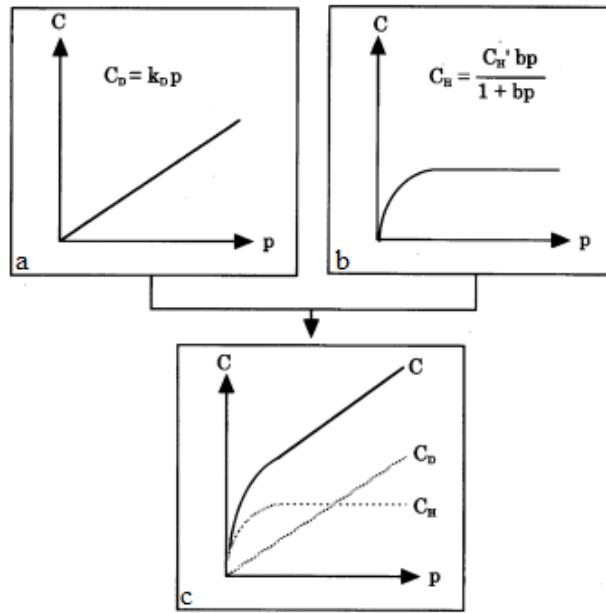


Figure 5.2 Schematic presentation of sorption mechanism (a) Henry-type sorption, (b) Langmuir-type sorption, (c) dual-mode sorption model (Tsujita 2003).

In the original dual-mode model firstly suggested by Barrer et al. 1958, it was assumed that the molecules sorbed in the Langmuir region were immobilized and did not have effect on the diffusive flux. Later on, this model was modified and it was admitted that molecules sorbed both Henry side and Langmuir side are mobile. Hence this model is also known as dual-mobility or partial-immobilization-model (Loat 2001).

The dual-mode sorption model can be presented by Eqn. 5.1 where C is the dual-mode sorption capacity and equal to the summation of C_D , Henry-type sorption capacity and C_H , Langmuir-type sorption capacity. P is pressure and k_D , b , C'_H are the coefficients of Henry type and Langmuir type sorption model, respectively (Tsujita 2003, Koros et al., 1981).

$$C = C_D + C_H = p k_D + \frac{C'_H b p}{1 + b p} \quad \text{Eqn. 5.1}$$

C_D is the concentration of the gas in the polymer matrix and increases proportionally with Henry's law solubility constant (k_D) as the pressure increases (Scholes et al., 2010). At constant temperature, the deviation from the linear Henry-type sorption curve is directly proportional to the condensation tendency of the absorbed molecule. Condensation tendency is characterized by the critical temperature or Leonard-Jones potential-well depth of the absorbed molecule. For example, when Helium's absorption curve in polycarbonate is examined, it was noticed negligible concavity, while CO_2 and heavy hydrocarbons (high condensation tendency) show a significant degree of concavity at low and moderate pressure range (Koros et al., 1981). k_D is related to penetrant-polymer interaction and thermodynamic properties of penetrant such as critical temperature, and Lennard-Jones force constant etc. k_D can be expressed as in the Eqn. 5.2, where χ is polymer-penetrant interaction parameter (Flory-Huggins theory) and it is related to solubility parameters of polymer and penetrants. V is the molar volume of penetrant and ε/κ is the Lennard-Jones potential well depth parameter, which measures the condensability of gases (Muruganandam et al. 1987).

$$k_D = \exp\left(\frac{-1-\chi+0.0255\varepsilon/\kappa}{V}\right) \quad \text{Eqn. 5.2}$$

The Langmuir capacity constant, C'_H , is related to the total sorption capacity of unrelaxed gap in glassy polymer for a certain molecules. The unrelaxed gas of a particular polymer at a specific temperature is essentially constant. The main reason of the difference in the Langmuir capacity constant between different gas molecules is the diversity of the sorption density of gas molecules at the saturation point of Langmuir side (Koros et al., 1981). C'_H , can be calculated by using Eqn. 5.3. V_g represents the actual glassy volume and V_l is volume at liquid state or densified glassy volume. The difference (V_g-V_l) is the unrelaxed volume. And V_p is the molar volume of the absorbed gas molecules (Koros and Paul 1978, Tsujita 2003, Masi et al. 1982). The Langmuir affinity constant 'b' is related to the tendency of the molecule to absorb in Langmuir mode. The Langmuir affinity constant (b) of non-condensable molecules such as helium or hydrogen is very small, while easily condensable polar or polarizable molecules have high 'b' (Koros

et al. 1981). In other words, “b” increases with tendency of condensability of penetrant gases and can be associated with Lennard-Jones parameter (ϵ/κ) (Muruganandam et al. 1987). “b” is mainly depend on gas type but slightly related to polymer structure (Masi, Paul and Barlow 1982). Dual mode sorption coefficients (k_D , b , C'_H) can be obtained by graphical interpolation or linear least square methods based on experimental data of concentration as a function of pressure (Loat 2001).

$$C'_H = \frac{V_g - V_l}{V_g} \times \frac{22400}{V_p} \quad \text{Eqn. 5.3}$$

Although it is commonly used, the dual-sorption-model has many aspects that are open to debate. One of the debated points is the existence of two different sorption sides. Sefcik and Schaefer, 1983; Higuchi and Nakagawa, 1994; Cain et al., 1991 tried to verify the existence of two distinct sorption sides Langmuir and Henry. They could not observe two distinct peak from NMR or FTIR spectrum. Hence if there are two distinct sorption sides, they should have similar spectroscopic property. On the other hand, Koros and Paul 1978 proved two distinct sorption sides. In this study, CO₂ sorption capacity of PET were measured [above and below the T_g (85 °C)]. Below T_g of PET, dual-mode sorption isotherm was obtained. Above T_g, only Henry-type sorption isotherm was obtained, because above T_g, mobilization of frozen backbone segments of the polymers led to disappearance of Langmuir-type sorption sides. Another weakness of the model is that it is only an empirical model and does not rely on any physical interpretations. The model parameters are strongly based on curve fitting method or initial guess. In this model, several parameters effecting the sorption properties of polymer such as relaxation time of the polymer chains, physical aging, structure or morphology of polymer, which is changing during experiment based on test duration or operating pressure, are not considered (Loat 2001).

In sorption studies, sometimes sorption capacity can be expressed by term solubility. The solubility of the gas in the polymer is expressed by the formula $S = C / f$. C is the ratio of the amount of sorbed gas to the polymer volume, and f is the

fugacity of the gas in contact with the polymer. For ideal gas, operating pressure (P) can be used instead of fugacity (f) (Raharjo et al., 2007, Chen et al. 1997).

5.1.2 Parameters Effect on Sorption Capacity

Both test conditions and polymer pre-treatment conditions alter the sorption capacity of polymer irreversibly. Heating polymer above T_g and then cooling to well below the T_g slowly, leads to decrease in the unrelaxed volume, hence sorption capacity decreased. Unrelaxed volume capacity is thermal history dependent (Koros and Paul 1978). It was also reported annealing just below the T_g leads to decrease enthalpy of quenched glassy polymer as well as excess volume (Chan and Paul 1979).

Moreover, operation or sorption test temperature is an important parameter, since the sorption enthalpy of gases by polymers is negative, in other word sorption process is exothermic. Hence the extend of gas sorption decreases gradually with temperature increase. The temperature dependence of solubility can be expressed by van't Hoff Equation as given in Eqn. 5.4. In this equation S_0 is pre-exponential and ΔH_S is heat of sorption which is the summation of the enthalpy of condensation of the gas (ΔH_{cond}) and the partial molar heat of mixing between the gas and polymer (ΔH_{mix}) can be seen in Eqn. 5.5. When the interaction between penetrant and polymer is weak, ΔH_{mix} is positive. For noble gases (such as H_2 , He, N_2 , and O_2) which are well above their critical temperature, ΔH_{cond} values are negligibly small compared to ΔH_{mix} . For these gases, sorption capacity increases with temperature since the ΔH_S is positive for those. However, for easy condensable gases such as CO_2 , CH_4 , SO_2 , NH_3 and several hydrocarbons, ΔH_{cond} is very large and negative. Therefore, ΔH_S is negative and sorption capacity or solubility decreases with increasing temperature. Moreover, penetrants condensability decreases as the temperature increases (Loat 2001, Costello and Koros 1994). Solubility selectivity (S_A/S_B) is also affected by change in temperature because interaction between polymer and penetrant changes depending on temperature. Moreover, the gases with low critical temperature are less affected by temperature increase than gases with high critical temperature (Costello and Koros 1994).

$$S = S_0 \exp\left(\frac{-\Delta H_S}{RT}\right) \quad \text{Eqn. 5.4}$$

$$\Delta H_S = \Delta H_{\text{cond}} + \Delta H_{\text{mix}} \quad \text{Eqn. 5.5}$$

The relative contribution of Langmuir term parameters reduces with increase in pressure as well as increase in temperature (Li, Chung and Paul, 2014).

Modifications in polymer also alter sorption extent. For example, aromatic group substitution in bisphenol-A connector in PC and PSF or replacement of fluorene group with isopropylidene unit in both PC and PSF increases the dual-mode sorption constants. Higher fractional free volume (FFV) associated with higher extent of sorption capacity. It was reported that k_D increases with FFV for broad range of polysulfones. Any modifications in polymer which results in increment in T_g leads to increase in C'_H value (Aguilar-Vega and Paul, 1993, Pixton and Paul 1995). Conditioning history of polymeric membrane is another parameter affecting sorption capacity. Exposure of certain chemical environment (for example CO_2 above 20 atm for a certain time) may lead to increase in excess volume (Chan and Paul 1979, Punsalan and Koros 2005, Muruganandam et al. 1987) or redistribution of the unrelaxed volume. Koros and Paul 1978 reported that exposing the high –pressure CO_2 for a reasonable time period led to increase the Langmuir capacity of PET. Generally, very long evacuation period (longer than 24 hour) is required to relax polymer and return to the original stage of the polymer. Polymers with dipolar oxygen-containing functional group are more tend to be affected from CO_2 conditioning (Puleo et al. 1989).

5.1.3 Mixed Gas Sorption in Glassy Polymer

Sorption capacity diminishes due to competition of penetrants for unrelaxed volume fraction of the glassy polymer which is limited in size (Koros et al. 1981).

Koros 1980 tried to generalize dual-mode sorption theory for binary gas mixtures. Based on this study, Henry-type sorption capacity of a binary mixtures (A+B) was calculated by Eqn. 5.6. Authors assumed that the components of the binary gas mixtures sorbed independently.

Probably, they thought that the competition of the penetrants was only for Langmuir side. The Henry-type sorption concentration of each component, $C_{D,A}$ or $C_{D,B}$, was taken directly proportional to its partial pressure.

$$C_D = C_{D,A} + C_{D,B} = p_A k_{D,A} + p_B k_{D,B} \quad \text{Eqn. 5.6}$$

Langmuir-type competitive sorption of binary gases expressed mathematically based on relations developed for competitive sorption of gases on catalysts (Koros 1980). The following mathematical expressions were for theoretical estimation of Langmuir side sorption concentration for binary gas mixtures. Eqn. 5.7 provided the fraction of unrelaxed volume taken by component A (θ_A) and component B (θ_B), where b_A and b_B are Langmuir affinity constant of pure A and pure B, respectively.

$$\theta_A = \frac{b_A p_A}{1 + b_A p_A + b_B p_B} \quad ; \quad \theta_B = \frac{b_B p_B}{1 + b_B p_B + b_A p_A} \quad \text{Eqn. 5.7}$$

$$(\theta_A) \text{ or } (\theta_B) \text{ can also be expressed; } \theta_A = \frac{C_{HA}/\rho_A^*}{C'_{HA}/\rho_{A0}^*}$$

Where C_{HA}/ρ_A^* is the unrelaxed volume occupied by component A and C'_{HA}/ρ_{A0}^* is the total unrelaxed volume.

- C_{HA} ; concentration of component A in the Langmuir mode
- ρ_A^* ; effective molar density of component A in the Langmuir mode in the presence of component B
- C'_{HA} ; Langmuir capacity constant for pure A
- ρ_{A0}^* ; effective molar density of pure component A in the Langmuir mode

Author assumed that $\rho_A^* = \rho_{A0}^*$ based on his experience. Hence, Langmuir-type sorption isotherm of component A in the presence of component B is as the given in Eqn. 5.8.

Eqn. 5.8;

$$C_{HA} = C'_{HA} b_A P_A / (1 + b_A P_A + b_B P_B); \quad C_{HB} = C'_{HB} b_B P_B / (1 + b_A P_A + b_B P_B)$$

Total mixture sorption capacity, component A sorption capacity in the existence of B and component B sorption capacity in the existence of polymers can be expressed by Eqn. 5.9, Eqn. 5.10, and Eqn. 5.11, respectively.

$$C = P_A k_{D,A} + P_B k_{D,B} + \frac{C'_{HA} b_A P_A + C'_{HB} b_B P_B}{(1 + b_A P_A + b_B P_B)} \quad \text{Eqn. 5.9}$$

$$C_{A|B} = P_A k_{D,A} + \frac{C'_{HA} b_A P_A}{(1 + b_A P_A + b_B P_B)} \quad \text{Eqn. 5.10}$$

$$C_{B|A} = P_B k_{D,B} + \frac{C'_{HB} b_B P_B}{(1 + b_A P_A + b_B P_B)} \quad \text{Eqn. 5.11}$$

The extended dual-mode sorption mechanism of mixture sorption of glassy polymer is simple and logical model but has a weakness; all sorption constants (k_D , b , C'_H) used in model belong to the pure components. Author assumed that plasticizing effect or penetrant-penetrant interaction effect on dual-mode parameters are negligible.

5.1.4 A Brief Literature Survey About CO₂ and CH₄ Sorption Capacity of PI Membranes and ZIF-8 Crystals

The purpose of this part of the study is to summarize sorption properties of PI and ZIF-8 introduced in the literature. There are different kinds of polyimides, and information provided in this part give a general idea or aspect about sorption behavior our polymer and our sorption test results. Table 5.1 is presented the CO₂ and CH₄ sorption extents of different kind of PI membranes and Table 5.2 is depicted dual-mode sorption parameters reported in the literature. The studies listed in Table 5.1 and discussed in the following pages were carried out for single gas sorption test.

Wind et al. 2003 studied CO₂ sorption behavior of 6FDA-DAM:DABA 2:1 type polyimide membranes. Effect of thermal treatment and cross-linking treatment on extent of sorption were also within the scope of this research. The CO₂ sorption capacity of the 6FDA-DAM:DABA 2:1 films with free carboxylic acid groups and CHDM groups tend to decrease with thermal treatments. The total sorption capacity of 6FDA-DAM:DABA 2:1 with CHDM monoesters was lower than that of 6FDA-

DAM:DABA 2:1 with free acids. Both Henry and Langmuir capacity constants decreased with increase in temperature of thermal treatments for free carboxylic acid groups. Langmuir capacity constant increased with annealing temperature for CHDM monoesters (Table 5.2).

In study by Moore and Koros 2007, researchers measured the sorption capacity inorganic fillers (HSSZ-13 and Zeolite-4A), polymers (ULTEM and Matrimid) and mixed matrix membranes made up of these fillers and ULTEM in order to signify gas sorption mechanism in mixed matrix membranes. Sorption extent of CO₂ and CH₄ in Matrimid at 35 °C were listed in Table 5.1 Both CO₂ and CH₄ sorption in Matrimid followed dual-mode sorption behavior (the percent increase in sorption extent decreases with increase in pressure), but the reduction in the increment in sorption extent with pressure is more significant for CH₄. The dual-mode parameters determined by fitting the isotherm was provided in Table 5.2.

The sorption capacity of mixed matrix membranes can be simply estimated by addition of sorption capacity of polymer and filler with proportional to their volume fraction as shown in Eqn. 5.12 (Moore and Koros, 2007). In this estimation, interfacial effects between sieve and polymer and contamination of sieve did not take into account.

$$C_{MMM} = C_{polymer} \phi_{polymer} + C_{filler} \phi_{filler}; \quad \phi \text{ volumetric fraction} \quad \text{Eqn. 5.12}$$

Moore and Koros 2007 tested the validity of this simple estimation method by comparing experimental N₂ and O₂ sorption isotherms of the ULTEM / HSSZ-13 mixed matrix membrane and the O₂ sorption isotherms of the ULTEM-Zeolite-4A mixed matrix membrane. It was concluded that estimated isotherms based on Eqn. 5.12 overlapped with experimental results in the ULTEM-HSSZ-13 mixed matrix membrane. However, the predicted O₂ sorption curves of ULTEM-Zeolite-4A mixed matrix membranes did not overlap experimental data. As the annealing temperature of the membrane increased, the experimental adsorption isotherms approached the estimated values based on the calculations. It was believed that this was due to the fact that Zeolite-4A was much more affected by the presence of

moisture, chemical contaminants or residual solvents compared to the HSSZ-13 (Moore and Koros, 2007). Authors was noted that the mixed matrix membrane could show a lower permeability than the estimated value due to the chain rigidification of polymer matrix near the sieve. However, according to the authors, polymer matrix rigidification near sieve could not make a measurable change in sorption data. As a conclude, this simple estimation (Eqn 5.12) works for some mixed matrix membranes but does not valid for some others.

O'Brain and Koros 1987 was measured the sorption capacity of the PMDA-ODA synthesized in laboratories and compared the extent of the sorption with commercially Kapton polyimide film which had the same chemical structure. As depicted in Table 5.1, gas sorption capacity of the polyimide (PMDA-ODA) produced in the laboratory environment is higher than that of the commercially available polyimide film. Authors suggested that the high sorption capacity arose from annealing in a vacuum environment for 24 hours at 210 ° C for 4 hours at 280 ° C. As the pressure increases, the difference between the absorption capacities of Kapton polyimide and PMDA-ODA increases. At 10 atm pressure, PMDA-ODA absorbs 68% of CO₂ and 50% more of CH₄ than does Kapton polyimide. At 10 atm, the CO₂ permeability of PMDA-ODA is 3 Barrer while that of Kapton polyimide 0.35 Barrer. The enhancement in sorption capacity led to increase in permeability tenfold. On the other hand, CO₂/CH₄ selectivity of Kapton polyimide is 25% higher than that of PMDA-ODA.

Costello and Koros 1995 studied sorption characteristic of two polyimide isomers 6FDA-6FpDA (with 320 °C T_g and 0.272 FFV) and 6FDA-6FmDA (with 254 °C T_g and 0.225 FFV) and the sorption extents were given in Table 5.1. At low temperature (35 °C), both showed high level of sorption with characteristic non-linear sorption isotherms. The higher sorption extent of 6FDA-6FpDA was explained by more open para-connected structure. Authors also repeated sorption test at 200 °C and reported that at high temperature, non-linearity of isotherm disappeared and sorption amount of two isomers became close to each other. Dual-mode sorption parameters depending on temperature were given in Table 5.2. All

three dual-mode parameters decreased with temperature increase. This phenomenon is related to both exothermic nature of sorption process and also relaxation of non-equilibrium voids of the polymer matrix.

Chung et al., 2003 investigated the sorption behavior of Matrimid 5218 in the existence of C₆₀ filler. Table 5.1 showed CH₄ and CO₂ sorption isotherm of both neat Matrimid and Matrimid/%5 C₆₀ mixed matrix membrane. The CH₄ sorption capacity of membrane was reduced by 14% while the CO₂ sorption capacity of that was reduced by 18% due to existence of C₆₀ filler. The decrease in sorption capacity was attributed to the rigidification of polymer chain due to C₆₀. The rigidification of the polymer chain was also confirmed by increased T_g and density values due to the presence of C₆₀ (Chung et al., 2003).

Dual-mode model parameters were given in Table 5.2. The presence of C₆₀ influenced Langmuir type sorption parameters more than Henry type sorption parameters. The presence of C₆₀ reduced Henry's sorption constant of CO₂ by 2%, while increased Henry's sorption constant of CH₄ by 46%. The Langmuir capacity constant (C'_H) decreased by 18% for CO₂ and by 27% for CH₄. The Langmuir tendency coefficient b decreased by 32% for CO₂ and by 22% for CH₄. The decrease in Langmuir constants has strengthened the interpretation that the C₆₀ filler modified with benzyl reduced the non-equilibrium free volume of the polymer since Langmuir type sorption is related to the free volume of the polymer. The permeability properties of Matrimid/ C₆₀ membrane were tested for CO₂, O₂, N₂, He and CH₄ single gas test. The ideals selectivity did not change. However, the permability of each single gas decreased with C₆₀ loadig. For example, CO₂ permeability decreased from 7.15 to 3.79 Barrer due to 10% C₆₀ loading.

Smith et al. 2012 investigated the effect of thermal rearrangement on the sorption capacity and solvent resistance of the HAB-6FDA type polyimide. Gas Sorption capacity of HAB-6FDA type polyimide, whose CO₂ and CH₄ sorption extents indicated in Table 5.1, increased due to thermal rearrangement. The increase in sorption capacity in CH₄ due to thermal rearrangement was more than that observed in CO₂. When the sorption capacity of PI membrane with 30 min. 450 °C

thermally rearranged compared to that of un-treated PI membrane, 75 % increase in CO₂ while 160% increase in CH₄ sorption capacity were noted. CO₂/CH₄ solubility selectivity decreased from 3.5 to 2.8. This reduction was attributed to the loss of the polar groups of the polymer during thermal rearrangement. During thermal regeneration, the HAB-6FDA lost its acetate and carboxyl groups. Hence, the increase in the polar CO₂ sorption capacity of polymer with degrading polar groups was not as high as nonpolar CH₄ (Smith et al., 2012).

Smith et al. 2012 investigated also impact of thermal rearrangement on the dual-mode sorption coefficients. The calculated values were listed in Table 5.2. As the thermal regulation temperature increased, the Langmuir type sorption coefficient C'_H increased. For methane, this value increased by 350% for 30 minutes at 450 °C, while it increased by 75% for CO₂. The Langmuir absorption capacity parameter is related to non-equilibrium excess free-volume for glassy polymers. Thus, the increase in this parameter was interpreted as the increase in the excess free-volume of the polymer due to thermal rearrangement.

Table 5.1 Comparison of sorption capacity of CO₂ and CH₄ in different kind of PI membranes at 35 °C.

Material	Operating Pressure (atm.)	Sorption Capacity (cm³ (STP)/(cm³ polymer)) (CO₂)	References
6FDA-DAM:DABA 2:1 (free acid-130 ° C)	2.5	37	Wind et al. 2003
	5.7	50	
	9.2	62.5	
	14	75	
	19.2	93	
	24	103.6	
	32.5	171.4	
6FDA-DAM:DABA 2:1 (free acid-220 ° C)	1.3	27.8	
	7.1	53.1	
	13	68.8	
	19.2	80	
	25	90	
	32.5	164.3	
6FDA-DAM:DABA 2:1 (CHDM-100 ° C)	2.1	22	
	6.2	40	
	12	52.5	
	20	67.5	
	26.2	79	
	33.3	97	
6FDA-DAM:DABA 2:1 (CHDM-220 ° C)	2.1	22	
	6.2	36.5	
	12	47.5	
	18	56.2	
	23.8	65	
	31	78	

Table 5.1 (Cont.) Comparison of sorption capacity of CO₂ and CH₄ in different kind of PI membranes at 35 °C.

Material	Operating Pressure (atm.)		Sorption Capacity (cm ³ (STP)/(cm ³ polymer))		References
	CO ₂	CH ₄	CO ₂	CH ₄	
Matrimid	1.8	4	10.5	4.5	Moore and Koros 2007
	4	9.5	21	8	
	7	15.5	28	11	
	12	20.8	37	12	
	17	22	45.5	13	
	21	29	51	14	
PMDA-ODA	1.5	2	15	2.2	O'Brain and Koros 1987
	3.8	4	22.5	5	
	4.6	5.5	26	6.5	
	7.8	8	31	7.5	
	9.5	9	36	8.5	
		10		9.2	
Kapton polyimide	1	3	4.5	2.5	
	2	5	9	3.9	
	5.5	7	17	5	
	10	9	21.7	5.8	
	-	11		6.5	
6FDA-6FpDA	0.8	-	13.3	-	Costello and Koros 1995
	2.5		24.9		
	4.3		32.5		
	6.2		39.5		
	8.3		45		

Table 5.1 (Cont.) Comparison of sorption capacity of CO₂ and CH₄ in different kind of PI membranes at 35 °C.

Material	Operating Pressure (atm.)		Sorption Capacity (cm ³ (STP)/(cm ³ polymer))		References
	CO ₂	CH ₄	CO ₂	CH ₄	
6FDA-6FmDA	1.1	-	10	-	Costello and Koros 1995
	2.8		17.5		
	4.75		22		
	6.7		26.7		
	9		30		
Matrimid (23 °C)	1		16	2	Chung et al. 2003
	4.5		31	8	
	7.8		41	11	
	11.1		47	14	
	14.5		52	16	
	18		58	17.7	
	21.5		63	18.5	
	25		68	20	
Matrimid / C ₆₀ (23 °C)	1		11	1	Chung et al. 2003
	4.5		25	6	
	7.8		31	8.5	
	11.1		40	11.5	
	14.5		45	14	
	18		51	15.5	
	21.5		56	17	
	25		60	18	

Table 5.1 (Cont.) Comparison of sorption capacity of CO₂ and CH₄ in different kind of PI membranes at 35 °C.

Material	Operating Pressure (atm.)		Sorption Capacity (cm ³ (STP))/(cm ³ polymer))		References
	CO ₂	CH ₄	CO ₂	CH ₄	
HAB-6FDA PI	1.3	4	15	5.5	Smith et al. 2012
	4.5	9	25	11	
	7.5	15	35	15	
	11	22	42.5	17.5	
	16	27	52.5	18.75	
	22	-	61	-	
	26		69		
HAB-6FDA PI Thermally rearranged TR 450 ° C 30 min	1.5	3.5	27.5	15	
	4	8.5	48.3	25	
	7	15	62	34	
	11	21.5	71	40	
	16.1	27	82.5	43.3	
	22	-	94	-	
	27		100		
Matrimid (2µm)	1.7	-	6.7	-	Simons et al. 2010
	3.3		12		
	6		17.5		
	11		25		
	21		39.5		
	31		46		
	41		55		

Table 5.2 Dual-mode sorption constants of polyimide for CO₂ and CH₄. The parameters obtained from isotherm at 35 °C unless otherwise specified.

Membrane	Penetrant		k_D (cm ³ (STP)/(cm ³ polymer atm))	C'_H (cm ³ (STP)/(cm ³ polymer))	b (1/atm)	Reference
6FDA- DAM:DA BA 2:1 (free acid- 130 ° C)	CO ₂		2.23	54.2	0.454	Wind et al. 2003
	CO ₂		1.77	46.6	0.689	
	CO ₂		1.82	31.1	0.51	
	CO ₂		1.36	37.0	0.58	
Matrimid	CO ₂		1.44	25.5	0.367	Moore and Koros 2007
	CH ₄		0.136	14.3	0.105	
6FDA- 6FpDA	35 °C	CO ₂	2.3	31	0.69	Costello and Koros 1995
	75 °C		1.1	23	0.25	
	100 °C		0.64	23	0.13	
	120 °C		0.68	16	0.11	
6FDA- 6FmDA	35 °C	CO ₂	1.4	22	0.60	
	75 °C		0.7	16	0.23	
	100 °C		0.75	5.8	0.31	
	120 °C		0.67	3.2	0.33	

Table 5.2 (Cont.) Dual-mode sorption constants of polyimide for CO₂ and CH₄. The parameters obtained from isotherm at 35 °C unless otherwise specified.

Membrane	Penetrant	k_D (cm ³ (STP)/(cm ³ polymer atm))	C'_H (cm ³ (STP)/(cm ³ polymer))	b (1/atm)	Reference
Matrimid	CO ₂	1.416	35.0	0.702	Chung et al. 2003
	CH ₄	0.249	17.7	0.136	
Matrimid+%5 C ₆₀	CO ₂	1.389	28.5	0.476	
	CH ₄	0.364	12.9	0.106	
HAB-6FDA PI	CO ₂	1.4	35	0.34	Smith et al. 2012
	CH ₄	0.44	11	0.11	
HAB-6FDA PI TR 450 ° C 30 min	CO ₂	1.6	62	0.53	
	CH ₄	0.49	36	0.16	

Punsalan and Koros 2005 showed that thickness of polyimide membrane has also influence sorption behavior and extent. In this study, CH₄ solubility in polyimide membrane with two different thickness (0.1 μm and 25 μm) was measured and compared. Since the active selective dense skin layer of asymmetric gas separation membrane is not more than 0.1 μm, sorption behavior of thin layer is meaningful. Previously, Weesling et al. 2001 showed that thin polymeric materials could plasticize at lower pressures than thick polymeric film. Sirard et al. 2001 induced that thin polymeric films can sorb differently from thick polymeric film made of the same polymer. Simons et al. 2010 studied the sorption behavior of Matrimid with thickness of 2 μm via Spectroscopic Ellipsometer. As listed in Table 5.2, the reported CO₂ sorption extent values were significantly lower than the values reported by Moore and Koros 2007.

The CH₄ sorption extent of thin Matrimid was lower than that of thick Matrimid. Moreover, thin film sorption capacity was affected by aging more than

the sorption capacity of thick film. The slope of the sorption isotherms at higher pressure regime (in the linear region) was equal to Henry- type sorption law coefficient (k_D). The slope of the isotherm at high pressure region was identical for both isotherms and this behavior is compatible with theory that k_D value is an intrinsic polymer-penetrant parameter. The Langmuir sorption capacity of the thinner films was lower than that of the thicker films. Therefore, it was deduced that the excess free volume (unrelaxed volume) of the thick dense film was higher than that of thin dense film. Authors explained this phenomenon by the free-volume diffusion theory (Punsalan and Koros 2005).

Vopicka et al. 2014 studied the sorption capacity of CO₂/CH₄ mixture by a glassy microporous polymer (PIM-1). Although (PIM-1) was not within the scope of this research, this study is very enlightening for understanding the sorption behavior of glassy polymer in the presence of the second penetrant. Feed composition dependent sorption isotherms are given in Figure 5.3. In the presence of the second penetrant, the sorption capacity of the polymer for each gas pair is lower than that of the pure states. This decrease in gas solubility is much more significant in methane. For example, at 10 atm, the CH₄ sorption capacity decreased from 40 (cm³ STP/cm³ polymer) to 10 (cm³ STP/cm³ polymer) as CO₂ concentration increased from 0 to 49% in the sorption mixture. The percent decrease in methane sorption capacity was approximately 75%. To get same percent decrease in sorption capacity of CO₂, the methane content of the mixture should be 80% at 10 atm. The suppression in sorption capacity of gases in the presence of the second penetrants is because of the competition between the penetrants (Vopicka et al., 2014).

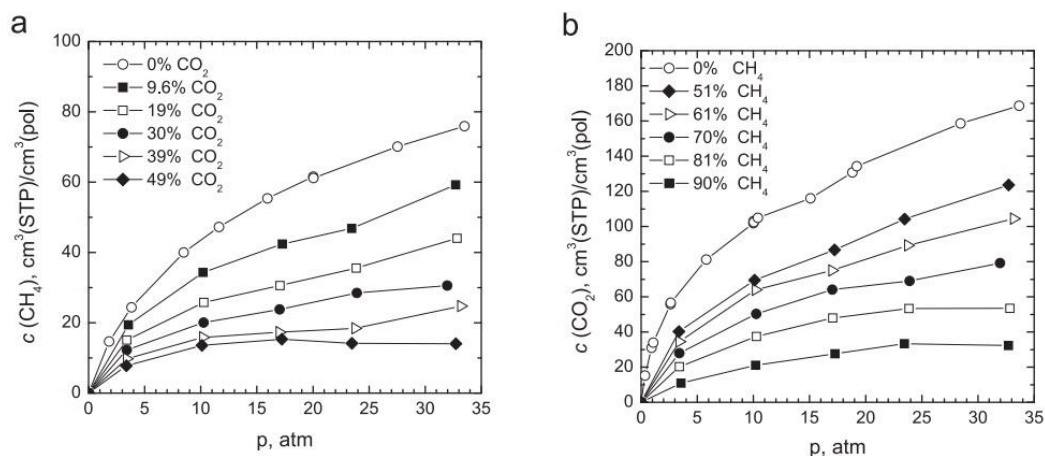


Figure 5.3 CO₂ and CH₄ sorption isotherms of PIM-1 for different mixing ratio of these two gases at 35 °C. (Vopicka et al. 2014).

5.1.5 CH₄ and CO₂ Sorption Behavior of ZIF-8

In the present study, ZIF-8 crystals were used to improve the sorption capacity of symmetric PI dense film membranes.

Metal organic frameworks (MOFs) are widely studied in scientific community, because the possibility of adapting the pores size and functional groups of these materials provides an opportunity for wide variety of applications. ZIFs are particular class of MOFs and their strong bonds between metal ions and imidazole group provides high thermal and moisture stability. The M-Im-M units in ZIFs, which are longer than the Si-O-Si units in Zeolite, provide larger cavities of ZIFs than those of corresponding Zeolites. The larger pore volumes result in higher sorption capacity. Moreover, the affinity of ZIFs for some specific molecules can be tunable by interposing functional groups to the imidazole links (Pérez-Pellitero et al., 2010, Zhang et al. 2014, Zhang et al. 2013). The ZIF-8 is better than many other MOFs in terms of gas storage capacity. Moreover, its hydrophobicity and high stability against moisture compared to other MOFs make it attractive in terms of industrial application (McEwen et al. 2013).

The CO₂/CH₄ separation is one of the application field of ZIF-8. The sieve aperture of ZIF-8 is approximately 3.4 Å, whereas the kinetic diameter of CO₂ and

CH₄ are 3.3 Å and 3.8 Å, respectively. Therefore, high CO₂/CH₄ selectivity is expected. However, because of the flexible nature of ZIF-8's aperture leads to moderate selectivity (Zhang et al. 2014, Fairen-Jimenez et al., 2011).

Figure 5.4 presented the adsorption isotherms of ZIF-8 for CO₂, CH₄ and N₂ at 30°C. The CO₂ sorption capacity of ZIF-8 is higher than that of CH₄ (Pérez-Pellitero et al., 2010). Polar nature of carbon-oxygen bonds in CO₂ (Venna and Carreon 2010) and high quadrupole moment of CO₂ (Banerjee et al., 2009) favors the adsorption by polar ZIF-8 walls. At 100 kPa (1bar) and at room temperature, CO₂/CH₄ adsorption selectivity of ZIF-8 was reported approximately 14 (Venna and Carreon, 2010). The study carried by McEven et al. 2013 conflicted with Venna and Carreon, 2010 findings and reported that CO₂/CH₄ adsorption selectivity was 2.75 at 1 bar and at 25 °C. At low pressures, ZIF-8 shows low CO₂/CH₄ selectivity, however at high pressures, ZIF-8s can provide better CO₂/CH₄ separation performance thanks to its large pore volume and less requirements of activation energy (McEven et al. 2013).

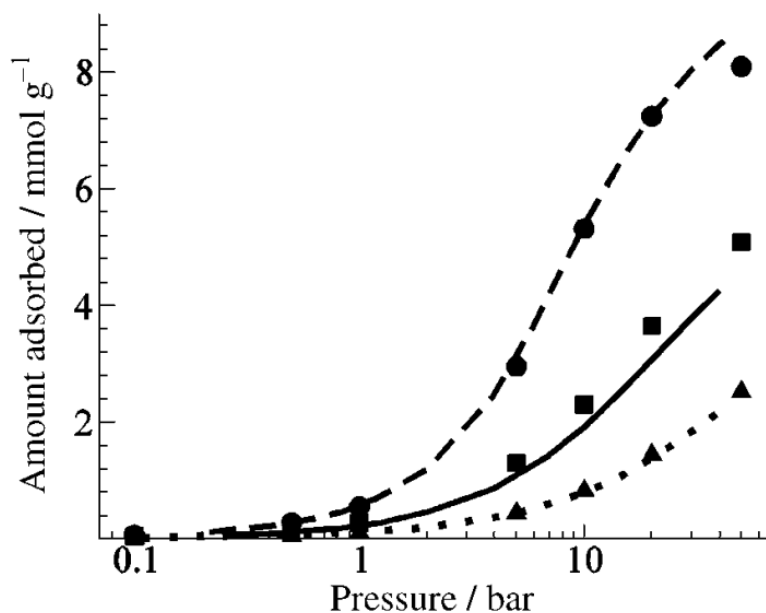


Figure 5.4 CO₂ (●), CH₄ (■) and N₂ (▲) adsorption isotherms of ZIF-8 at 30 °C. Symbols showed simulation results and lines showed experimental results (Pérez-Pellitero et al., 2010).

Zhang et al. 2013 improved the CO₂ sorption capacity of ZIF-8s by modifying synthesized ZIF-8s with ethylenediamine linker. The sorption extent of CO₂ in ZIF-8 increased by 80% at 5 bar and the enhancement was increased with pressure. The enhancement of the CO₂ sorption capacity of ZIF-8 was explained by the increased basicity of ZIF-8 and introducing N-H group due to ethylenediamine linker.

5.2 Materials and Experimental Methods of PI Membrane Production and Sorption Test

5.2.1 Materials

Polyimide resin, Matrimid[®]5218 with 1.2 g/cm³ density, 588,000 g/mol molecular weight and 305°C glass transition temperature (T_g) was used as polymer, further detail about the polymer can be found in Chapter 3.2. N,N-Dimethylformamide (DMF) with high purity (>99%) was used as solvent and provided by Sigma-Aldrich. ZIF-8 with 65 nm average particle size was used as filler. The details of ZIF-8 synthesis and pre-treatment procedures were already expressed in Chapter 2. ZIF-8 crystals were used after thermal annealing (Treatment Type-3).

5.2.2 Preparation of Dense Symmetric neat PI and PI/ZIF-8 Membranes via Solvent Evaporation

The neat dense symmetric PI membranes were produced by solvent evaporation method. For this purpose, a homogeneous polymer (17.4 wt.%) solution consisting of 2 g. PI and 10 ml (9.5 g.) DMF was prepared. PI was kept at 80°C overnight in order to remove humidity before mixing solvent. The PI-DMF solution was stirred by a magnetic stirrer at 300 rpm and at room temperature. The essential amount of PI was primed in three steps to avoid agglomeration and sudden increase of viscosity. Between each steps, the solution was ultrasonicated for 10 min in order to ease the dispersion and to provide degassing. The homogeneous PI-DMF (17.4 wt.%) was poured on a glass plate by automatic film applicator. The thickness of casting film was adjusted by doctor-blade as 500 μm. The solvent DMF

was then removed from casting film by standing it at oven for 7-8 hours, at 80 °C and under vacuum atmosphere. After 7 or 8 hours, the membrane film was peeled off from the glass plate and was annealed at 100 °C under nitrogen atmosphere at least one week.

In order to prepare PI/ZIF-8 dense symmetric mixed matrix membrane, ZIF-8 at 10% or 20% by mass of the polyimide was dispersed in 9.5 g DMF solvent. Before adding ZIF-8 with 65 nm average particle size, ZIF-8 crystals treated thermally as explained in Chapter 4 in detail. The ZIF-8/DMF solution was stirred at 300 rpm and at room temperature. The necessary amount of ZIF-8 was added at three or four step based on the amount. The solution was ultrasonicated for 30 min between each step. The homogeneous dispersion of ZIF-8 took at least two days. After dispersion of necessary amount of ZIF-8 in the 9.5 g DMF solvent, the 2 g. of PI was added in three steps; 15 wt.% of total PI, 35 wt.% of total PI, and 50 wt.% of total PI, respectively. Before each addition, membrane solution was ultrasonicated for 10 minutes. The casting and annealing methodologies of mixed matrix PI/ZIF-8 membranes were the same as those of neat PI membranes.

5.2.3 Experimental Test Set-up and Sorption Test

Gas sorption test can be carried out in several ways. Most common two are gravimetric sorption and pressure-decay sorption. Gravimetric sorption test is suitable for highly sorbing gases and vapors and low pressures. Pressure decay sorption test is widely preferred for low sorbing gases and high pressure tests (Moore and Koros 2007).

Pressure decay sorption test is more suitable for our low sorbing gases and our moderate pressures (1-10 bar). The sorption test set-up installed in this study was dual-volume and dual-transducer system as suggested by Koros and Paul 1976. This system was connected to GC for analyzing mixture sorption.

Figure 5.5 shows the laboratory-built sorption test system. Initially, the system was designed as three volumes, namely reservoir volume, sample volume and residual analyze volume. These volumes are made up of the chambers and the

tubing connecting these chambers with the same name as the volumes. Chambers (reservoir chamber, sample chamber and residual analyze chamber) were prepared by burrowing a cylindrical hollow with 2.5 cm in diameter and 3 cm in depth into 304-quality stainless steel billet with 80 mm in diameter. The sealing of these chamber was provided with two Viton o-rings which was placed between the flange-shaped cover and the stainless steel blank with cylindrical slot. These three volumes were connected to the system via weld-union with 1/8" in size. Membranes to be tested were placed in the sample chamber. The reservoir volume was a section added to the system to adjust the pressure value and temperature of the gas to be sent to the sample chamber. The residual analysis volume was added to the system in order to test the composition of the non-sorbed gas volume while the sorption of mixture gases was studied. The polymeric membrane sorbed components in the gas mixture at different proportion. The gas that was not absorbed by the sample was sent to the analysis volume and tested with GC to determine the composition. By the help of this residual analyze chamber, the pressure of the non-sorbed gas in the sample chamber can be reduced to such a degree that can be sent to the GC without the risk of saturation or disrupt the GC column. The GC test of the residual gas was repeated at least three times and each test took 5 minutes. Between each run the GC column was evacuated for at least 5 minutes. The residual analysis volume is necessary to keep the composition of non-sorbed gases constant until the GC test finished. Otherwise, the depressurization of sample chamber led to desorption of gases and composition varies during the GC test.

The mixing tank was added to the system later according to the requirements of the system. The mixture was prepared by using the pressure ratios of the feed gases. This large mixing tank provides a suitable environment for the mixing of gases. In addition, the mixing tank has a large volume and provides sufficient amount of gases until the entire pressure range test has been completed.

The sorption capacity is very sensitive to variation in temperature, hence controlling and keeping constant the test temperature is crucial for reliable and repeatable test results. The reservoir chamber and the sample chamber were placed

in a home-made oven. The oven was insulated by placing 20 mm stone wool. Heating was provided by an electric heating plate and a fan was used to obtain uniform temperature in the oven. The temperature which kept at 35 °C during sorption test was controlled by a thermocouple equipped PID controller (GEMO D104A).

The most important part of the system is the pressure transducers used to monitoring pressure variation. Super TJE transducer Honeywell Sensotec (accuracy 0.05%) (Ribeiro and Freeman, 2010), Delta Metrics 0.05% accuracy (Kim et al. 2015), Statham Schlumberger model PA8224-1M-24050 accuracy 0.09% (Costello and Koros 1992) are pressure gauge models used in literature studies. When these models were examined, it was noted that the precision of the transducer was higher than 0.2%. Indeed, according to Costello and Koros 1992' study, the precision value which is smaller than 0.25%, may led to inaccuracy in measurement. In our system, MKS-Baratron® with product-ID 750C13PFE2RA is used. The pressure operating range is 0-1000 psia with 0.1 % precision in full-scale and operating temperature range is 0-50 °C.

The sorption feed whose temperature and pressure were adjusted in reservoir chamber was send to sample volume chamber which was under vacuum. Transferring gases from high pressures to low pressures may lead to Joule-Thomson type or iso-enthalpic expansion, hence freezing may be observed. This is why gas transfer or purging should be slow, reliable and be done in a controlled manner. To provide this requirement, Hoke brand stainless steel needle valves (NV) with "regulating stem type" tip were used which can stand up to 345 bars. The connection between system components (pressure chambers, valves, pressure transducers) were provided via stainless steel fittings and tubing with 1/8" size, which can stand up to 207 bars.

Determination of the Volume of the Sample Chamber

Estimation accuracy of volume of the sample chamber is vital since it is used in all the subsequent calculations. Moreover, Smith et al. 2012 indicated that

the largest error in the sorption measurements comes from the volume calibration of the sorption cell, which has the greatest effect on low sorbing gases in the polyimide. Volume estimation is performed using the following two methods. In the first method, the sample chamber was filled with water. Next, it was poured in to a beaker whose weight was measured. Then, the corresponding volume was calculated. By this method, volume of the sample chamber was calculated to be 24 cm³. However, the volume inside transducer could not be taken into account. Since contact with water could have damaged the transducer. In the second method, we tested sorption capacity of PES/SAPO34(%20 w/w) membrane which has already been reported in Ülgen Çakal's work. The volume of the sample chamber of the system under test was changed until we met the sorption capacity reported and it was calculated to be 28 cm³

The closer look at the parts of the system was provided in the following figures. In Figure 5.5-A, the sorption feed preparation unit and manifold part are seen. V-1 and V-2 are ball valves. The V-1 valve was used to pressurize the system with CO₂ while the V-2 was used to pressurized the system with CH₄. V-3, V-4, V-5, V-6, and V-7 are both needle valves. The needle valve, V-3 was distinguished the mixing tank from the rest of the system. The needle valve, V-4 was used to depressurized or evacuate the mixing tank when it is necessary. The needle valve, V-5 is connected to the mixing tank to the reservoir. In Figure 5.5-B shows the reservoir volume and sample volume. The zone restricted to V-5, V-6 and V-7 with reservoir chamber are comprised the reservoir volume of the system. The pressure and temperature of this part was monitored by pressure transducer number 2 (PT-2). The zone restricted to V-7, and V-8 with sample chamber are formed the sample volume of the system. The pressure of the sample volume was monitored by pressure transducer number 1 (PT-1). The residual volume shown in Figure 5.5-C is residual chamber with the zone restricted by V-8, V-9, V-10, V-11 and V-12. The needle valve, V-8 was used to send the residual gas to the residual volume. The needle valve V-10 was to purge the volume in a controlled manner. V-9, V-11 and V-12 are ball valve. V-12 provides the GC connection, while V-10 is used to

evacuate the volume. V-11 is provided a connection between reservoir volume and residual volume by a plastic pipe and plastic quick-connect. When the composition of the prepared gas mixture is to be measured, this gas mixture is sent to the residual volume via the valve V-11.

Flow diagram of sorption test system is shown in Figure 5.6

VARIAN® Star 3800, Gas Chromatography was used to analyze the relative amount of gases in the residual mixture based on the difference between the sorption properties of CO₂ and CH₄ by the GC column. He was used both sweep gas and reference gas. Dry-air was used to automatic injection of sample gas. Before injection and between two injections, injection port of the GC was evacuated. The peak area from the gas chromatograph provides the information about the partial pressure of each gas in the mixture. For calculations, the pure CO₂ and pure CH₄ GC calibration test results were used. The properties of GC test condition were provided in Table 5.3. Table 5.4 provided the codes, contents and casting parameters of the membranes tested for sorption experiment. In further discussion, these abbreviations were used.

Table 5.3 Gas chromatography test operation condition.

Column	Chromosorp 102, 80-100 mesh
Detector	Thermal conductivity detector (TCD)
Detector Temperature	100
Column Temperature	80
Valve Temperature	80
Column Pressure	50 psi
Sample Flow rate	50 ml/min
Reference gas and flow rate	He, 30 ml/min

Table 5.4 Dense symmetric membranes prepared by solvent evaporation for sorption test. Solvent evaporation was taken place at 80 °C under vacuum and annealing was carried out 100 °C at N₂ atm. for 1 week.

Membrane Code	Polymer (g)	ZIF-8 (g)	Non-volatile Solvent (g)	Weight of tested membrane sample (g)
PI-1	2 g PI	No	9.5 g DMF	0.43
PI-2		No		1.43
MM-PI-1		0.4 g.		1.29
MM-PI-2		0.8 g.		1.40

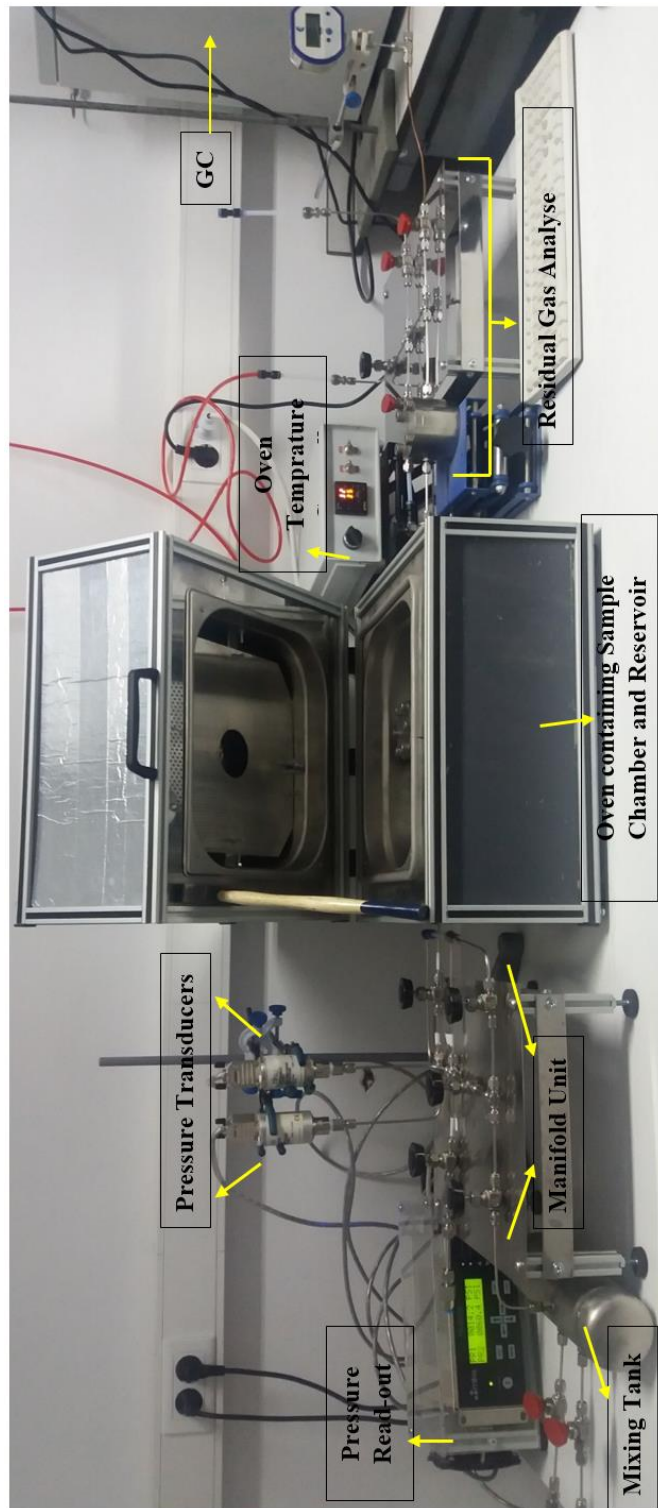


Figure 5.5 Pressure-Decay type sorption test system.



Figure 5.5-A Pressure-Decay type sorption test system-sorption feed part.



Figure 5.5-B Pressure-Decay type sorption test System-Reservoir Volume and Sample Volume.



Figure 5.5-C Pressure-Decay type sorption test System-Residual Volume.

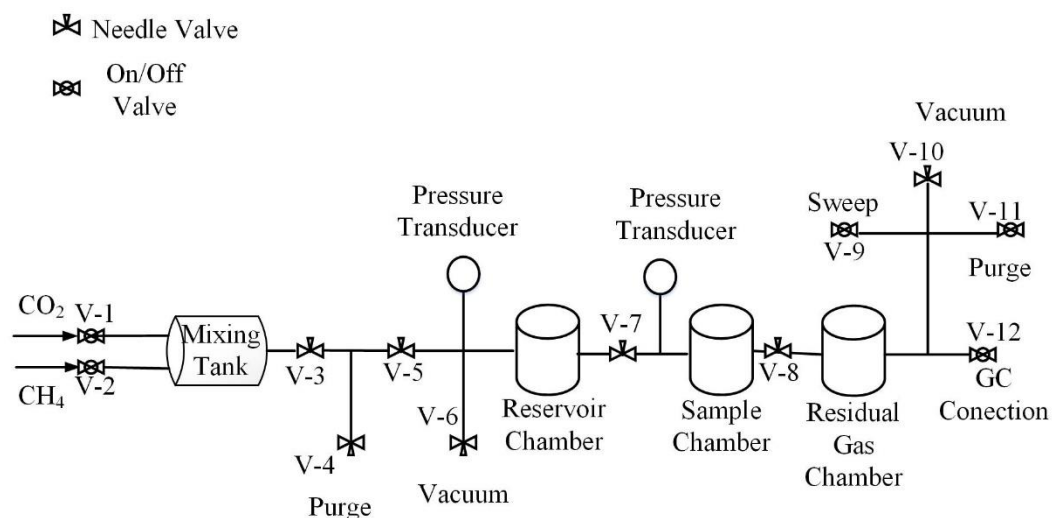


Figure 5.6 Flow diagram of sorption test system.

Single (pure) Gas Sorption Test,

After, the temperature of the sample volume and reservoir chamber was adjusted at 35 °C, the polymer sample was emplaced in the sample chamber. The whole apparatus was kept under vacuum for one day before experiment. Before pressurized the system, pressure transducers were calibrated to zero under vacuum. After the vacuum period, the whole system was separated by closing all valves. Then the volume containing sample was separated from the rest of the apparatus by closing needle valve 7 (V-7) and needle valve 8 (V-8). System was pressurized through valve 1 (V-1) with CO₂ or through valve 2 (V-2) with CH₄. The gas tank and reservoir chamber were filled with the penetrant gas up to 180 psi. The sorption experiment was started by opening needle valve 7 (V-7). Sorption equilibrium was indicated by constant reading of pressure reading from pressure transducer 1 (PR1) and occurred within 3 hours for CO₂ and within 6 hours for CH₄ from the start.

Mixed Gas Sorption Test

The polymer sample preparation method and vacuum period are the same as the procedure implemented for pure gas sorption experiment. The differences came from sorption feed preparation period and gas chromatography connection. After vacuum period and separation of sample volume by closing V-7 and V-8

valves, the feed tank and reservoir chamber were pressurized through V-2 with CH₄. Then V-2 was closed and mixture tank was further pressurized through V-1 with CO₂. Pressure of the feed was read from pressure transducer 2 (PR2). The composition of feed gas was adjusted based on the pressure ratio of pressurized gases. For example, for %70 CH₄-%30 CO₂ mixture, the reservoir was pressurized with CH₄ up to 70 psia, then the system was further pressurized with CO₂ up to 100 psia. After waiting for one night for mixing the feed, V-1 was closed and the mixing tank was isolated from the capillary region. Before analyzing and sending the gas mixture to the sample volume, the capillary region was evacuated. After evacuation, V-1 was opened and reservoir volume was filled with gas mixture. The composition of feed gas was analyzed by GC before pressurizing the sample volume. For this purpose, reservoir volume and residual volume were connected by a plastic pipe between valves (V-6 and V-11). The mixed gas sorption test was started by opening V-7 and ended after equilibrium which was indicated by constant pressure reading of PR1. After sorption equilibrium, non-sorbed gas composition was analyzed by gas chromatography for subsequent calculation. First, residual volume was evacuated and then the non-sorbed gas in the sample chamber was sent to residual volume which was connected to sample volume via V-8 and to gas chromatography device via valve 12 (V-12).

5.3 Sorption Capacity Test Results of the Neat Dense Symmetric PI Membranes

The sorption capacity isotherms of pure gases CO₂ and CH₄ were measured using the procedures described previously. Figure 5.7 showed the sorption isotherms of pure CH₄ and pure CO₂ in symmetric dense PI membranes; PI-1 and PI-2 at 35 ° C. Literature values of CO₂ and CH₄ sorption capacity of PI (Moore and Koros 2007) were also provided on the same graph. The CO₂ sorption capacity values of PI-1 membrane are 19% higher than those reported in literature at test pressure above 5 bar. When the test pressure was below 5 bar, the deviation of CO₂ sorption capacity of PI-1 from literature decreased to 10%. The CH₄ sorption capacity values of PI-1 membrane are approximately 30% higher than the values

reported in the literature. The reasons of this variation may be due to different membrane casting method, different pre-treatment of tested samples, purities of penetrant or differences between the test apparatus. Especially a small miscalculation in sample volume and in-sufficient precision of PT-1 have a great influence on the final result. The same sorption tests were repeated by increasing the amount of the testing polymeric membrane in order to eliminate the adverse effect of low sensitivity of the pressure gauge. PI-1 and PI-2 were produced with the same methods and conditions. The only difference between them is the tested part of the PI-1 was 0.43 gr while tested part of the PI-2 was 1.43 gr. As observed in Figure 5.7, by increasing the amount of the testing polymeric film, the determined sorption capacity values became closer to the literature values. Small differences may be considered to be the nature of the polymer sorption process. Because a lot of studies have shown that a small temperature variation in the pre-treatment process of the polymer (Scholes et al. 2010), or even the thickness of the tested polymer (Punsalan and Koros 2005, Simons et al. 2010, Sirard et al. 2001) film, has a significant effect on the sorption capacity.

The chemical associations between CO₂ and Matrimid are more thermodynamically favorable (Scholes et al. 2010) and hence the sorbed CO₂ concentration substantially higher than that for CH₄ at similar pressures. One of the reasons of the higher sorption capacity of CO₂ compared to CH₄ is higher condensation tendency of CO₂. The critical temperature of CO₂ is 304.3 K while that of CH₄ is 190.6. Hence CO₂ is condensable even at room temperature and more easily sorbed when compared less condensable CH₄ (Pixton and Paul 1995; Zhang et al. 2014, Chung et al. 2003, Smith et al. 2012). Polymers (for example; poly-methy methacrylate, polyetherdiimide, cellulose acetate- acetate or pendant group are also polar-) containing high density carbonyl group have high sorption capacity of CO₂ relative to CH₄ and show high CO₂/CH₄ sorption selectivity (Koros 1985, Pixton and Paul 1995, Smith et al. 2012). The Matrimid®5218 used in the present study includes high density of carbonyl group; five at each repeating unit as indicated in Figure 5.8. Therefore, similar sorption behavior was observed for PI-1 and PI-2 as expected. Polar nature, high quadrupole moment of CO₂, leads to high

interaction between polar polymer, hence larger CO₂ solubility is observed compared to the CH₄ (Smith et al. 2012).

CO₂ and CH₄ isotherms demonstrate standard dual-sorption behavior. Isotherms are non-linear and concave to the pressure axis (Chung et al. 2003, Smith et al. 2012). This means rapid increase in gas sorption concentration at low pressures. By increasing in pressure, increase in the gas sorption concentration are tapered off. As the pressure increases, free microvoid space in polymer matrix becomes limited and concentration increase is reduced. This trend is valid for sorption in all glassy polymers (Scholes et al. 2010, Koros et al. 1981).

The CO₂/CH₄ sorption selectivity of PI-1 and PI-2 is shown in Figure 5.9. The highest sorption selectivity was observed at 1 bar, by increasing the test pressure sorption selectivity decreased slightly and then fixed at a constant value. This constant value was approximately 3.5 for our PI-1, PI-2 membrane and calculated value based on dual-mode model. On the other hand, the constant sorption selectivity of Moore and Koros 2007's study was 4.5.

Dual-mode sorption parameters of neat PI tested in the present study was determined based on the average sorption values of PI-1 and PI-2 via grid search approach to numerically solve a nonlinear least squares (NLS) problem. The dual parameters were calculated also based on just only sorption data of PI-2 since the PI-2 sorption isotherms were closer to the isotherms provided Moore and Koros 2007. The results were provided in Table 5.5. The CO₂ and CH₄ sorption isotherm determined based on the estimated dual-mode parameters according to average sorption extent of PI-1 and PI-2 were also provided in Figure 5.7. The dual mode parameters for Matrimid studied by Moore and Koros 2007 and Chung et al. 2003 were the suitable candidates to compare with our results. The dual mode parameter b of CO₂ and CH₄ and C'_{H-CH_4} were within the range of the value provided in literature (see Table 5.2). However, the C'_{H-CO_2} value estimated based on average sorption extent of PI-1 and PI-2 was lower than the values in the literature, and the K_{D-CO_2} value of average of PI-1 and PI-2 was greater than the all K_{D-CO_2} values listed in Table 5.2. This value was found to be less than 2.55 even for polymers

specifically modified to increase the CO₂ sorption capacity. The dual mode parameters based on PI-2 were very close the values provided by Moore and Koros 2007.

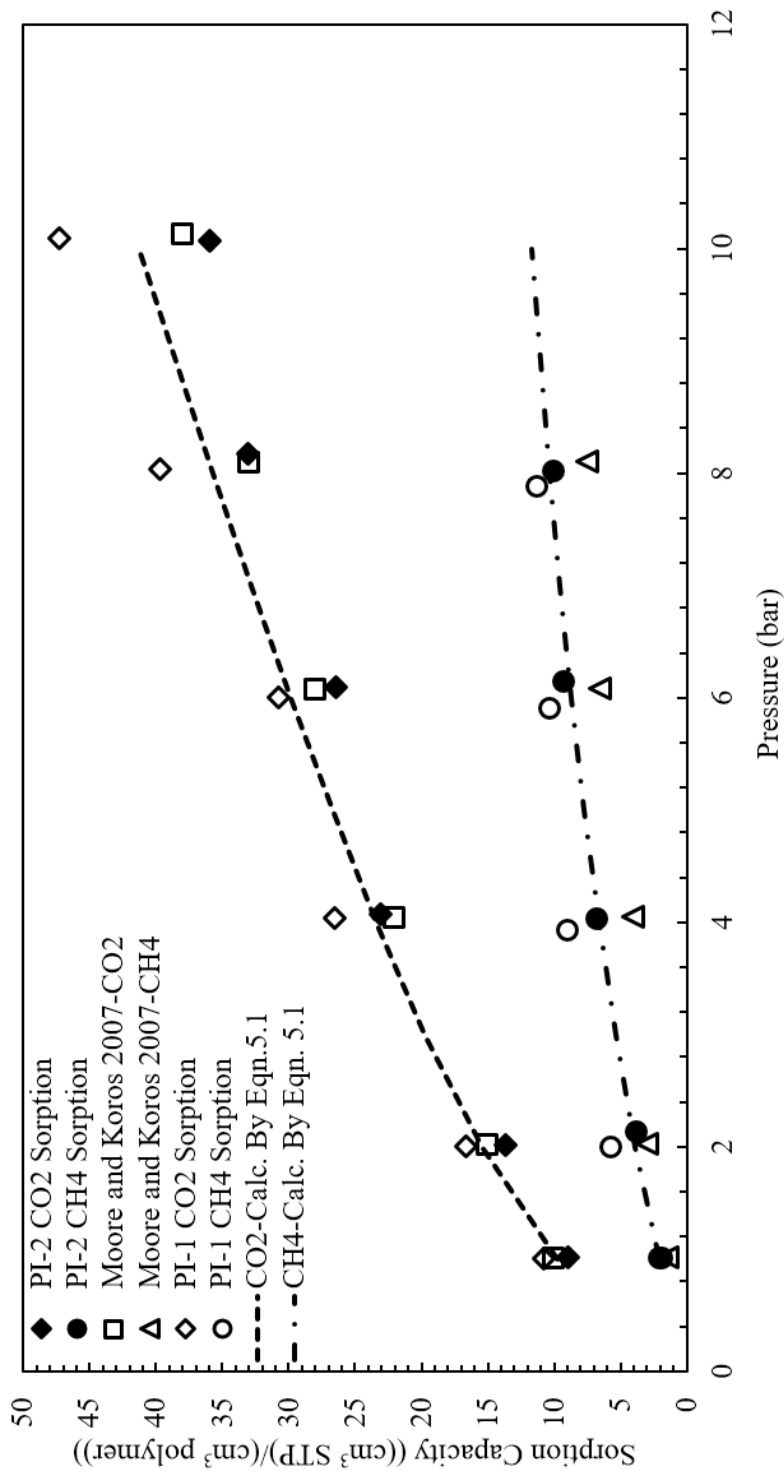


Figure 5.7 Pure methane and pure carbon dioxide sorption isotherm of neat symmetric dense PI membranes (PI-1 and PI-2) at 35 °C. 'REF' values were taken from Moore and Koros 2007.

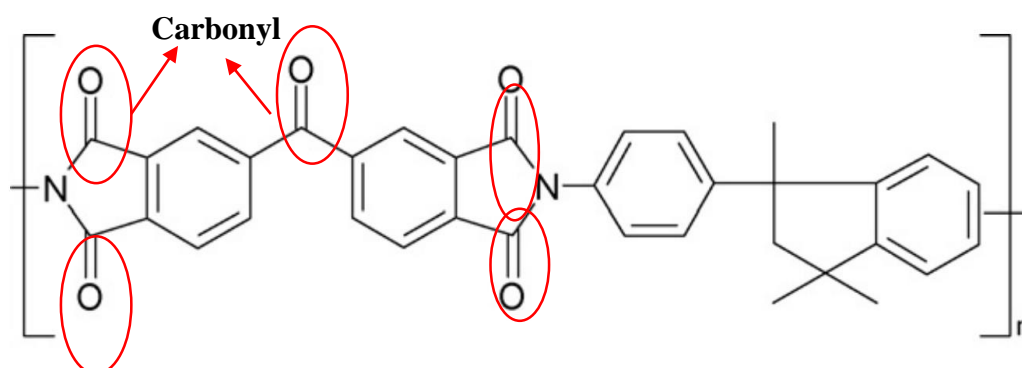


Figure 5.8 Matrimid®5218 repeating monomer (retrieved from Zhang et al., 2008).

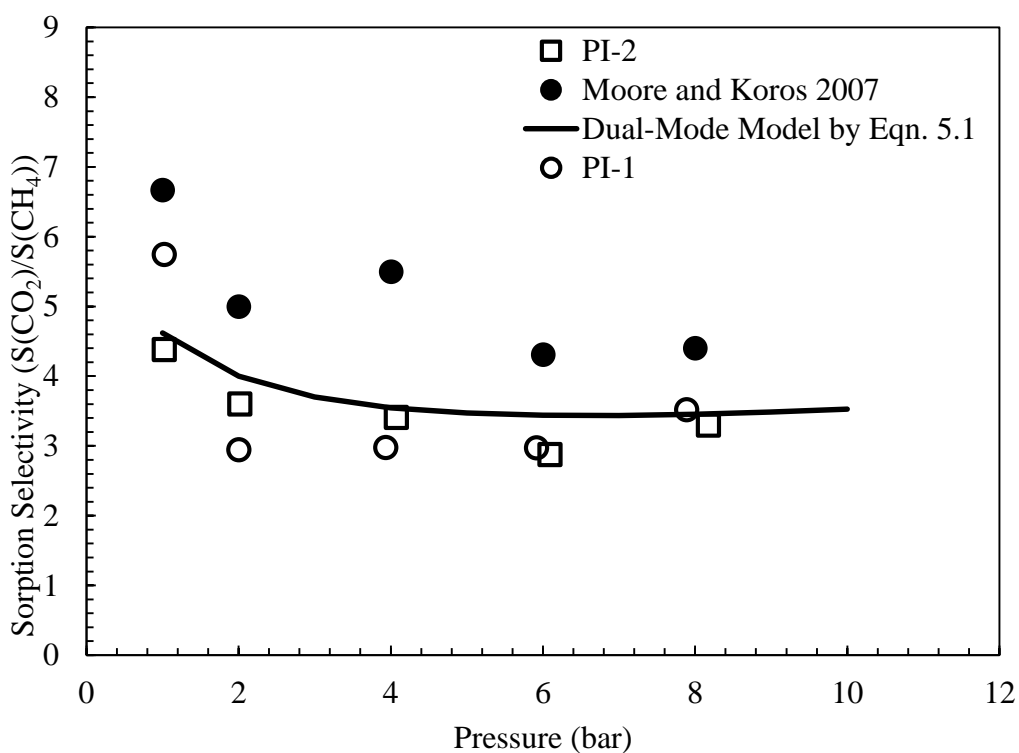


Figure 5.9 Solubility selectivity of dense PI membranes (PI-1 and PI-2) and reference Moore and Koros 2007.

Dual-mode sorption parameters of neat PI tested in the present study was determined based on the average sorption values of PI-1 and PI-2 via grid search approach to numerically solve a nonlinear least squares (NLS) problem. The dual parameters were calculated using sorption data of PI-2 since the PI-2 sorption isotherms were closer to the isotherms provided by Moore and Koros 2007.

The results were provided in Table 5.5. The CO₂ and CH₄ sorption isotherm determined based on the estimated dual-mode parameters according to average sorption extent of PI-1 and PI-2 were also provided in Figure 5.7. The dual mode parameters for Matrimid studied by Moore and Koros 2007 and Chung et al. 2003 were the suitable candidates to compare with our results because their type of membranes and test method were similar to ours. The dual mode parameter b of CO₂ and CH₄ and C'_{H-CH_4} were within the range of the value provided in literature (see Table 5.2). However, the C'_{H-CO_2} value estimated based on average sorption extent of PI-1 and PI-2 was lower than the values in the literature, and the k_{D-CO_2} value of average of PI-1 and PI-2 was greater than the all k_{D-CO_2} values listed in Table 5.2. This value was found to be less than 2.55 even for polymers specifically modified to increase the CO₂ sorption capacity. The dual mode parameters based on PI-2 were very close the values provided by Moore and Koros 2007.

Table 5.5 Dual-mode sorption constants for CO₂ and CH₄ based on sorption test average of PI-1 and PI-2.

Membrane	Penetrant	k_D (cm ³ (STP)/(cm ³ polymer bar))	C'_H (cm ³ (STP)/(cm ³ polymer))	b (1/bar)
PI-1 and PI-2 average	CO ₂	2.55	18.23	0.66
	CH ₄	0.3	14	0.2
PI-2	CO ₂	1.43	28.16	0.34
	CH ₄	0.22	16.73	0.13
Moore and Koros 2007	CO ₂	1.44	25.5	0.367
	CH ₄	0.136	14.3	0.105
Chung et al. 2003	CO ₂	1.42	35.0	0.702
	CH ₄	0.249	17.7	0.136

5.3.1 CO₂ - CH₄ Mixture Sorption Capacity of Neat Symmetric Dense Polyimide Membrane

The solubility of binary mixtures of CO₂ and CH₄ in PI-2 were measured at three fixed values of molar fraction of CH₄ in the gaseous phase: 29.64 mol%, 49 mol%, 69.42 mol%. The CO₂ and CH₄ sorption isotherms as a function of both pressure and mixture composition were provided in Figure 5.10 and Figure 5.11, respectively. The sorption behavior of PI-2 in the presence of the two penetrants were also calculated according to the approximation (Eqn. 5.10 and Eqn. 5.11) developed by Koros 1980.

The experimentally observed CO₂ sorption capacity were higher than the estimated CO₂ sorption capacity. On the other hand, the obtained CH₄ sorption capacities were much lower than the calculated values.

Experimental results showed that the highest reduction in CO₂ sorption capacity for the case of the 29.6% CH₄-70.6% CO₂ mixture due to the competition effect was about 22% at 1 bar. At the same concentration and test pressure, the percent decrease in methane sorption capacity was 90%. For 29.6% CH₄-70.4% CO₂ composition, the percent reduction in sorption capacity of CO₂ was in the range of 22%-and 9%. However, this decline was not correlated with pressure but oscillated. The average decline for CO₂ sorption capacity at 29.6%CH₄ - 70.4% CO₂ mixture was approximately 15%.

For the 49%CH₄-51%CO₂ mixture, the percent of decrease for CO₂ sorption capacity was observed at 1 bar, approximately 40%. The average decline in CO₂ sorption capacity at this concentration was approximately 31% with respect to pure CO₂. At this concentration, the maximum decrease in methane sorption capacity was observed at 4 bar and approximately 83% with respect to pure CH₄. For mixture including 51% CO₂, the average percent reduction of CH₄ sorption capacity was found approximately 77% relative to the pure CH₄.

Figure 5.10 and Figure 5.11 indicated that in the multicomponent sorption in glassy polymers the solubility of all gases was depressed with different extents. This behavior is due to a competitive effect that lowers the ability of the penetrant to be absorbed in the matrix when a second penetrant is present within the same environment. Because of competitive nature of mixed gas solubility in glassy polymers, for each species the deviations from the ideal pure gas case increase as mole fractions of the second gas increase (Koros 1981, Chern et al. 1984, Visser et al. 2005, Vopicka et al. 2014, Dorosti et al. 2015, Saberi et al. 2016)

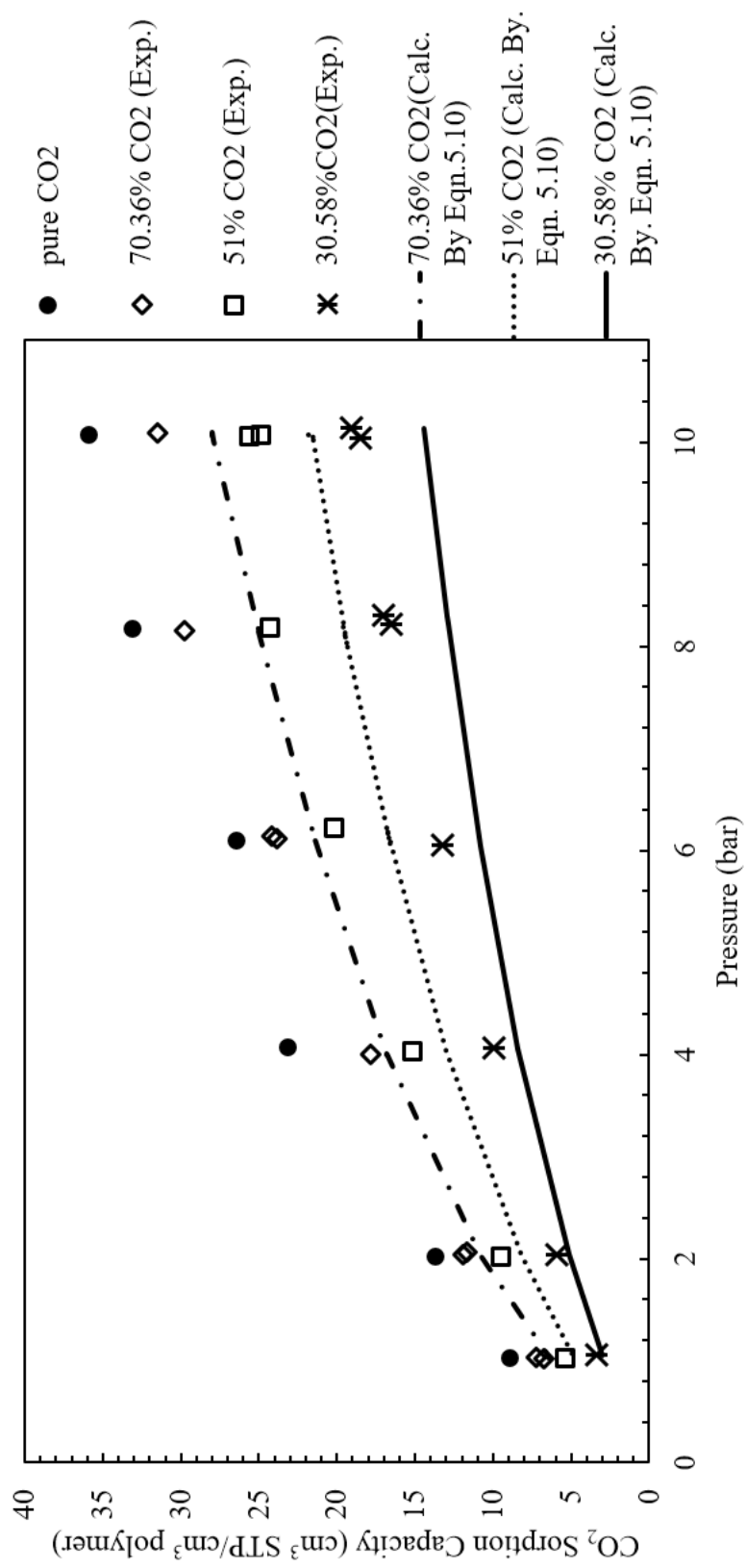


Figure 5.10 Pure and mixed gas solubility of CO₂ in symmetric PI-2 membrane at 35 °C at different mole fractions of CO₂ in the gaseous mixture.

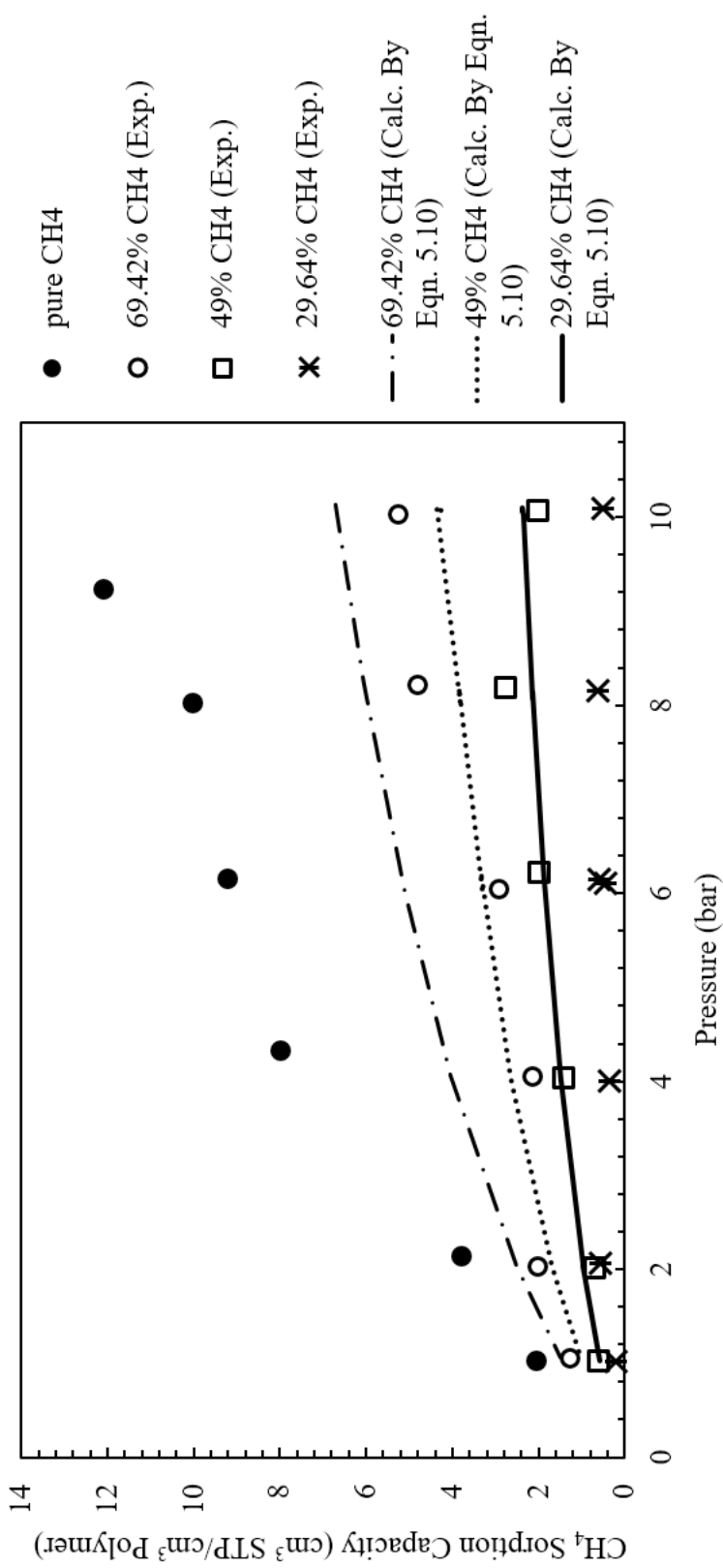


Figure 5.11 Pure and mixed gas sorption capacity of CH₄ in symmetric PI-2 membrane at 35 °C at different mole fractions of CH₄ in the gaseous mixture.

5.4 Sorption Capacity of the Mixed Matrix Dense Symmetric PI/ZIF-8 Membranes

CO₂ and CH₄ sorption capacity isotherms of mixed matrix membranes (MM-PI-1 and MM-PI-2) were given in Figure 5.12 and Figure 5.13, respectively. In these figures, both experimental sorption data and estimated sorption capacity were provided. The theoretical sorption capacity of mixed matrix membrane was estimated by the simple formula as Eqn. 5.12 (Moore and Koros, 2007). In our calculations, CO₂ and CH₄ sorption capacity of PI-2 membrane were used as polymer sorption capacity. The sorption capacity values of ZIF-8 were taken from the study of Perez-Pellitero et al. 2010. In all comparison (sorption capacity or dual mode sorption parameters), for the reference parameters, PI-2 was used because its properties were closer to those in literature relative to PI-1.

At first glance on Figure 5.12 and Figure 5.13, both CH₄ and CO₂ sorption capacity of membrane enhanced due to ZIF-8 loading. Several researchers experienced enhancement of solubility of gases in polymeric membranes due to addition of MOFs (Song et al. 2012, Bushell et al. 2013, Ge et al. 2013 Lin et al. 2014), or zeolites (Moore and Koros 2007).

The percent increment in CO₂ sorption capacity of the MM-PI-1 was determined approximately 2% at 1 bar, 5.5 % at 2 bar, 11% at 6 bar and 22% at 10 bar due to adding ZIF-8 at 10%. The CO₂ sorption capacity of MM-PI-2 are approximately 14%, 18%, 30% and 40% higher than that of PI-2 at 1 bar, 2 bar, 6 bar and 10 bar, respectively. The CO₂ sorption capacity of the MM-PI-2 was determined at least 10% greater than that of the MM-PI-1 at each test pressures. For both MM-PI-1 and MM-PI-2, the CO₂ sorption capacities estimated according to Eqn. 5.12 were higher than the experimentally determined CO₂ sorption values. At low pressures, 1 and 2 bars, the calculated CO₂ sorption values corresponded to the experimental values, perfectly. However, with increasing test pressures (>3 bar), the experimental data began to deviate from the calculated values. The percent of deviations changed depending on test pressures, however, drawing a trend is not possible. The relatively higher calculated CO₂ sorption capacity was actually

expected. One of the possible reason for that the ZIF-8 CO₂ sorption values used in the calculations were taken from the literature and may be higher than the ZIF-8s which we synthesized. Because in many studies in the literature, ZIF-8 has been subjected to many modifications, especially to increase CO₂ sorption capacity. The second possible explanation is partially-closed pores of ZIF-8 by polymer chain which might suppress the effect of ZIF-8s.

The CH₄ sorption capacity of MM-PI-1 are approximately 13%, 15%, and 20% higher than that of PI-2 at 4 bar, 6 bar, and 10 bar, respectively. At 1 bar, the CH₄ sorption capacity of MM-PI-1 and PI-2 was determined close to each other. For MM-PI-1, the estimated CH₄ sorption capacity values were pretty agreeing with the experimental data. The enhancement in CH₄ sorption extent was reached %33 at 2 bar, %51 at 4 bar, %56 at 6 bar and %62 at 10 bar with addition ZIF-8 at 20% of PI. The estimated CH₄ sorption capacity values of the MM-PI-2 were determined approximately 10% lower than experimental data at each testing pressures.

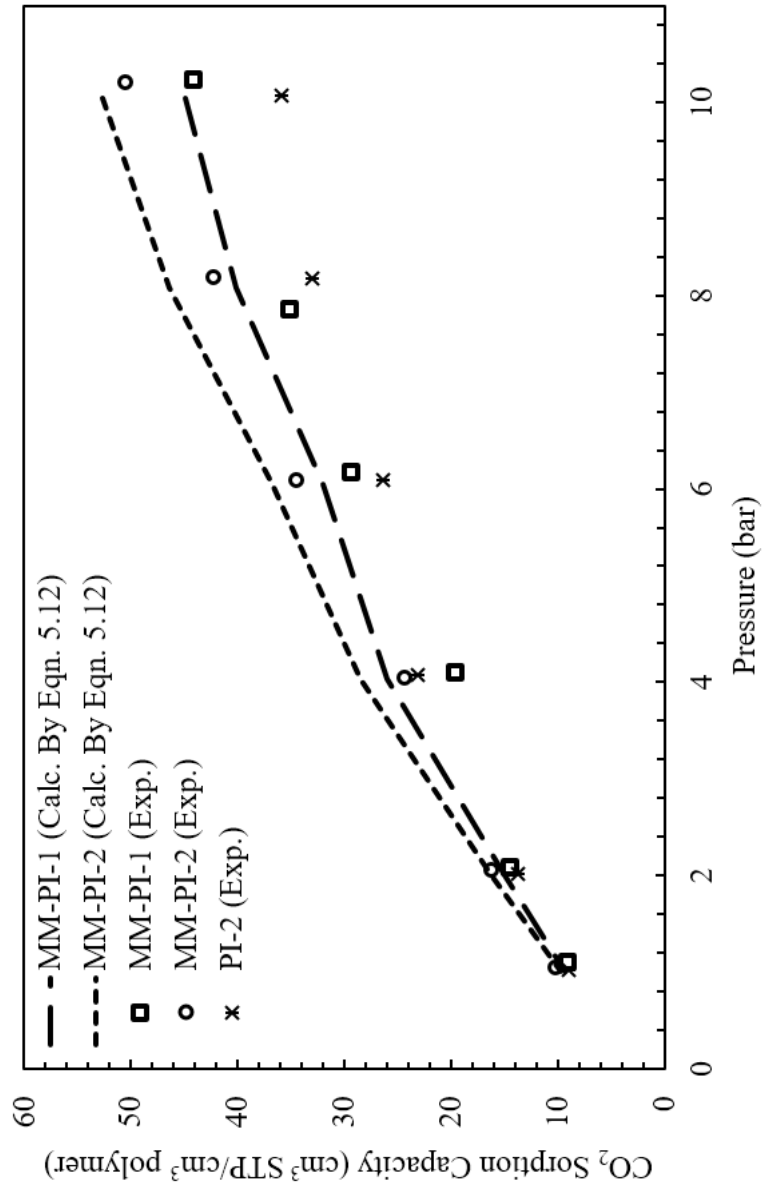


Figure 5.12 CO₂ sorption capacity of mixed matrix PI/ZIF-8 dense symmetric membranes at 35 °C.

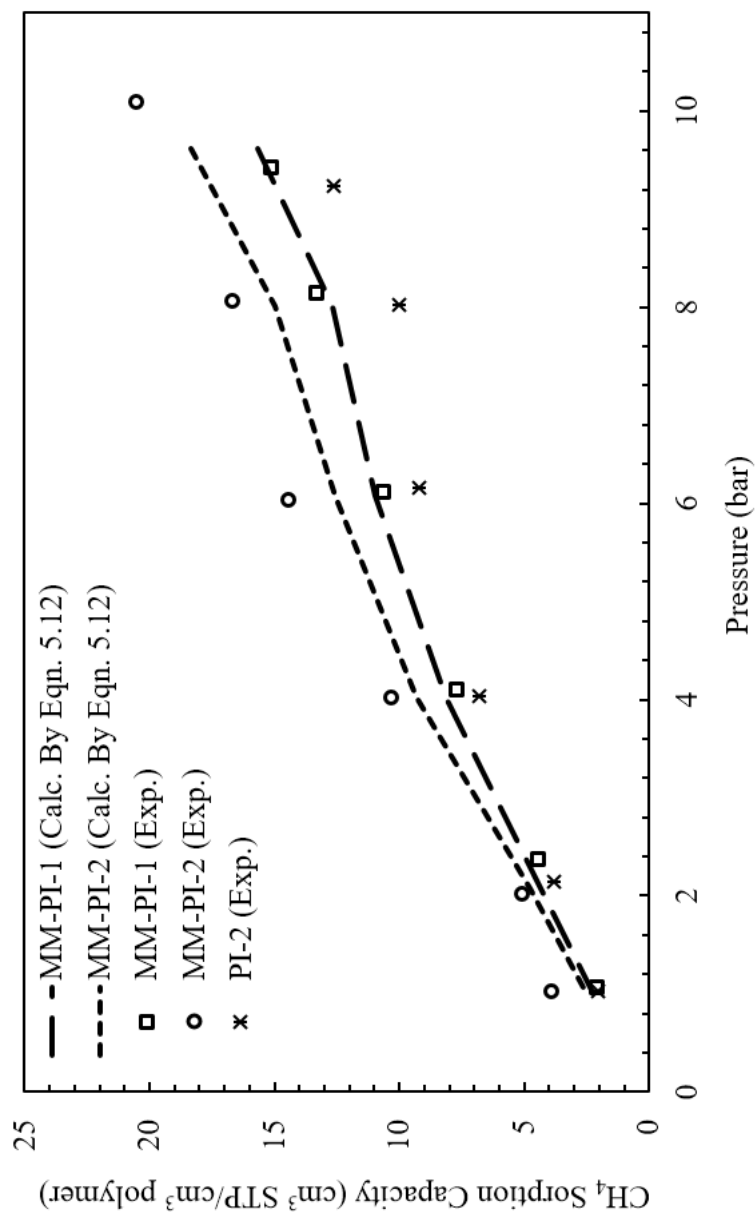


Figure 5.13 CH₄ sorption capacity of mixed matrix PI/ZIF-8 dense symmetric membranes at 35 °C.

The dual-mode sorption model constants of MM-PI-1 and MM-PI-2 were tabulated in Table 5.6. ZIF-8 loading leads to smaller C'_H values and larger k_D and b values as compared to neat PI-2 membrane.

The most influenced parameter due to ZIF-8 loading was k_D . The k_{D-CO_2} of MM-PI-1 was twice that of neat PI. The k_{D-CO_2} of MM-PI-2 was approximately two and a half times greater than the k_{D-CO_2} of neat PI. The increment in k_{D-CH_4} values were higher than that in k_{D-CO_2} values. The k_{D-CH_4} of MM-PI-1 was roughly 4.5 times and the k_{D-CH_4} of MM-PI-2 was roughly 6 times greater than that of neat PI. k_D is related to penetrant-polymer interactions and solubility of penetrant (Muruganandam et al. 1987). ZIF-8 loading into polymeric membrane increased the affinity between membrane and penetrants (CO_2 and CH_4) and also solubility of penetrant. Hence higher k_D values were obtained. The higher increment in the k_D of CH_4 as relative to the increase in the k_D of CO_2 was associated with the higher affinity between CH_4 and ZIF-8 in comparison with interaction between CH_4 and neat PI.

The percent decrease in C'_H of CO_2 were calculated 54% and 57% while that of CH_4 were estimated as 31% and 35% corresponding to 10% and 20% ZIF-8 loading, respectively. Since C'_H is associated with the unrelaxed free volume of the polymer (Koros et al. 1981, Chung et al. 2003), the decrease in the C'_H values was interpreted the diminish in the free volume of the polymer (Simons et al. 2010) due to ZIF-8 loading. The other possible explanation for reduction may be the tight polymer chain packing and stronger molecular interaction due to ZIF-8 particles (Chung et al. 2003).

Langmuir affinity constant b of CO_2 increased almost 66% in the presence of ZIF-8s. However, it was not affected by the increase in the amount of ZIF-8s. Langmuir affinity constant b of CH_4 was not changed significantly. The parameter, b is related to the ratio of penetrant sorption and desorption rate constants in Langmuir site (Solovyov and Goldman 2008, Scholes et al. 2010) and also condensability of penetrants (Muruganandam et al. 1987) and slightly related to structure of membrane (Masi, Paul and Barlow 1982). The ZIF-8 loading could not

change the condensability of gases. It may alter the structure but in this case I expected that a certain variation in b_{CH_4} . The presence of ZIF-8 particles may lead to increase sorption rate of CO_2 or decrease the desorption rate of CO_2 , hence higher b was obtained. This is the most logical explanation, since strong affinity between ZIF-8 and CO_2 is widely accepted phenomena (Venna and Carreon 2010, Banerjee et al., 2009).

Table 5.6 Dual-mode sorption constants for CO_2 and CH_4 based on sorption test of MM-PI-1 and MM-PI-2.

Membrane	Penetrant	k_D (cm^3 (STP)/(cm^3 polymer bar))	C'_H (cm^3 (STP) /(cm^3 polymer))	b (1/bar)	Squared Error
MM-PI-1	CO_2	3.0	13.0	1.0	3.45
	CH_4	1.0	11.6	0.1	0.11
MM-PI-2	CO_2	3.86	12.05	1.01	1.19
	CH_4	1.3	10.9	0.17	1.71

5.4.1 Mixed Gas Sorption Behavior of the Mixed Matrix Dense Symmetric PI/ZIF-8 Membranes

The sorption extent of MM-PI-1 for binary mixtures of CO_2 and CH_4 were measured at three fixed values of molar fraction on CH_4 in the gaseous phase: 27.6 mol%, 48.7 mol%, 69.4 mol%. Figure 5.14 and Figure 5.15 are the CO_2 and CH_4 sorption isotherms of MM-PI-1, respectively. Pure gas sorption extent and the sorption trend of MM-PI-1 for binary mixtures calculated based on Eqn. 5.10 and Eqn. 5.11 were also provided on the same isotherms. In calculations, the dual-mode sorption parameters listed in Table 5.6 were used.

As depicted in Figure 5.14, the CO_2 sorption extent of MM-PI-1 diminished due to presence of CH_4 . The average percent of diminishment in CO_2 sorption extent (cm^3 STP/ cm^3 polymer) with respect to pure CO_2 was approximately 19%, 33% and 56% in the presence of 27.6 mol%, 48.7 mol%, 69.4 mol% CH_4 in the feed gas, respectively. The experimental sorption data of CO_2 is very close to the corresponding data points calculated according to the Eqn. 5.10.

The reduction in sorption extent of CH₄ is higher than that of CO₂ due to competition effect (see isotherm in Figure 5.15). The CH₄ sorption extent (cm³ STP/cm³ polymer) of MM-PI-1 reduced by approximately 57%, 82% 98% due to presence of CO₂ at 30.5 mole %, 51.3 mole % and 72.4 mole% in the feed mixture. The experimental sorption data of CH₄ deviated strongly from the corresponding data points calculated according to the Eqn. 5.10. For example, for binary mixture 72.4 mole % CO₂- 27.6 mole % CH₄, the measured CH₄ sorption capacity points were lower than 0.5 cm³ STP/cm³ polymer even at 10 bar while the calculated CH₄ sorption capacity at 10 bar was estimated as 3.17 cm³ STP/cm³ polymer. The experimentally obtained CH₄ sorption points for the 48.7 % CH₄- 51.3 % CO₂ mixture coincided with the CH₄ sorption curve calculated for the 27.6% CH₄- %72.5% CO₂ mixture, while the experimentally obtained CH₄ sorption points for the 69.4 % CH₄- 30.6 % CO₂ mixture coincided with the CH₄ sorption curve calculated for the 48.7% CH₄- %51.3% CO₂ mixture. The reason of the large deviation between experimentally obtained CH₄ sorption values and corresponding calculated values is the fact that CH₄ sorption capacity measurement was affected more strongly by experimental errors than CO₂ since CH₄ is low sorbed gas. For example, for 48.7% CH₄- 51.3% CO₂ mixture sorption experiment at 10 bar, the GC test of residual gases was 55.26% CH₄. When 56% was used instead of 55.26% in the further calculations, the percent of variation in the CH₄ sorption extent was 41.82%, while that of variation in the CO₂ sorption amount was 4.1%. In this study, the GC test result of the two subsequent tests of the same mixture can be deviate 1.1% from each other. Hence, the low sensitivity of our GC may lead to sharp deviation in CH₄ test results. Smith et al 2012 suggested that largest possible error in sorption test is observed due to the volume calibration and its effect on low sorbing gases is higher than that on high sorbing gases. However, in our calculations, deviations in sample volume effected both CH₄ and CO₂ at the same amount. However, as suggested by Smith et al. 2012 and Robeson et al., low sorbing gas CH₄ affected 10 times higher than high sorbing gas CO₂ from the variation in GC results.

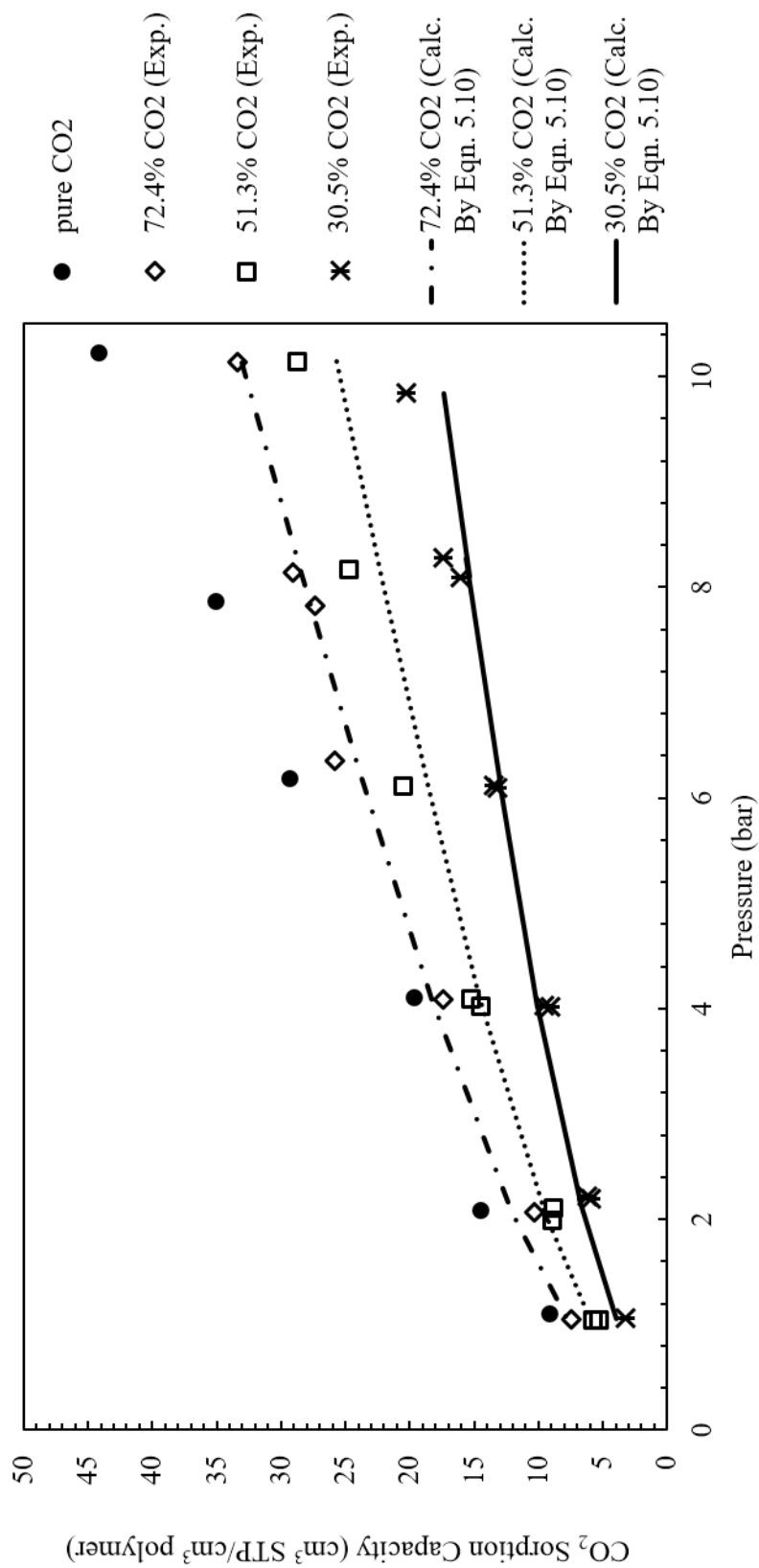


Figure 5.14 Pure and mixed gas sorption capacity of CO₂ in symmetric mixed matrix MM-PI-1 membrane at 35 °C at different mole fractions of CO₂ in the gaseous mixture.

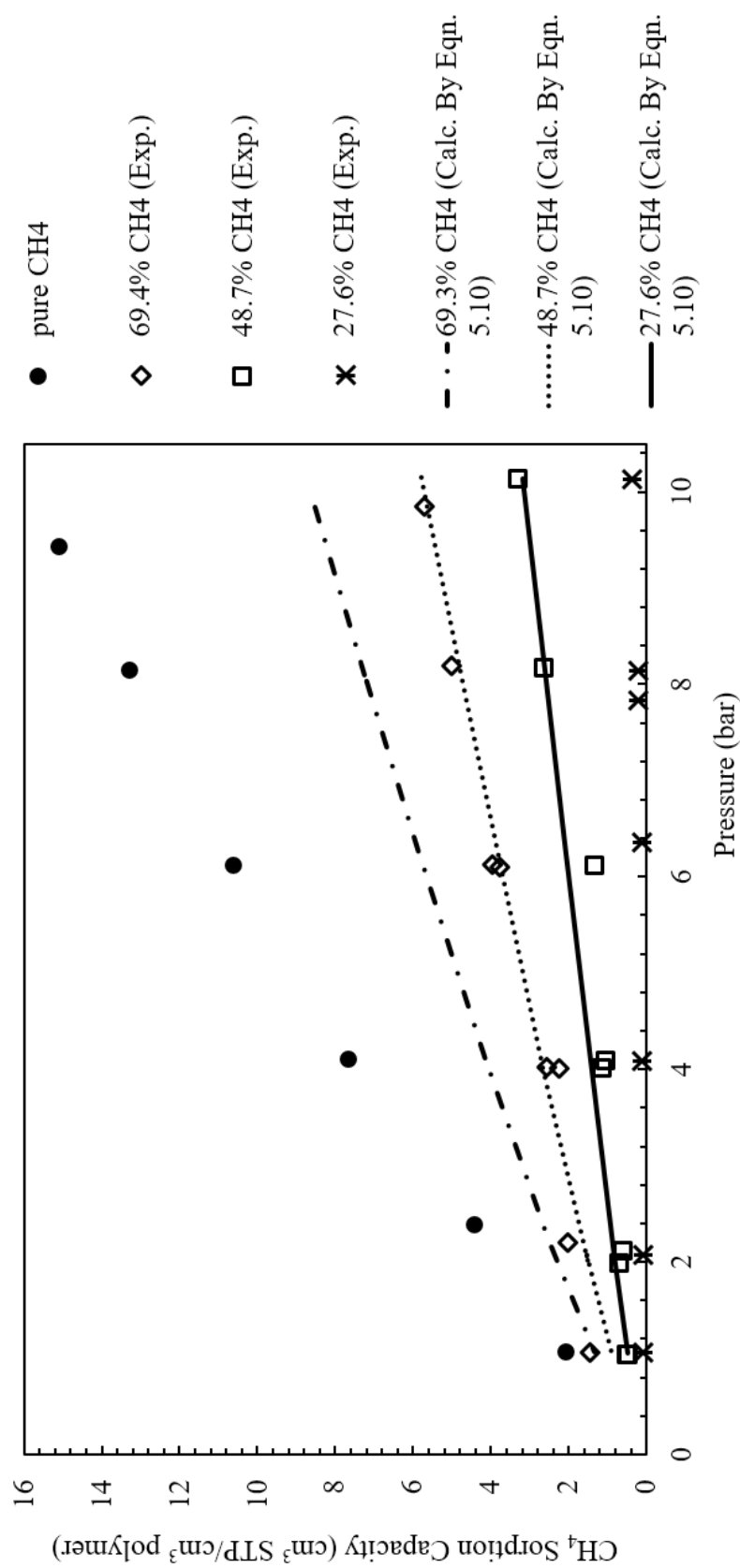


Figure 5.15 Pure and mixed gas sorption capacity of CH₄ in symmetric mixed matrix MM-PI-1 membrane at 35 °C at different mole fractions of CH₄ in the gaseous mixture.

Figure 5.16 showed the CO₂ sorption isotherms of MM-PI-2 for pure CO₂, CO₂ and CH₄ binary mixture in the presence of 27.6 mol%, 48.7 mol%, 69.4 mol% CH₄ in the feed gas and also estimated sorption extents of CO₂ in the mixtures test. The average percent of reduction in CO₂ sorption extent (cm³ STP/cm³ polymer) with respect to pure CO₂ was approximately 24%, 40% and 60% in the presence of 29.4 mol%, 49 mol%, 69.3 mol% CH₄ in the feed gas, respectively. The experimental sorption data of CO₂ is very close to the corresponding data points calculated according to the Eqn. 5.10.

The CH₄ sorption isotherms for pure gas, binary mixtures and estimated sorption curves of MM-PI-2 were given in Figure 5.17. The diminishment in sorption extent of CH₄ was calculated approximately 52%, 71% and 87% due to presence of CO₂ at 30.7 mole %, 51 mole % and 70.6 mole% in the feed mixture. The experimental sorption data of CH₄ in MM-PI-2 deviated from the corresponding data points calculated based on the Eqn. 5.10 as observed for MM-PI-1. However, the deviation was not as sharp as observed in MM-PI-1. The experimental points approached to the calculated curve.

The percent of reduction in CH₄ sorption of MM-PI-2 decreased and the percent of reduction in CO₂ of MM-PI-2 increased compared to the sorption extents of MM-PI-1. The reason is the increased affinity between CH₄ and MM-PI-2 due to high ZIF-8 content.

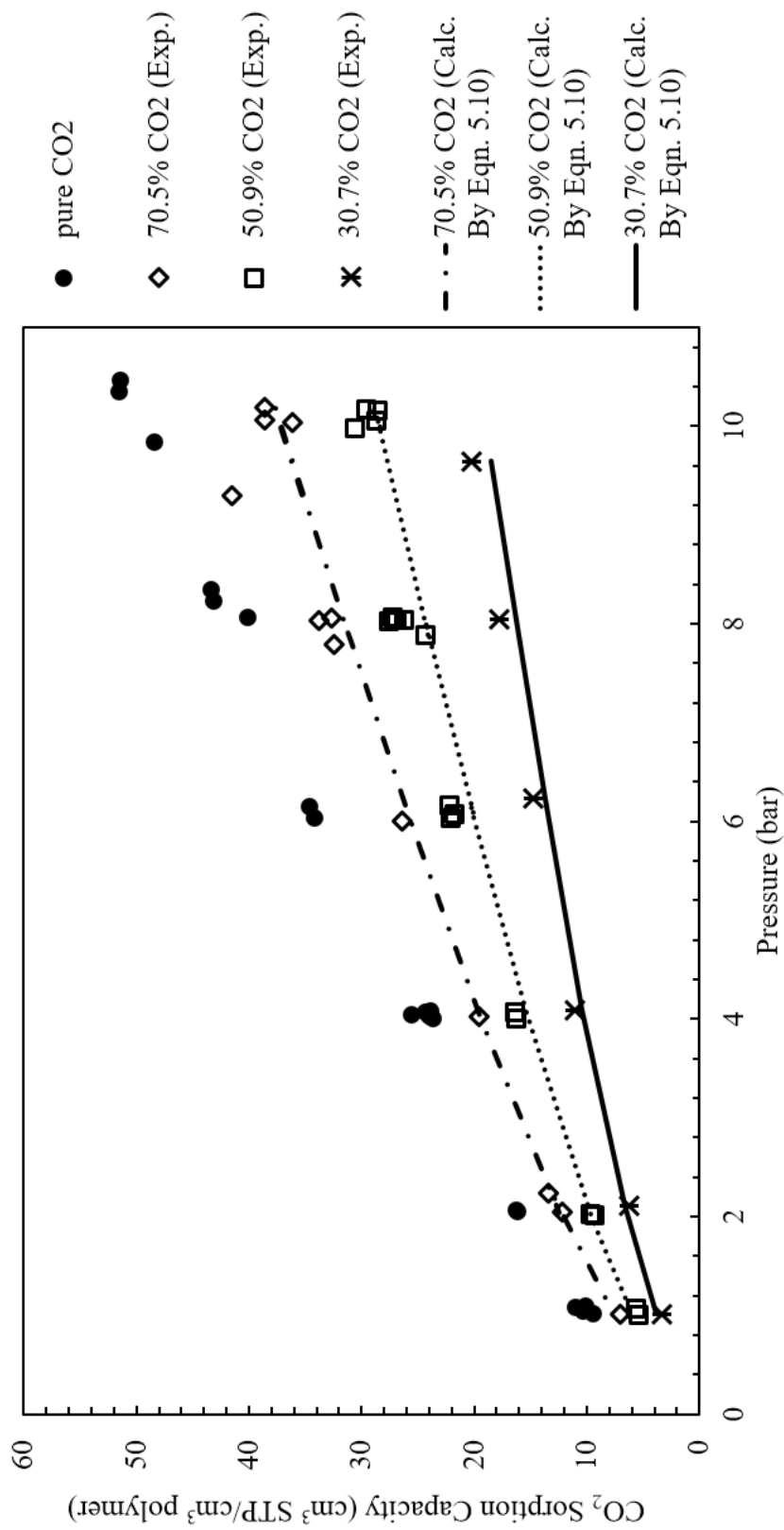


Figure 5.16 Pure and mixed gas sorption capacity of CO₂ in symmetric mixed matrix MM-PI-2 membrane at 35 °C at different mole fractions of CO₂ in the gaseous mixture.

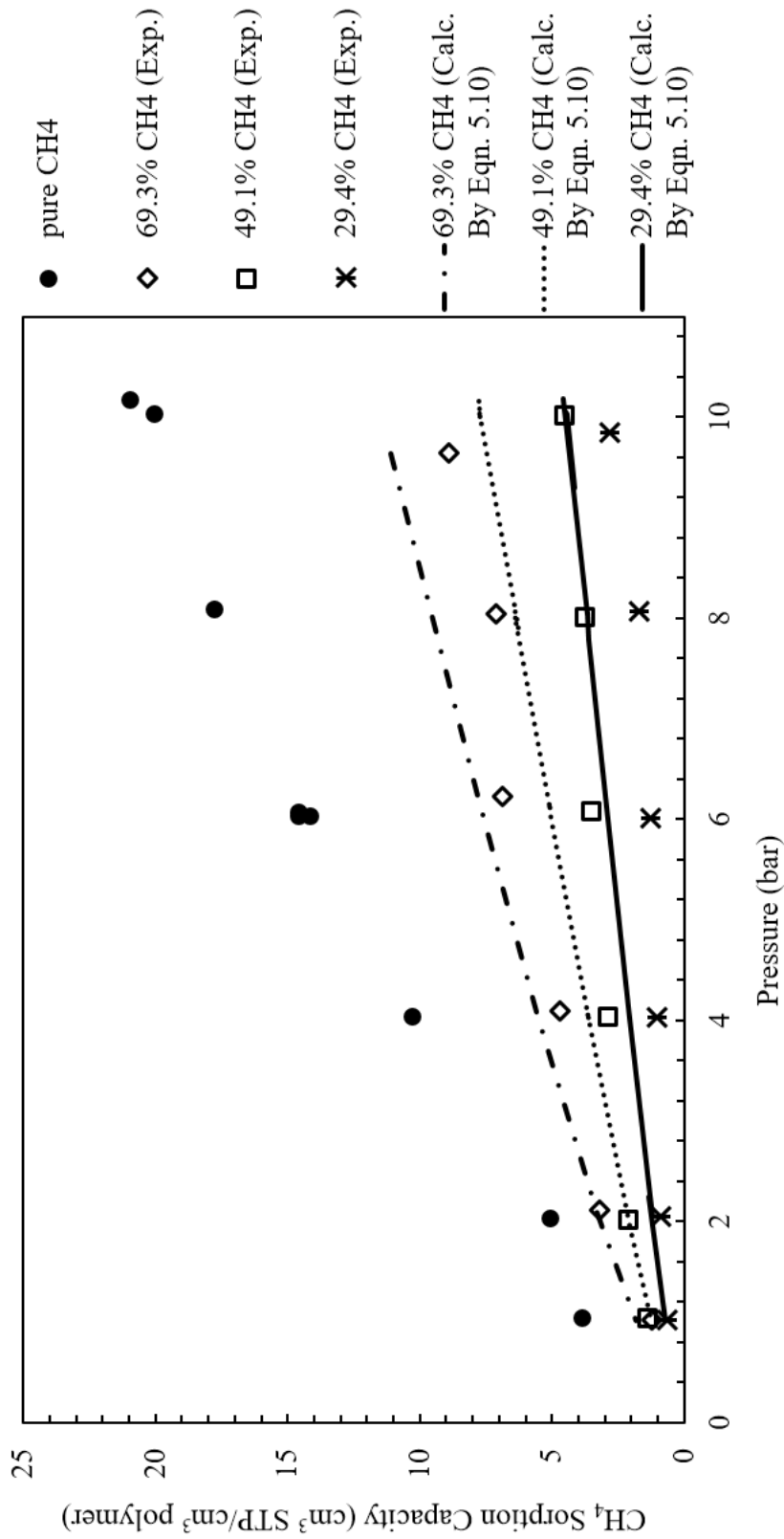


Figure 5.17 Pure and mixed gas sorption capacity of CH₄ in symmetric mixed matrix MM-PI-2 membrane at 35 °C at different mole fractions of CH₄ in the gaseous mixture.

5.5 Conclusions

The dense neat PI and ZIF-8/PI membranes were produced solvent evaporation method. The pressure decay method was used to determine CO₂ and CH₄ sorption capacity of membranes following conclusions have been drawn.

- CO₂ and CH₄ isotherms all demonstrate standard dual-sorption behavior. Isotherms are non-linear and concave to the pressure axis.
- The chemical associations between CO₂ and Matrimid are more thermodynamically favorable and hence the sorbed CO₂ concentration substantially higher than that for CH₄ at similar pressures.
- For mixture sorption experiment, the competitive effect lowers the ability of the penetrant to be sorbed in the matrix when a second penetrant is present within the same environment. The competition has a much stronger impact on CH₄ than on CO₂ sorption content.
- Sorption capacity of CO₂ and CH₄ were increased due to ZIF-8 incorporation.
- The dual-mode sorption model constants of MM-PI-1 and MM-PI-2 were calculated by non-linear least square curve fitting method. ZIF-8 loading leads to smaller C_H values and larger k_D and b values as compared to neat PI-2 membrane.

REFERENCES

- Aguilar-Vega, M., & Paul, D. R. (1993). Gas transport properties of polycarbonates and polysulfones with aromatic substitutions on the bisphenol connector group. *Journal of Polymer Science Part B: Polymer Physics*, 31(11), 1599-1610. doi:10.1002/polb.1993.090311116
- Banerjee, R., Furukawa, H., Britt, D., Knobler, C., O'Keeffe, M., & Yaghi, O. M. (2009). Control of Pore Size and Functionality in Isorecticular Zeolitic Imidazolate Frameworks and their Carbon Dioxide Selective Capture Properties. *Journal of the American Chemical Society*, 131(11), 3875-3877. doi:10.1021/ja809459e
- Barrer, R. M., Barrie, J. A., & Slater, J. (1958). Sorption and diffusion in ethyl cellulose. Part III. Comparison between ethyl cellulose and rubber. *Journal of Polymer Science*, 27(115), 177-197. doi:10.1002/pol.1958.1202711515
- Baschetti, M. G., Doghieri, F., & Sarti, G. C. (2001). Solubility in Glassy Polymers: Correlations through the Nonequilibrium Lattice Fluid Model. *Industrial & Engineering Chemistry Research*, 40(14), 3027-3037. doi:10.1021/ie000834q
- Boudouris, D., & Panayiotou, C. (1998). On the Solubility of Gas Molecules in Glassy Polymers and the Nonequilibrium Approach. *Macromolecules*, 31(22), 7915-7920. doi:10.1021/ma980382h
- Bushell, A. F., Attfield, M. P., Mason, C. R., Budd, P. M., Yampolskii, Y., Starannikova, L., ... Isaeva, V. (2013). Gas permeation parameters of mixed matrix membranes based on the polymer of intrinsic microporosity PIM-1 and the zeolitic imidazolate framework ZIF-8. *Journal of Membrane Science*, 427, 48-62. doi:10.1016/j.memsci.2012.09.035
- Cain, E. J., Wen, W., Jones, A. A., Inglefield, P. T., Cauley, B. J., & Bendler, J. T. (1991). A dual-mode interpretation of spin relaxation for ¹³CO₂ sorbed in polycarbonate. *Journal of Polymer Science Part B: Polymer Physics*, 29(8), 1009-1020. doi:10.1002/polb.1991.090290811
- Chan, A. H., & Paul, D. R. (1979). Influence of history on the gas sorption, thermal, and mechanical properties of glassy polycarbonate. *Journal of Applied Polymer Science*, 24(6), 1539-1550. doi:10.1002/app.1979.070240615
- Chen, S. (1997). Sorption and transport mechanism of gases in polycarbonate membranes. *Journal of Membrane Science*, 134(2), 143-150. doi:10.1016/s0376-7388(97)00132-4
- Chern, R. T., Koros, W. J., Yui, B., Hopfenberg, H. B., & Stannett, V. T. (1984). Selective permeation of CO₂ and CH₄ through kapton polyimide: Effects of penetrant competition and gas-phase nonideality. *Journal of Polymer Science: Polymer Physics Edition*, 22(6), 1061-1084. doi:10.1002/pol.1984.180220610
- Chung, T., Chan, S. S., Wang, R., Lu, Z., & He, C. (2003). Characterization of permeability and sorption in Matrimid/C60 mixed matrix membranes. *Journal of Membrane Science*, 211(1), 91-99.

- doi:10.1016/s0376-7388(02)00385-x
- Conforti, R. M., Barbari, T. A., Vimalchand, P., & Donohue, M. D. (1991). A lattice-based activity coefficient model for gas sorption in glassy polymers. *Macromolecules*, 24(11), 3388-3394. doi:10.1021/ma00011a054
- Costello, L. M., & Koros, W. J. (1992). Temperature dependence of gas sorption and transport properties in polymers: measurement and applications. *Industrial & Engineering Chemistry Research*, 31(12), 2708-2714. doi:10.1021/ie00012a012
- Costello, L. M., & Koros, W. J. (1994). Effect of structure on the temperature dependence of gas transport and sorption in a series of polycarbonates. *Journal of Polymer Science Part B: Polymer Physics*, 32(4), 701-713. doi:10.1002/polb.1994.090320412
- Costello, L. M., & Koros, W. J. (1995). Thermally stable polyimide isomers for membrane-based gas separations at elevated temperatures. *Journal of Polymer Science Part B: Polymer Physics*, 33(1), 135-146. doi:10.1002/polb.1995.090330114
- Doghieri, F., & Sarti, G. C. (1996). Nonequilibrium Lattice Fluids: A Predictive Model for the Solubility in Glassy Polymers. *Macromolecules*, 29(24), 7885-7896. doi:10.1021/ma951366c
- Dorosti, F., Omidkhah, M., & Abedini, R. (2015). Enhanced CO₂/CH₄ separation properties of asymmetric mixed matrix membrane by incorporating nanoporous ZSM-5 and MIL-53 particles into Matrimid®5218. *Journal of Natural Gas Science and Engineering*, 25, 88-102. doi:10.1016/j.jngse.2015.04.033
- Duda, J. L., & Zielinski, J. M. (1996). Free-Volume Theory. *Plastics Engineering*, 32(143).
- Fairen-Jimenez, D., Moggach, S. A., Wharmby, M. T., Wright, P. A., Parsons, S., & Düren, T. (2011). Opening the Gate: Framework Flexibility in ZIF-8 Explored by Experiments and Simulations. *Journal of the American Chemical Society*, 133(23), 8900-8902. doi:10.1021/ja202154j
- Ge, L., Zhou, W., Rudolph, V., & Zhu, Z. (2013). Mixed matrix membranes incorporated with size-reduced Cu-BTC for improved gas separation. *Journal of Materials Chemistry A*, 1(21), 6350. doi:10.1039/c3ta11131h
- Higuchi, A., & Nakagawa, T. (1994). Infrared spectroscopic studies of CO₂ sorbed in glassy and rubbery polymeric membranes. *Journal of Polymer Science Part B: Polymer Physics*, 32(1), 149-157. doi:10.1002/polb.1994.090320118
- Kanehashi, S., & Nagai, K. (2005). Analysis of dual-mode model parameters for gas sorption in glassy polymers. *Journal of Membrane Science*, 253(1-2), 117-138. doi:10.1016/j.memsci.2005.01.003
- Kim, S., Seong, J. G., Do, Y. S., & Lee, Y. M. (2015). Gas sorption and transport in thermally rearranged polybenzoxazole membranes derived from polyhydroxylamides. *Journal of Membrane Science*, 474, 122-131. doi:10.1016/j.memsci.2014.09.051

- Koros, W. J. (1980). Model for sorption of mixed gases in glassy polymers. *Journal of Polymer Science: Polymer Physics Edition*, 18(5), 981-992. doi:10.1002/pol.1980.180180506
- Koros, W. J. (1985). Simplified analysis of gas/polymer selective solubility behavior. *Journal of Polymer Science: Polymer Physics Edition*, 23(8), 1611-1628. doi:10.1002/pol.1985.180230813
- Koros, W. J., Chern, R. T., Stannett, V., & Hopfenberg, H. B. (1981). A model for permeation of mixed gases and vapors in glassy polymers. *Journal of Polymer Science: Polymer Physics Edition*, 19(10), 1513-1530. doi:10.1002/pol.1981.180191004
- Koros, W. J., & Paul, D. R. (1976). Design Considerations for Measurement of Gas Sorption in Polymers by Pressure Decay. *Journal of Polymer Science*, 14, 1903-1907.
- Koros, W. J., & Paul, D. R. (1978). CO₂ sorption in poly(ethylene terephthalate) above and below the glass transition. *Journal of Polymer Science: Polymer Physics Edition*, 16(11), 1947-1963. doi:10.1002/pol.1978.180161105
- Koros, W. J., & Paul, D. R. (1980). Sorption and transport of CO₂ above and below the glass transition of poly(ethylene terephthalate). *Polymer Engineering and Science*, 20(1), 14-19. doi:10.1002/pen.760200104
- Lin, R., Ge, L., Hou, L., Strounina, E., Rudolph, V., & Zhu, Z. (2014). Mixed Matrix Membranes with Strengthened MOFs/Polymer Interfacial Interaction and Improved Membrane Performance. *ACS Applied Materials & Interfaces*, 6(8), 5609-5618. doi:10.1021/am500081e
- Li, P., Chung, T., & Paul, D. (2013). Gas sorption and permeation in PIM-1. *Journal of Membrane Science*, 432, 50-57. doi:10.1016/j.memsci.2013.01.009
- Li, P., Chung, T., & Paul, D. (2014). Temperature dependence of gas sorption and permeation in PIM-1. *Journal of Membrane Science*, 450, 380-388. doi:10.1016/j.memsci.2013.09.030
- Lipscomb, G. G. (1990). Unified thermodynamic analysis of sorption in rubbery and glassy materials. *AIChE Journal*, 36(10), 1505-1516. doi:10.1002/aic.690361006
- Loat, C. M. (2001). *Gas Transport Properties in Polycarbonate Influence of the Cooling Rate, Physical Aging, and Orientation* (Unpublished doctoral dissertation). Virginia Polytechnic Institute and State University, Blacksburg, Virginia, VA.
- Masi, P., Paul, D. R., & Barlow, J. W. (1982). Gas sorption and transport in a copolyester and its blend with polycarbonate. *Journal of Polymer Science: Polymer Physics Edition*, 20(1), 15-26. doi:10.1002/pol.1982.180200102
- McEwen, J., Hayman, J., & Ozgur Yazaydin, A. (2013). A comparative study of CO₂, CH₄ and N₂ adsorption in ZIF-8, Zeolite-13X and BPL activated carbon. *Chemical Physics*, 412, 72-76. doi:10.1016/j.chemphys.2012.12.012
- Moore, T. T., & Koros, W. J. (2007). Gas sorption in polymers, molecular sieves, and mixed matrix membranes. *Journal of Applied Polymer Science*, 104(6), 4053-4059. doi:10.1002/app.25653

- Muruganandam, N., Koros, W. J., & Paul, D. R. (1987). Gas sorption and transport in substituted polycarbonates. *Journal of Polymer Science Part B: Polymer Physics*, 25(9), 1999-2026. doi:10.1002/polb.1987.090250917
- O'Brien, K. C., Koros, W. J., & Husk, G. R. (1987). Influence of casting and curing conditions on gas sorption and transport in polyimide films. *Polymer Engineering and Science*, 27(3), 211-217. doi:10.1002/pen.760270306
- Pixton, M. R., & Paul, D. R. (1995). Gas transport properties of polyarylates part I: Connector and pendant group effects. *Journal of Polymer Science Part B: Polymer Physics*, 33(7), 1135-1149. doi:10.1002/polb.1995.090330717
- Puleo, A., Paul, D., & Kelley, S. (1989). The effect of degree of acetylation on gas sorption and transport behavior in cellulose acetate. *Journal of Membrane Science*, 47(3), 301-332. doi:10.1016/s0376-7388(00)83083-5
- Punsalan, D., & Koros, W. J. (2005). Thickness-dependent sorption and effects of physical aging in a polyimide sample. *Journal of Applied Polymer Science*, 96(4), 1115-1121. doi:10.1002/app.21544
- Pérez-Pellitero, J., Amrouche, H., Siperstein, F., Pirngruber, G., Nieto-Draghi, C., Chaplais, G., Bats, N. (2010). Adsorption of CO₂, CH₄, and N₂ on Zeolitic Imidazolate Frameworks: Experiments and Simulations. *Chemistry - A European Journal*, 16(5), 1560-1571. doi:10.1002/chem.200902144
- Raharjo, R. D., Freeman, B. D., Paul, D. R., & Sanders, E. S. (2007). Pure and mixed gas CH₄ and n-C₄H₁₀ permeability and diffusivity in poly(1-trimethylsilyl-1-propyne). *Polymer*, 48(25), 7329-7344. doi:10.1016/j.polymer.2007.10.024
- Rein, D., Baddour, R., & Cohen, R. (1992). Gas solubility in glassy polymers—a correlation with excess enthalpy. *Polymer*, 33(8), 1696-1700. doi:10.1016/0032-3861(92)91069-e
- Ribeiro, C. P., & Freeman, B. D. (2010). Carbon dioxide/ethane mixed-gas sorption and dilation in a cross-linked poly(ethylene oxide) copolymer. *Polymer*, 51(5), 1156-1168. doi:10.1016/j.polymer.2010.01.012
- Saberi, M., Hashemifard, S. A., & Dadkhah, A. A. (2016). Modeling of CO₂/CH₄ gas mixture permeation and CO₂ induced plasticization through an asymmetric cellulose acetate membrane. *RSC Adv*, 6(20), 16561-16567. doi:10.1039/c5ra23506e
- Scholes, C. A., Tao, W. X., Stevens, G. W., & Kentish, S. E. (2010). Sorption of methane, nitrogen, carbon dioxide, and water in Matrimid 5218. *Journal of Applied Polymer Science*, 117(4), 2284-2289. doi:10.1002/app.32148
- Sefcik, M. D., & Schaefer, J. (1983). Solid-state ¹³C NMR evidence for gas-polymer interactions in the carbon dioxide-poly(vinyl chloride) system. *Journal of Polymer Science: Polymer Physics Edition*, 21(7), 1055-1062. doi:10.1002/pol.1983.180210706
- Simons, K., Nijmeijer, K., Sala, J. G., Van der Werf, H., Benes, N. E., Dingemans, T. J., & Wessling, M. (2010). CO₂ sorption and transport behavior of OPA-based polyetherimide polymer films. *Polymer*, 51(17), 3907-3917. doi:10.1016/j.polymer.2010.06.031

- Sirard, S. M., Green, P. F., & Johnston, K. P. (2001). Spectroscopic Ellipsometry Investigation of the Swelling of Poly(Dimethylsiloxane) Thin Films with High Pressure Carbon Dioxide. *The Journal of Physical Chemistry B*, 105(4), 766-772. doi:10.1021/jp002592d
- Smith, Z. P., Sanders, D. F., Ribeiro, C. P., Guo, R., Freeman, B. D., Paul, D. R., ... Swinnea, S. (2012). Gas sorption and characterization of thermally rearranged polyimides based on 3,3'-dihydroxy-4,4'-diamino-biphenyl (HAB) and 2,2'-bis-(3,4-dicarboxyphenyl) hexafluoropropane dianhydride (6FDA). *Journal of Membrane Science*, 415-416, 558-567. doi:10.1016/j.memsci.2012.05.050
- Solovyov, S., & Goldman, A. (2008). *Mass transport & reactive barriers in packaging: Theory, applications, & design*. Lancaster, Pa.: DEStech Pub.
- Song, Q., Nataraj, S. K., Roussanova, M. V., Tan, J. C., Hughes, D. J., Li, W., Sivaniah, E. (2012). Zeolitic imidazolate framework (ZIF-8) based polymer nanocomposite membranes for gas separation. *Energy & Environmental Science*, 5(8), 8359. doi:10.1039/c2ee21996d
- Tsujita, Y. (2003). Gas sorption and permeation of glassy polymers with microvoids. *Progress in Polymer Science*, 28(9), 1377-1401. doi:10.1016/s0079-6700(03)00048-0
- Venna, S. R., & Carreon, M. A. (2010). Highly Permeable Zeolite Imidazolate Framework-8 Membranes for CO₂/CH₄ Separation. *Journal of the American Chemical Society*, 132(1), 76-78. doi:10.1021/ja909263x
- Visser, T., Koops, G., & Wessling, M. (2005). On the subtle balance between competitive sorption and plasticization effects in asymmetric hollow fiber gas separation membranes. *Journal of Membrane Science*, 252(1-2), 265-277. doi:10.1016/j.memsci.2004.12.015
- Vopička, O., De Angelis, M. G., Du, N., Li, N., Guiver, M. D., & Sarti, G. C. (2014). Mixed gas sorption in glassy polymeric membranes: II. CO₂/CH₄ mixtures in a polymer of intrinsic microporosity (PIM-1). *Journal of Membrane Science*, 459, 264-276. doi:10.1016/j.memsci.2014.02.003
- Wessling, M., Lidon Lopez, M., & Strathmann, H. (2001). Accelerated plasticization of thin-film composite membranes used in gas separation. *Separation and Purification Technology*, 24(1-2), 223-233. doi:10.1016/s1383-5866(01)00127-7
- Wind, J. D., Sirard, S. M., Paul, D. R., Green, P. F., Johnston, K. P., & Koros, W. J. (2003). Carbon Dioxide-Induced Plasticization of Polyimide Membranes: Pseudo-Equilibrium Relationships of Diffusion, Sorption, and Swelling. *Macromolecules*, 36(17), 6433-6441. doi:10.1021/ma0343582
- Zhang, L., Wu, G., & Jiang, J. (2014). Adsorption and Diffusion of CO₂ and CH₄ in Zeolitic Imidazolate Framework-8: Effect of Structural Flexibility. *The Journal of Physical Chemistry C*, 118(17), 8788-8794. doi:10.1021/jp500796e
- Zhang, Z., Xian, S., Xia, Q., Wang, H., Li, Z., & Li, J. (2013). Enhancement of CO₂ Adsorption and CO₂/N₂ Selectivity on ZIF-8 via Postsynthetic Modification. *AIChE Journal*, 59(6), 2195-2206. doi:10.1002/aic.13970
- Zielinski, J. M., & Duda, J. L. (1996). Solvent Diffusion in Polymeric Systems. *Plastics Engineering*, 33(35).

APPENDICES

A. EXPERIMENTAL RESULTS OF PES MEMBRANES PRODUCED VIA LIDWPI METHOD

Production Method

Asymmetric PES Membrane Preparation via Dry-Wet Phase Inversion: A homogeneous polymer solution made up of 4 g of PES, 4 g of Acetone and 10 mL (9.5 g) of DMF (23 wt.% PES- 23 wt.% Acetone- 54 wt. % DMF) solution was prepared by priming at three step. PES solution film casted at 500 μm by automatic film applicator was kept in an air-dried vessel with zeolite at room temperature for 15 minutes for dry phase inversion. 500 ml of distilled water was used for wet phase change. Solvent removing and annealing procedure were the same as those applied for wet phase inversion PES membranes and was already narrated in Chapter 2. In order to investigate the effects of the acetone content on the properties of membrane, the polymer solution was prepared by increasing the amount of acetone to 5 and 6 grams. In order to keep the polymer concentration constant, the amount of DMF was reduced to 8.5 and 7.5 grams. The some of the produced membranes were coated with PDMS to plug the pin holes by dip coating method. Membranes were immersed in 3% PDMS-n hexane solution and allowed to stand overnight. These were cured under vacuum for one hour at 60 ° C.

Forced Dry-Wet Phase Inversion for PES Membranes: The polymer solution was prepared as described previously. To increase the evaporation rate of acetone in solution, it was exposed to light for 2.5 to 15 minutes. Hence denser polymer surface layer was formed. We estimated that this denser layer will reduce the formation of surface defects. A light lamp with energy class D of 77 W, 250 V was used as light source. All other membrane preparation processes are the same as the dry-wet phase inversion method. PES membranes prepared via dry-wet phase inversion and light induced dry-wet phase inversion method were listed in Table A.1 with their production specifications and their codes.

Table A.1 PES membranes produced via DWPI and LIDWPI methods.

Membrane Codes	Membrane Solution (g)		Dry Inversion Period
PP-37	PES	4	15 min free evaporation
	Acetone	4	
	DMF	9.5	
PP-39	PES	5	
	Acetone	4	
	DMF	9.5	
PP-41	PES	4	
	Acetone	4	
	DMF	9.5	
PP-42	PES	4	
	Acetone	4	
	DMF	9.5	
PP-43	PES	4	
	Acetone	4	
	DMF	9.5	
PP-44	PES	4	
	Acetone	4	
	DMF	9.5	
PP-45	PES	4	
	Acetone	5	
	DMF	8.5	
PP-46	PES	4	
	Acetone	2	
	DMF	11.5	
PP-47	PES	4	
	Acetone	2	
	DMF	11.5	

Table A.1 (Cont.) PES membranes produced via DWPI and LIDWPI methods.

Membrane Codes	Membrane Solution (g)		Dry Inversion Period
PP-48	PES	4	15 min free evaporation
	Acetone	4	
	DMF	9.5	
PP-53	PES	4	
	Acetone	6	
	DMF	7.5	
PP-55	PES	4	
	Acetone	6	
	DMF	7.5	
PP-56	PES	4	
	Acetone	5	
	DMF	8.5	
PP-60	PES	4	15 min incandescent lamp exposure
	Acetone	4	
	DMF	9.5	
PP-61	PES	4	15 min incandescent lamp exposure
	Acetone	4	
	DMF	9.5	
PP-62	PES	4	10 min incandescent lamp exposure
	Acetone	4	
	DMF	9.5	
PP-64	PES	4	10 min incandescent lamp exposure
	Acetone	5	
	DMF	8.5	
PP-66	PES	4	15 min incandescent lamp exposure
	Acetone	5	
	DMF	8.5	

Experimental Results of PES

In this part of the study, I investigated the variation of morphological and gas transport properties of PES membranes due to addition of co-solvent acetone in PES-DMF polymer solution. Co-solvent additives in the polymer solution is applied because it is known that volatile solvent can change liquid-liquid demixing behavior during phase inversion (Aroon et al. 2010). Furthermore, its volatility promotes the evaporation rate during dry-inversion period.

The Hansen solubility parameter differences for PES-acetone, Acetone-DMF, Acetone-water, Water-PES and Water-DMF were provided in Table A.2. The Hansen solubility parameters was taken from Guillen et al. 2011 and the parameter difference was calculated according to Eqn. 2.2 (Chapter 2). Since the $\Delta\delta_{\text{PES-Acetone}}$ and $\Delta\delta_{\text{DMF-Acetone}}$ are both less than 8, hence we can assume that PES-DMF-Acetone trio quite miscible with each other. The $\Delta\delta_{\text{Water-Acetone}}$ is very close $\Delta\delta_{\text{Water-DMF}}$, hence the interaction between water and acetone is similar to the interaction between water and DMF.

Table A.2 Hansen solubility parameter difference ($\Delta\delta$) between polymer (PES)-solvent (DMF)-co-solvent(Acetone)-quench medium(Water).

Chemicals	DMF	Acetone	Water
PES	4.3	5.19	34.4
Solvent (DMF)	-	7.12	31.1
Co-solvent (Acetone)	7.12	-	33.2

There are several studies in literature about effect of acetone on membrane properties (Vogrin et al. 2002, Krol et al. 2001, Visser et al. 2007, Barth et al. 2000, Madaeni et al. 2005, Ahmed et al. 2014, Chabot et al. 1997, Ahmed et al. 2013) (Note that the references given in Appendix A are provided in the REFERENCE part of the Chapter 3). They used acetone to facilitate evaporation step.

Effect of Acetone Content of the Casting Solution on Morphological Properties of Asymmetric PES Membranes Produced via DWPI Method for 15 min free-evaporation

Figure A.1 showed the SEM micrographs of asymmetric PES membranes; PP-47, PP-37, PP-56, PP-55 which are prepared PES solutions containing 11.4%, 22.9%, 28.6%, 34.3% AC. During casting period these membranes were standing free-evaporation for 15 minutes and quenched in 500 ml DI water. At first glance, membranes seemed to be composed of pores in different size.

PP-47 included both sponge like and finger like pores. Total thickness of PP-47 was nearly 500 μm . Size of the finer like pores closer to dense layer was smaller than that of the finger like pores settled on the middle. A closer look at surface layer; it was measured a dense layer with approximately 400 nm supported with fine pores.

PP-37 was made up of only sponge like pores; it cannot be detected finger like pores from SEM micrographs. However, locally small sponge like pores combined and forms larger sponge like pores. A closer look at dense layer, it was observed approximately 300 nm dense layer at upon the layer with nearly 5 μm thickness made up of very tiny pores. I named this finely pored thin region as transition zone.

The morphology of membranes PP-55 and PP-56 have very similar structure. Both of them have pores in elliptical shape rather than finger like or sponge like and pores walls were in reticular form. Based on eye investigation, the thickness of transition zone and porosity of it increased with increase in the content of AC.

Table A.3 was given the quantitative analyses of morphological properties of membranes based on SEM images. The thickness of dense skin layer was about 100-200 nm. The thickness of skin layer of membrane did not change with increasing amount of acetone, which is unexpected results. Because it was presumed that the skin layer will be formed by the evaporation of AC during dry phase change. Based on this assumption, the thickness of the skin layer becomes

thicker as the amount of AC increases. Our observation was also conflicted with Krol et al. 2001 who revealed enlargement in thickness of skin layer of PI membrane from 0.4 to 1.3 μm due to increasing AC content of PI/NMP/AC solution from 30 wt.% to 37.5 wt.%. On the other hand, Barth et al. 2000 could not detect an obvious change in morphological structure of PES and PSF membranes despite including 3% acetone in the polymer-DMF solution. This observation enhanced the suggestion that the membrane morphology is mainly determined by wet phase inversion step. Although the evaporation of volatile solvent creates denser polymer layer and also the formation of skin layer begins in this period; a new thermodynamic equilibrium will be established in the quenching medium and the thickness and properties of skin layer is mainly depending on this new thermodynamic equilibrium. For our polymer-solvent-nonsolvent system, a sharp concentration gradient and fast solvent-nonsolvent exchange may be formed within a thin layer which will be constituted the dense skin layer, laterally.

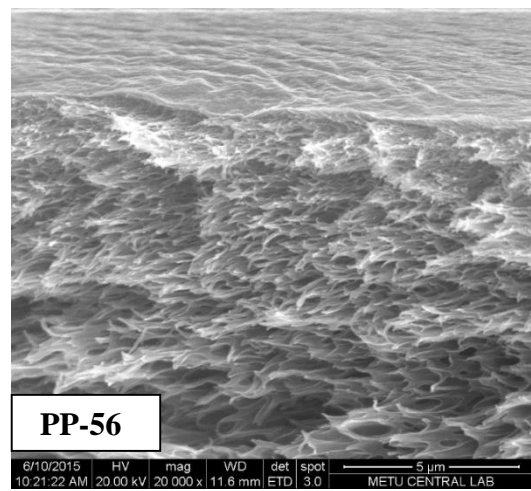
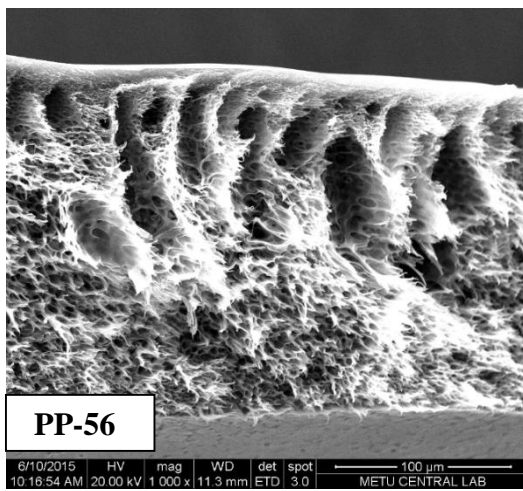
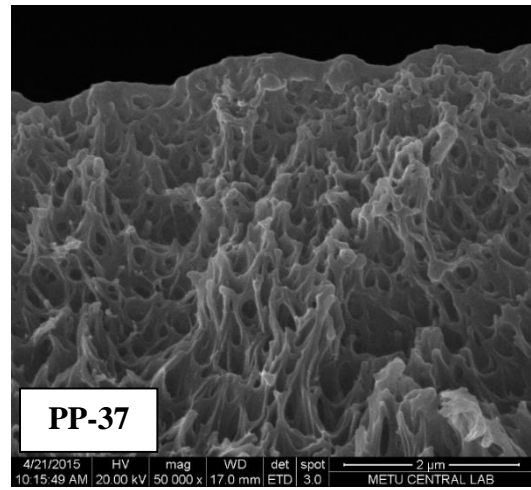
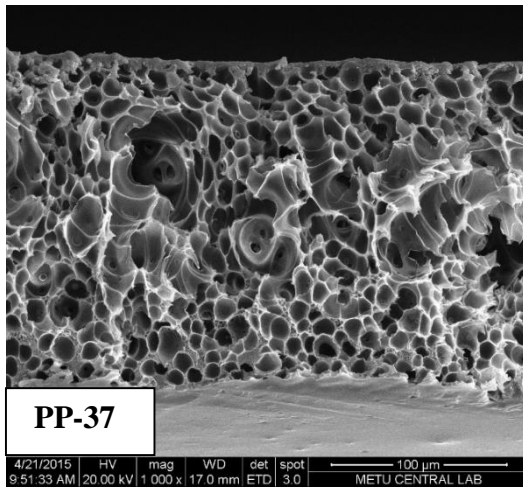
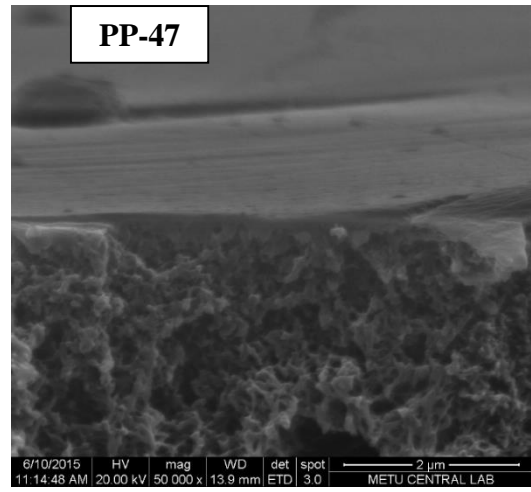
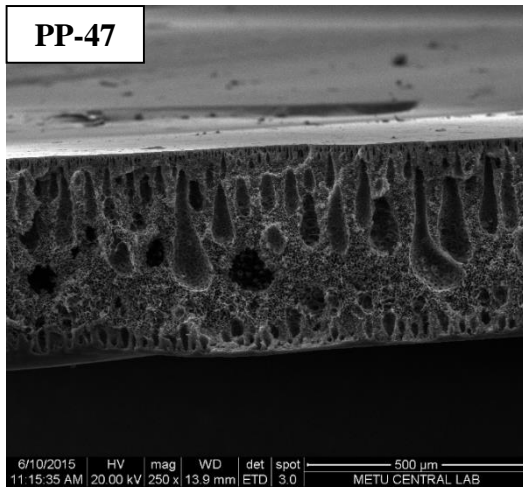
The thickness of transition zone increased in proportion to the amount of acetone content of polymer solution. This is attributed to the increment in the thickness of densified polymer layer due to evaporation of higher amount of acetone. The formation of transition layer was observed by several authors (Yuenyao et al. 2015, Ismail et al. 2011, and Ismail and Lai 2003).

The largest total thickness of membrane was measured as 461 μm belonging to PP-47 (11.4% AC solution). When the amount of acetone increased twofold in the casting polymer solution, the total thickness of membrane PP-37 decreased to 180 μm . This observation is compatible with my expectation. Because as the amount of acetone increased in the casting solutions more acetone evaporated during dry inversion, hence denser polymer solution quenched in wet inversion and volume of membrane shrank as expected. However, further increase in the content of acetone (from 22.9% to 34.3%) led to increment in the total thickness of membrane. The tendency of increase in the total thickness despite the densified polymer solution can be explained by the pore structure. While the acetone content was 22.9%, the membrane support layer was made up of only spongy pores. While

the amount of acetone increased, larger pores in elliptical form formed which provided larger volumes. In literature, general opinion is decrease in the size of the pores because of acetone incorporation. Madaeni et al. 2005 observed decline in the size of the pores and number of fingerlike pores due to involving of 6 wt.% acetone into PSF/NMP solution. This is attributed to the densified skin layer provided by evaporation of acetone during dry inversion. On the other hand, according to Ahmed et al. 2013, adding acetone shifted the PES/DMF/acetone solution towards binodal curve, thereby coagulation of casting polymer solution was enhanced. Furthermore, the viscosity of polymer solution decreased with increasing the acetone content, which accelerated the solvent-nonsolvent diffusion rate. As a results, the pore size and skin thickness of membrane prepared with Acetone/DMF/PES solution were larger and thinner, respectively compared to the membrane prepared with DMF/PES solution. The concentration of acetone was between the range 23-25 wt.% in the study carried by Ahmed et al. 2013. Our observation about pore morphology for acetone content less than 22.9 wt. % was compatible with Madaeni et al. 2005 who studied polymer solution with acetone content 6 wt.%. Our observation about pore morphology for acetone content higher than 22.9 wt. % was compatible with Ahmed et al. 2013 who studied polymer solution with acetone content 23-25 wt.%. Hence it was deduced that depending on the acetone concentration morphology of membrane may show different trend.

Table A.3 Morphological properties of asymmetric PES membranes prepared via DWPI method. AC content of the membrane solution was the investigated parameter. Casting film was standing 15 min free-evaporation before wet phase inversion in 500 ml water quench bath.

Code	Membrane solution content	Skin layer thickness (μm)	Transition zone thickness (μm)	Total Thickness (μm)	Pore shape
PP-47	11.4%AC- 22.9%PES- 65.7%DMF	0.13	2.81	461.79	Spongy + Finger like
PP-37	22.9%AC- 22.9%PES- 54.3%DMF	0.200	5.88	183.76	Spongy
PP-56	28.6%AC- 22.9%PES- 48.6%DMF	0.128	12.27	192.41	Spongy
PP-55	34.3%AC- 22.9%PES- 42.9%DMF	Non- measurable	14.35	213.68	Spongy



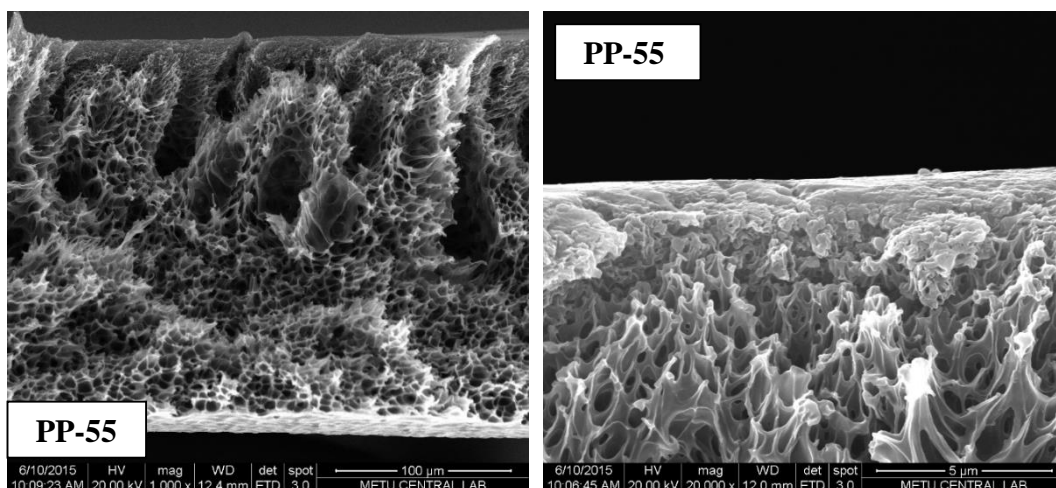


Figure A.1 PES asymmetric membranes prepared from PES-DMF-Acetone solution with different acetone (AC) content via DWPI method for 15 min free evaporation during dry inversion period. PP-55 with 34.3% AC.

Effect of Acetone Content of the Casting Solution on Gas Separation Properties of Asymmetric PES Membranes Produced via DWPI Method for 15 min free-evaporation

The gas test results of DWPI membranes were listed in Table A.4. The gas permeance of membranes (PP-37, PP-41, PP-44) were 67.80 GPU for H₂, 19.33 GPU for CO₂ and 11.57 GPU for CH₄. These values were more than 100 times higher than the permeance of PES membranes prepared via wet phase inversion in IPA quenching bath. These values were well above the CO₂ permeance values for neat asymmetric flat PES membranes reported in the studies carried by Saedi et al. 2014 (11 GPU CO₂ with 25 CO₂/CH₄ selectivity), Saedi et al. 2012 (6.75 GPU CO₂ with 18.1 CO₂/CH₄ selectivity), Ismail et al. 2015 (0.94 GPU CO₂ with 16.94 CO₂/CH₄ selectivity). The H₂/CO₂, CO₂/CH₄ and H₂/CH₄ ideal selectivity values were 3.53, 1.74, and 6.10; respectively, which were significantly lower than listed in literature. The Knudsen diffusivity selectivity values were calculated as 4.69, 0.60, 2.83 for H₂/CO₂, CO₂/CH₄ and H₂/CH₄, respectively. The experimental ideal selectivity values are well below the intrinsic selectivity values of PES (CO₂/CH₄ = 30, Li and Chung, 2008) and slightly higher than Knudsen diffusivity selectivity. This was attributed that gas permeation through membrane was mainly carried out

Knudsen diffusion mechanism instead of solution-diffusion mechanism. This was an evidence that the dense layer included non-selective voids with size of 2-50 nm in which Knudsen diffusivity is dominant. However, the porosity of membrane (closed pores or thin skin layer) an additional permeance retardancy hence the experimental selectivity values were larger than Knudsen selectivity.

The 6% increase in AC content of the casting solution led to 24.5% and 24.8% and 43.6% of decrease in H₂, CO₂ and CH₄ permeance, respectively with slight enhancement in ideal selectivity values. Further increase in AC content is provided by further reduction in permeance without any enhancement in selectivity.

The variation in the gas separation performance of the membranes depending on AC content had been tried to be explained by the morphological structures of the membranes. As observed previously and according to my previous experience (see Chapter 2), gas permeance of PES membrane was inversely proportional to its dense skin layer thickness. Based on SEM micrographs of DWPI PES membranes (Figure A.1 or Table A.3), the thickness of dense skin layer was remaining constant despite the change in the AC content. However, the thickness of transition zone increased by 2 fold corresponding to redounding the AC content of casting solution by 11.4% and 6%. Probably, this zone was made up of closed and fine pores and the main resistance against the gas permeance was provided by this transition zone. The decrease in permeance with enhancement in selectivity was experienced by several authors in literature. Krol et al. 2001 reported that by increasing acetone content from 30% w/w to 37.5% w/w the O₂ permeance of polyimide membrane decreased from 4 GPU to 1.2 GPU which was attributed to the reinforced evaporation step because of acetone. Barth et al. 2000 reported reduction in flux and very high retention of solutes due to including 3% acetone in the polymer-DMF solution and this phenomenon was ascribed by densified and concentrated polymer layer on the upper part of the membrane despite the fact that it could not be observed any significant change in morphological structure based on SEM images. Madaeni et al. 2005 observed decline in milk flux due to involving of 6 wt.% acetone into PSF/NMP solution. Chabot et al. 1997 prepared PVDF

membranes and documented that evaporation of acetone prior to wet phase inversion increased the density of membrane and resulting in higher selectivity. Ahmed et al. 2013 indicated that the lower permeance and excellent rejection of solute for PES membranes, despite the thinner skin layer. This result shows that the quality of the skin layer such as porosity or defects is as important as its thickness.

Mixed matrix DWPI-PES membranes gas separation performance were also listed in Table A.4. Such a high gas permeance value (340 GPU for CH₄) with low selectivity indicated the existence of non-selective voids because of both clustering of ZIF-8s and nature of DWPI production method. Hence the effect of ZIF-8s loading could not be investigated objectively.

PDMS coating is widely used method in membrane technology to plug the pores. The several authors who prepared asymmetric mixed matrix polymeric membrane for gas separation, used and suggested PDMS or Poly methyl hydrosiloxan (PMHS) coating for effective separation (Dorosti et al. 2015, Zuhairun et al. 2014-a, Ismail et al. 2015). Coating the membrane with dilute PDMS solution dominates the sorption-diffusion mechanism by plugging the non-selective pores. The performance of PDMS coated membranes was also provided in Table A.4. After PDMS coating, permeance of each membrane decreased. For each membrane type, the H₂/CO₂ selectivity decreased to nearly 2.5 which is the intrinsic H₂/CO₂ selectivity of PES while H₂/CH₄ and CO₂/CH₄ selectivity increased after PDMS coating, however those were still well below the intrinsic CO₂/CH₄ and H₂/CH₄ selectivity of dense PES film. The ideal selectivity of neat PDMS membrane were reported as 3.3 for CO₂/CH₄ (Hussain and König 2012, Sridhar et al. 2007); approximately 0.6-0.7 for H₂/CH₄ (Orme et al. 2003, Basu et al. 2010) and ~0.3-0.2 for H₂/CO₂ (Orme et al. 2003, Basu et al. 2010). Ideal CO₂/CH₄ selectivity values of DWPI- neat PES membranes coated with %3 PDMS solution were 9.76, 25.2, 11.8 corresponding to the AC content of membrane 22.9%, 28.6%, 34.3%, respectively. After PDMS coating, ideal H₂/CH₄ selectivity values of neat PES membranes were increased to 23.2, 57.7, and 24 corresponding to the AC content of membrane 22.9%, 28.6%, 34.3%, respectively. These ideal

selectivity values are considerably higher than that of neat PDMS membranes. This phenomenon is strong evidence that PES membrane layer was dominant in gas separation, and PDMS coating layer acted only as plug for non-selective voids. The reason that the selectivity values of the membrane were lower than the intrinsic selectivity of dense PES membrane is attributed to the expansion of free-volume of the polymer which changed the gas separation properties of polymer significantly.

Among PDMS coated membranes, the highest selectivity values belong to membranes (PP-45, PP-56) prepared from solution including %28.6 acetone. For this type of membranes; H₂, CO₂ and CH₄ permeances were 12.69, 5.55 and 0.20 GPU, respectively. On the other hand, H₂/CO₂, H₂/CH₄ and CO₂/CH₄ selectivities were 2.29, 57.72 and 25.25 respectively. Among the membranes prepared wet phase inversion method, the highest selectivity belongs to membrane coagulated in %2 water- %98 IPA bath (Table 2.9). H₂, CO₂ and CH₄ permeance of this type of membranes are 0.41 GPU, 0.18 GPU and 0.0050 GPU, respectively. When we compared these two types of membranes, it was observed that CO₂ permeance increased approximately 30 fold meanwhile CO₂/CH₄ selectivity reduced by half.

The highest permeance values belong to membranes (PP-37, PP-41, PP-44) prepared from solution including %22.9 acetone. For this type of membranes; H₂, CO₂ and CH₄ permeances were 24.16, 10.16 and 1.16 GPU, while H₂/CO₂, H₂/CH₄ and CO₂/CH₄ selectivities were 2.37, 23.21 and 9.76 respectively. Among the membranes prepared wet phase inversion method, the highest permeances belong to membrane coagulated in %10 water- %90 IPA bath (Table 2.9). CO₂ permeance of this type of membranes is 0.44 GPU with 15.3 ideal selectivity of CO₂/CH₄. By comparing these two types of membranes, it was observed that CO₂ permeance increased 23 fold while the CO₂/CH₄ selectivity decreased slightly from 14.6 to 9.76 by means of DWPI method.

Mixed matrix PES/ZIF-8 membranes via DWPI method were also tested in terms of gas separation performance. The results were as indicated in Error! Reference source not found.6. MMMs did not show any selectivity unless PDMS coating. CO₂ permeance of MMM-31 prepared from solution including 0.1gr 65 nm ZIF-8 and %22.9 acetone was 44.5 GPU and CO₂/CH₄ ideal selectivity is 3.27 after PDMS coating. Among MMMs prepared via NIPS method, the highest selectivity and permeance belong to MMMs (MMM-10, MMM-25) including %10 65 nm non-annealed ZIF-8 (Table 4.14). CO₂ permeance of this type of membrane was 0.38 GPU and CO₂/CH₄ selectivity of them was 37.6. By comparing MMMs prepared via two different methods (DWPI and NIPS), it was depicted that CO₂ permeance increased more than 100 fold while the CO₂/CH₄ selectivity decreased sharply from 37.6 to 3.27. Increase in acetone content of solution (MMM-30) caused to approximately 45% decrease in H₂ and CO₂ permeance and approximately 20% decrease in CH₄ permeance without any enhancement in ideal selectivity. The increment in AC content in the membrane created denser membrane layer, however the variation in both morphology and free-volume of polymer layer due to existence of ZIF-8s prevented the high selectivity.

Effect of Light Exposure: Morphological Properties of Asymmetric PES Membranes Produced via Forced Dry Inversion LIDWPI Method for 15 min Light Exposure

Figure A.2 showed the SEM micrographs of asymmetric PES membranes; PP-60 and PP-62 which were prepared PES solutions made up of 22.9%PES-22.9%AC-54.2%DMF and exposed 15 min and 10 min IL light, respectively.

The PP-66 and PP-64 which were prepared from 22.9%PES-28.6%AC-48.5%DMF and exposed 15 min and 10 min IL light during dry inversion, respectively. Their SEM images were provided in Figure A.3.

At first glance on SEM micrographs, the morphological properties of membranes produced via LIDWPI method were not affected by neither IL exposure period nor content of AC. Their common properties were very-thin skin layer, finely-pored transition zone, support layer with spongy and finger like pores. The

only difference can be noticed was the reticular form of the pores walls of membranes prepared from solution with 28.6% AC.

If these two figures are compared it is observed that the selective skin layer of membranes prepared via LIDWPI is more pronounced than that of membranes prepared via DWPI method. This phenomenon is indicative of the fact that light energy induction enhances evaporation of volatile solvent (acetone). Therefore, denser and more pronounced skin layer was obtained. The support layer morphology of these two membranes which were prepared by two different methods is similar. Since the support layer formed during wet inversion step, this result is as expected.

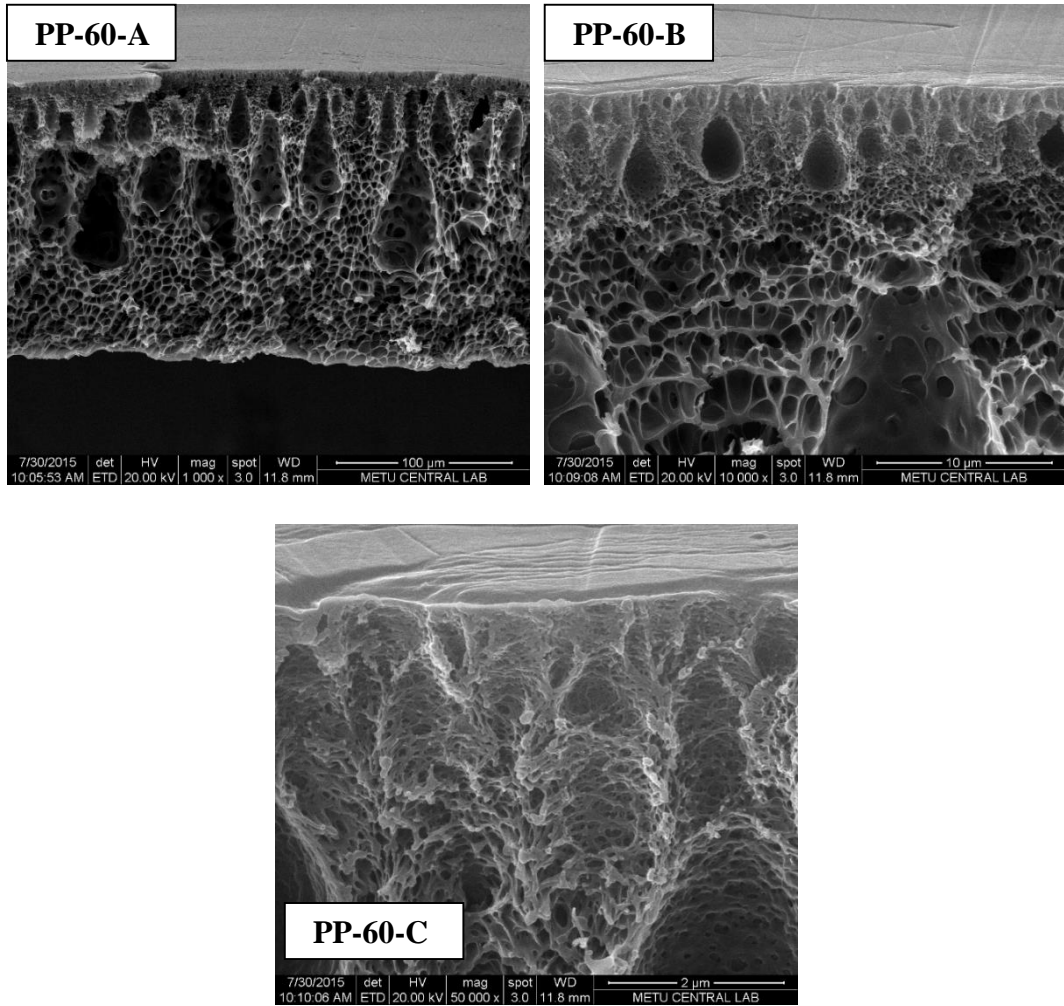


Figure A.2 SEM micrographs of membrane prepared from 22.9%AC-22.9%PES-54.2%DMF solution DMF solution and exposed 15 min. incandescent lamp light for dry inversion. (A) cross-section, (B) transition layer and (C) selective skin layer.

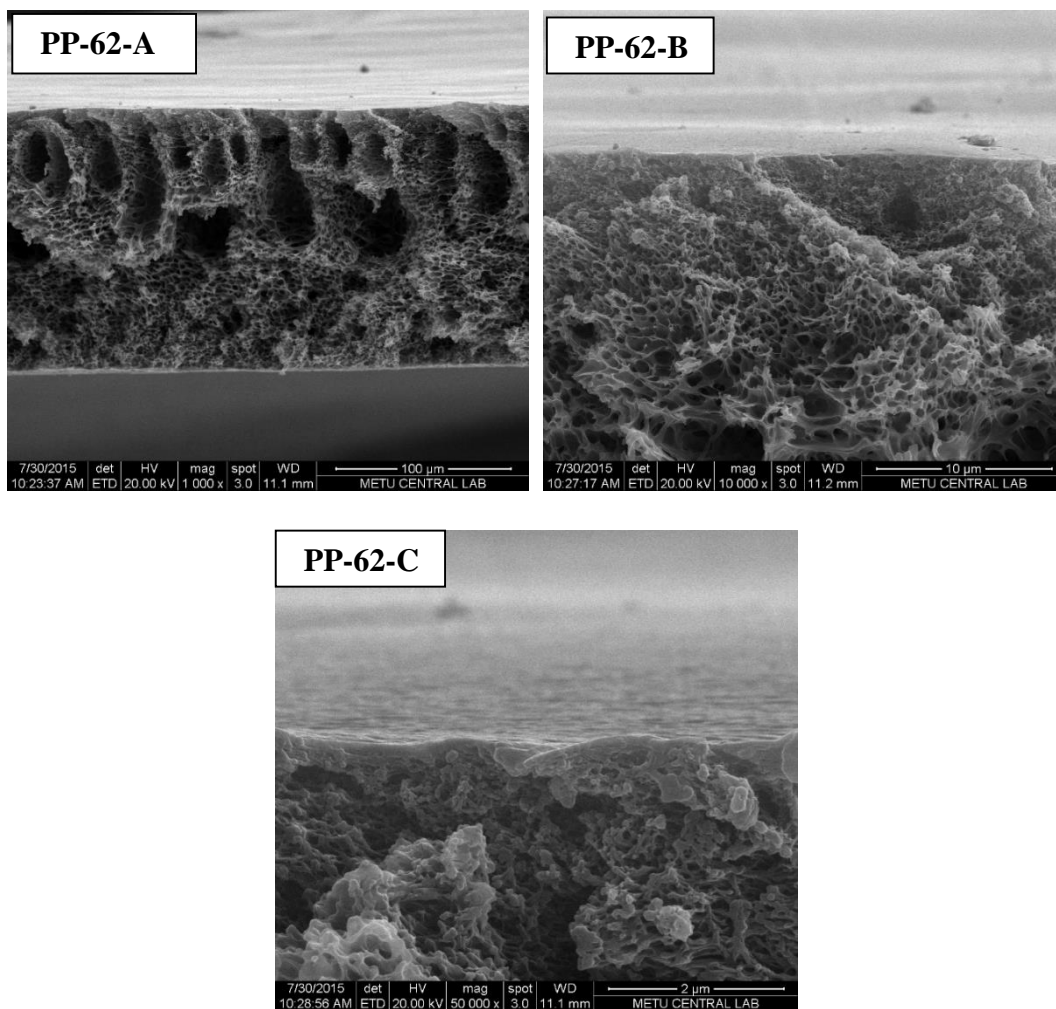


Figure A.2 (Cont.) SEM micrographs of membrane prepared from 22.9%AC-22.9%PES-54.2%DMF solution DMF solution and exposed 10 min. incandescent lamp light for dry inversion. (A) cross-section, (B) transition layer and (C) selective skin layer.

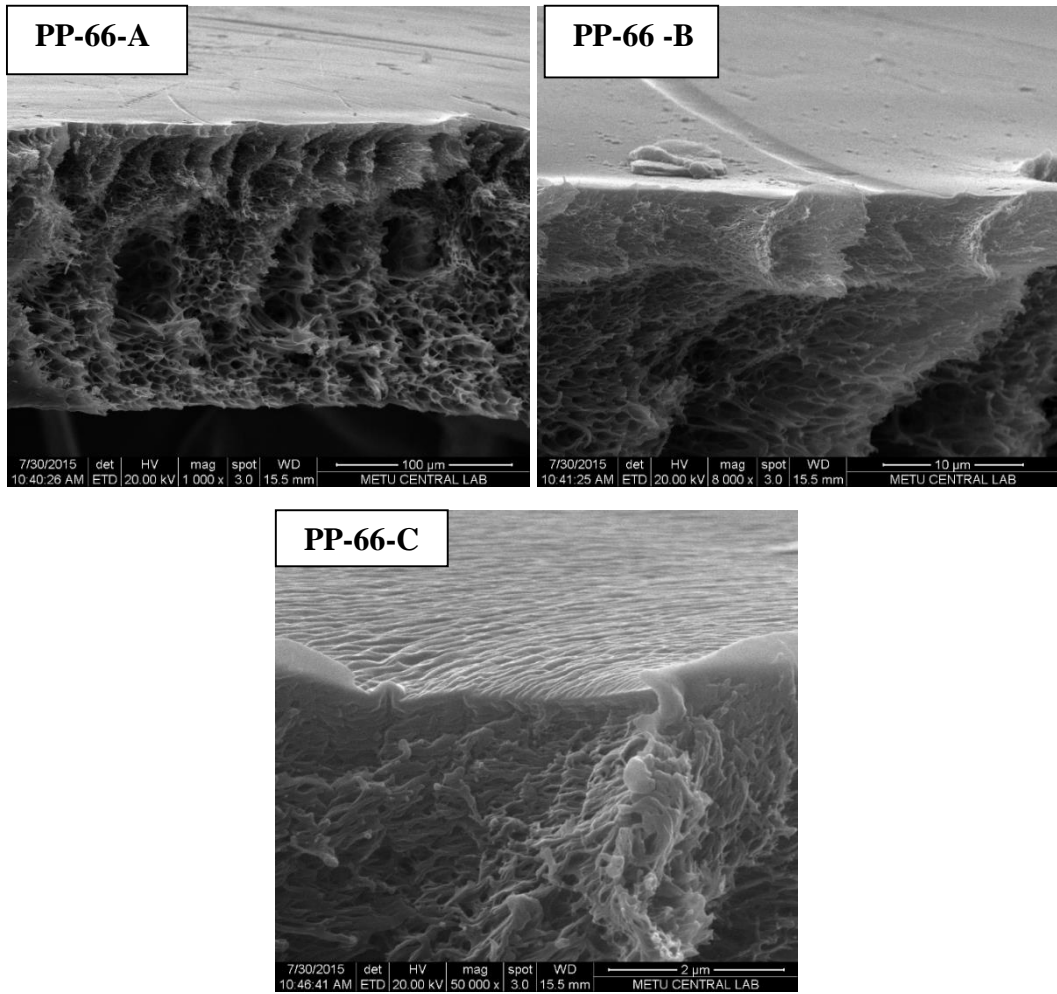


Figure A.3 SEM micrographs of membrane prepared from 28.6%AC-22.9%PES-48.6%DMF solution DMF solution and exposed 15 min. incandescent lamp light for dry inversion. (A) cross-section, (B) transition layer and (C) selective skin layer.

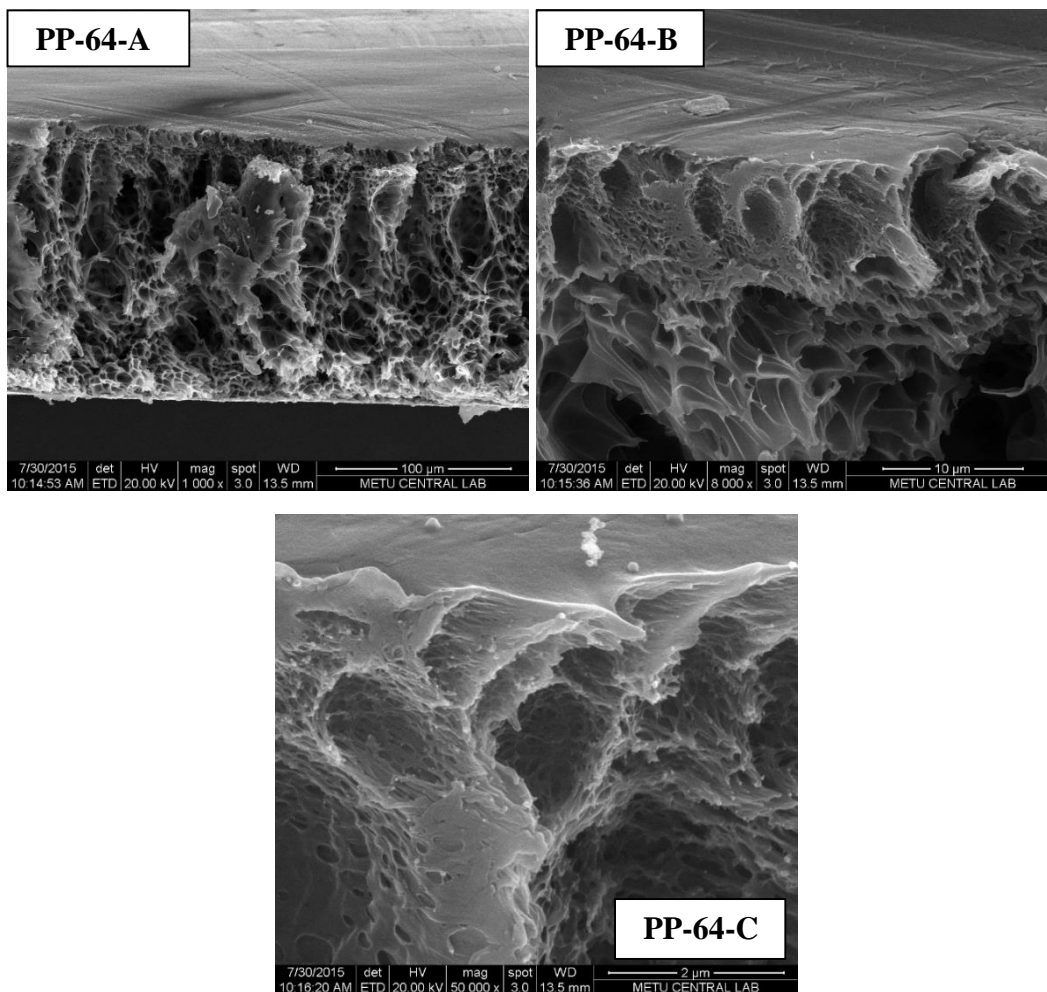


Figure A.3 (Cont.) SEM micrographs of membrane prepared from 28.6%AC-22.9%PES-48.6%DMF solution DMF solution and exposed 10 min. incandescent lamp light for dry inversion. (A) cross-section, (B) transition layer and (C) selective skin layer.

The quantitative investigation results of PP-60, PP-62, PP-64 and PP-66 were provided in Table A.5. For two different AC content (22.9% and 28.6%), increasing IL exposure period from 10 min to 15 min did not affect the thickness of skin layer and the thickness of transition zone. Probably, the thickness of dense skin layer or transition zone layer fixed during IL exposure period for less than 10 min. Hence further increase in exposure interval did not alter the properties of dimensions. However, by increasing IL exposure 5 min, the total thickness of membrane increased by 9.5 % and 7.5 % corresponding to membrane including

22.9% and 28.6% AC, respectively. One of the possible explanation was the thermal expansion of polymer chain.

When the IL exposure kept constant, the increase in the AC content of the solution from 22.9% to 28.6% led to 3-fold increment in transition zone thickness while its effect on total membrane thickness was insignificant. The percent extension in skin layer thickness was approximately 20% due to additional AC in the solution. The extension in both dense skin layer and transition zone thickness was a result of the densified polymer solution due to larger amount of AC evaporation as suggested by Krol et al. 2001. As suggested by Shieha and Chung 1998, the denser or thicker skin layer leads to retard interfacial solvent-nonsolvent exchange in subsequent coagulation. Probably, the significant increase the transition zone layer with approximately 30 nm increase in skin layer may be originated from the retardation of solvent-nonsolvent exchange rate because of resistance of denser and thicker skin layer. Hence the region of small-pores increased.

Membranes produced by the LIDWPI method have a thinner total cross-sectional thickness and a thinner transition zone thickness and thicker dense skin layer thickness than the membranes produced by the DWPI method. Since the IL exposure enhanced the evaporation of AC., casting polymer solution became denser and more stable for wet phase inversion step. As a result, shrinking in porous layer (such as porous support layer thickness or finely-pored transition zone thickness) or increasing in the thickness or density of non-porous dense skin layer can be observed.

Table A.5 Morphological properties of asymmetric PES membranes prepared via LIDWPI method. AC content of the membrane solution and IL exposure period were the parameters inquired. The wet phase inversion period was performed in 500 ml water quench bath.

Code	Membrane solution content	IL exposure period (min.)	Skin layer thickness (nm)	Transition zone thickness (μm)	Total Thickness (μm)
PP-60	22.9% AC- 22.9% PES- 54.3% DMF	15	150	1.74	163.07
PP-62	22.9% AC- 22.9% PES- 54.3% DMF	10	150	1.91	148.7
PP-66	28.6% AC- 22.9% PES- 48.6% DMF	15	180	5.43	161.3
PP-64	28.6% AC- 22.9% PES- 48.6% DMF	10	190	6.1	150.1

Gas Separation Properties of Asymmetric PES Membranes Produced via LIDWPI Method

The gas test performances of PES membranes prepared LIDWPI method were listed in Table A.6. For the membranes prepared from solution with 28.6% AC, the permeance of membrane via LIDWPI was very close to that of membrane produced by DWPI and coated with PDMS. This made us think that by the help of the light induction, it will be possible to change the gas separation property of the membrane without coating. However, the selectivity values were the same as the selectivity values of the DWPI membrane, which did not be coated with PDMS. Presumably the interaction between PES and water and the rate of displacement of water and solvent interfered with the formation of a completely defect-free PES membrane. The polymer surface was tried to rigidify to prevent these defects by IL induction, but it was not enough.

The permeance of PP-60 was lower than that of PP-66, but had almost the same ideal selectivity. This is the opposite of what is expected, according to our experience, as the AC content of solution increased, the permeance of membrane decreased. Probably, 15 minutes IL exposure caused to evaporation of large amount of AC, when the AC content of the solution was low, the degree of rigidification of polymer layer hindered the high permeance. For this reason, exposure to IL reduced to 10 minutes, considering 15 minutes was too long. The 5 minutes' decrease in the IL exposure provided to enhancement in H₂ and CO₂ permeance by 2 fold and in CH₄ permeance by 2.8 fold, when the AC content of the solution was 28.6%. For membranes prepared solution with 22.9% AC, H₂ and CO₂ permeance increased 9-fold while CH₄ permeance increased 20 fold due to decreasing IL exposure period from 15 minutes to 10 minutes. However, the ideal selectivity values were still considerably lower than the intrinsic selectivity values of dense PES membrane.

If membranes prepared two different methods; namely LIDWPI and DWPI were compared, it was observed that permeances of membranes decreased due to exposure of light energy. However, the selectivity enhanced slightly.

Table A.6 Gas separation performance of neat PES membranes prepared via LIDWPI method.

IL	Content	Code	Permeance (GPU)			Ideal Selectivity		
			H ₂	CO ₂	CH ₄	H ₂ /CO ₂	H ₂ /CH ₄	CO ₂ /CH ₄
15'	%23 Act- %23 PES- %54 DMF	PP-60	9.44	3.16	1.13	2.99	8.35	2.80
	%29 Act- %23 PES- %48 DMF	PP-66	14.83	4.54	1.83	3.28	8.1	2.48
10'	%23 Act- %23 PES- %54 DMF	PP-62	86.82	27.88	22.48	3.12	3.87	1.24
	%29 Act- %23 PES- %48 DMF	PP-64	30.79	8.56	5.24	3.59	7.26	2.04

In order to increase these selectivity values, it was decided to use different polymer instead of coating PES with PDMS. Because, as described in the previous part, the selectivity values were significantly lower than the intrinsic selectivity values of the PES despite PDMS coating. When the PES membrane prepared by IL exposure, the selectivity values were still well below the target values, despite the low permeance values (for example PP-60). The low selectivity even at low permeance made me think that the characteristic of PES film which determines the gas separation properties of membrane such as free-volume changed during phase inversion (Kesting et al. 1990, Fritzsche et al. 1990).

Comparison of Membranes produced via NIPS, DWPI and LIDWPI Methods in terms of Morphological Properties

Membranes produced by the NIPS method have very thick dense selective layer with 25 μm and support layer with spongy pores. For NIPS method, when the water content of quenching medium increased to 25%, the dense skin layer could

not be obtained, only porous membrane layer with spongy and finger like shape were observed. Membranes produced by DWPI method were composed of three layer, namely dense skin layer with thickness less than 200 nm, transition zone with finely pores, support layer with both spongy and finger like pores. At first sight, DWPI membranes and LIDWPI membranes have very similar morphological features. At a closed examination, the thickness of skin layer increased by 30% and the thickness of transition zone and total membrane decreased by approximately 65% and 10%, respectively with respect to those of DWPI membranes. Because IL exposure during dry inversion produced denser polymer casting layer before wet quenching step.

B. CALIBRATION OF GC

For the analysis of feed and permeate gas compositions, gas chromatograph was calibrated for CO₂ and CH₄ gases. For calibration, each gas was fed to GC separately at several pressures between 0 and 100 Torr, and the areas under the peaks were recorded for all pressures. Then, the pressure versus the corresponding area were plotted as calibration curve for both gases. Pure gas calibration curves for CO₂ and CH₄ are shown in Figures B.1 and B.2, respectively. These pure gas calibration curves were used so as to calculate the partial pressures of each component in binary gas mixtures.

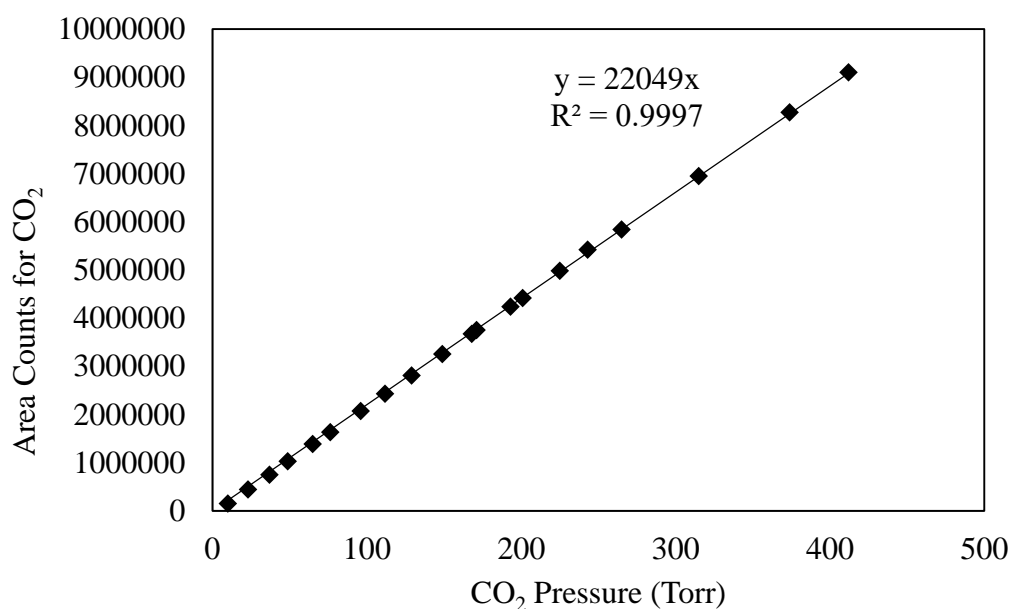


Figure B.1 The calibration curve of CO₂ for GC analysis.

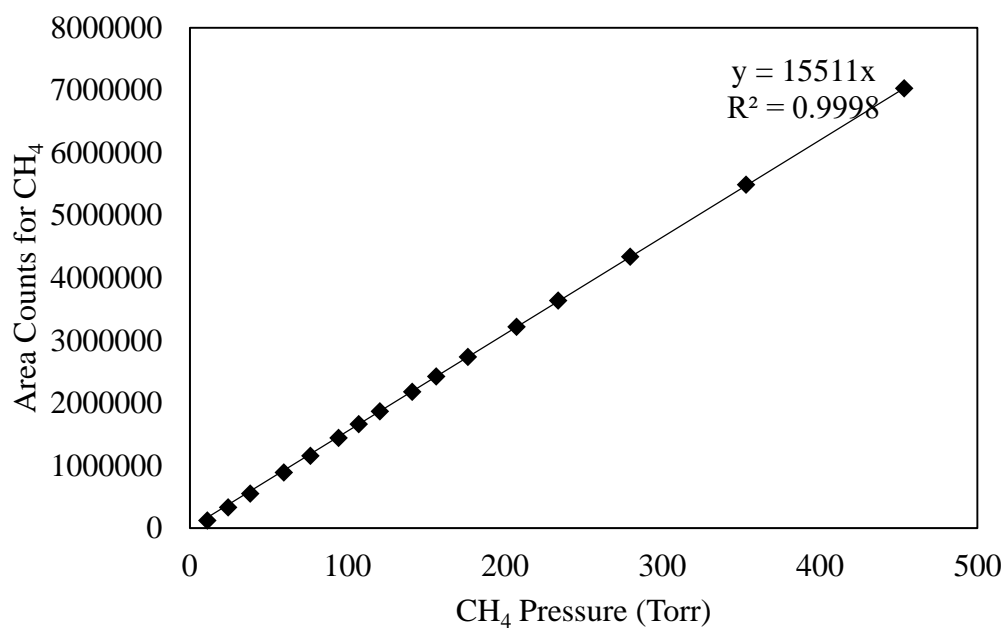


Figure B.2 The calibration curve of CH₄ for GC analysis.

CURRICULUM VITAE

PERSONAL INFORMATION

Surname, Name: Antepli Tüzün, Burcu

Nationality: Turkish (TC)

Date and Place of Birth: 29 July 1986, Ankara

Marital Status: Married

email: burcutuzun.metu@gmail.com

EDUCATION

- Ph.D,** **Middle East Technical University (METU)**
Chemical Engineering, CGPA:3.93/4.00
Thesis Title: Gas Permeation and Sorption Properties of ZIF-8 Filled Polymeric Membranes Prepared by Infrared and Incandescent Light Induced Liquid and Vapor Phase Inversion
Graduation: 03.2012-12.2017
- M.S** **Middle East Technical University (METU)**
Micro and Nanotechnology, CGPA:3.57/4.00
Thesis Title: Structural Properties of Defected Graphene Nanoribbons under Tension: Molecular-Dynamics Simulations
Graduation: 01.2010-02.2012
- B.S** **Middle East Technical University (METU)**
Chemical Engineering, CGPA:3.35/4.00
Graduation: 09.2004-06.2009
- High School** **Çankaya Anadolu High School, 4.98/5.00**

HONORS AND AWARDS

- HASAN ORBEY Award in Graduate Studies Ph.D.2014, METU, Dept. of Chemical Engineering
- Dean's Honor List, Dept. of Chemical Engineering, METU, 2005-2009

EXPERIENCE

- Teaching assistantship in METU, Dept. Of Chemical Engineering (November 2015 - January 2018)
- Project assistantship in International Research Fellowship, The Scientific and Technological Research Council of Turkey, (March 2014 - November 2015)
- Internship in Baştaş Çimento, Ankara/TURKEY
- Internship in Samur Halı, Ankara/TURKEY

COMPUTER AND LANGUAGES

- Microsoft Office Applications (Word, Excel, Power Point)
- LATEX
- POLYMATH
- MATHCAD
- English (Advanced)
- Germany (Beginner)

PUBLICATIONS

- B. Tuzun, S. Erkoc, "Structural and electronic properties of unusual carbon nanorods", Quantum Matter 1, 136(2012).
- B. Tuzun, S. Erkoc, "Molecular dynamic simulations of pristine and defective graphene nanoribbons under strain", J. Comput. Theor. Nanosci. 10, 470(2013).

CONFERENCES ATTENDED

- Burcu Tüzün Antepi, Levent Yılmaz, Halil Kalıpçılar; Asimetrik Poliimid Gaz Ayırım Membranlarının Hazırlanması ve Karakterizasyonu; Oral presentation, 12th National Congress of Chemical Engineering, Izmir High Technology Enstitute, Izmir, Turkey, August 2016.
- Burcu Tüzün Antepi, Halil Kalıpçılar, Levent Yılmaz; Asymmetric Mixed Matrix PES/ZIF-8 Membrane for CO₂ Removal from CH₄; Short Presentation, EUROMEMBRANE 2015, Aachen, Germany, September 2015.
- Burcu Tüzün Antepi, Levent Yılmaz, Halil Kalıpçılar; Asimetrik Polietersülfon Gaz Ayırım Membranlarının Hazırlanması ve Karakterizasyonu; Oral presentation, 11th National Congress of Chemical Engineering, Eskişehir Osmangazi University, Eskişehir, Turkey, September 2014.